

**Low Speed Orthogonal Hot Machining with a Virtual Quick Stop Device**

by

Jonathan Maxmillian Edward Patillo

A thesis submitted to the Graduate Faculty of  
Auburn University  
in partial fulfillment of the  
requirements for the Degree of  
Master of Science

Auburn, Alabama  
May 7, 2016

Keywords: orthogonal milling, hot machining, force reduction

Approved by

Lewis N. Payton (Chair), Associate Research Professor, Mechanical Engineering  
Robert L. Jackson, Professor, Materials Engineering  
Dan B. Marghitu, Professor, Mechanical Engineering

## **Abstract**

Cocquillat first documented (1851) how heat in a tool shortens the life of the tool. Research since his time has generally concluded that the tool gives up a relatively higher percentage of its “cold hardness and toughness” as compared to the work stock. This interpretation suggests that if the workpiece itself were pre-heated it might alternatively lose a large percentage of its “cold hardness”.

This thesis looks at the advantages and disadvantages which may be gained by pre-heating the work stock thereby preferentially shifting the ratio/percentages back toward the tool. A body centered cubic (BCC) steel and face centered cubic (FCC) aluminum were chosen to test common commercially machined crystalline structures. The materials were heat treated and/or aged to provide various levels of hardness within the crystalline structures. Both alloys at two levels of hardness/temper were machined with two different depths of cut and three tool rake angles using the Videographic Quick Stop Device (VQSD) originally developed at Auburn University. Steel parts were machined at three different temperatures. Aluminum samples were cut at four different temperatures. Parts were preheated immediately prior to the machining operations. Tensile specimens of all the samples were undertaken to establish the cold working flow stress values of the materials tested. Machining was conducted in a specially modified Cincinnati Horizontal Milling machine using an improved Videographic Quick Stop Device (VQSD) to capture the geometry of the cutting formation simultaneously with the forces in the X, Y and Z-axes

using a standard Kistler force plate dynamometer. Utilizing the VQSD greatly increases the number of replicates available for statistical analysis by the metal cutting researcher. This allows for comprehensive multivariate analysis of the data with high confidence (> 95 %) in the meaning of the results obtained. Forces were collected and analyzed using low speed orthogonal machining equations. Wear was measured on the face of each tool using white light microscopy. The results of the data collection and statistical analysis are then used to populate the various historical models predicting the flow stress in metal cutting. The results indicate that one model is superior utilizing the criteria established by Kobayashi-Thomsen. The **Normal** force data indicated there is a definite advantage to be had in pre-heating the workpiece. This, combined with improved tool cooling methods, may result in all tools living a longer time while undergoing less chatter and/or deflection.

## **Acknowledgments**

This experiment was a team effort. I would like to thank God for His blessings and guidance throughout this experiment. All that is mentioned in the paper below came about because of the opportunity that Dr. Payton laid out before me. I would like to thank him for the opportunity to expand my knowledge and skill base by working in the Design Manufacturing Lab. I would also like to thank John Marcell for his electric expertise which tremendously helped my experimental setup and safety. I would like to thank my committee members (Dr. Jackson and Dr. Marghitu) for agreeing to evaluate my results.

I would also like to thank my fellow researchers in the Design Manufacturing Lab (past and present) for their contributions to my experiment. Their advice and aid was invaluable. Both the graduate teaching assistants and the undergraduate teaching assistants played a role in allowing me to work on my experiment and I truly appreciate them.

My family and other friends' support was immeasurable throughout this process. I want to thank them for helping keep my life outside of the Design Manufacturing Lab in order.

## Table of Contents

Abstract .....	ii
Acknowledgments.....	iv
List of Tables .....	viii
List of Figures .....	vix
List of Symbols .....	viii
I. Introduction .....	1
II. Scope and Objectives .....	2
III. Literature Review.....	3
Orthogonal Machining.....	3
Shear Zone .....	5
Dislocations and Hardness .....	11
High-Speed Camera Usage .....	12
Hot Machining .....	15
Laser Assisted Machining (LAM) .....	16
Flame/ Plasma Arc (PEM) .....	20
Induction .....	29
The Normal Force and Tool Wear .....	31
IV. Experimental Equipment and Techniques .....	41
Design and Construction of the Thermal Videographic Quick Stop Holder .....	47

Videographic Analysis.....	52
Video Analysis.....	52
Heating the Samples .....	53
Thermal Resistance Network.....	56
Materials .....	57
Hardness Test.....	58
Wear Analysis Setup.....	58
VI. Statistical Design of the Experiment .....	60
VI. Results.....	62
Effects of temperature upon Friction ( $F$ ) and Normal ( $N$ ) force results .....	62
Effects of temperature upon the Specific Horsepower ( $HP_s$ ) .....	63
Effects of Temperature upon the Calculated Wear Rate (Equation 22) .....	64
Analysis of Variance.....	65
Tool Wear Results.....	67
Miscellaneous Items.....	69
VI. Conclusions.....	70
Recommendations for Future Work.....	72
References.....	73
Appendix.A: Equations Used.....	78
Appendix.B: Raw Data .....	81
Appendix.C: Calculated Data Table .....	93
Appendix.D: Friction and Normal Force Graphs .....	135
Appendix.E: Specific Horsepower Graphs .....	142

Appendix.F: Wear Rate Graphs .....	152
Appendix.G: ANOVA Tables.....	162
Appendix.H: Tool Edge Summary Table .....	182
Appendix.I: Program Files.....	184
Appendix.J: Kobayashi-Thomsen Graphs .....	191
Appendix.K: Load Cell Calibration Certificate .....	201

## **List of Tables**

Table 1: Chang's ANOVA Table (24) .....	18
Table 2: Parameters in Kim's experiment (26).....	19
Table 3: Kim AISI 1045 Steel Results (26).....	20
Table 4: Kim Inconel 718 Results (26).....	20
Table 5: Case 1 ANOVA (28) .....	24
Table 6: Case 2 ANOVA (28) .....	24
Table 7: Case 3 ANOVA (28) .....	24
Table 8: Ranganathan's ANOVA table results (29) .....	25
Table 9: Ganta's ANOVA table (33).....	29
Table 10: Fixture 1 Displacement Results .....	50
Table 11: Fixture 2 Displacement Results .....	50
Table 12: Ranked multivariate outcomes .....	66
Table 13: Comparison of Optimal Factor Level Combinations.....	70
Table 14: Overall Optimal Factor Level Combinations for Steel 4130.....	71
Table 15: Overall Optimal Factor Level Combinations for Aluminum 6061 .....	71

## List of Figures

Figure 1: Type 1, 2 and 3 Chips Respectively (3) .....	3
Figure 2: Merchant Force Diagram (3).....	4
Figure 3: Merchant's observation of chip formation (3) .....	6
Figure 4: Merchant's Stack of Cards Model (3).....	7
Figure 5: Okushima and Hitomi's Model (4) .....	8
Figure 6: Huang's Observation of Flow in Shear Zone (6).....	9
Figure 7: Huang's "New" Stack of Cards Model (6).....	10
Figure 8: Payton Copper 10102 alloy observed geometry (36) .....	14
Figure 9: Feed rate variation results (27).....	22
Figure 10: Temperature and feed rate variation results (27).....	22
Figure 11: Temperature and cutting depth variation results (27) .....	22
Figure 12: Specific energy comparison (32).....	27
Figure 13: Material removal comparison (32) .....	28
Figure 14: Lajis' analysis results (34) .....	30
Figure 15: Enlarged view of the contact conditions between tool-chip interface.....	32
Figure 16: Tool damage mechanisms and cutting temperaturas (Childs 2000) .....	36
Figure 17: Merchant Force Diagram as modified by Payton (51) .....	37
Figure 18: Elevated View of Equipment Setup .....	43
Figure 19: Rotary Encoder.....	44
Figure 20: Kistler Dual Mode Amplifiers.....	44

Figure 21: National Instruments USB-6008 .....	45
Figure 22: Modified Load Lift Camera Stand .....	46
Figure 23: DRS Technologies Lightning RDT Camera .....	47
Figure 24: Final Fixture .....	48
Figure 25: Deformed Model of Fixture .....	49
Figure 26: 4130 42 HRC steel sample with hole drilled into leading edge .....	51
Figure 27: DRS TECHNOLOGIES Lighting RDT Camera.....	52
Figure 28: (Top) McMaster 120 V Strip Heater, (bottom) Cadco Buffet Range .....	54
Figure 29: Omega CN7523 Temperature Controller and Crydon Solid State Relay .....	54
Figure 30: Modified Cincinnati Horizontal Mill .....	55
Figure 31: (Left) Wood's E-trac AC Inverter, (right) Baldur Industrial electric motor....	55
Figure 32: Thermal Resistance Network .....	56
Figure 33: Paragon Industries Double Barrel furnace .....	58
Figure 34: Representative $F$ and $N$ trend as temp increased.....	63
Figure 35: Representative specific horsepower ( $HP_s$ ) trend as temp increased .....	64
Figure 36: Trend of tool wear rate in (in/sec) with increasing temperatures.....	65
Figure 37: Representative optical sample of edge wear documented in Appendix H.....	68
Figure 38: Representative optical sample of aluminum adhesion documented in Appendix H.....	68

## List of Symbols

$\phi$	Shear Plane Angle
$\phi_c$	Calculated Shear Plane Angle
$\alpha$	Tool Rake Angle
$A$	Area
$A_s$	Area of the Shear Plane
$A_{sK}$	Actual Shear Area
$\beta$	Angle between the Normal Force and the Resultant Force
$F$	Frictional Force
$F_c$	Cutting Force
$F_n$	Force Normal to the Shear Plane
$F_s$	Shearing Force along the Shear Plane
$F_t$	Feed/ Thrust Force
$F_y$	Y-axis Force
$F_z$	Z-axis Force
$k$	Conduction Coefficient
$k'$	Constant
$h$	Convection Coefficient
$k_y$	Kobayashi-Thomsen Trendline Y-intercept
$l$	Sliding Distance Along the Tool Face
$N$	Normal Force

$\sigma_y$	Yield Stress
$P_c$	Pixel to Inch Conversion Factor
$q$	Heat Transfer Rate
$R$	Resultant Force
$r_c$	Ratio Chip/Uncut Chip Thickness
$R_{cond}$	Conduction Resistance
$R_{conv}$	Convection Resistance
$R_T$	Total Thermal Resistance
$\tau_{sr}$	Resultant Shear Stress on Shear Plane
$\Delta T$	Temperature Difference
$t$	Thickness
$t_1$	Uncut Chip Thickness/Depth of Cut
$t_{1actual}$	Actual Depth of Cut
$t_{1pixels}$	Depth of Cut in Pixels
$t_2$	Cut Chip Thickness
$\tau_s$	Shear Stress on Shear Plane
$T_{max}$	Maximum Temperature Allowed for Load Cell
$T_{mr}$	Average Material Removal Temperature
$\tau_{sK}$	Kobayashi-Thomsen Shear Stress
$\mu$	Friction Coefficient
$V_c$	Velocity Along Chip-Tool Interface
$\psi$	Shear Front Angle
$\psi_c$	Calculated Shear Front Angle

$W$	Volume of Material Removed from Tool
$w$	Width of Chip/Thickness of Sample
$\chi$	Ratio- Shear Force over Force Normal to Shear Plane
$\gamma$	Shear Strain
$\gamma_C$	Chandrasekaran Shear Strain
$\gamma_M$	Merchant Shear Strain
$\gamma_P$	Payton Shear Strain

## **I. Introduction**

A literature review of "hot machining" was conducted including orthogonal machining techniques and the various heating techniques (traditional heating, induction heating and laser assisted machining (LAM), and flame/plasma arc (PEM) heating). The literature review concluded with an analysis of the normal force and wear mechanisms during metal cutting.

The literature review indicated that no one has conducted low speed orthogonal machining using a pre-heated work piece. An experiment was developed that looks at the effects of preheating the workpiece using a low speed orthogonal Videographic Quick Stop Device (VQSD) developed here at Auburn University in the Design and Manufacturing Laboratory (DML). The results of preheating the work piece indicated a general reduction in the Normal Force acting against the tool face. Since all forms of wear are directly proportional to the Normal Force, this indicates the possibility of extended tool life in general practice when the work-piece is preheated to low temperatures prior to machining.

## **II. Scope and Objectives**

The literature review indicated the absence of orthogonal machining data during hot machining of metal. An experiment was devised using the Low Speed Videographic Quick Stop Device (VQSD) developed at Auburn University. This device coordinates the simultaneous capture of tool chip geometry using a high speed, high magnification camera with a KISTLER Force Dynamometer. This allows for a complete statistical analysis of the classic metal cutting formula results. The objectives of the experiment are summarized here:

- Study the effects of hot machining on a Body Centered Cubic (BCC) material, Steel alloy 4130 at two levels of hardness (22 and 42 Rockwell Hardness (C-scale)).
- Study the effects of hot machining on Face Centered Cubic (FCC) materials, Aluminum alloy 6061 at two levels of temper (T0 and T6).
- Analyze the combined and individual effects of material, hardness / temper, tool rake angle, depth of cut and temperature upon the sliding Friction and Normal forces.
- Conduct post-mortem wear analysis of tools using white light microscopy.
- Compare the Kobayashi-Thomsen results of two predictive orthogonal models (Merchant and Payton).

### **III. Literature Review**

#### **Orthogonal Machining**

Orthogonal machining is only practiced in the research laboratory. It assumes that the cutting edge is perfectly perpendicular to the narrow workpiece. It completely overtops the workpiece thereby effectively becoming an infinitely wide tool. This simplified geometry allows for accurate and relatively easy force collection along with tool geometry. These measurements would consist of the shear plane angle, depth of cut, and chip thickness for example. The addition of a high-speed camera allows for the measurements to be taken as well as observation of chip formation.

Ernst (1) first denoted the three basic chip types formed from this process. The three types are as follows: type 1 is a discontinuous or segmented chip, type 2 is a continuous and smooth chip, and type 3 is continuous with a buildup of chip material between the tool and the chip or a “built-up edge” (BUE). Figure.1 shows an example of each chip type.

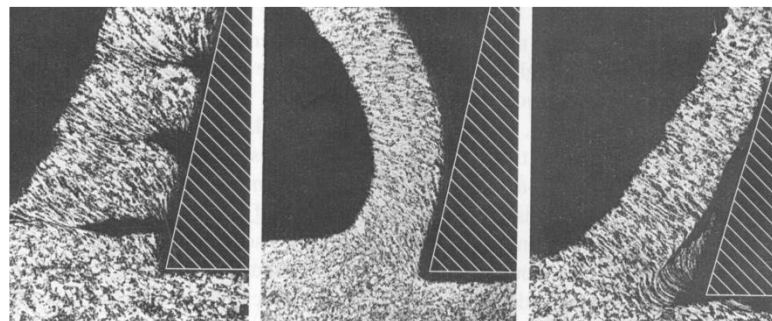


**Figure 1: Type 1, 2 and 3 Chips Respectively (3)**

Both Merchant and Piispanen independently developed similar concepts for a force diagram which illustrated the geometrical relationship between the cutting force components during orthogonal machining. Both researchers viewed the chip as an independent body held in mechanical equilibrium by the two equal and opposing resultant forces  $\mathbf{R}$  and  $\mathbf{R}'$ . The force  $\mathbf{R}$  is due to the force exerted by the work-piece on the chip. The force  $\mathbf{R}$  is composed of two components; the shearing force along the shear plane ( $\mathbf{F}_s$ ) and a force normal to the shear plane ( $\mathbf{F}_n$ ). The force  $\mathbf{R}$  may also be resolved into two other components, the cutting force ( $\mathbf{F}_c$ ) and the Feed Force ( $\mathbf{F}_t$ ). Figure.2 shows these relationships in what is now commonly referred to as the Merchant force diagram.

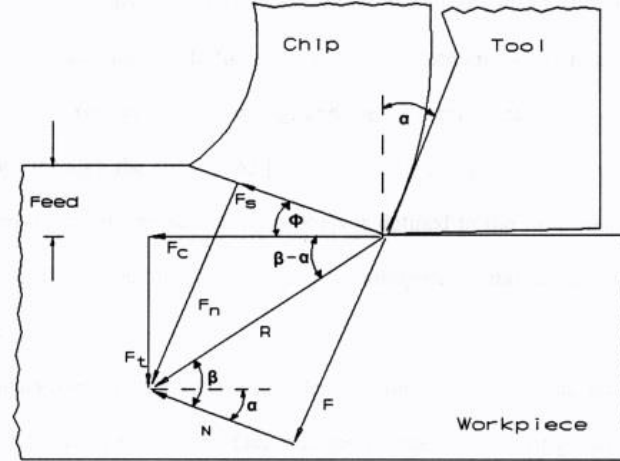


**Figure 2: Merchant Force Diagram (3)**

Analysis of Merchant's model produced the following equations:

$$F = F_c \times \sin \alpha + F_t \times \cos \alpha \quad (1)$$

$$N = F_c \times \cos \alpha - F_t \times \sin \alpha \quad (2)$$

$$R = \sqrt{F_c^2 + F_t^2} \quad (3)$$

$$F_s = F_c \times \cos \phi - F_t \times \sin \phi \quad (4)$$

$$F_n = F_c \times \sin \phi + F_t \times \cos \phi \quad (5)$$

$$\mu = \frac{F}{N} = \tan \beta \quad (6)$$

$F$  is the frictional force and  $N$  is the normal force. The friction coefficient,  $\mu$ , can be found by the equation 6 above which also yields  $\beta$ , the angle between the normal force and the resultant force (Degarmo (2)).

### Shear Zone

As mentioned above, the shear plane angle can be measured through this form of machining. Regardless of the metal cutting process, the shearing of metal takes place. Over the years, researchers have worked to determine where this shear plane is in relation to the tool and how it varies relative to the tool. Whereas the shear plane was originally a single line, further research has shown that it is actually a "zone." Merchant (3), Okushima and Hitomi (4) for example developed models which depicted a zone connected to the shear plane which showed how material flows when it is cut. Merchant's model represented the shear zone as a single plane, or thin-zone model. The angle of inclination of the shear plane to the cutting direction was defined by the angle  $\phi$ . Merchant observed that the crystal structure of the material was elongated by the shear process and gave the direction of crystal elongation the direction  $\psi$ .

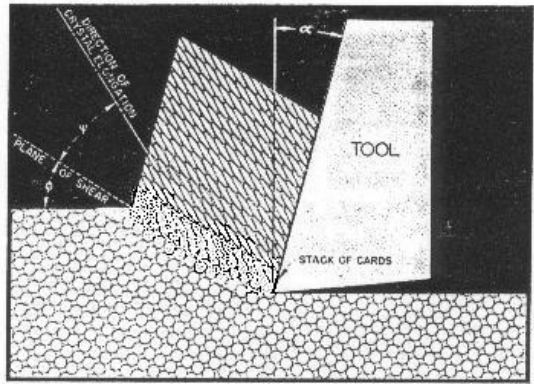


**Figure 3: Merchant's observation of chip formation (3)**

Merchant did not develop the plastic deformation aspect of his observations. Both Merchant and Piispanen used a “deck of cards” concept to visualize the shear zone process, where the shear mechanism during chip formation could be illustrated by the incremental displacement of cards in a stack (Figure.4). Each card moves forward a small amount in respect to the next card in the stack as the cutting process occurs. Merchant (5) proposed that the crystalline structure of the metal was elongated by the shear process, and that the direction of elongation was in a different direction than the shear plane.

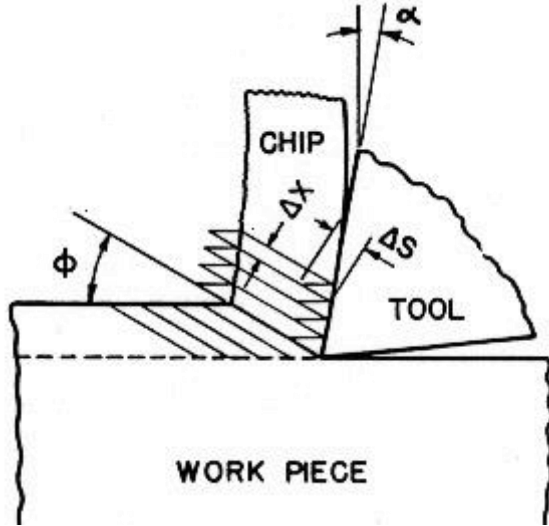


**Figure 4: Merchant's Stack of Cards Model (3)**

The following equation for the shear strain and shear front were developed from Merchant's chip formation bubble (Degarmo (2)).

$$\gamma = \frac{\cos\alpha}{\sin(\phi + \psi) \times \cos(\phi + \psi - \alpha)} \quad (7)$$

$$\varphi = 45 - \phi + \frac{\alpha}{2} \quad (8)$$

Okushima and Hitomi's (4) model consisted of an AOB zone between the work-piece and the tool. The boundary regions of this zone were considered rigid. Plastic deformation began to occur at the starting boundary line of the shear zone, OA, and the plastic strain gradually increased as the cut progressed. Figure.5 below shows their model.

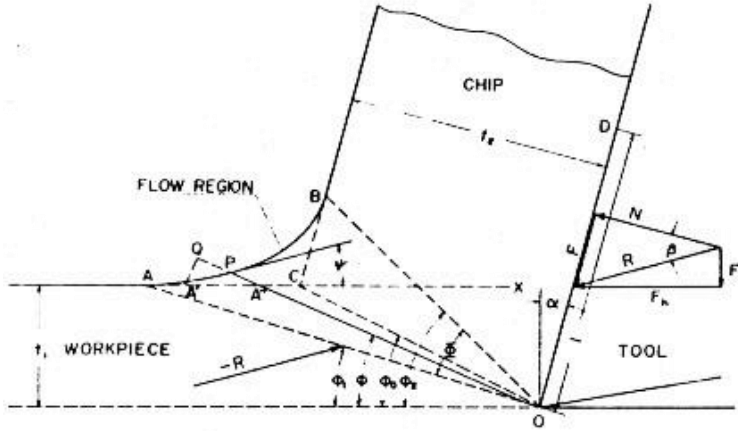


**Figure 5: Okushima and Hitomi's Model (4)**

Shear strain inside the shear zone AOB was expressed as follows:

$$\gamma = \cot\phi - \cot(\phi - \Psi) \quad (9)$$

Here  $\phi$  is the inclination angle of the arbitrary radial plane, and  $\psi$  is the tangent to the free surface (curve between A and B in Figure.5) with the machined surface. This model predicted that the shear strain was zero at the lower boundary of the shear zone and obtained the maximum at the upper boundary of the shear zone.

Another shear zone model was suggested in 1996 by Huang (6), working as a graduate student for J.T. Black. During a review of Brigg's (7) experiment using high speed magnification to observe the cutting of aluminum, Huang developed a new "stack of cards" model and a new shear strain equation of orthogonal machining. In reviewing the tapes made by Briggs, they observed that the material deformed in a totally different fashion than that which had been described in the machining literature. The plastic deformation of material as observed by Huang and Black is depicted in Figure.6.

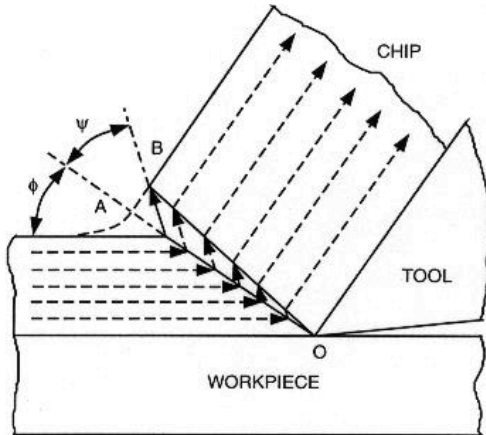


**Figure 6: Huang's Observation of Flow in Shear Zone (6)**

As the material in the work-piece moves from left to right, toward the cutting tool along the cutting direction, it approaches the shear zone, designated by the triangle AOB. When the material encounters the onset shear plane AO, it changes direction and appears to move at an inclination angle,  $\psi$ , to the plane. This is the shearing of the metal caused by the massive movement of many dislocations. Upon reaching the plane BO, the shearing process stops, and the material changes direction a final time and moves in a direction parallel to the tool face. The shape of AOB is triangular and the onset shear plane is flat. The material encounters plane AO simultaneously and shear is in mass all along the boundary. This onset of shear fronts creates the shear plane and defines the lower boundary of the shear zone. Thus  $\phi$  has been more properly termed by Black "the Onset of Shear Plane angle" (7). The termination of the shear fronts forms the upper boundary of the shear zone as noted by Black and Briggs (8). The shear fronts are inclined at an angle,  $\psi$ , originating from the plane connecting the tool tip to the free surface. His reasoning behind

this movement was the presence of dislocations in the material. Figure.7 details the angular relationships as derived by Huang.

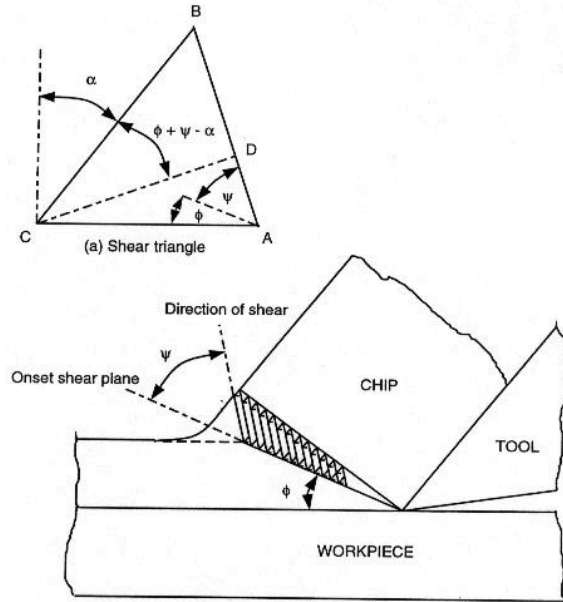


**Figure 7: Huang's "New" Stack of Cards Model (6)**

Huang's model is significantly different than Merchant's model. In the new card model, an element shears at the direction  $\psi$  relative to the onset shear plane. (In Merchant's model, an element shears in the direction of the shear plane  $\phi$ . In Zorev's model the work material shears tangentially to a shear line that is approximately parallel to the initial shear plane.) Using a minimum energy criteria, Huang developed the following relationships for  $\psi$  and  $\gamma$ :

$$\varphi = 45 - \phi + \frac{\alpha}{2} \quad (10)$$

$$\gamma = \frac{2 \times \cos \alpha}{1 + \sin \alpha} \quad (11)$$

## Dislocations and Hardness

Several attempts have been made to associate grain dislocations and hardness to factors in the metal cutting process. Material hardness is determined by the size and arrangement of these grains. Work-hardening material dislocates these grains, compressing them and thus making the material harder. P.K. Wright (10) suggested work-hardening as a major influence of the shear angle in 1982. However, he was not able to produce a predictable model and he ignored the frictional constraints in his analysis. Black (11) proposed a model in 1979 with regards to the plastic deformation in metal cutting. He demonstrated that the magnitude of the flow stress and the onset of shear angle  $\varphi$  correlated to the stacking fault energy of the material being cut. His resultant flow stress model predicts a catastrophic shear front (or shear plane) ahead of the tool created by the annihilation and subsequent heat generation as the metastable cells in his model rearrange themselves. The model observes that dislocation sources originate near the tool tip, driving dislocations into the cell networks. There is a rapid buildup of applied stress levels as the number of dislocations increase, causing a force hardening effect at the tip of the tool (Cottrell (11)).

Black's paper notes that more than one shear front would be crossing the material from the tool tip to the free surface at any one point in time, comparing this effect to waves at the seashore. Waves from the ocean will intersect a jetty at many different point along the length of the jetty, but always at the same angle. This is a good analogy to the effect observed by Huang in aluminum as he developed his "new" stack of cards model. Further,

Black's theory predicts that as work-hardening increases, the resistance to the onset of shear will also increase. This delay in the initiation of shear would translate into an increase in the shear plane angle  $\phi$ .

### **High-Speed Camera Usage**

One of the earliest attempts at capturing images of the shear zone was Coker's photoelastic attempts in the 1930s. The development of the scanning electron microscopes and other such technologies has aided researchers such as Black (12), Ueda and Iwata (13), and others.

Cook and Shaw (14) used magnified cinematography as early as 1951 to analyze the shear process. They observed a thick shear zone and at various times two shear zones. One zone (the primary zone) extended from the tip of the tool along the shear plane while the secondary zone at times appeared adjacent to the tool face. They noted that the frequency of the two zones was "perhaps" more pronounced when cutting materials that strain harden easily and produce thick chips.

Agrawal and Amstead (15) examined the cutting of mild steels with a FASTEX high speed motion camera in the 1960s. They detected the presence of Built-Up Edges (BUE), crack formations, and deformation ahead of and below the tool. Their study would also indicate that the shear zone region was not a simple, narrow zone problem. Agrawal and Amstead recognized that their system had technique problems common to all photographers: control of lighting, vibration, movement of the target, focal length, depth of field and magnification.

Black and James (16) were more successful using high speed motion pictures to record at up to 4000 frames per second as they analyzed the results of their Quick Stop

Device (QSD) experiments for orthogonal machining. They were instrumental in studying the disengagement process of the chip from the tool.

Briggs (7) used a high quality Kodak Ektapro Imaging System (using the EM Model 1012 Processor) and an Infinity K2 Lens with an intensified imager to conduct an experiment examining some of the classical factors ( $a$ , depth of cut,  $V$ , tool contact length, and temperature) in an experiment whose primary video objective was to produce a classroom video for metal cutting. The tapes produced of the shear zone were without doubt the best produced to date and formed the basis without further experimentation of Black and Huang's "new" deck of cards model. The existence of a definitive, easily viewed zone of plastic deformation was strongly supported by his studies of aluminum. The primary drawback with the system being used was the cost and availability. The unit was borrowed and usage was limited to a very small amount of time. Since then, simpler video cameras at a fraction of the cost have emerged on the top end of the consumer market that may be useful in a continued study of the shear zone.

Payton (36) developed an improved Videographic Quick Stop device to observe the slip plane of Copper 10102 alloy. The video system also provide the means to accurately measure the shear front angle  $\psi$ . Tape replay permitted multiple measurements coordinated with the forces and VQS photographs. The angle was measured during each run, with the average of 5 observations. Measured shear angles were compared to the calculated values of Merchants model with extremely good effect. The system greatly reduced the time required for measurements and decreased the margin of error typically associated with measuring chip thickness (uncut as well as cut). Observation also established the following observed geometry for the shear zone in Copper 10102 alloy shown in the figure below.

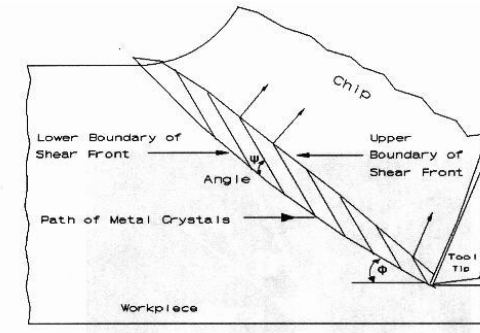


**Figure 8: Payton Copper 10102 alloy observed geometry (36)**

Scanning Electron Microscope (SEM) technology has been invaluable in establishing the role of dislocations in the cutting process. Black (12) studied single and polycrystals using the SEM and published the work (12). Von Turkovich and Black (17) used SEM in studies of chip and workpiece deformation. Ramplingham and Black (18) developed the first in-situ machining technique (machining microscopically within the SEM itself on a stage they developed) and observed the formation of shear fronts and heterogeneous plastic flow during chip formation. It also established the validity of post cut (static) examination of chip morphology to explain the mechanics of chip formation. Black and Cohen (19) would later extend in-situ techniques to measure, for the first time, shear velocity directly, along with chip velocity, shear strain and the strain rate. Scanning electron microscopy is important also because it permits the before and after analysis of dislocation generation during work hardening by the tool face.

Sutter's (20) experiment involved high-speed measurement of chip geometry and formation. Orthogonal machining was the metal cutting method employed and the material used in this experiment was low carbon steel. Cutting speed was varied between 17 and 60 m/s. These speeds were achieved due to the unorthodox setup utilized. The sample was

propelled into the cutting tool by an air gun and a high-speed camera captured the cutting process. Sutter used Merchant's equations to obtain forces and shear angles with the maximum shear angle around 45 °.

## **Hot Machining**

Hot machining is the process of heating a work-piece to a set temperature and then cutting it. Junior (21) also attempts to review hot machining techniques which have been employed. The author detailed the types of heat sources used in experiments which are as follows: a furnace, electric resistance, flame, induction, electric arc, electric current localized between the piece and the tool, plasma arc, and laser assisted machining. One of the authors that mentioned Junior's paper, Barrow, divides heating techniques into bulk heating and localized heating. Bulk heating involves heating the whole work-piece or a considerable part while localized heating only heats up the immediate area of the shear zone. The disadvantage of bulk heating is the danger to the operator as well as thermal distortions, but the advantage is that these methods are simple and cheap. This is flipped for localized heating where it is expensive and more complex, but it obtains better results.

In all of these hot machining techniques there exists the risk of adhesion, abrasion, and the built-up edge effect (BUE). If the temperature is brought too close to the recrystallization temperature of the material, the material will become too ductile and lead to BUE on the tool. Several authors have found that 400 °C was a good temperature for steel and harder metals in their experiments. Some of these experiments will be detailed later on in this literature review.

## **Laser Assisted Machining (LAM)**

Venkatesan (22) created a detailed review of laser assisted machining findings in his paper. Information from this paper explained that the two main types of lasers at that period were CO<sub>2</sub> and Nd: YAG (neodymium-doped yttrium aluminum garnet). Since then other types of lasers are Solid-state, gas, excimer, dye, and semiconductor (38). The difference was in the absorptivity in relation to the material. Nd:YAG lasers have higher absorptivity while CO<sub>2</sub> lasers have lower absorptivity. Venkatesan states that a CO<sub>2</sub> laser would be better suited for heating Inconel, hardened steel, and composites. Other parameters to consider when using LAM are work-piece surface temperature, cutting speed, feed rate, depth of cut, laser spot diameter, laser-tool lead distance, and focal length. Taking these parameters into account helps avoid surface damage and premature failure of the cutting tools.

Venkatesan (23) explains that titanium has excellent strength-to-weight ratio, strong corrosion resistance, ability to retain high strength at high temperature, a low modulus of elasticity, and low thermal conductivity which makes it extremely difficult to machine. Ferrous alloys such as low carbon ductile steels, stainless steel, and hardened steel are also difficult to machine due to high hardness and fracture toughness with conventional machining technology.

Another LAM experiment was conducted by Wang. The heating apparatus used in Wang's (23) experiment was a YAG continuous laser with 200 W average power output. The machine used in this experiment was a S28-lathe and the material was Al<sub>2</sub>O<sub>3</sub>p/Al which was cut with a carbide cutting tool. The cutting forces were measured using a Kistler piezoelectric dynamometer.

A force reduction of 50 % was observed in the axial and radial components. In addition the z-axis force ( $F_z$ ) was reduced by 10 %. Unfortunately, no temperatures were mentioned in Wang's paper. While the material was an aluminum composite, with no temperature range mentioned, these results are left to speculation.

Chang (24) evaluated the use of laser assisted machining of aluminum oxide ceramic parts. A 60 W Nd: YAG laser, FEMCO-CNC lathe, and CBN tools were used. The conditions measured in this experiment were depth of cut (mm), rotational speed (rpm), feed (mm/rev), and frequency (kHz). Transient temperature measurements were taken with a minimum temperature of 25.4 °C. At one point the temperature exceeded 850 °C (the glass transition temperature) which the author explained to be the optimum point to cut the material. The reason for this is that the aluminum oxide ceramics become more viscous, expand volumetrically, and transform into elastomers which also causes the grains or groups of grains to detach from the surface.

The Taguchi method was used to analyze the results. An ANOVA table was constructed and depth of cut, rotational speed, and feed were most important with pulsed frequency in fourth. These values are shown in Table.1 below. The frequency is used for the temperature measurement for this experiment. Similar to other experiments reviewed in this paper, it was neglected. The author found that the optimum operating conditions were as follows: 1500 rpm rotational speed, 0.013 mm/rev feed rate, 0.2 mm depth of cut, and 40 kHz laser frequency.

**Table 1: Chang's ANOVA Table (24)**

Analysis of variation

Factor	Sum of square	D.O.F.	Sum of mean square	Contribution
A	41.39	2	20.69	0.207319
B	85.21	2	42.60	0.426808
C	45.08	2	22.54	0.22582
D	27.97	2	13.98	0.140112
Total	199.65	8	99.82	

**Factor A = Depth of Cut**

**Factor B = Rotational Speed**

**Factor C = Feed Rate**

**Factor D = Work-piece Temperature**

Ding (25) investigated the use of laser assisted machining as an alternative to grinding hardened steel. A 20 Hp Jones and Lambson CNC lathe, a CO<sub>2</sub> laser, and a 1 kW Nd: YAG laser were used as the equipment in this experiment. A PCBN insert (grade BNC 200, made by Sumitomo) was used as the tool for OD turning operations. Its dimensions were as follows: 1.19 mm tool nose radius, -5 ° side rake angle, and 0 ° back rake angle. The work-piece was a hollow shaft of heat-treated AISI 4130 steel with 50 Rockwell hardness (C-scale). The work-piece was sandblasted and painted with Cotronics 931 graphite adhesive powder/binder in order to increase absorption of the laser energy. The author states that this step can be avoided with the use of a more powerful laser. A Kistler 9121 dynamometer and a FLIR SC300 infrared camera were used for force and temperature measurements respectively.

The temperature effect on the cutting force or the specific cutting energy is significant and consistent for all the conditions. Compared to conventional machining, the specific cutting energy during LAM drops by about 20 % as the  $T_{mr}$  increased to above

200 °C. No microstructure change of the material was observed in this experiment compared to conventional machining. This experiment showed four-times faster material removal rate with LAM operation versus the two-step hard turning and grinding operations.

Kim (26) used LAM to mill Inconel 718 and AISI 1045 steel. Kim chose his temperatures for the AISI steel in the range of 550 °C and 726 °C, the annealing and transformation temperatures. A similar process was taken with the Inconel and the temperature range was 659 °C to 950 °C.

The experiment was conducted on a tilting table on a CNC milling machine (Hyundai WIA Inc., Type Hi-V560M). The laser used was a Laserline Inc. Type LDM 1000-100 diode-laser. The laser had a wavelength of 940-980 nm and was held at an angle relative to the angle of the work-piece. Whenever the work-piece angle was adjusted so was the angle of the laser in order to maintain the same angular relation. A Kistler Type 9257B dynamometer was used to measure the forces. A two flute carbide ball end mill was the tool for the experiment.

Kim (26) utilized five parameters in this experiment which are as follows: feed rate, depth of cut, tool diameter, rotational speed, and laser power. Each parameter had two values as shown in the table below.

**Table 2: Parameters in Kim's experiment (26)**

Parameters	Levels
Rotational speed (rpm)	3000, 9000
Feed rate (mm/min)	150, 300
Depth of cut (mm)	0.2, 0.4
Tool diameter (mm)	6, 8
Laser power (W)	80, 100

The tables of values for the measured and predicted Cutting forces and Preheating temperatures are shown below.

**Table 3: Kim AISI 1045 Steel Results (26)**

Verification experiments using coded units for AISI 1045 steel.							
Exp. no.	Rotational speed (rpm)	Feed rate (mm/min)	Depth of cut (mm)	Cutting force (N)		Preheating temperature (°C)	
				Measurement	Prediction	Measurement	Prediction
1	-1	1	0	32	32.94	855	852.50
2	1	0	1	33	32.05	805	800.62
3	0	0	0	30	30.93	860	861.67
4	0	-1	-1	26	27.55	980	981.88
5	1	0	-1	23	23.55	960	958.12

**Table 4: Kim Inconel 718 Results (26)**

Verification experiments using coded units for Inconel 718.							
Exp. no.	Rotational speed (rpm)	Feed rate (mm/min)	Depth of cut (mm)	Cutting force (N)		Preheating temperature (°C)	
				Measurement	Prediction	Measurement	Prediction
1	-1	0	1	80	78.27	1200	1198
2	-1	-1	0	62	62.11	1390	1376
3	0	0	0	62	61.69	1280	1290
4	1	0	-1	49	50.77	1210	1211
5	0	1	1	75	75.11	1110	1116

Statistical analysis was done in Minitab and the experimental runs were compared against predicted values. The error between the theoretical and experimental values for the AISI steel and the Inconel were 6 and 4 % respectively. Likewise, preheating calculations had an error of 0.5 and 1 % respectively.

### Flame/ Plasma Arc (PEM)

The material that Ozler (27) used in the experiment was Austenite manganese steel. The experiment was conducted on a lathe and the main focus was a study on tool life after cutting heated materials. Austenite manganese steel was chosen due to its wear resistance and reduced machinability. Heating was done using a gas flame torch which was mounted onto the carriage of the lathe.

The steel was heat treated in an induction furnace at 1100 °C and the mean hardness of the steel was 243 HB. Cutting speeds were 22, 33, 46, 62, and 75 m/min. The temperatures used in the cutting operation were 200 °C, 400 °C, and 600 °C.

In Ozler's experiment, hot machining yielded similar wear patterns to room temperature machining regardless of the cutting speed. Increases in tool life were noticed when the heating temperatures were increased. In this study, the longest tool lives were noticed at 600°C machining. However the fastest increases in the tool lives were obtained at machining carried out at 200°C. Because at high heating temperatures the difference between the heating temperature and the temperature of tool chip interface is reduced, the tool lives obtained at 600°C machining were approximately similar to those obtained at 400°C machining. As austenitic manganese steel has a recrystallization temperature range of 500–650°C, the high heating temperatures might induce unwanted structural changes. Thus, in machining performed at temperatures higher than 600°C, the possibility of unwanted structural changes and an increased wearing of tool exist. Consequently, in hot machining of manganese steel, the selection of 400°C as the heating temperature might be appropriate in view of the cost and workpiece considerations. These results are graphically shown in the three figures below.

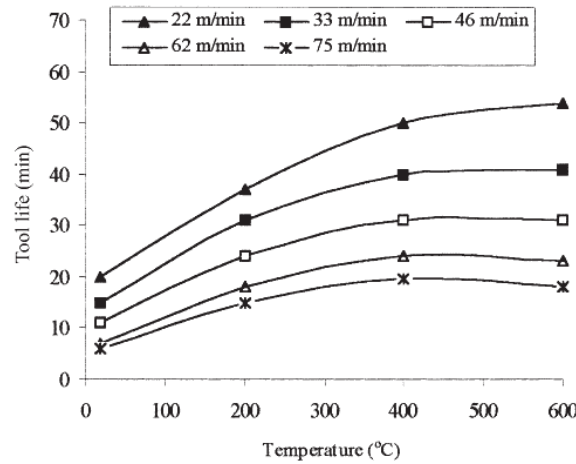


**Figure 9: Feed rate variation results (27)**

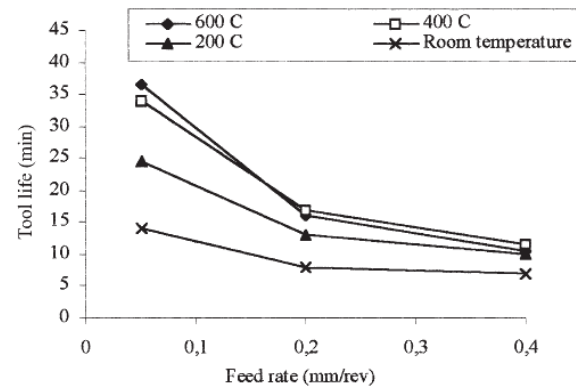


**Figure 10: Temperature and feed rate variation results (27)**

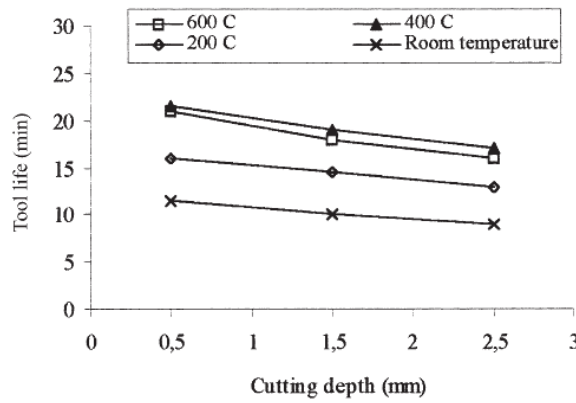


**Figure 11: Temperature and cutting depth variation results (27)**

Feed rate is another factor influencing the tool life. The tool life was decreased as the feed rate was increased. The effect of feed rate was smaller than that of cutting speed and heating temperature. In experiments at 600 °C hot machining and conventional machining, 14 min tool lives were obtained from 0.4 and 0.1 mm/rev feed rates, respectively. These results showed that in hot machining higher feed rates would be used without producing significant reductions in tool life. The depth of cut seemed to have the least influence on the tool life. An increase in the depth of cut reduced the tool life, however, this reduction seemed inconsequential.

A researcher named Tosun (28) attempted to optimize hot turning operations with multiple parameters. The experiment was performed on a lathe with different feed rates, depths of cut, cutting speeds, and work-piece temperatures. A liquid petroleum gas torch was used to heat the work-piece. An M20 sintered carbide tool was used to cut the material (high manganese steel).

Similar to other experiments, cutting speed and feed rate were more significant than work-piece temperature, but work-piece temperature was still an important factor. Similarly, Tosun constructed ANOVA tables to quantify the importance of the results. The tables for each case are shown below.

**Table 5: Case 1 ANOVA (28)**

Cutting parameter	Degree of freedom ( <i>df</i> )	Sum of square ( $SS_A$ )	Variance ( $V_A$ )	<i>F</i>	Contribution %
Cutting speed	2	80.96	40.48	121.01	26.66
Depth of cut	2	17.33	8.66	25.90	5.71
Feed rate	2	173.17	86.58	258.83	57.03
Workpiece temperature	2	29.16	14.57	43.58	9.60
Error	9	3.01	0.33		1
Total	17	303.63			100

**Table 6: Case 2 ANOVA (28)**

Cutting parameter	<i>df</i>	$SS_A$	$V_A$	<i>F</i>	Contribution (%)
Cutting speed	2	62.04	31.02	121.02	21.38
Depth of cut	2	15.94	7.97	31.10	5.49
Feed rate	2	184.28	92.14	359.49	63.49
Workpiece temperature	2	25.67	12.83	50.08	8.85
Error	9	2.31	0.25		0.79
Total	17	290.24			100

**Table 7: Case 3 ANOVA (28)**

Cutting parameter	<i>df</i>	$SS_A$	$V_A$	<i>F</i>	Contribution (%)
Cutting speed	2	47.19	23.59	128.40	16.78
Depth of cut	2	14.40	7.20	39.18	5.12
Feed rate	2	195.07	97.53	530.79	69.38
Workpiece temperature	2	22.85	11.42	62.16	8.13
Error	9	1.65	0.18		0.59
Total	17	281.16			100

Stainless steel (type 316) was the material used in researcher Ranganathan's (29) experiment. The steel was heated using a liquid petroleum gas flame burned with oxygen.

The purpose of this paper was optimization of machining parameters based on the Taguchi technique. Stainless steel was chosen based on its excellent wear resistance and corrosive resistance. The experiment was conducted on an all-gearied lathe.

The parameters varied in this experiment were cutting speed, feed, depth of cut, and temperature. The temperatures used in this experiment were 200 °C, 400 °C, and 600 °C. Results evaluated were surface roughness, tool life, and metal removal rate. An ANOVA table was constructed to evaluate the significance of these parameters. Feed rate was the most significant with cutting speed in second and temperature in third. The optimal hot turning process parameter revealed through the Taguchi orthogonal array from the experiments were A<sub>3</sub>, B<sub>3</sub>, C<sub>2</sub>, and D<sub>2</sub> (113.1 m/min, 0.381 mm/rev, 0.8 mm, and 400 °C).

**Table 8: Ranganathan's ANOVA table results (29)**

Source	df	Mean square	Sum of square	F value	% contribution
A	2	0.029	0.059	12.79	22.7
B	2	0.06	0.12	25.87	46.2
C	2	0.011	0.022	4.88	8.5
D	2	0.019	0.038	8.19	14.6
Error	9	0.0023	0.021		8

**Factor A = Cutting Speed**

**Factor B = Feed Rate**

**Factor C = Depth of Cut**

**Factor D = Temperature**

Based on the Taguchi method and ANOVA, feed rate has a dominant effect of almost 46.2 % in contribution ratio, while cutting speed has 22.7 % and work-piece temperature has 14.6 % influence on the surface roughness, tool life, and metal removal rate in hot turning of stainless steel (type 316). The cutting speed, feed rate, and work-piece

temperature are primary factors that affect the quality of hot turning of stainless steel (type 316), while the depth of cut is considered a secondary factor.

Muhammad (30) combined ultrasonic machining with hot machining to turn down Ti alloy. A torch was not used as the heating method for this experiment to prevent carbon deposits from forming a layer on the Ti sample. Instead a band-resistance heater encapsulated the work-piece and heated it to  $300\text{ }^{\circ}\text{C}$   $\pm 10\text{ }^{\circ}\text{C}$ . A universal lathe machine was used for the turning operation. Cemented carbide inserts were used as the cutting tools. Three different cutting methods used in this experiment were conventional turning (CT), hot conventional turning (HCT), and hot ultrasonically assisted turning (HUAT).

Cutting forces were measured in real time and substantial reduction in the tangential and radial force components were observed. When the work-piece was heated to  $300\text{ }^{\circ}\text{C}$ , force was reduced by 78 % and when heated to  $500\text{ }^{\circ}\text{C}$ , force was reduced by 80 %. These cutting force reductions were seen at a  $500\text{ }\mu\text{m}$  depth of cut.

The machine used for Maity's (31) experiment was a lathe and the heating apparatus was a petroleum gas and oxygen torch. The purpose of this experiment was to determine tool life. A carbide tool was used in this experiment with the following dimensions:  $4.625\text{ }^{\circ}$  side rake angle,  $0.925\text{ }^{\circ}$  back rake angle,  $9.7\text{ }^{\circ}$  orthogonal clearance angle, and  $5.2\text{ }^{\circ}$  orthogonal rake angle. Forces were measured using a Syscon strain gauge type turning dynamometer.

The material used in this experiment was high manganese steel. It was observed that when the piece was heated to  $350\text{ }^{\circ}\text{C}$ , the thrust force increased as feed increased. Regardless, in the author's analysis work-piece temperature, cutting speed, depth of cut,

and feed were all important factors. Work-piece temperature was observed as the most important factor on tool life.

A researcher named Leshock (32) used plasma enhanced machining (PEM) to machine Inconel 718. The heating was systematically characterized through numerical modeling and experimental investigation using infrared radiation thermometry. The setup consisted of a 7 Hp lathe, a plasma heating system with a torch, and a control unit. A three axis Kistler dynamometer was also used to measure forces and a fiber optic radiation thermometer capable of measuring temperatures between 450 °C and 1000 °C was used.

The tool used was a WG-300 insert (aluminum oxide reinforced with silicon carbide whiskers). Forces dropped between 250 °C and 400 °C, and then again between 600 °C and 700 °C. There was also a reduction in shear energy with PEM over other methods. PEM yielded a 30 % reduction in the resultant cutting force, two-fold improvement in surface roughness, and about 40 % increase in tool life compared to conventional machining. Comparative figures of the different techniques are shown below.

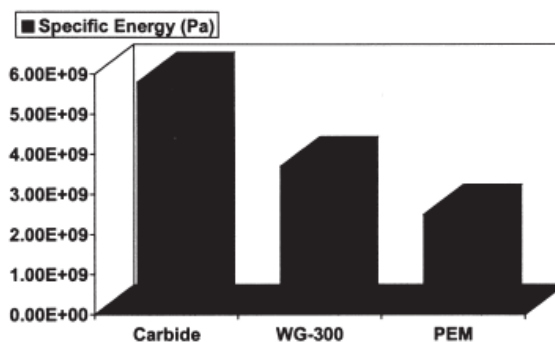
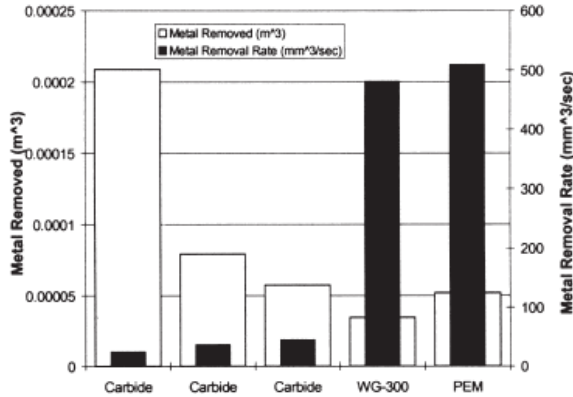


Figure 12: Specific energy comparison (32)



**Figure 13: Material removal comparison (32)**

The material used Ganta's (33) experiment was precipitation hardenable martensitic stainless steel or 15-5PH which has a hardness of 40 HRC. The experiment was conducted on a lathe with different speeds, feeds, depth of cut, and work-piece temperature. The heated apparatus was an oxyacetylene torch. The temperature was measured using a K-type thermocouple. The temperature ranged from 200 °C to 400 °C to 600 °C.

An ANOVA table was used to quantify the results and work-piece temperature ended up being negligible in terms of Grey Relational Analysis. In the grey relation analysis, grey relation coefficient is calculated for different process characteristics and an average of these grey relation coefficients give the grey relation grade. Statistical ANOVA analysis is performed to find out the significant process parameters, with the grey relation analysis and the statistical analysis of variance, the optimum combination of process parameters can be predicted. It instead showed that cutting speed was the most significant.

**Table 9: Ganta's ANOVA table (33)**

Source	dof	Sum of squares	Mean square	F value	% contribution
A	2	37.4067	18.7033	38.56	46.42
B	2	24.3653	12.1826	25.11	30.23
C	2	9.8262	4.9131	10.13	12.19
D	2	0.2478	0.1239	0.26	0.3075
Error	18	8.7316	0.4851		
Total	26	80.5775			

**Factor A = Cutting Speed**

**Factor B = Feed Rate**

**Factor C = Depth of Cut**

**Facotr D = Work-piece Temperature**

The F-values showed that cutting speed was most significant while work-piece temperature was least significant just as the Grey Relational Analysis showed.

### **Induction**

Lajis (34) machined AISI D2 hardened steel on a Vertical Machining Center. Cutting speed, feed, and temperature were varied in this experiment. Temperatures used in this experiment were 250 °C, 335 °C, and 450 °C. The work-piece was heated using a 25 kVA induction heating device. The surface temp was measured using an infrared pyrometer (Omega, OS-651 with a range of -29 °C to 1093 °C and accuracy of 1 %).

The hardness of the steel was 56-62 HRC. Heating of the material resulted in longer tool life at a temperature of 450 °C. Surface roughness was also measured in this experiment. The results of Lajis' tool wear results are shown below.

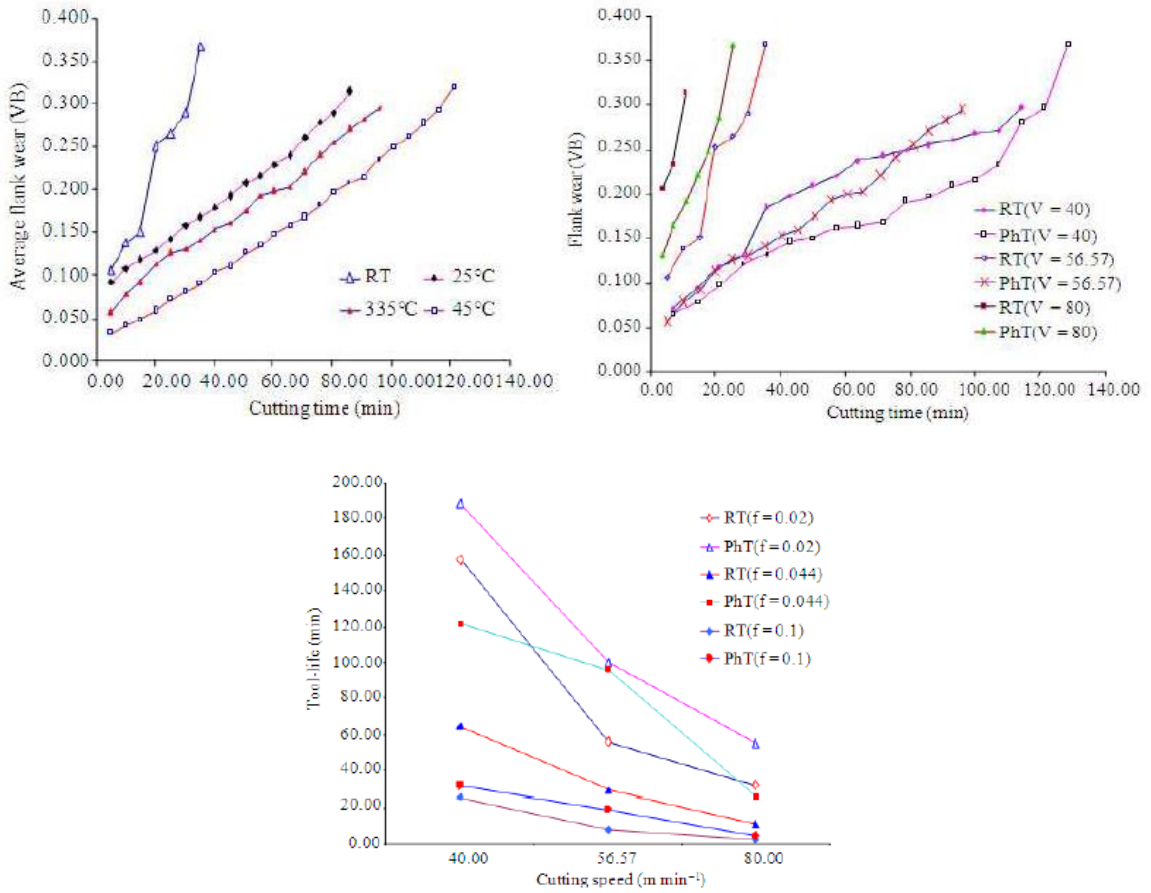


**Figure 14: Lajis' analysis results (34)**

Titanium (Ti-6Al-4V) was the material for Hossain's (35) experiment. The experiment was also conducted on a Vertical Machining Centre with an endmill as the cutting tool. High frequency induction heating was the heating method and a temperature of 420 °C was maintained.

This experiment showed that although tool life increased with temperature, lower cutting speeds undermined this result. The resultant cutting force was reduced by around 10 % to 12 %. Vibration of the machine was also observed in this experiment and found to be reduced under preheated conditions.

The experiments detailed in this literature review all applied hot machining techniques to difficult to cut materials. Several resorted to lasers to heat up the material, while others used induction heating. The purpose of several of the papers was to determine quantitatively tool life in addition to observe force reduction, surface roughness, and even microstructural changes.

### **The Normal Force and Tool Wear**

In all manufacturing operations, with the exception of those based on chemical action, heat or electrical forces, the material being shaped is caused to deform by means of mechanical contact with a “tool” of some sort. Therefore the interfacial conditions of friction and wear become an important economic consideration in the manufacturing process analysis. In manufacturing, the cost of any process is largely dictated by the speed at which it can be carried out, and that speed is limited by rate of wear of the tooling involved. One type of mass-production tool may be completely worn out in 5-10 minutes of high speed machining and another type may last for several months in, for example, a punch die press. Most modern manufacturing tools are loaded so high as to produce plastic deformation in the workpiece indicative of high interfacial contact stresses. The interfacial temperatures often approach or exceed 1500-2000 °F (815.6-1093 °C).

When one enlarges a microscopic region of the tool face, it becomes apparent that the adjacent surfaces are very rough (**Error! Reference source not found.**

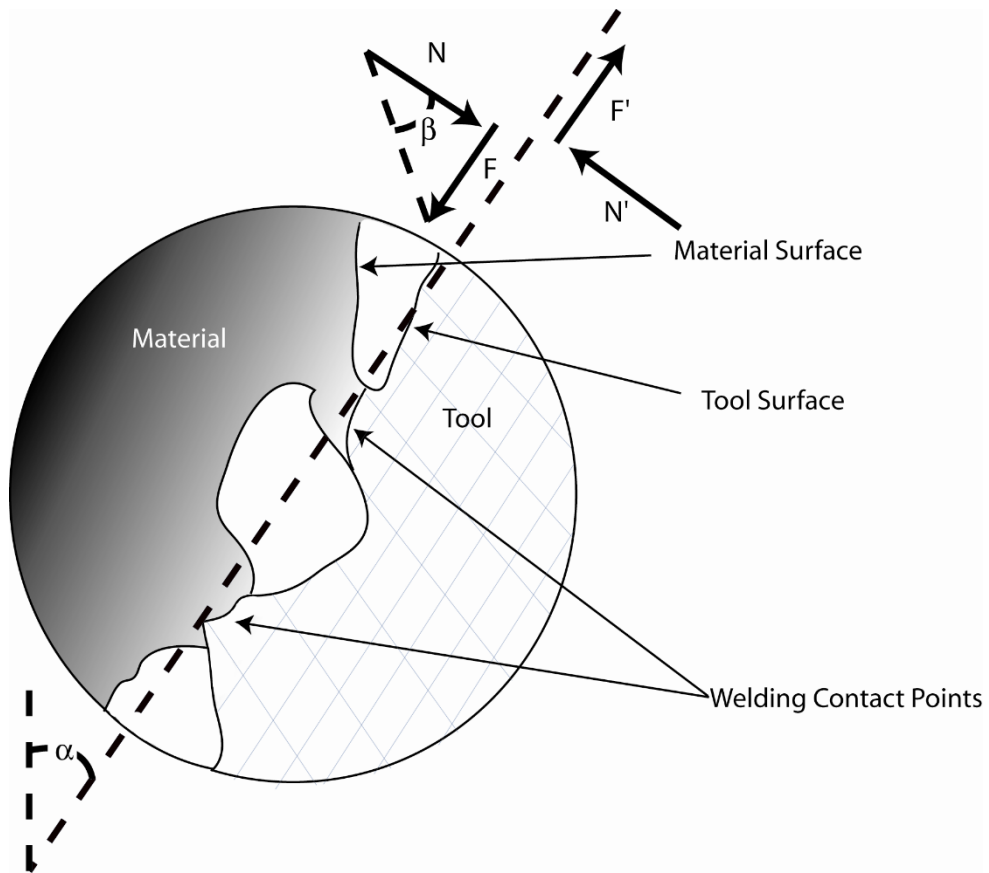


**Figure 15:** Enlarged view of the contact conditions between tool-chip interface.

Therefore, the apparently “in contact” faces of the chip and tool are actually in contact over a smaller, more discrete area, the sum of which is the actual area of real contact. Under very light loads, the area of contact may be very small. Increasing the normal force ( $N$ ) in this diagram increases the contact area and generally increases the wear rate. Tool life is therefore shortened whenever  $N$  increases. Although the ratio of the sliding force to normal force is generally of the form normally associated with the coefficient of sliding friction:

$$\mu = \frac{F}{N} \quad (12)$$

and it's associated friction angle:

$$\beta = \tan^{-1} \mu = \tan^{-1} \left[ \frac{F}{N} \right] \quad (13)$$

it will be shown that the ratio is more important to the life of the tool than the concept of a friction angle. The friction coefficient  $\mu$  in metal cutting practice is not limited to a unitary value of 1. It frequently exceeds one when the shearing force exceeds the normal force because of various wear mechanisms (Childs (42)). The text by Childs provides an excellent discussion on metal cutting systems and a coefficient of friction that is greater than one. Indeed, the concept of  $\beta$  as “the friction angle” in metal cutting has frequently been the focus of many papers (Williams, Smart and Milner (43); Finnie and Shaw (44)), as will be discussed in detail later. This is contrary to the common perception that using a lubricant “reduces the coefficient of friction”.

Wear mechanisms along the tool chip interface face three special conditions not normally encountered in the ideal physics definition for friction represented by equations (12) and (13) (Shaw (45)):

- The surface against which the tool is rubbing is newly cut from the work material and there is little time for oxide or other films to form.
- The surface on which the tool is rubbing has severely work-hardened in the plastic processes involved in forming the chip.
- The temperatures and pressures at the sliding interface are exceptionally high.

The kinetics involved on metal cuttings shear plane ( $\phi$ ) cannot be underestimated. Metal cutting, particularly at high speeds, approaches the strain rates that are normally seen in high energy military armor penetrators. In another departure from common tribological considerations, Shaw (45) points out that in most wear studies, the material of interest is the wear of the softer material being rubbed by the harder. In metal cutting, where the softer material is being shaped by the much harder tool, the inverse is true. The economic question of how long the harder tool lives is of primary importance, not the material being formed.

The mechanisms commonly used to describe the wear of the tool are:

- Material Fracture
- Adhesive (Attrition Wear)
- Abrasive Wear
- Diffusion Wear
- High Temperature Shearing
- Fatigue Wear
- Oxidation Effect
- Electrochemical Effect
- Chemical Decomposition

The more readily visualized and documented wear mechanisms are in column 1. Material fracture of the tool occurs due to a defect in its manufacture or design. Adhesive or attrition wear occurs when particles from the softer material adhere to a few high spots on the tool. This continues as the flow of softer material piles up around the “stuck” particles. Eventually, these built up areas are torn away by the passage of the metal being cut, leaving the tool with a “nibbled” appearance. When the softer material contains small trace or deliberately included hard particles, the now relatively softer tool material may be “scoured” by this abrasive wear as frequently happens in the machining of aluminum castings retaining pockets of sand. The tool itself may compound this problem under the

extreme temperature that exists at the tool-chip interface through diffusion. Diffusion wear occurs when atoms from the harder tool material migrate into the chip, becoming the source of “abrasive grit” for its own wear. These same high temperatures which promote diffusion wear also lower the shear stress of the harder tool. Although both the tool and the work material see the same temperatures, the tool is weakened by that temperature and the severely deforming work material becomes work hardened in addition. The relative hardness between the tool and chip decreases, promoting wear of the tool through all of the preceding mechanisms.

The other mechanisms of wear are well known, but are intrinsically harder to study and visualize. Fatigue wear occurs when the surface asperities of one material mechanically locks into those of another. Because of the relative motion of the two materials, one side of the asperity sees a compressive stress and the other a tensile stress. Eventually the stresses are relieved when their inter-lock fails, but only after one cycle of stress. This repeats itself continuously and surface cracks form, which eventually combine with each other and leads to a crumbling substrate of material. The electrochemical effect pre-supposes that a thermoelectric EMF is set up in the closed circuit represented by the hot junction of the tool-chip interface and the surrounding environment (Childs (42)). The presence of the electric current may promote diffusion of atoms from the tool to the workpiece, facilitating the diffusion wear process. Similarly, the so called oxidation effect may aide the formation of abrasive oxides when machining is done in an atmosphere rich in oxygen. Finally, the material being machined and the tool may react chemically through the formation of compounds at the interface which weaken the tool or its protective coatings.

Many of the wear mechanisms coexist at the same time in varying proportions which may be modeled in terms of the cutting speed and/or the temperature at the interface of the tool-chip. Childs (42) provides an excellent summary diagram of the predominate effects as a function of removal rate (dependent on velocity) and cutting temperature (Figure.16).

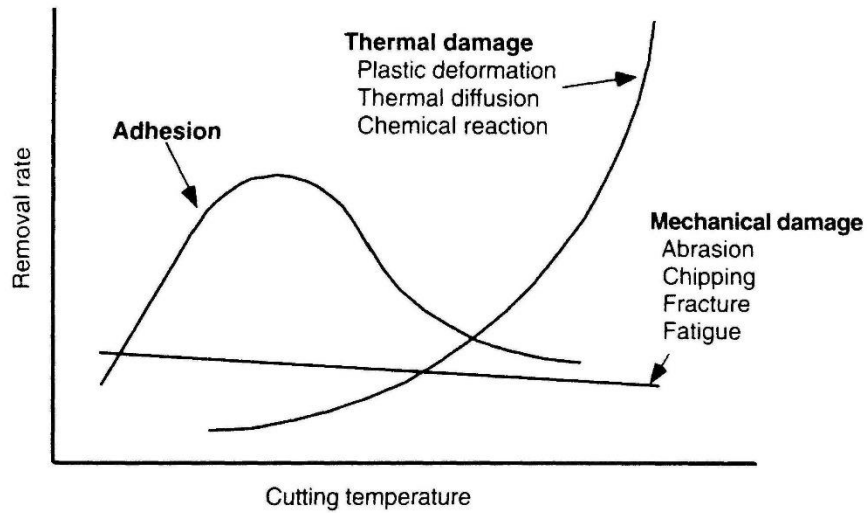


**Figure 16: Tool damage mechanisms and cutting temperatures (Childs 2000)**

There are many books and articles which discuss the details of tribology at great length (e.g. (Buckley (46); Dawson (47); Kopalinsky, Li and Oxley (48); Suh (49); Schey (50)). There are a great many mathematical formulations for the wear  $W$  and the associated wear rate. All of these formulations are generally of the following form:

$$\frac{dW}{dt} \propto N \quad (14)$$

In general, the wear rate is proportional to the normal force  $N$  acting between the two surfaces. Controlling  $N$  controls the wear rate, independently of the concept of a coefficient of friction. This presumes that there is a metal cutting model which can accurately predict the values of  $N$  which are to be expected and controlled. One of the earliest and most successful models for doing that is Merchant's orthogonal machining force diagram. Another is Payton's Modified Merchant Force Diagram.

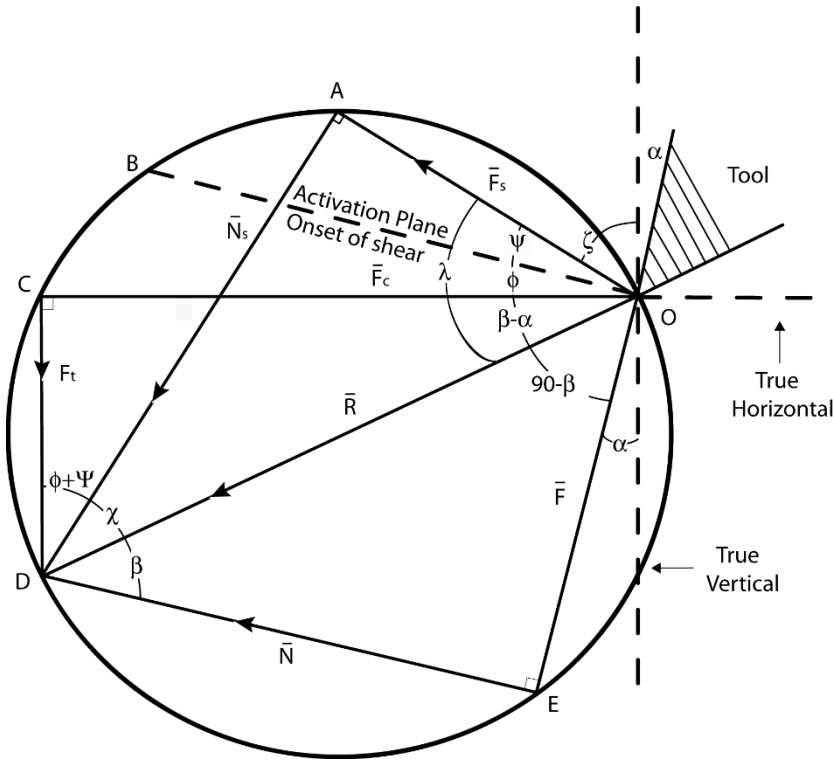


**Figure 17: Merchant Force Diagram as modified by Payton (51)**

Archard (1953) modeled the wear of a material (represented as volume of material removed  $W$ ) in terms of the following variables:

$$W = k' \frac{N}{3\sigma_y} l \quad (15)$$

where  $k'$  was a constant dependent upon the temperature and material combinations,  $N$  was the normal force acting between the two surfaces,  $\sigma_y$  is the yield stress of the lower strength material and  $l$  is the sliding distance along the tool face. Taking the time derivative of this expression, the wear rate in terms of the velocity along the chip tool interface ( $V_c$ ) becomes

$$\dot{W} = k' \frac{N}{3\sigma_y} V_c \quad (16)$$

or consistent with equation (17),

$$\dot{W} \propto \frac{N}{3\sigma_y} V_c \quad (17)$$

Now, from metal cutting literature (Payton 2002), the chip velocity may be expressed in terms of the input velocity of the work stock and chip ratio (uncut chip thickness  $t$  divided by the formed chip thickness  $t_c$ ):

$$\frac{V_c}{V} = \frac{t}{t_c} \quad (18)$$

to give:

$$\dot{W} \propto \frac{N}{3\sigma_y} V \frac{t}{t_c} \quad (19)$$

However, using Payton's Force Diagram,

$$N = \frac{F}{\tan \beta} = \frac{F_c \sin \alpha + F_t \cos \alpha}{\tan \left[ \frac{\pi}{4} + \frac{\alpha}{2} - \tan^{-1} \left[ \frac{F_s}{F_n} \right] \right]} \quad (20)$$

Therefore:

$$\dot{W} \propto \frac{\frac{F_c \sin \alpha + F_t \cos \alpha}{\tan \left[ \frac{\pi}{4} + \frac{\alpha}{2} - \tan^{-1} \left[ \frac{F_s}{F_n} \right] \right]}}{3\sigma_y} V \frac{t}{t_c} \quad (21)$$

or simplifying:

$$\dot{W} \propto \frac{F_c \sin \alpha + F_t \cos \alpha}{\tan \left[ \frac{\pi}{4} + \frac{\alpha}{2} - \tan^{-1} \left[ \frac{F_s}{F_n} \right] \right]} V \frac{t}{t_c} \quad (22)$$

## **IV. Experimental Equipment and Techniques**

Many different materials, instruments, machines, electrical hardware, and software were used during this experiment. The following lists and figures describe in great detail what was used to obtain the results presented in this thesis. All figures will include a detailed description of the particular piece of equipment and how it was used.

The equipment and instruments listed below were used together to create the virtual quick stop device in its entirety. The equipment listed includes everything from the base machine, upgrades to the machines, fixturing of the workpiece specimens, cutting tools, recording equipment for forces and feeds, lighting, video recording hardware, and software used data acquisition.

CINCINNATI No. 2 HM Horizontal Milling Machine

BALDOR 1/8 Horsepower Three Phase Induction Electric Motor

WOOD'S E-Trac AC Inverter

Re-Designed Thermal Quick-Stop Workpiece Holder

HSS Stick Tools, 0.75 x 0.75 inches (19 x 19 mm) at Various Rake Angles

YUMO Rotary Encoder

KISTLER Dual Mode Amplifier

KISTLER Dynamometer

NATIONAL INSTRUMENTS USB-6008

DOLAN JENNER Fiber-Lite A-200

STOCKER AND YALE Imagelite Lite Mite Model 20

Fiber Optic Ring Light

Modified Load Lift Camera Stand

Cross Slide Vice

DRS TECHNOLOGIES Lightning RDT Camera

INFINITY InfiniVar Lens

NATIONAL INSTRUMENTS LabVIEW

XCITEX Midas 2.0 Video Capture Software

The following equipment was used to prepare the various aluminum and steel specimens to the appropriate dimensions and properties before undergoing the orthogonal machining process. This list also includes any machinery used to create any custom fixtures or tooling required as well as the material testing equipment used to obtain the material properties of the final specimens. Software used for design and post processing of data also listed.

CINCINNATI Arrow VMC-750 CNC Mill

BRIDGEPORT Vertical Milling Machine

SOUTHBEND Lathe

WILTON Belt Sander

ROCKWELL Hardness Tester

BRINELL Hardness Tester

DASSAULT SYSTEMS Solidworks Modeling Software

MATHWORKS MATLAB

STATGRAPHICS Statistical Analysis Software

MICROSOFT Excel 2010

## GIMP Image Manipulation Software

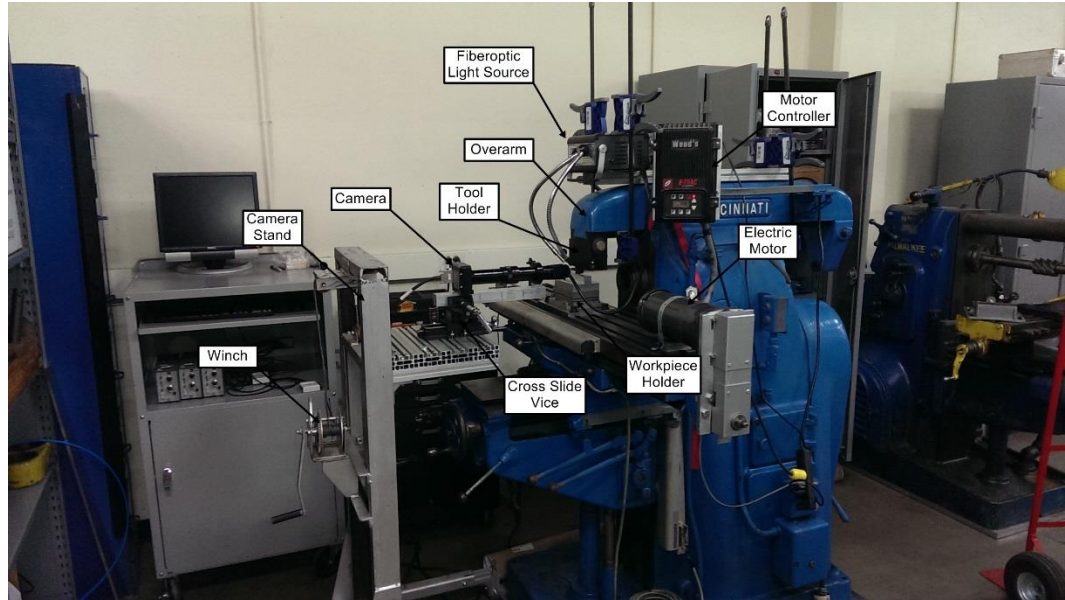


**Figure 18: Elevated View of Equipment Setup**

An elevated view of the testing area is shown in Figure 18 above. The major components are noted. A computer cart containing the data acquisition PC is seen in the left hand corner. The cart also holds the NI USB modules as well as the amplifiers for the dynamometer.

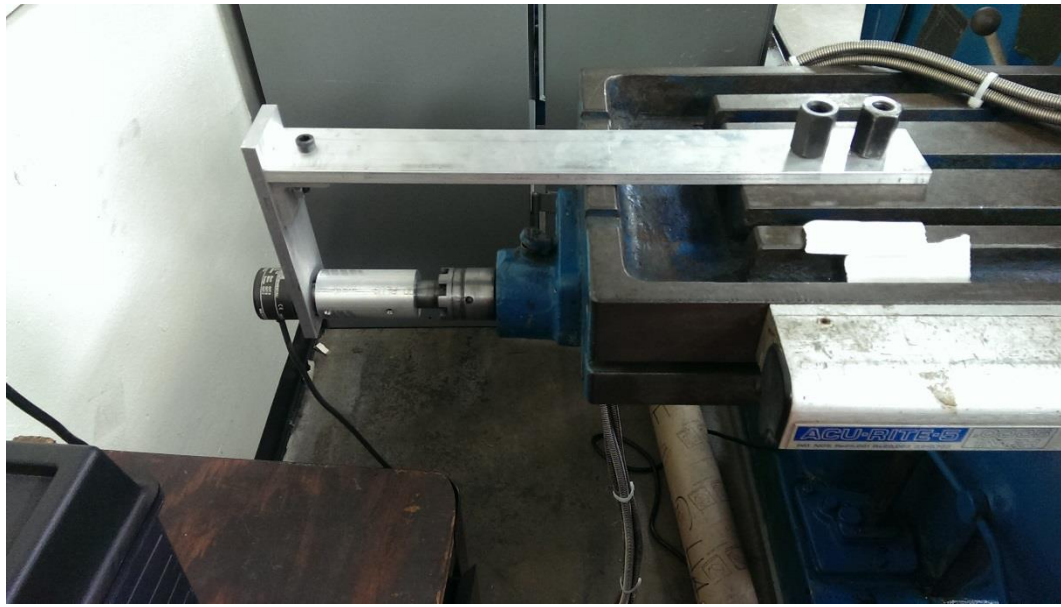


**Figure 19: Rotary Encoder**

In the Figure.19 on the previous page, the rotary encoder can be seen attached to the lead screw of the horizontal milling machine. A coupler was machined on the lathe that would couple the lead screw to the rotary encoder shaft. The supporting bars going from the table to the encoder are there to make sure that the encoder does not rotate with the shaft. The supports were attached to the horizontal milling table with T-nuts and bolts.



**Figure 20: Kistler Dual Mode Amplifiers**

The Kistler dual mode amplifiers can be seen in Figure.20 above. Each axis of the dynamometer has its own amplifier. All of the functions for the amplifiers are located on the front as shown for easy operation.



**Figure 21: National Instruments USB-6008**

The National Instruments USB-6008 can be seen on the above. Two of these data acquisition device was used for many different purposes. The rotary encoder connected to one and the other one took in the amplifier signals for data logging. The device that took in the data from the amplifiers also output a signal to the high speed camera letting it know when to start recording. This allowed software triggers to be defined for to aid in the capture of images for processing.



**Figure 22: Modified Load Lift Camera Stand**

The camera stand can be seen in full in Figure.22. Figure.23 shows a close up view of the camera and how it is attached to the custom made camera stand. Notice how the stand has a modular table that allows many different attachments. The cross slide vise is mounted to the camera stand table with bolts and nuts that slide into the T-slot grooves in the table. The camera is attached to a rectangular piece of aluminum which is clamped in the cross slide vice. The piece of aluminum extends out to support the weight of the camera lens as well. The cross slide vice made adjusting the camera position on a very fine scale a much easier task.



**Figure 23: DRS Technologies Lightning RDT Camera**

The DRS high speed camera can be seen above with some of the hardware specifications marked.

### **Design and Construction of the Thermal Videographic Quick Stop Holder**

Construction of the work holder (Figure.24 on next page) required that a rigid, deflection free thermally isolated holder be developed whose thermal properties were very well understood and documented. Several versions were constructed while addressing these problems as detailed herein.

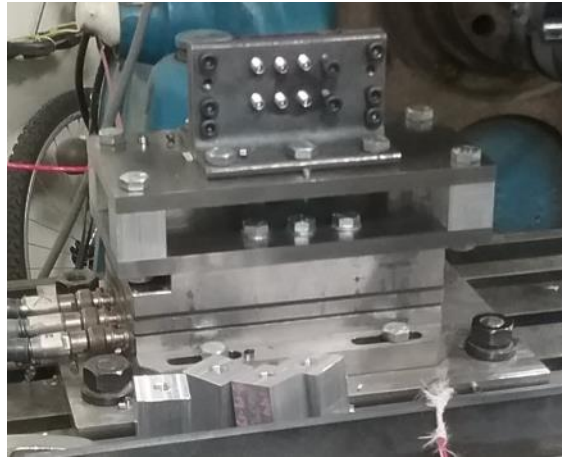


**Figure 24: Final Fixture**

The Kistler load cell had to be protected from the heat while also insulating the workpiece to minimize heat loss. One early solution was to place a ceramic layer between the jig and the load cell. However, when the jig was bolted to the load cell through the ceramic, the heat would conduct through the bolts. If the jig was bolted to the ceramic and then the ceramic to the load cell, the ceramic would shear. In the final setup, an open-air box design was chosen. The original intent then was to place a ceramic layer in the open section of the box. The ceramic proved to be far too brittle to withstand the machining forces. Fortunately, by increasing the height of the air gap, the low heat transfer coefficient of air itself proved to be completely sufficient when temperatures were measured.

Two modified 1018 steel  $90^{\circ}$  angle bars were mounted on the top of the thermal isolation box which actually held the sample in place. On one  $90^{\circ}$  bar was an array of fasteners meant to secure the sample against the other  $90^{\circ}$  bar. The other  $90^{\circ}$  bar had a pocket milled on the inside for the sample to sit in while the outside was kept flat for the strip heater to be mounted. The initial box had 0.250 inch (6.35 mm) thick top and bottom

plates with 1.500 inch tall x 1.500 inch (38.1 x 38.1 mm) square pillars composed of 6061-T6 aluminum. The Solidworks CAD deflection analysis model is shown in the figure below. The simulation indicated that this design would resist deflection at loads expected. This proved to not be the case during testing.

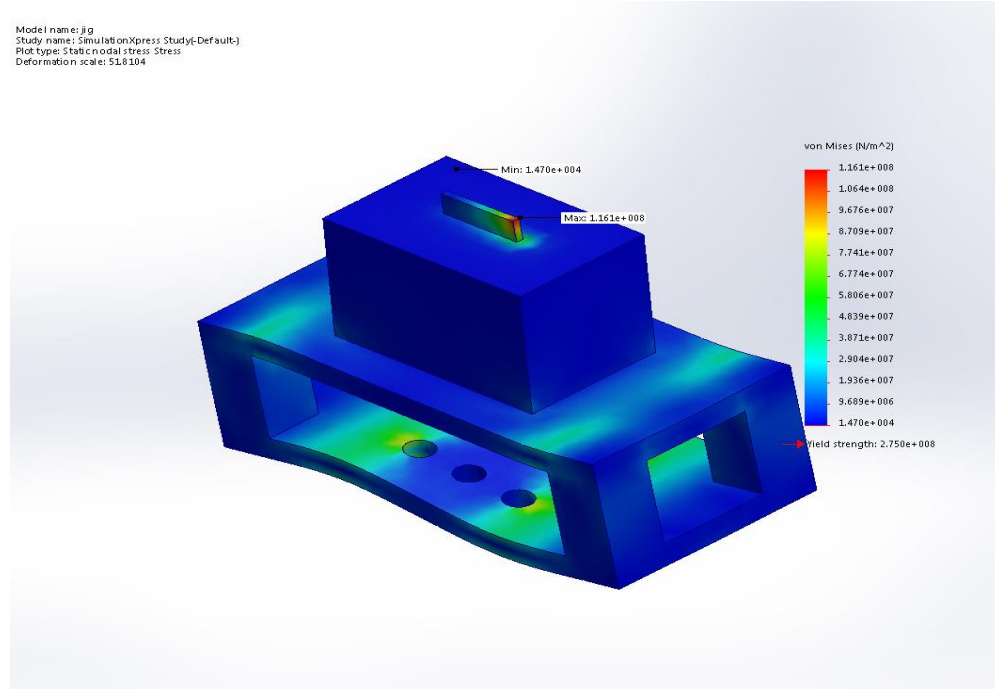


**Figure 25: Deformed Model of Fixture**

Unheated runs were conducted with the first version of the fixture and the results were not acceptable. Deflection was excessive for the aluminum and quite excessive for the steel samples. Several times the tool went deeper than the set depth of cut into the steel. Therefore, the top and bottom plate thicknesses were increased to 0.375 inches (9.525 mm) and the pillars were shortened to 1.000 inch tall x 1.000 inch (25.4 x 25.4 mm) square to prevent lateral deflection as well. The Solidworks model was then subjected to a higher 600 pound force (lbf) (2669 N) to be used to load both models without physically

performing the setup. The deflection was measured when both models were analyzed in Solidworks and the tables below show the results.

**Table 10: Fixture 1 Displacement Results**

Name	Type	Min	Max
Displacement	URES: Resultant Displacement	0 mm Node: 1	0.395131 mm Node: 1447

**Table 11: Fixture 2 Displacement Results**

Name	Type	Min	Max
Displacement	URES: Resultant Displacement	0 mm Node: 1	0.138878 mm Node: 1447

The key difference is that the maximum displacement is less than half from Fixture 2 (0.138878 mm) to Fixture 1 (0.395131 mm). When the y-direction displacement was measured on the Fixture 1 design, the displacement was around 3 mils (0.0762 mm). The new box design had less than 1 mil (0.0254 mm) displacement when tested the same way. Regardless, displacement was expected for this design and the objective of this analysis was to minimize the displacement. Stiffness performed quite well in practice.

The fixture was machined using a 2 Horsepower Bridgeport mill. Hole locations were scribed using precision metrology equipment and then drilled on the mill. Some holes were a few thousandths of an inch bigger than the bolts to aid in alignment of the fixture while others were drilled close to the size of the bolt. The holes close to the size of the bolt

were positioned towards the front of the fixture to prevent a pivoting motion from occurring.

Early on in trial runs, another problem with the work holder emerged. As mentioned above, discrepancies with the steel runs were due to the heating process. Excess space left in the sample slot of the fixture enabled the sample to move and throw off the depth of cut. This led to several unusable runs for the steel. There were also incidents where the tool was forced further into the sample despite the fixture redesign. The steel samples began sliding upon contact with the tool because the bottom of the screws securing it had worn down. To counter future occurrences, the screws were replaced with stainless steel set screws and a hole was drilled in the leading edge of each sample as shown below.



**Figure 26: 4130 42 HRC steel sample with hole drilled into leading edge**

The bottom right set screw was capable of screwing through the sample which locked it to the fixture. Although the tool was assumed rigid for this experiment, several videos showed a noticeable deflection in the tool upon impact with the sample. Any movement of the workpiece in the fixture led to an immediate rejection of the run's validity.

## Videographic Analysis

Prior to development of the Auburn University Videographic Quick Stop Device, measurement were conducted post-mortem on samples which had been cut. In order to make comparison easier, a high-speed camera was used to record each run. Chip formation was frozen in time in coordination with the forces cutting the geometry at the time. The camera used was a DRS TECHNOLOGIES Lighting RDT Camera. An image is shown in the figure below.



**Figure 27: DRS TECHNOLOGIES Lighting RDT Camera**

This added the ability to measure shear angles, depth of cut, and chip thickness. A pixel calibration run was required for every change of the fixture and camera location. The pixel calibration was recorded for each run. The actual depth of cut, chip thickness and all geometric angles were obtained using the high-speed camera's videos.

## Video Analysis

A software program called Kinovea was used to perform the measurements on the videos obtained via the high-speed camera. The same person reviewed and created the

measurements for all of the videos used in this experiment. While this did not eliminate error, it provided consistency in the processing of the videos. The videos were played until the shear plane was clearest in each video. Angles were placed and afterwards the depth of cut and chip thickness were measured. Determination of the depth of cut was more difficult for the 6061-T0 aluminum and the 4130 42 HRC steel. For the 6061-T0, the difficulty arose from the reflectivity of the material and the deburred edge of its top surface. In several of the videos, jagged edges from the previous cut obscured the shear plane which made deburring necessary. The problem with the steel was the low reflectivity. Several of the videos were dim, but the shear plane was still obtainable.

The measured angles were in degree units, but the depth of cut and chip thickness measurements were in pixels. A conversion factor (pixels to inches) was created by imaging a calibration slide after any adjustment of the camera's position. The image of the calibration slide was also analyzed in the Kinovea software.

The varying reflectivity of the materials made video observation difficult. Coating the samples was considered, but dismissed due to possible concealment of the slip plane.

### **Heating the Samples**

Heating for the fixture was done by a McMaster 120 V Strip Heater. Preheating for the steel samples was done using a Cadco Buffet Range as shown in the figure below.



**Figure 28: (Top) McMaster 120 V Strip Heater, (bottom) Cadco Buffet Range**

The temperature for the strip heater was controlled by the Omega CN7523 Temperature Controller and Crydon Solid State Relay setup shown in the figure below.

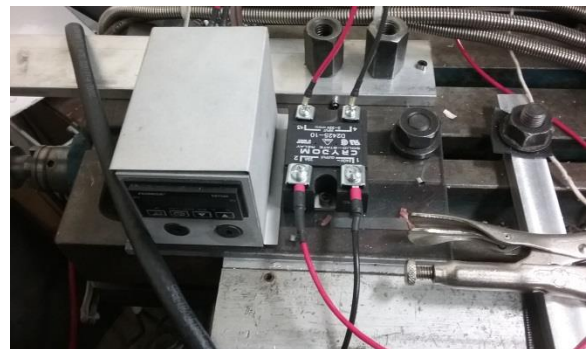


**Figure 29: Omega CN7523 Temperature Controller and Crydon Solid State Relay**

The mill upon which all this equipment was used was a heavily modified, extremely rigid Cincinnati Horizontal Mill. It is shown in the figure below.



**Figure 30: Modified Cincncinnati Horizontal Mill**

The table of the mill was move by a Baldur Industrial electric motor and the speed of the motor was adjusted by a Wood's E-trac AC Inverter. This allowed for precision table velocities. Both are shown in the figure below.

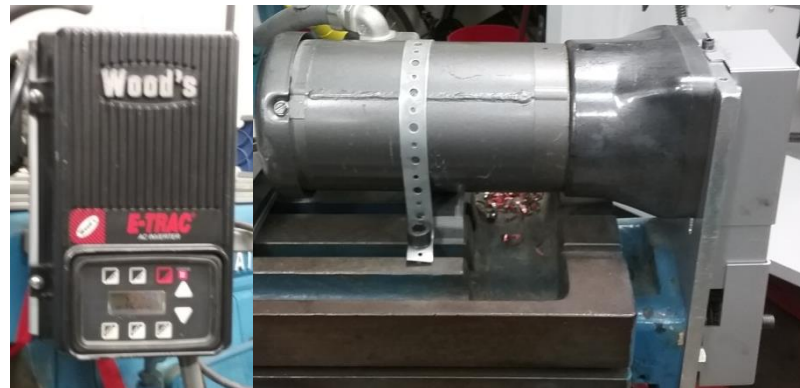


**Figure 31: (Left) Wood's E-trac AC Inverter, (right) Baldur Industrial electric motor**

## Thermal Resistance Network

A thermal resistance network (Figure.32) was constructed to aid in the development of a testing fixture. The primary purpose of the network was to determine how heat flowed through  $90^\circ$  angle steel to the top plate of the fixture box. The resistance network entails everything above the top plate of the entire fixture.

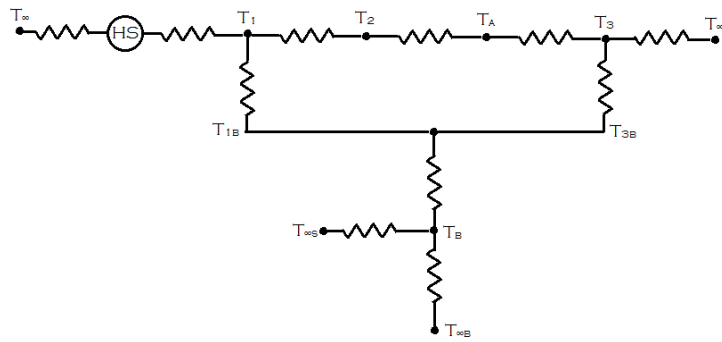


Figure 32: Thermal Resistance Network

The variable  $T_\infty$  represents the ambient temperature while  $T_A$  represents the air temperature between the  $90^\circ$  angle steel bars. These variables are separated because the gap for air in between the plates is so small and isolated. The symbol  $HS$  represents the strip heater as the heat source. All other temperature variables will be explained by subscript as follows:  $1$  is the temperature between the heated  $90^\circ$  angle steel bar and the sample,  $2$  is the temperature between the sample and air,  $3$  is the temperature between the unheated  $90^\circ$  angle steel bar and ambient air,  $1B$  is the temperature at the base of the heated  $90^\circ$  angle steel bar,  $3B$  is the temperature at the base of the unheated  $90^\circ$  angle steel bar,  $B$  is the temperature at the top of the top plate,  $\infty S$  is the ambient temperature on the sides of the top plate, and  $\infty B$  is the ambient temperature at the bottom of the top plate.

The thermal resistance network helped in dimensioning the final fixture. The resistance between the strip heater and the sample helped determine what thickness of the 90 ° steel to leave. The main aid was determining the thickness of the air gap between the top plate and the bottom plate of the box. Though the thermal resistance network above shows the resistance above the top plate, it gave a more accurate number of the temperature going through the top plate. The equations used are shown in Appendix.A. These equations are from the Fundamentals of Heat and Mass Transfer 7th Edition book by Incropera (40).

## Materials

The two materials used in this experiment were Face Centered Cubic 6061 aluminum and Body Centered Cubic 4130 steel. Two different hardness values were chosen for the 4130 steel were 22 HRC and 42 HRC and two tempers for the 6061 aluminum were T0 and T6. The 4130 22 HRC steel, 6061-T0, and 6061-T6 aluminum were purchased and used as received while the 4130 42 HRC hardness was achieved in house. Each sample hardened, underwent the same process and all were water quenched. The steel was hardened using a Paragon Industries Double Barrel furnace and also tempered using the same furnace (air cooled). An image of the furnace is shown in the figure below.



**Figure 33: Paragon Industries Double Barrel furnace**

## **Hardness Test**

The hardness of all samples was measured using a Rockwell Hardness Tester. Once sample hardness was confirmed to be in an acceptable range, the samples were green lit for use. The hardness tester had an accuracy of 3 HRC; therefore, the range of acceptable hardness values for the samples was +/- 3 HRC.

## **Wear Analysis Setup**

Tools were observed under a Keyence white light 3D microscope once the heated runs for a sample had been completed. When the observations were complete, the tools were reground for further use.

Images of the tool cutting edges were taken using the Keyence 100-1000x microscope. Magnifications varied from tool to tool due to the amount of the cutting edge present, image quality, and magnification effectiveness. Images were made to incorporate the cutting edge that came into contact with the material as well as some of the uncut edge for comparison. The tools were held under the microscope by a vice and angled to make the cutting edge relatively level. However, several of the tools could not be made completely level. When measuring the length of the cutting edge and the uncut edge, these

measurements are not very reliable due to the image creation process. The opposite side of the image varied (meaning that the worn edge and the uncut edges could have the same measurement but be completely different). To correct this, the side of the tool was roughly aligned so that the tool was square in the microscope's view. Images of the tools will be shown in the results chapter.

## **VI. Statistical Design of the Experiment**

Two different alloys were chosen for the experiment to allow a comparison between a body centered cubic crystalline structure (Steel 4130) and a face centered cubic crystalline structure. Each alloy is conducted as a separate multivariate experiment since the nature of steels “hardness” varies from the nature of aluminums “temper”.

The Steel 4130 alloy was heat treated and/or annealed locally in the Design and Manufacturing Laboratory to provide two comparative hardness values (22 HRC and 42 HRC). Three tool angles were selected (25, 30 and 35 °) to be used at two different depths of cut (0.004 or 0.008 inches, or 4 mils (0.1016 mm) and 8 mils (0.2032 mm) respectively). Room temperature trials were conducted as a baseline for comparison at 22 °C. Two elevated temperatures were chosen for comparison to the room temperature samples (100 °C and 200 °C). Three replicates of each factor level combination were required to achieve a confidence of 95 % in the statistical results.

The Aluminum alloy 6061 was purchased directly from the vendor at two certified hardness tempers (T0 and T6). Two tool angles were selected (25 and 30 °) to be used at two different depths of cut (0.004 or 0.008 inches, or 4 mils (0.1016 mm) and 8 mils (0.2032 mm) respectively). Trials with the aluminum and a 35 ° tool proved to be too inconsistent for use. Room temperature trials were conducted as a baseline for comparison at 22 °C. Three elevated temperatures were chosen for comparison to the room temperature samples (50 °C, 75 °C and 100 °C). Three replicates of each factor level combination were again required to achieve a confidence of 95 % in the statistical results.

Samples were taken in a randomized manner. Upon conclusion, 204 total runs had been accomplished to allow for statistical comparisons with a 95 % confidence when testing statistically.

Although random optical samples were measured for wear as discussed later, no attempt was made to achieve a powerful statistical result since it can take up to 10 hours to do one sample with the available Keyence microscope. The optical samples were conducted to allow for additional subjective observations.

## VI. Results

Upon the completion of data runs (Appendix.B), all of the classic manufacturing research calculations (Appendix.A) were conducted to support future researchers (results in Appendix.C). As discussed in the literature review, the focus of this thesis is upon the effectives of temperature on the external and internal cutting forces along with the sliding friction and normal friction at the tool-chip interface. The plane defined by angle  $\phi$  was included in the analysis of variance along with the friction coefficient, specific horsepower and the Wear Rate. Optical tool wear at the leading edge was also observed in a non-statistical manner for general comments.

### **Effects of temperature upon Friction ( $F$ ) and Normal ( $N$ ) force results**

Appendix.D provides friction force ( $F$  in lbf) and normal force ( $N$  in lbf) for all factor level combinations at all temperature levels. In general, both the friction force  $F$  and the normal force  $N$  decreased in value as the temperature increased. Figure.34 below is illustrative of the general trend in all cases.

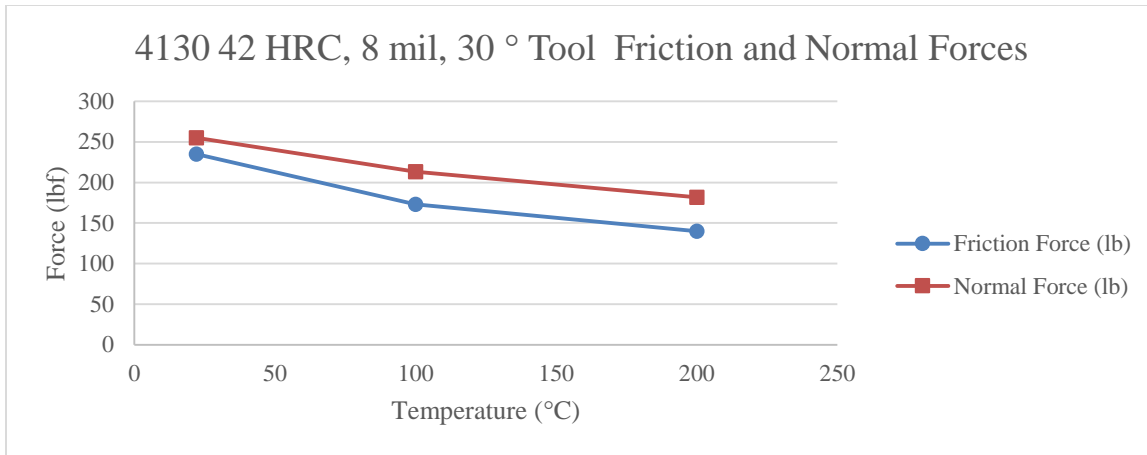


**Figure 34: Representative  $F$  and  $N$  trend as temp increased**

### Effects of temperature upon the Specific Horsepower ( $HP_s$ )

Specific Horsepower is the amount of horsepower required to achieve a given material removal rate (units hp x min/in<sup>3</sup>). It represents the amount of power required to remove a unit volume of material in a defined time. Anything which causes a decrease in the specific horsepower reduces the amount of work going into heating the tool as well as the workpiece. Appendix.E provides detailed  $HP_s$  graphs for each factor level combination in both materials. In general, elevating the temperature decreased the specific horsepower as illustrated in Figure.35 for one combination.

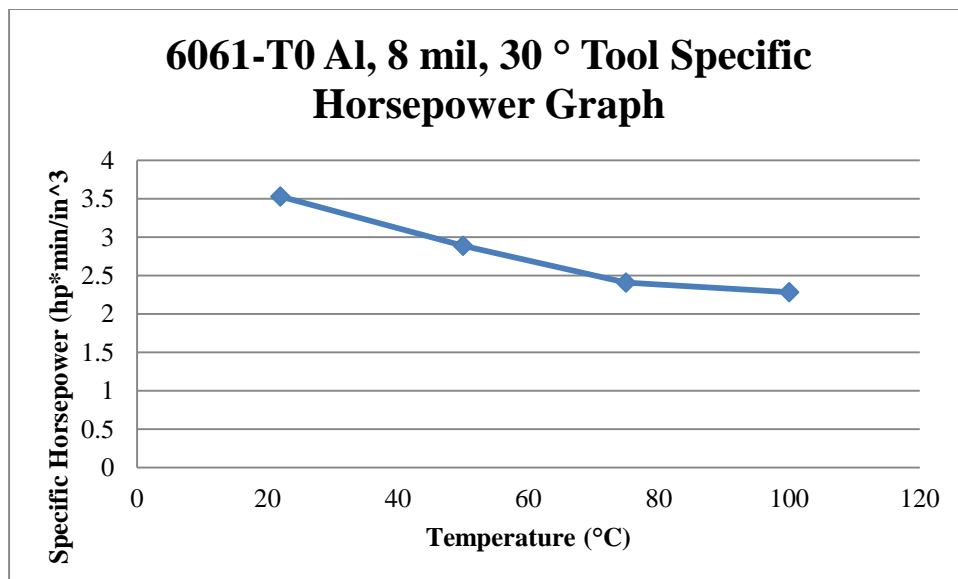


**Figure 35: Representative specific horsepower ( $HP_s$ ) trend as temp increased**

### Effects of Temperature upon the Calculated Wear Rate (Equation 22)

Appendix.F provides graphs of the calculated wear rate (equation 22) for all factor level combinations conducted in this experiment on both alloys. In general, the calculated wear rate had a downward trend as temperature increased. This is consistent with the decreasing values of the normal force ( $N$ ) as temperature was increased. Since all forms of wear are directly proportional to the normal force ( $N$ ), one would expect the wear rate to decrease with decreasing values of ( $N$ ) as the temperature increases. Figure.36 is illustrative of the general trend.

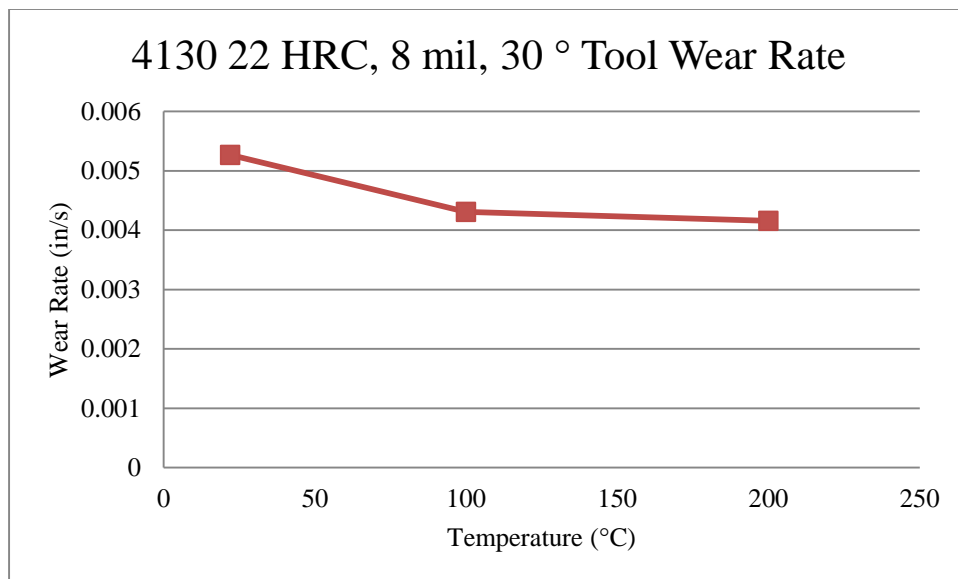


**Figure 36: Trend of tool wear rate in (in/sec) with increasing temperatures**

### Analysis of Variance

The great advantage of the Videographic Quick Stop Device (VQSD) is its ability to collect large amounts of coordinated force and geometrical measurements in a short period of time. Previous methods were manually intensive and extremely slow making multivariate analysis of variance impossible. A single sample a day was the benchmark of the most skilled laboratory technician.

Appendix G provides the analytical results of the multivariate ANOVA conducted upon the results using STATGRAPHICS as the analytic tool. Table.12 summarizes the ranked effects for the metal cutting forces in Payton's modified Merchant force diagram (Figure 17), shear plane angle  $\phi$ , friction coefficient, specific horsepower and the wear rate. All main effects were ranked even if they were not found to be significant.

**Table 12: Ranked multivariate outcomes**

Measured Outcome		A	B	C	D	AB	AC	AD	BC	BD	CD
Wear Rate (in/sec)	Steel	2	6-	1	5	3*		4-*			
	Aluminum	1	5-	2	4		3				
Specific HP (Hp/in <sup>3</sup> min)	Steel	2	3	4	1						5
	Aluminum	5-	3	4-	1		2*				
Friction Coefficient	Steel	5-	1	3	2	4					
	Aluminum	1	3	4	2						5
Normal Shear Force ( $F_n$ )	Steel	5	3	1	2	6					4
	Aluminum	4	3	1	2						5
Internal Shear Force ( $F_s$ )	Steel	3-	2	1	4-						
	Aluminum	2	3	1	4	9	7	8	5		6*
Normal Force (N)	Steel	5	2	1	3					6-	4
	Aluminum	4	2	1	3	6			5		
Friction Force ( $F_f$ )	Steel	4	6	1	2	5*					3
	Aluminum	3	5-	1	2		6-				4
Angle $\phi$	Steel	2	1	3	6-	5-					4*
	Aluminum	5-	1	3	2				4*		
Thrust Force ( $F_t$ )	Steel	6	3	2	1				7	5	4
	Aluminum	2	4	5	1		6*	7			3
Cutting Force ( $F_c$ )	Steel	5	3	1	2	6					4
	Aluminum	6-	3	1	2	4-					5-
		A	B	C	D	AB	AC	AD	BC	BD	CD
		Hardness	Tool Angle	Depth of Cut	Temperature	Hard x Angle	Hard x Depth	Hard x Temp	Angle x Depth	Angle x Temp	Depth x Temp

Any result that was ranked but not statistically significant is indicated by a – sign following the ranking. Any interaction where there was a dramatic crossover is indicated by a \* symbol following the ranking. There are a few with both symbols.

## Tool Wear Results

Given the short time that each tool was used for each factor level combination (a maximum of 45 s), the amount of wear upon each tool face was not expected to be significant. This was in fact the case for cratering which was nonexistent. Cratering is the predominant wear result associated with tool failure. There was notable edge wear however on all of the random samples that were drawn out of the experiment. All of the tools selected were visually imaged with a Keyence 100x-1000x microscope. The profile data was recorded by the Keyence software and then processed in Excel. The maximum, minimum, and average profile heights were stated for each tool.

Additionally, the edge length for the worn part of the tool cutting edge and the unworn part were stated and compared (Figure.37). The worn edge length was always subtracted from the unworn edge length; therefore, any negative value indicated either an uneven edge or a buildup of material from the cut. The table showing the edge differences as well as sample of how the images were measured is shown in Appendix.H. In general, the steel wore the edges more than the aluminum as might be expected by any layman. The aluminum was observed to adhere to the steel tools on occasion as shown in Figure.38 on the next page.



**Figure 37: Representative optical sample of edge wear documented in Appendix.H**  
**(Left) 4130 42 HRc 35 ° validation, (mid) 4130 42 HRc 35 ° 100 °C, (right) 4130 42 HRc 35 ° 200 °C**



**Figure 38: Representative optical sample of aluminum adhesion documented in Appendix.H**  
**(Left) 6061-T6 25 ° validation, (middle left) 6061-T6 25 ° 50 °C, (middle right) 6061-T6 25 ° 75 °C,  
(right) 6061-T6 25 ° 100 °C**

## **Miscellaneous Items**

Computer program utilized to process images is included in Appendix.I. Kobayashi-Thomsen test graphs are included in Appendix.J at the request of the advisor. Appendix.K contains the certificate of calibration for the Kistler dynamometer.

## VI. Conclusions

Table.12 summarized all the significant factor level combinations. Table.13 below summarizes the statistical optimal for each factor level combination. Any cell that is “grayed” illustrates a difference between alloys (crystalline structure). Table.14 summarizes the optimal factor level combinations when machining steel. Table.15 summarizes the optimal factor level combinations when machining aluminum. The optimal goals seek to minimize power required at the spindle and tool wear.

**Table 13: Comparison of Optimal Factor Level Combinations**

c		Hardness /Temper	Tool Angle	Depth of Cut	Temp
Wear Rate (in/sec)	Steel	L	H	L	H
	Aluminum	L	L	L	H
Specific HP ( $\text{HP/in}^3\text{min}$ )	Steel	L	H	H	H
	Aluminum	L	H	L	H
Friction Coefficient	Steel	Y	H	L	H
	Aluminum		H	L	H
Normal Shear Force ( $F_n$ )	Steel		L	H	L
	Aluminum		H	H	L
Internal Shear Force ( $F_s$ )	Steel	Y	L	H	L
	Aluminum		L	H	L
Normal Force (N)	Steel		L	H	L
	Aluminum		L	H	H
Friction Force (F)	Steel		L	H	L
	Aluminum		H	H	H
Angle $\phi$	Steel		H	H	L
	Aluminum		H	H	H
Thrust Force ( $F_t$ )	Steel		L	H	L
	Aluminum		H	H	H
Cutting Force ( $F_c$ )	Steel		L	H	L
	Aluminum		H	H	H

Shaded cells indicate a different between materials.  
**L** means lowest choice for that material.  
**H** means highest choice for that material

**Table 14: Overall Optimal Factor Level Combinations for Steel 4130**

	<b>Hardness /Temper</b>	<b>Tool Angle</b>	<b>Depth of Cut</b>	<b>Temp</b>
Wear Rate (in/sec)	L	H	L	H
Specific HP (Hp/in <sup>3</sup> min)	L	H	H	H
Friction Coefficient	H	L	H	H
Normal Shear Force (F <sub>n</sub> )	L	H	L	H
Internal Shear Force (F <sub>s</sub> )	L	H	L	L
Normal Force (N)	L	H	L	H
Friction Force (F)	L	H	L	H
Angle $\phi$	H	H	L	L
Thrust Force (F <sub>t</sub> )	L	H	L	H
Cutting Force (F <sub>c</sub> )	L	H	L	H
<b>Best Overall Alloy 4130</b>	<b>L</b>	<b>H</b>	<b>L</b>	<b>H</b>

**Table 15: Overall Optimal Factor Level Combinations for Aluminum 6061**

	<b>Hardness /Temper</b>	<b>Tool Angle</b>	<b>Depth of Cut</b>	<b>Temp</b>
Wear Rate (in/sec)	L	L	L	H
Specific HP (Hp/in <sup>3</sup> min)	L	H	L	H
Friction Coefficient	H	L	H	H
Normal Shear Force (F <sub>n</sub> )	H	H	L	H
Internal Shear Force (F <sub>s</sub> )	L	H	L	L
Normal Force (N)	L	H	H	H
Friction Force (F)	H	H	L	H
Angle $\phi$	H	H	L	H
Thrust Force (F <sub>t</sub> )	H	H	H	H
Cutting Force (F <sub>c</sub> )	H	H	L	H
<b>Best Overall Alloy 6061</b>	<b>H</b>	<b>H</b>	<b>L</b>	<b>H</b>

The results for hardness/temper, tool angle and depth of cut are consistent with observed industry practice during high speed machining operations. Soft steels (the low setting) are generally more machinable than hard steels. Aluminum 6061-T6 (the high factor setting) is well known for its superior machinability compared to the “gummier” 6061-T0 alloy. During high speed machining the sharpest tool (high setting) is used with the shallowest depth of cut (low setting). Since the tool is “weaker” as it gets sharper due

to the removal of material, there is always a tradeoff requiring less depth of cut. However this is compensated for by the ability to maintain very high feed rates.

The new result is that increasing the temperature of the work piece makes a statistical difference (at 95 %) in reducing all measured forces, leading to a reduction in the horsepower required to remove a given swept volume of material (the specific horsepower). The Normal force ( $N$ ) is reduced in ALL combinations where the temperature has been elevated. Since all forms of wear are directly proportional to the Normal force ( $N$ ) in some form, one would expect a general reduction in tool wear. Equation (22) predicts that the wear rate will decrease in all cases as well. It seems that elevating the temperature of the workpiece should require less horsepower at the spindle of the machines doing the work while simultaneously improving tool life.

### **Recommendations for Future Work**

The results of this experiment indicate that elevating the workpiece temperature has the dual benefits or reducing machine size (less horsepower, perhaps less rigidity) while reducing tool wear (prolonging tool life). If an elevated temperature in the work piece is combined with thru tool cryogenic cooling, large reductions in wear may result.

This experiment needs to be conducted at higher cutting speeds over longer periods of time which will produce enough visible wear on the tool face (cratering and lip erosion) to become easily measurable with a profilometer, a scanning electron microscope or a 3D white light microscope manned by an efficient operator. The results of this experiment, while encouraging and suggestive, are limited to the limited laboratory case of slow sleep orthogonal machining.

## References

1. Ernst, H., "The Physics of Metal Cutting," *ASM Symposium, Machining of Metals*, 1938.
2. DeGarmo, E. Paul, J. T. Black, and Ronald A. Kohser. Materials and Processes in Manufacturing. 9th ed. Hoboken, NJ: Wiley, 2003. Print.
3. Merchant, M. E., "Mechanics of the Metal Cutting Process—I. Orthogonal Cutting and a Type Chip," *Journal of Applied Physics*, Vol. 16, pp. 267-317, 1945.
4. Okushima, K. and Hitomi, K., November, "An Analysis of the Mechanism of Orthogonal Cutting and Its Application to Discontinuous Chip Formation," *ASME Journal of Engineering for Industry*, pp. 545-556, 1961.
5. Merchant, M. E., "Mechanics of the Metal Cutting Process—II. Plasticity Conditions in Orthogonal Cutting," *Journal of Applied Physics*, Vol. 16, pp. 318-324, 1945.
6. Huang, J., "Theoretical and Numerical Studies of Machining," PhD Dissertation, Auburn University, 1996.
7. Briggs, N. D., "Observation of the Orthogonal Machining Process Using High Speed Videography," *Master's Thesis*, Auburn University, 1993.
8. Black, J. T. and Briggs, N. D., High Speed Videographs of the Orthogonal Machining of Aluminum," *Tribology Symposium, ASME*, PD-Vol. 61, 1994, pp. 41-54, 1994.
9. Wright, P. K., "Predicting the Shear Plane Angle in Machining From Workmaterial Strain Hardening Characteristics," *Journal of Engineering for Industry*, Vol. 104, pp. 285-292, 1982.
10. Cottrell, A.H., Theory of Crystal Dislocations, Gordon and Breach, London, England, 1964.
11. Black, J. T., "Flow Stress Model in Metal Cutting," *ASME Journal of Engineering for Industry*, Vol. 101, pp. 403-415, 1979.

12. Black, J T., "On the Fundamental Mechanism of Large Strain Plastic Deformation Electron Microscopy of Metal Cutting Chips," *ASME Journal of Engineering for Industry*, Vol. 93, pp. 507-526, 1971.
13. Ueda, K. and Iwata, K., "Chip Formation Mechanism in Single Crystal Cutting of /3 Brass," *Anna/s of the C/RP*, Vol. 29/1, pp. 41-46, 1980.
14. Cook, N. H., Finnie, L., and Shaw, M. C., "Discontinuous Chip Formation," *ASME Transactions*, Vol. 76, pp. 153-163, 1954.
15. Agrawal, S.N., Amstead, B.H., "Study Reveals Mechanics of Chip Formation," *Machinery*, pp. 114-119 March 1961.
16. Black, J T. and James, C. R., "The Hammer QSD-Quick Stop Device for High Speed Machining and Rubbing," *Journal of Engineering for Industry*, Vol. 103, pp. 13 21, 1981.
17. Von Turkovich, B. F., Black, J.T., "Micro-machining of Copper and Aluminum Crystals," *Journal of Engineering for Industry*, pp. 130-134, February 1970.
18. Ramalingham, S., Black J T., "On the Metal Physical Considerations in the Machining of Metals," *Journal of Engineering for Industry*, December, 1971.
19. Cohen, P. H. and Black, J T., "Strain, Strain Rate and Shear Velocity Measurements in Metal Cutting," *High Energy Rate Fabrication*, Edited by Berman and Shroeder, ASME, pp. 271-278, 1978.
20. Sutter, G. "Chip Geometries during High-speed Machining for Orthogonal Cutting Conditions." *International Journal of Machine Tools & Manufacture* 45 (2005): 719-26. Science Direct. 23 Nov. 2004. Web. 11 Aug. 2015.
21. Junior, Adhemar Jose Spinelli, Luiz Eduardo De Angelo Sanchez, and Hamilton Jose De Mello. "HOT MACHINING: A REVIEW." Proceedings of COBEM 2003. 17<sup>th</sup> International Congress of Mechanical Engineering, Sao Paulo. N.p., n.d. Web.
22. Venkatesan, K., R. Ramanujam, and P. Kuppan. United States. Global Conference on Manufacturing and Management. Laser Assisted Machining of Difficult to Cut Materials: Research Opportunities and Future Directions A Comprehensive Review. 12th sess. Cong. Bill. N.p., n.d. Web. <[www.sciencedirect.com](http://www.sciencedirect.com)>.

23. Wang, Y., L. J. Yang, and N. J. Wang. "An Investigation of Laser-insisted Machining of AL<sub>2</sub>O<sub>3</sub> Particle Reinforced Aluminum Matrix Composite." *Journal of Materials Processing Technology* 129 (2002): 268-72. Web.
24. Chang, Chih-Wei, and Chun-Pao Kuo. "Evaluation of Surface Roughness in Laser assisted Machining of Aluminum Oxide Ceramics with Taguchi Method." *International Journal of Machine Tools & Manufacture* 47 (2007): 141-47. Science Direct. Web.
25. Ding, Hongtao, and Yung C. Shin. "Laser-assisted Machining of Hardened Steel Parts with Surface Integrity Analysis." *International Journal of Machine Tools & Manufacture* 50 (2010): 106-14. Web.
26. Kim, Dong-Hyeon, and Choon-Man Lee. "A Study of Cutting Force and Preheating temperature Prediction for Laser-assisted Milling of Inconel 718 and AISI 1045 Steel." *International Journal of Heat and Mass Transfer* 71 (2014): 264-74. Science Direct. 8 Jan. 2012. Web. 12 Aug. 2015.
27. Ozler, L., A. Inan, and C. Ozel. "Theoretical and Experimental Determination of Tool Life in Hot Machining of Austenitic Manganese Steel." *International Journal of Machine Tools & Manufacture* 41 (2001): 163-72. Web.
28. Tosun, N., and L. Ozler. "Optimisation for Hot Turning Operations with Multiple Performance Characteristics." *International Journal of Manufacturing Technology* 23 (2004): 777-82. Web.
29. Ranganathan, S., and T. Senthilvelan. "Multi-response Optimization of Machining Parameters in Hot Turning Using Grey Analysis." *International Journal of Manufacturing Technology* 56 (2011): 455-62. Web.
30. Muhammad, Riaz, Agostino Maurotto, Murat Demiral, Anish Roy, and Vadim V. Silberschmidt. "Thermally Enhanced Ultrasonically Assisted Machining of Ti Alloy." *Science Direct*. CIRP Journal of Manufacturing Science and Technology, n.d. Web.
31. Maity, K. P., and P. K. Swain. "An Experimental Investigation of Hot-machining to Predict Tool Life." *Journal of Materials Processing Technology* 198 (2008): 344-49. Web.
32. Leshock, Carl E., Jin-Nam Kim, and Yung C. Shin. "Plasma Enhanced Machining of Inconel 718: Modeling of Workpiece Temperature with Plasma Heating and Experimental Results." *International Journal of Machine Tools & Manufacture* 41 (2001): 877-97. Web.

33. Ganta, Venkatesh, and D. Chakradhar. "Multi Objective Optimization of Hot Machining of 15-5PH Stainless Steel Using Grey Relation Analysis." *Procedia Materials Science* 5 (2014): 1810-818. *Science Direct*. Web.
34. Lajis, M. A., A. K.M.N. Amin, A. N.M. Karim, H. C.D.M. Radzi, and T. L. Ginta. "Hot Machining of Hardened Steels with Coated Carbide Inserts." *American Journal of Engineering and Applied Sciences* (2009): 421-27. *Science Direct*. Web.
35. Hossain, M. I., A. K.M. Nurul Amin, A. U. Patwari, and A. Karim. "Enhancement of Machinability by Workpiece Preheating in End Milling of Ti-6Al-4V." *Journal of Achievements in Materials and Manufacturing Engineering* 31.2 (2008): n. pag. Web
36. Payton, Lewis Nathaniel. "Orthogonal Machining of Copper Using a Virtual Quick Stop Device." Thesis. Auburn University, 2000. 13 Apr. 2000. Web.
37. Shaw, M. C., Metal Cutting Principles, Clarendon Press, Oxford, 1984.
38. "Laser Types and Classification." *Oregon State*. Oregon State University, n.d. Web. 31 Mar. 2016.
39. Chandrasekaran, Vishnu V. *A Study on Forces, Tool Wear and Surface Finish in Orthogonal Machining of Aluminum 6061 T6 Alloy and AISI 1020 Steel with HSS and Uncoated Carbide Tool Inserts under Different Gaseous Cutting Environments*. Diss. Auburn U, 2013. N.p.: n.p., n.d. Auburn, Alabama. Auburn University, 14 Dec. 2013. Web.
40. Incropera, Frank P. "Chapter 3 One-Dimensional, Steady-State Conduction." *Fundamentals of Heat and Mass Transfer*. 7th ed. Hoboken: John Wiley, 2011. 111-35. Print.
41. "Machinability Ratings." *All Metals Forge Group*. N.p., 22 Jan. 2013. Web. 07 Apr. 2016. <<http://www.steelforge.com/literature/machinability-ratings/>>.
42. Childs, Thomas. Metal Machining : Theory and Applications. London
43. Finnie, I., Shaw, M.C. "The Friction Process in Metal Cutting." *Transactions of ASME*. November, 1956 (1956): 1649-57.
44. Williams, J.E., E. Smart, and D. Milner. "The Metallurgy of Machining, Part I." Metallurgia 81.1970 (1970): 3.

45. Shaw, Milton Clayton. Metal Cutting Principles. Oxford: Oxford University Press, 1984. Metal Cutting Principles. Oxford Series on Advanced Manufacturing ; 3. Oxford [Oxfordshire] New York: Clarendon Press ; Oxford University Press, 1984.
46. Buckley, D.H. "Tribology in the 80's." NASA Conference Publication 2300, 1983. 19-44. Vol. 1.
47. Dawson, D. History of Tribology. Longman, 1979.
48. Kopalinsky, E.M., X. Li, and P.L.B Oxley. Tribological Aspects in Manufacturing. Eds. Ranga Komanduri and M.H. Attia: ASME, 1991.
49. Suh, Nam P. Tribophysics. Englewood Cliffs, N.J.: Prentice-Hall, 1986.
50. Schey, John A. Tribology in Metalworking : Friction, Lubrication, and Wear. Metals Park, Ohio: American Society for Metals, 1983.
51. Payton, Lewis N. "AN UPDATE TO THE MERCHANT ORTHOGONAL FORCE DIAGRAM (MFD)." Proc. of ASME 2010 International Mechanical Engineering Congress and Exposition, Vancouver, British Columbia. N.p., 12 Nov. 2010. Web.

## Appendix.A: Equations Used

Data	Symbol	Units	Equation
Ratio Chip-Uncut Chip Thickness	$r_c$	none	$r_c = t_1/t_2$
Frictional Force upon Chip	$F$	lbf	$F = F_c \times \sin \alpha + F_t \cos \alpha$
Normal Force Upon Chip	$N$	lbf	$N = F_c \times \cos \alpha - F_t \times \sin \alpha$
Friction Coefficient	$\mu$	none	$\mu = \tan^{-1} \left( \frac{F}{N} \right)$
Resultant Force Upon Chip	$R$	lbf	$R = \sqrt{F_c^2 + F_t^2}$
Mean Friction Angle at Tool	$\beta$	deg	$\beta = \arctan [F/N]$
Shear Force on Plane (Merchant)	$F_s$	lbf	$F_s = F_c \times \cos \phi - F_t \times \sin \phi$
Normal Force on Plane (Merchant)	$F_n$	lbf	$F_n = F_c \times \sin \phi - F_t \times \cos \phi$
Area of the Shear Plane	$A_s$	in <sup>2</sup>	$A_s = t_1 \times w / \sin \phi$
Shear Stress on Shear Plane	$\tau_s$	lbf/in <sup>2</sup>	$\tau_s = F_s / A_s$
Resultant Shear Stress on Shear Plane	$\tau_{sr}$	MPa	$\tau_{sr} = \frac{F_R}{A_s} * 0.001550031$
Shear Force on Plane (Payton)	$F_s$	N	$F_s = \frac{1}{\sqrt{2}} * \left( \left( (F_c - F_t) * \cos \frac{\alpha}{2} \right) - \left( (F_c + F_t) * \sin \frac{\alpha}{2} \right) \right)$

Normal Force on Plane (Payton)	$F_n$	N	$F_n = \frac{1}{\sqrt{2}} * \left( \left( (F_c + F_r) * \cos \frac{\alpha}{2} \right) + \left( (F_c - F_r) * \sin \frac{\alpha}{2} \right) \right)$
Data	Symbol	Units	Equation
Area of the Shear Plane	$A_s$	in <sup>2</sup>	$A_s = \frac{t_1 * 0.125}{\sin \varphi}$
Shear Strain (Merchant)	$\gamma$	none	$\gamma = \frac{\cos \alpha}{(\sin \varphi_c * \cos(\varphi_c - \alpha))}$
Shear Strain (Payton)	$\gamma$	none	$\gamma = \frac{2 * \cos \alpha}{1 + \sin \alpha}$
Shear Strain (Chandrasekaran)	$\gamma$	none	$\gamma = \frac{\sin \varphi_c}{\sin \psi_c}$
Shear Front Angle (Payton)	$\psi_c$	°	$\psi_c = 45 + \frac{\alpha}{2} - \phi$
Shear Plane Angle	$\phi_c$	°	$\phi_c = \tan^{-1} \frac{(r_c) * \cos \alpha}{1 - (r_c) * \sin \alpha}$
Measured Shear Angle	$\phi_m$	°	$\phi = 90 - (\text{angle measure in Kinovea})$
Actual Depth of Cut	$t_{1actual}$	in	$t_{1actual} = t_{1pixels} * P_c$
Ratio- Shear Force over Force Normal to Shear Plane	$\chi$	radians	$\chi = \tan^{-1} \frac{F_s}{F_n}$
Kobayashi-Thomsen Shear Stress	$\tau_{sk}$	MPa	$\tau_{sk} = \frac{F_c}{t * w} \left[ \frac{\sin \left( \frac{\pi}{4} + \frac{\alpha}{2} \right) * \sin x}{\left( \cos \left( \frac{\pi}{4} - \frac{\alpha}{2} - x \right) \right)} \right]$
Kobayashi-Thomsen Trendline	$A_{sk}$	in <sup>2</sup>	$A_{sk} = m * F_s + k_y$
Conduction Resistance	$R_{cond}$	K/W	$R_{cond} = \frac{t}{A * k}$

Convection Resistance	$R_{conv}$	K/W	$R_{conv} = \frac{1}{A * h}$
Heat Transfer Rate	$q$	W	$q = \frac{\Delta T}{R_T}$
Data	Symbol	Units	Equation
Force Reduction	$FR$	%	$FR = \frac{F_V - F_H}{F_V} * 100$
Horsepower	$HP$	hp	$HP = \frac{F_c \times V}{33,000}$
Metal Removal Rate	$MRR$	in <sup>3</sup> /min	$MRR = V \times w \times t_1$
Specific Horsepower	$HP_s$	hp*min/ in <sup>3</sup>	$HP_s = \frac{HP}{MRR}$

## Appendix.B: Raw Data

Raw Collected Data Table

No.	Run	Material	Hardness/ Temper	Temperature (°C)	Depth of Cut (mils)	Depth of Cut (inches)
1	4130_22_25d_vali_9315_4mils	4130	22	22	4	0.004
2	4130_22_25d_vali_9315_4mils2	4130	22	22	4	0.004
3	4130_22_25d_vali_9315_4mils3	4130	22	22	4	0.004
4	4130_22_25d_100C_81815_4mi ls3	4130	22	100	4	0.004
5	4130_22_25d_100C_81815_4mi ls5	4130	22	100	4	0.004
6	4130_22_25d_100C_81815_4mi ls6	4130	22	100	4	0.004
7	4130_22_25d_200C_82015_4mi ls3	4130	22	200	4	0.004
8	4130_22_25d_200C_82015_4mi ls4	4130	22	200	4	0.004
9	4130_22_25d_200C_82015_4mi ls5	4130	22	200	4	0.004
10	4130_22_30d_vali_9315_4mils	4130	22	22	4	0.004
11	4130_22_30d_vali_9315_4mils2	4130	22	22	4	0.004
12	4130_22_30d_vali_9315_4mils3	4130	22	22	4	0.004
13	4130_22_30d_100C_81815_4mi ls2	4130	22	100	4	0.004
14	4130_22_30d_100C_81815_4mi ls3	4130	22	100	4	0.004
15	4130_22_30d_100C_81815_4mi ls4	4130	22	100	4	0.004
16	4130_22_30_200_4216_4mils	4130	22	200	4	0.004
17	4130_22_30_200_4216_4mils2	4130	22	200	4	0.004
18	4130_22_30_200_4216_4mils3	4130	22	200	4	0.004
19	4130_22_35d_vali_9315_4mils	4130	22	22	4	0.004
20	4130_22_35d_vali_9315_4mils2	4130	22	22	4	0.004
21	4130_22_35d_vali_9315_4mils3	4130	22	22	4	0.004
22	4130_22_35d_100C_81815_4mi ls	4130	22	100	4	0.004
23	4130_22_35d_100C_81815_4mi ls3	4130	22	100	4	0.004
24	4130_22_35_100_4216_4mils	4130	22	100	4	0.004
25	4130_22_35_200_1416_4mils	4130	22	200	4	0.004
26	4130_22_35_200_1416_4mils2	4130	22	200	4	0.004
27	4130_22_35_200_1416_4mils3	4130	22	200	4	0.004
28	4130_22_25d_vali_9315_8mils	4130	22	22	8	0.008
29	4130_22_25d_vali_9315_8mils2	4130	22	22	8	0.008
30	4130_22_25d_vali_9315_8mils3	4130	22	22	8	0.008
31	4130_22_25d_100C_81815_8mi ls	4130	22	100	8	0.008

No.	Run	Material	Hardness/ Temper	Temperature (°C)	Depth of Cut (mils)	Depth of Cut (inches)
32	4130_22_25d_100C_81815_8mi ls2	4130	22	100	8	0.008
33	4130_22_25d_100C_81815_8mi ls3	4130	22	100	8	0.008
34	4130_22_25d_200C_82115_8mi ls	4130	22	200	8	0.008
35	4130_22_25d_200C_82115_8mi ls2	4130	22	200	8	0.008
36	4130_22_25d_200C_82115_8mi ls5	4130	22	200	8	0.008
37	4130_22_30d_vali_9315_8mils	4130	22	22	8	0.008
38	4130_22_30d_vali_9315_8mils2	4130	22	22	8	0.008
39	4130_22_30d_vali_9315_8mils3	4130	22	22	8	0.008
40	4130_22_30d_100C_81715_test 8mils2	4130	22	100	8	0.008
41	4130_22_30d_100C_81715_test 8mils3	4130	22	100	8	0.008
42	4130_22_30_100_4216_8mils	4130	22	100	8	0.008
43	4130_22_30d_200C_82415_8mi ls	4130	22	200	8	0.008
44	4130_22_30d_200C_82415_8mi ls2	4130	22	200	8	0.008
45	4130_22_30d_200C_82415_8mi ls3	4130	22	200	8	0.008
46	4130_22_35d_vali_9315_8mils	4130	22	22	8	0.008
47	4130_22_35d_vali_9315_8mils2	4130	22	22	8	0.008
48	4130_22_35d_vali_9315_8mils3	4130	22	22	8	0.008
49	4130_22_35_100_121915_8mils	4130	22	100	8	0.008
50	4130_22_35_100_121915_8mils 2	4130	22	100	8	0.008
51	4130_22_35_100_121915_8mils 3	4130	22	100	8	0.008
52	4130_22_35_200_122915_8mils 2	4130	22	200	8	0.008
53	4130_22_35_200_41216_8mils	4130	22	200	8	0.008
54	4130_22_35_200_41216_8mils2	4130	22	200	8	0.008
55	4130_42_25_vali_41016_4mils	4130	42	22	4	0.004
56	4130_42_25d_vali_9915_4mils2	4130	42	22	4	0.004
57	4130_42_25d_vali_9915_4mils3	4130	42	22	4	0.004
58	4130_42_25d_100C_83115_4mi ls5	4130	42	100	4	0.004
59	4130_42_25d_100C_83115_4mi ls3	4130	42	100	4	0.004
60	4130_42_25d_100C_83115_4mi ls4	4130	42	100	4	0.004
61	4130_42_25d_200_9815_4mils	4130	42	200	4	0.004
62	4130_42_25_200_1516_4mils	4130	42	200	4	0.004
63	4130_42_25_200_1516_4mils3	4130	42	200	4	0.004

No.	Run	Material	Hardness/ Temper	Temperature (°C)	Depth of Cut (mils)	Depth of Cut (inches)
64	4130_42_30d_vali_9915_4mils	4130	42	22	4	0.004
65	4130_42_30d_vali_9915_4mils2	4130	42	22	4	0.004
66	4130_42_30d_vali_9915_4mils3	4130	42	22	4	0.004
67	4130_47_30d_100C_9115_4mils	4130	42	100	4	0.004
68	4130_47_30d_100C_9115_4mils3	4130	42	100	4	0.004
69	4130_42_30_100_4416_4mils2	4130	42	100	4	0.004
70	4130_42_30_200_101315_4mils2	4130	42	200	4	0.004
71	4130_42_30_200_101315_4mils3	4130	42	200	4	0.004
72	4130_42_30_200_4416_4mils3	4130	42	200	4	0.004
73	4130_42_35d_vali_9915_4mils	4130	42	22	4	0.004
74	4130_42_35d_vali_9915_4mils2	4130	42	22	4	0.004
75	4130_42_35d_vali_9915_4mils3	4130	42	22	4	0.004
76	4130_42_35d_100C_9215_4mils2	4130	42	100	4	0.004
77	4130_42_35d_100C_9215_4mils3	4130	42	100	4	0.004
78	4130_42_35d_100C_9215_4mils4	4130	42	100	4	0.004
79	4130_42_35d_200C_9315_4mils	4130	42	200	4	0.004
80	4130_42_35d_200C_9315_4mils2	4130	42	200	4	0.004
81	4130_42_35d_200C_9315_4mils3	4130	42	200	4	0.004
82	4130_42_25d_vali_9915_8mils	4130	42	22	8	0.008
83	4130_42_25d_vali_9915_8mils2	4130	42	22	8	0.008
84	4130_42_25d_vali_9915_8mils3	4130	42	22	8	0.008
85	4130_42_25d_100C_83115_8mils2	4130	42	100	8	0.008
86	4130_42_25_100_1816_8mils2	4130	42	100	8	0.008
87	4130_42_25_100_1816_8mils3	4130	42	100	8	0.008
88	4130_42_25_200_41016_8mils2	4130	42	200	8	0.008
89	4130_42_25_200_1716_8mils	4130	42	200	8	0.008
90	4130_42_25_200_1716_8mils2	4130	42	200	8	0.008
91	4130_42_30d_vali_9915_8mils	4130	42	22	8	0.008
92	4130_42_30d_vali_9915_8mils2	4130	42	22	8	0.008
93	4130_42_30d_vali_9915_8mils3	4130	42	22	8	0.008
94	4130_47_30d_100C_9115_8mils	4130	42	100	8	0.008
95	4130_47_30d_100C_9115_8mils2	4130	42	100	8	0.008
96	4130_47_30d_100C_9115_8mils3	4130	42	100	8	0.008

No.	Run	Material	Hardness/ Temper	Temperature (°C)	Depth of Cut (mils)	Depth of Cut (inches)
97	4130_42_30_200_101415_8mils 2	4130	42	200	8	0.008
98	4130_42_30_200_41216_8mils	4130	42	200	8	0.008
99	4130_42_30_200_41216_8mils2	4130	42	200	8	0.008
100	4130_42_35d_vali_9915_8mils	4130	42	22	8	0.008
101	4130_42_35d_vali_9915_8mils2	4130	42	22	8	0.008
102	4130_42_35d_vali_9915_8mils3	4130	42	22	8	0.008
103	4130_42_35_100_41216_8mils2	4130	42	100	8	0.008
104	4130_42_35d_100C_9215_8mil s2	4130	42	100	8	0.008
105	4130_42_35d_100C_9215_8mil s3	4130	42	100	8	0.008
106	4130_42_35d_200_9415_8mils2	4130	42	200	8	0.008
107	4130_42_35d_200_9415_8mils3	4130	42	200	8	0.008
108	4130_42_35d_200_9415_8mils5	4130	42	200	8	0.008
109	T0_25d_vali_9215_4mils	6061	0	22	4	0.004
110	T0_25d_vali_9215_4mils2	6061	0	22	4	0.004
111	T0_25d_vali_9215_4mils3	6061	0	22	4	0.004
112	T0_25d_50C_73015_4mil2	6061	0	50	4	0.004
113	T0_25_50_22516_4mils2	6061	0	50	4	0.004
114	T0_25_50_22516_4mils3	6061	0	50	4	0.004
115	T0_25_75_2816_4mils	6061	0	75	4	0.004
116	T0_25_75_2816_4mils2	6061	0	75	4	0.004
117	T0_25_75_41316_4mils2	6061	0	75	4	0.004
118	T0_25_100_2816_4mils	6061	0	100	4	0.004
119	T0_25_100_2816_4mils2	6061	0	100	4	0.004
120	T0_25_100_2816_4mils3	6061	0	100	4	0.004
121	T0_30d_vali_9215_4mils	6061	0	22	4	0.004
122	T0_30d_vali_9215_4mils2	6061	0	22	4	0.004
123	T0_30d_vali_9215_4mils3	6061	0	22	4	0.004
124	T0_30d_50C_73015_4mils	6061	0	50	4	0.004
125	T0_30d_50C_73015_4mils2	6061	0	50	4	0.004
126	T0_30d_50C_73015_4mils3	6061	0	50	4	0.004
127	T0_30_75_101615_4mils	6061	0	75	4	0.004
128	T0_30_75_101615_4mils2	6061	0	75	4	0.004
129	T0_30_75_101615_4mils3	6061	0	75	4	0.004
130	T0_30d_100C_73115_4mils2	6061	0	100	4	0.004
131	T0_30d_100C_73115_4mils3	6061	0	100	4	0.004
132	T0_30_100_4116_4mils	6061	0	100	4	0.004
133	T0_25d_vali_9215_8mils	6061	0	22	8	0.008

No.	Run	Material	Hardness/ Temper	Temperature (°C)	Depth of Cut (mils)	Depth of Cut (inches)
134	T0_25d_vali_9215_8mils2	6061	0	22	8	0.008
135	T0_25d_vali_9215_8mils3	6061	0	22	8	0.008
136	T0_25_50_4116_8mils2	6061	0	50	8	0.008
137	T0_25d_50C_73015_8mil2	6061	0	50	8	0.008
138	T0_25_50_41316_8mils	6061	0	50	8	0.008
139	T0_25_75_41316_8mils	6061	0	75	8	0.008
140	T0_25d_75C_73015_8mil2	6061	0	75	8	0.008
141	T0_25d_75C_73015_8mil3	6061	0	75	8	0.008
142	T0_25d_100C_73115_8mil	6061	0	100	8	0.008
143	T0_25d_100C_73115_8mil2	6061	0	100	8	0.008
144	T0_25d_100C_73115_8mil3	6061	0	100	8	0.008
145	T0_30d_vali_9215_8mils	6061	0	22	8	0.008
146	T0_30d_vali_9215_8mils2	6061	0	22	8	0.008
147	T0_30d_vali_9215_8mils3	6061	0	22	8	0.008
148	T0_30d_50C_73015_8mils	6061	0	50	8	0.008
149	T0_30d_50C_73015_8mils2	6061	0	50	8	0.008
150	T0_30d_50C_73015_8mils3	6061	0	50	8	0.008
151	T0_30d_75C_73015_8mils2	6061	0	75	8	0.008
152	T0_30d_75C_73015_8mils3	6061	0	75	8	0.008
153	T0_30_75_4116_8mils2	6061	0	75	8	0.008
154	T0_30_100_4116_8mils	6061	0	100	8	0.008
155	T0_30_100_4116_8mils2	6061	0	100	8	0.008
156	T0_30_100_4116_8mils3	6061	0	100	8	0.008
157	T6_25d_vali_9115_4mils	6061	6	22	4	0.004
158	T6_25d_vali_9115_4mils2	6061	6	22	4	0.004
159	T6_25d_vali_9115_4mils3	6061	6	22	4	0.004
160	T6_25_50_41216_4mils	6061	6	50	4	0.004
161	T6_25_50_41216_4mils2	6061	6	50	4	0.004
162	T6_25d_50C_81915_4mils3	6061	6	50	4	0.004
163	T6_25d_75C_72615_4mils	6061	6	75	4	0.004
164	T6_25_75_41316_4mils2	6061	6	75	4	0.004
165	T6_25_75_2516_4mils3	6061	6	75	4	0.004
166	T6_25_100_22216_4mils2	6061	6	100	4	0.004
167	T6_25_100_22216_4mils3	6061	6	100	4	0.004
168	T6_25_100_4316_4mils3	6061	6	100	4	0.004
169	T6_30d_vali_9115_4mils	6061	6	22	4	0.004
170	T6_30d_vali_9115_4mils2	6061	6	22	4	0.004
171	T6_30d_vali_9115_4mils3	6061	6	22	4	0.004
172	T6_30d_50C_72615_4mils2	6061	6	50	4	0.004

No.	Run	Material	Hardness/ Temper	Temperature (°C)	Depth of Cut (mils)	Depth of Cut (inches)
173	T6_30d_50C_81915_4mils2	6061	6	50	4	0.004
174	T6_30d_50C_81915_4mils3	6061	6	50	4	0.004
175	T6_30d_75C_72815_4mils	6061	6	75	4	0.004
176	T6_30_75_41316_4mils	6061	6	75	4	0.004
177	T6_30_75_41316_4mils2	6061	6	75	4	0.004
178	T6_30d_100C_8315_4mils3	6061	6	100	4	0.004
179	T6_30d_100C_91415_4mils	6061	6	100	4	0.004
180	T6_30d_100C_91415_4mils2	6061	6	100	4	0.004
181	T6_25d_vali_9115_8mils	6061	6	22	8	0.008
182	T6_25d_vali_9115_8mils2	6061	6	22	8	0.008
183	T6_25d_vali_9115_8mils3	6061	6	22	8	0.008
184	T6_25_50_41216_8mils3	6061	6	50	8	0.008
185	T6_25d_50C_72315_8milsr2	6061	6	50	8	0.008
186	T6_25d_50C_72315_8milsr3	6061	6	50	8	0.008
187	T6_25_75_2516_8mils	6061	6	75	8	0.008
188	T6_25_75_2516_8mils2	6061	6	75	8	0.008
189	T6_25_75_41316_8mils2	6061	6	75	8	0.008
190	T6_25_100_22216_8mils2	6061	6	100	8	0.008
191	T6_25_100_22216_8mils3	6061	6	100	8	0.008
192	T6_25_100_4316_8mils	6061	6	100	8	0.008
193	T6_30d_vali_9115_8mils	6061	6	22	8	0.008
194	T6_30d_vali_9115_8mils2	6061	6	22	8	0.008
195	T6_30d_vali_9115_8mils3	6061	6	22	8	0.008
196	T6_30d_50C_81915_8mils	6061	6	50	8	0.008
197	T6_30d_50C_81915_8mils2	6061	6	50	8	0.008
198	T6_30d_50C_81915_8mils3	6061	6	50	8	0.008
199	T6_30d_75C_72815_8mils	6061	6	75	8	0.008
200	T6_30_75_4116_8mils	6061	6	75	8	0.008
201	T6_30_75_4116_8mils2	6061	6	75	8	0.008
202	T6_30d_100C_91415_8mils	6061	6	100	8	0.008
203	T6_30d_100C_91415_8mils2	6061	6	100	8	0.008
204	T6_30_100_4516_8mils2	6061	6	100	8	0.008

No.	Tool Angle (degrees)	Replicate	cutting force (lbs force)	thrust force (lbs force)	measured shear angle (Phi) (degrees)	Depth of Cut (pixels)	Cut Chip thickness (pixels)	Psi measured (degrees)	V (in/mi n)
1	25	1	203.587	62.032	31	21.31	41.64	30.500	7.5
2	25	2	204.504	62.134	28	22.81	49.61	30.500	7.5
3	25	3	205.834	62.736	32	22.75	45.85	30.500	7.5
4	25	1	159.729	41.260	28	19.03	43.68	30.500	7.5
5	25	2	221.834	49.291	18	23	81.93	30.500	7.5
6	25	3	150.080	39.784	24	19.03	48.72	30.500	7.5
7	25	1	164.340	24.642	28	27.01	56.47	30.500	7.5
8	25	2	127.633	17.943	32	23.01	45.69	30.500	7.5
9	25	3	142.033	20.369	27	15.01	34.77	30.500	7.5
10	30	1	127.158	31.434	43	16.68	25.88	21.000	7.5
11	30	2	186.129	44.249	34	25.44	39.52	29.000	7.5
12	30	3	172.527	41.881	38	21.15	35.98	21.000	7.5
13	30	1	121.264	15.640	29	19	40.6	29.000	7.5
14	30	2	125.866	11.599	30	23	48.02	29.000	7.5
15	30	3	113.086	10.455	30	19	40.89	29.000	7.5
16	30	1	125.121	28.350	28	18.34	46.04	29.000	7.5
17	30	2	128.782	24.172	32	20.78	42.87	29.000	7.5
18	30	3	108.093	23.759	36	22.77	40.94	29.000	7.5
19	35	1	144.223	25.992	36	27.19	52.42	23.500	7.5
20	35	2	150.039	27.345	35	18.86	33.64	23.500	7.5
21	35	3	156.105	30.129	30	20.79	45.77	23.500	7.5
22	35	1	102.290	15.474	45	18.45	32.37	23.500	7.5
23	35	2	104.109	14.542	34	30	53.44	23.500	7.5
24	35	3	111.095	14.595	30	25.66	53.17	23.500	7.5
25	35	1	135.947	7.545	41	24.94	43.95	23.500	7.5
26	35	2	101.193	11.128	34	18.94	36.53	23.500	7.5
27	35	3	126.516	5.152	46	22.96	32.21	23.500	7.5
28	25	1	375.632	100.782	21	33.97	99.1	30.500	7.5
29	25	2	343.881	95.892	21	34.23	99.35	30.500	7.5
30	25	3	365.208	101.674	22	40.77	107.21	30.500	7.5
31	25	1	231.280	44.886	30	39	81.41	30.500	7.5
32	25	2	251.620	53.356	29	35.01	74.01	30.500	7.5
33	25	3	302.944	56.353	28	43	90.94	30.500	7.5
34	25	1	242.457	33.101	22	39.01	106.59	30.500	7.5
35	25	2	345.068	34.305	26	47.01	104.35	30.500	7.5
36	25	3	272.904	24.677	23	43.01	114.88	30.500	7.5
37	30	1	384.926	84.174	29	45.63	91.83	29.000	7.5

No.	Tool Angle (degrees)	Replicate	cutting force (lbs force)	thrust force (lbs force)	measured shear angle (Phi) (degrees)	Depth of Cut (pixels)	Cut Chip thickness (pixels)	Psi measured (degrees)	V (in/mi n)
38	30	2	315.468	76.173	37	32.39	56.66	29.000	7.5
39	30	3	339.690	81.066	29	32.39	68.53	29.000	7.5
40	30	1	233.320	43.070	27	39	90.34	29.000	7.5
41	30	2	310.971	51.420	29	43	88.49	29.000	7.5
42	30	3	363.717	68.318	29	52.51	113.53	29.000	7.5
43	30	1	266.128	18.592	37	39	66.22	29.000	7.5
44	30	2	238.396	19.376	35	39	71.94	29.000	7.5
45	30	3	229.641	18.628	25	39	95.01	29.000	7.5
46	35	1	314.583	56.698	27	29.79	69	30.000	7.5
47	35	2	261.899	59.931	24	36.32	79.77	30.000	7.5
48	35	3	289.363	63.587	22	34.07	76.87	32.000	7.5
49	35	1	242.591	18.235	27	38.46	94.37	28.000	7.5
50	35	2	206.826	15.946	31	34.49	70.97	23.500	7.5
51	35	3	188.637	17.049	32	32.49	64.38	23.500	7.5
52	35	3	187.754	15.261	33	29.51	55.79	23.500	7.5
53	35	1	186.175	36.872	29	39.02	84.12	30.000	7.5
54	35	2	183.287	29.778	35	39.35	70.08	23.500	7.5
55	25	1	175.005	47.780	40	25.7	42.23	18.500	7.5
56	25	2	205.115	54.295	26	21.24	48.93	30.000	7.5
57	25	3	190.175	49.591	32	21.26	39.18	18.500	7.5
58	25	1	199.096	38.936	27	27	62.93	26.000	7.5
59	25	2	184.055	42.914	28	23.02	47.34	25.000	7.5
60	25	3	180.862	33.213	27	23	48.31	25.000	7.5
61	25	1	200.023	39.069	30	29.25	65.99	18.500	7.5
62	25	2	144.246	26.430	36	16.25	27.86	18.500	7.5
63	25	3	129.891	27.153	35	21	39.46	18.500	7.5
64	30	1	145.785	37.488	38	15.97	27.68	27.670	7.5
65	30	2	167.037	38.082	37	17.89	29.03	27.670	7.5
66	30	3	177.100	40.358	34	19.63	34.02	27.670	7.5
67	30	1	177.030	42.817	25	26.02	62.79	27.670	7.5
68	30	2	145.977	32.173	30	15.01	34.44	27.670	7.5
69	30	3	148.939	23.374	42	19	26.87	27.670	7.5
70	30	1	169.405	14.970	33	23	46.14	27.670	7.5
71	30	2	177.218	18.274	28	23.01	46.43	27.670	7.5
72	30	3	167.409	20.557	34	27	49.65	27.670	7.5
73	35	1	152.462	35.063	40	18.25	28.65	23.330	7.5
74	35	2	163.612	36.350	39	18.19	28.6	23.330	7.5
75	35	3	154.811	37.123	40	15.72	22.71	23.330	7.5

No.	Tool Angle (degrees)	Replicate	cutting force (lbs force)	thrust force (lbs force)	measured shear angle (Phi) (degrees)	Depth of Cut (pixels)	Cut Chip thickness (pixels)	Psi measured (degrees)	V (in/mi n)
76	35	1	138.459	40.377	49	20.34	26.55	23.330	7.5
77	35	2	158.170	39.276	46	24.34	32.06	23.330	7.5
78	35	3	155.015	42.287	39	16	27.91	23.330	7.5
79	35	1	150.314	12.016	41	23	32.53	23.330	7.5
80	35	2	106.031	17.751	45	15	23.81	23.330	7.5
81	35	3	141.160	16.145	39	18	29.15	23.330	7.5
82	25	1	420.699	107.057	26	35	83.07	24.000	7.5
83	25	2	367.249	96.157	24	27	67.62	25.000	7.5
84	25	3	375.646	97.415	29	35	73.96	24.000	7.5
85	25	1	333.263	73.338	24	35	91.48	28.000	7.5
86	25	2	285.517	52.495	23	36.96	87.56	31.000	7.5
87	25	3	228.746	51.767	24	34.2	84.75	31.000	7.5
88	25	1	280.955	48.826	35	36.47	68.66	18.500	7.5
89	25	2	272.005	45.546	38	30.21	52.22	18.500	7.5
90	25	3	264.836	36.156	45	29.46	43.92	18.500	7.5
91	30	1	349.668	78.304	32	37.37	76.96	27.670	7.5
92	30	2	344.465	75.626	28	30.36	71.34	27.670	7.5
93	30	3	321.160	73.629	35	35.57	63.95	27.670	7.5
94	30	1	308.987	50.119	22	34.03	93.79	30.000	7.5
95	30	2	235.354	34.703	29	29.67	60.26	27.670	7.5
96	30	3	268.962	44.455	30	31.02	66.53	27.670	7.5
97	30	2	214.044	11.745	34	40.99	80.75	27.670	7.5
98	30	1	220.482	38.061	40	31.01	50.71	27.670	7.5
99	30	3	247.720	41.158	40	43.01	68.51	27.670	7.5
100	35	1	344.754	64.176	29	33.66	63.91	30.000	7.5
101	35	2	289.535	61.215	38	31.68	50.97	23.330	7.5
102	35	3	291.502	59.914	42	35.11	51.33	23.330	7.5
103	35	1	258.155	27.039	41	46.01	70.94	23.330	7.5
104	35	2	259.359	46.506	46	28.33	40.07	23.330	7.5
105	35	3	279.952	41.123	40	44.01	70.68	23.330	7.5
106	35	1	257.192	21.019	32	39.34	73.42	23.330	7.5
107	35	2	270.055	11.958	35	35	64.36	23.330	7.5
108	35	3	292.068	6.326	37	36.33	61.4	23.330	7.5
109	25	1	72.298	24.985	21	25.21	77.16	28.000	7.5
110	25	2	61.366	21.222	28	22.79	48.08	24.670	7.5
111	25	3	66.816	22.643	29	22.98	50.41	24.670	7.5
112	25	1	54.500	15.947	23	27.01	73.62	28.000	7.5
113	25	2	55.363	15.421	26	27.48	64.07	24.670	7.5

No.	Tool Angle (degrees)	Replicate	cutting force (lbs force)	thrust force (lbs force)	measured shear angle (Phi) (degrees)	Depth of Cut (pixels)	Cut Chip thickness (pixels)	Psi measured (degrees)	V (in/mi n)
114	25	3	62.013	16.718	30	25.7	55.33	24.670	7.5
115	25	1	60.600	16.586	36	23.48	44.38	24.670	7.5
116	25	2	58.246	15.874	31	27.75	58.25	24.670	7.5
117	25	3	60.442	13.756	30	23.04	47.3	24.670	7.5
118	25	1	47.747	15.998	33	25.23	45.83	24.670	7.5
119	25	2	45.607	13.485	25	23.22	60.18	27.000	7.5
120	25	3	52.538	14.743	25	25.72	63.51	26.000	7.5
121	30	1	54.171	15.278	26	27	61.9	36.000	7.5
122	30	2	55.583	15.157	16	23	90.11	36.000	7.5
123	30	3	58.013	16.316	35	23	42.16	30.000	7.5
124	30	1	50.979	12.796	27	31.02	69.02	36.000	7.5
125	30	2	53.690	10.325	26	23.01	51.93	36.000	7.5
126	30	3	49.303	11.785	33	23	43.85	36.000	7.5
127	30	1	44.944	13.063	26	23	59.04	36.000	7.5
128	30	2	60.870	15.392	26	27.02	63.37	36.000	7.5
129	30	3	59.188	15.346	27	23.01	53.22	36.000	7.5
130	30	1	53.438	7.927	31	23.02	42.72	36.000	7.5
131	30	2	45.399	4.248	38	19.01	33.01	31.000	7.5
132	30	3	46.511	6.610	29	30	65	36.000	7.5
133	25	1	124.499	39.834	26	27.26	72.02	24.670	7.5
134	25	2	109.599	37.231	27	39.02	89.07	24.670	7.5
135	25	3	121.961	40.045	21	40.72	109.44	31.000	7.5
136	25	2	102.000	32.060	32	47.01	90.78	24.670	7.5
137	25	3	98.391	28.387	18	43.01	145.8	40.000	7.5
138	25	1	103.995	26.758	36	35	59.2	24.670	7.5
139	25	1	99.927	22.797	30	31.02	61.69	24.670	7.5
140	25	2	93.911	13.801	23	47	110.13	40.000	7.5
141	25	3	93.284	13.615	28	45.67	99.58	24.670	7.5
142	25	1	88.215	8.149	28	31.01	70.96	24.670	7.5
143	25	2	92.716	11.117	20	27	76.44	34.000	7.5
144	25	3	95.375	11.241	22	39.01	108.89	35.000	7.5
145	30	1	98.380	25.087	23	27	73.85	36.000	7.5
146	30	2	120.969	42.836	31	36.36	68.44	36.000	7.5
147	30	3	122.509	49.138	18	39	128.49	36.000	7.5
148	30	1	77.865	14.376	29	27	57.02	36.000	7.5
149	30	2	85.877	16.156	29	34.01	70.91	36.000	7.5
150	30	3	79.063	14.135	28	31.01	65.95	36.000	7.5
151	30	1	79.042	13.011	22	39.01	112.67	36.000	7.5

No.	Tool Angle (degrees)	Replicate	cutting force (lbs force)	thrust force (lbs force)	measured shear angle (Phi) (degrees)	Depth of Cut (pixels)	Cut Chip thickness (pixels)	Psi measured (degrees)	V (in/mi n)
152	30	2	73.807	10.200	28	31.01	68.59	36.000	7.5
153	30	3	80.945	12.233	35	39.01	71.28	27.000	7.5
154	30	1	75.591	5.268	32	39.02	76.09	36.000	7.5
155	30	2	78.988	4.297	29	39	79.84	36.000	7.5
156	30	3	73.829	5.948	32	39	76.04	36.000	7.5
157	25	1	67.385	15.420	19	19.03	64.2	34.377	7.5
158	25	2	72.177	16.300	19	19	59.15	34.377	7.5
159	25	3	72.599	16.503	22	19	56.34	34.377	7.5
160	25	1	57.198	9.327	28	20.71	57.07	34.377	7.5
161	25	2	53.375	7.856	31	22.77	53.29	34.377	7.5
162	25	3	53.770	7.718	26	22	51.74	34.377	7.5
163	25	1	53.560	9.791	39	25.02	45.62	27.000	7.5
164	25	2	58.582	6.851	30	23.02	47.3	34.377	7.5
165	25	3	54.996	4.569	30	22.76	46.41	34.377	7.5
166	25	1	46.483	2.992	24	23.27	62.43	34.377	7.5
167	25	2	55.880	3.937	26	25.51	65.41	34.377	7.5
168	25	3	50.262	2.705	34	19.03	39.83	28.000	7.5
169	30	1	60.499	10.425	21	18.03	53.88	31.500	7.5
170	30	2	60.111	10.340	24	19	47.49	31.500	7.5
171	30	3	59.652	10.148	20	15.39	49.78	31.500	7.5
172	30	1	44.405	3.855	36	23	40.8	31.500	7.5
173	30	2	43.073	4.587	31	22	41.85	31.500	7.5
174	30	3	46.493	3.288	34	21.3	41.51	31.500	7.5
175	30	1	53.551	4.619	45	19.04	28.25	26.000	7.5
176	30	2	50.638	5.293	32	19.03	37.22	31.500	7.5
177	30	3	53.333	4.816	35	15	27.18	31.500	7.5
178	30	1	45.775	3.693	30	25.55	57.15	31.500	7.5
179	30	2	51.486	4.953	25	20.34	47.87	31.500	7.5
180	30	3	52.863	5.543	24	23.02	55.04	31.500	7.5
181	25	1	118.873	23.321	20	32.33	92.07	34.377	7.5
182	25	2	120.672	23.051	24	36.36	89.42	34.377	7.5
183	25	3	128.621	23.588	27	39.35	89	34.377	7.5
184	25	1	95.195	10.321	28	41.22	90.86	34.377	7.5
185	25	2	91.693	11.104	30	42.01	81.58	34.377	7.5
186	25	3	92.466	10.229	22	39	109.87	34.377	7.5
187	25	1	94.330	5.097	22	36.76	100.87	34.377	7.5
188	25	2	97.403	5.106	28	43.23	97.28	34.377	7.5
189	25	3	96.912	8.347	30	39	78.68	34.377	7.5

No.	Tool Angle (degrees)	Replicate	cutting force (lbs force)	thrust force (lbs force)	measured shear angle (Phi) (degrees)	Depth of Cut (pixels)	Cut Chip thickness (pixels)	Psi measured (degrees)	V (in/mi n)
190	25	1	102.598	10.300	17	36.19	128.26	34.377	7.5
191	25	2	106.311	11.302	22	41.2	120.63	34.377	7.5
192	25	3	94.407	4.074	28	41.19	92.14	34.377	7.5
193	30	1	98.062	13.739	27	39.18	84.62	31.500	7.5
194	30	2	100.823	14.005	21	33.98	100.49	31.500	7.5
195	30	3	105.235	15.038	32	41.44	72.11	31.500	7.5
196	30	1	81.945	2.573	32	43.01	82.26	31.500	7.5
197	30	2	83.492	2.854	35	39.01	67.78	31.500	7.5
198	30	3	85.651	1.888	28	39.01	88.25	31.500	7.5
199	30	1	78.841	2.496	37	37	58.58	31.500	7.5
200	30	2	77.872	1.882	29	39.01	85	31.500	7.5
201	30	3	78.286	3.000	26	43	100.35	31.500	7.5
202	30	1	75.843	4.080	32	27.99	50.72	31.500	7.5
203	30	2	71.181	4.095	31	23.03	50.09	31.500	7.5
204	30	3	84.820	3.073	34	35.01	64.35	31.500	7.5

## Appendix.C: Calculated Data Table

No.	actual depth of cut (inches)	actual depth of cut (mm)	Cut chip thickness (inches)	Cut chip thickness (mm)	chip thickness ratio	phi calculated (radians)	phi calculated (degrees)	Psi calculated (degrees)	Psi-calculated (radians)
1	0.005	0.125	0.010	0.245	0.512	0.534	30.618	26.5	0.463
2	0.005	0.134	0.011	0.292	0.460	0.477	27.348	29.5	0.515
3	0.005	0.134	0.011	0.270	0.496	0.517	29.641	25.5	0.445
4	0.004	0.108	0.010	0.247	0.436	0.451	25.825	29.5	0.515
5	0.005	0.130	0.018	0.464	0.281	0.281	16.102	39.5	0.689
6	0.004	0.108	0.011	0.276	0.391	0.401	22.977	33.5	0.585
7	0.007	0.165	0.014	0.346	0.478	0.498	28.516	29.5	0.515
8	0.006	0.141	0.011	0.280	0.504	0.525	30.107	25.5	0.445
9	0.004	0.092	0.008	0.213	0.432	0.446	25.574	30.5	0.532
10	0.004	0.098	0.006	0.152	0.645	0.689	39.474	17	0.297
11	0.006	0.150	0.009	0.232	0.644	0.688	39.423	26	0.454
12	0.005	0.124	0.008	0.212	0.588	0.625	35.791	22	0.384
13	0.004	0.095	0.008	0.204	0.468	0.487	27.883	31	0.541
14	0.005	0.116	0.009	0.241	0.479	0.499	28.609	30	0.524
15	0.004	0.095	0.008	0.205	0.465	0.483	27.663	30	0.524
16	0.004	0.096	0.010	0.242	0.398	0.407	23.305	32	0.559
17	0.004	0.109	0.009	0.226	0.485	0.506	28.989	28	0.489
18	0.005	0.120	0.008	0.215	0.556	0.588	33.712	24	0.419
19	0.006	0.160	0.012	0.308	0.519	0.544	31.167	26.5	0.463
20	0.004	0.111	0.008	0.198	0.561	0.595	34.095	27.5	0.480
21	0.005	0.122	0.011	0.269	0.454	0.466	26.710	32.5	0.567
22	0.004	0.093	0.006	0.163	0.570	0.606	34.748	17.5	0.305
23	0.006	0.151	0.011	0.268	0.561	0.596	34.147	28.5	0.497
24	0.005	0.135	0.011	0.280	0.483	0.500	28.663	32.5	0.567
25	0.006	0.141	0.010	0.249	0.567	0.603	34.572	21.5	0.375
26	0.004	0.107	0.008	0.207	0.518	0.544	31.152	28.5	0.497
27	0.005	0.130	0.007	0.183	0.713	0.779	44.647	16.5	0.288
28	0.008	0.200	0.023	0.583	0.343	0.348	19.966	36.5	0.637
29	0.008	0.201	0.023	0.584	0.345	0.350	20.076	36.5	0.637
30	0.009	0.240	0.025	0.630	0.380	0.390	22.325	35.5	0.620
31	0.009	0.221	0.018	0.461	0.479	0.499	28.563	27.5	0.480
32	0.008	0.198	0.017	0.419	0.473	0.492	28.185	28.5	0.497
33	0.010	0.244	0.020	0.515	0.473	0.492	28.172	29.5	0.515
34	0.009	0.239	0.026	0.652	0.366	0.374	21.424	35.5	0.620
35	0.011	0.288	0.025	0.638	0.451	0.467	26.762	31.5	0.550
36	0.010	0.263	0.028	0.703	0.374	0.383	21.954	34.5	0.602

No.	actual depth of cut (inches)	actual depth of cut (mm)	Cut chip thickness (inches)	Cut chip thickness (mm)	chip thickness ratio	phi calculated (radians)	phi calculated (degrees)	Psi calculated (degrees)	Psi-calculated (radians)
37	0.011	0.268	0.021	0.540	0.497	0.520	29.795	31	0.541
38	0.007	0.190	0.013	0.333	0.572	0.606	34.730	23	0.401
39	0.007	0.190	0.016	0.403	0.473	0.492	28.190	31	0.541
40	0.009	0.221	0.020	0.512	0.432	0.445	25.491	33	0.576
41	0.010	0.244	0.020	0.501	0.486	0.507	29.069	31	0.541
42	0.011	0.276	0.024	0.597	0.463	0.480	27.522	31	0.541
43	0.009	0.239	0.016	0.405	0.589	0.626	35.864	23	0.401
44	0.009	0.239	0.017	0.440	0.542	0.572	32.784	25	0.436
45	0.009	0.239	0.023	0.581	0.410	0.421	24.099	35	0.611
46	0.007	0.175	0.016	0.406	0.432	0.439	25.177	35.5	0.620
47	0.008	0.214	0.018	0.469	0.455	0.467	26.785	38.5	0.672
48	0.008	0.200	0.018	0.452	0.443	0.453	25.958	40.5	0.707
49	0.009	0.218	0.021	0.535	0.408	0.411	23.542	35.5	0.620
50	0.008	0.196	0.016	0.402	0.486	0.504	28.896	31.5	0.550
51	0.007	0.184	0.014	0.365	0.505	0.527	30.191	30.5	0.532
52	0.007	0.167	0.012	0.316	0.529	0.556	31.882	29.5	0.515
53	0.008	0.205	0.017	0.442	0.464	0.478	27.371	33.5	0.585
54	0.008	0.207	0.015	0.369	0.562	0.596	34.155	27.5	0.480
55	0.006	0.151	0.010	0.248	0.609	0.639	36.595	17.5	0.305
56	0.005	0.125	0.011	0.288	0.434	0.449	25.725	31.5	0.550
57	0.005	0.125	0.009	0.230	0.543	0.568	32.543	25.5	0.445
58	0.006	0.155	0.014	0.360	0.429	0.443	25.406	30.5	0.532
59	0.005	0.132	0.011	0.271	0.486	0.506	29.017	29.5	0.515
60	0.005	0.132	0.011	0.277	0.476	0.495	28.377	30.5	0.532
61	0.007	0.172	0.015	0.388	0.443	0.459	26.304	27.5	0.480
62	0.004	0.092	0.006	0.158	0.583	0.612	35.052	21.5	0.375
63	0.005	0.119	0.009	0.224	0.532	0.557	31.893	22.5	0.393
64	0.004	0.094	0.006	0.163	0.577	0.612	35.078	22	0.384
65	0.004	0.105	0.007	0.171	0.616	0.657	37.646	23	0.401
66	0.005	0.115	0.008	0.200	0.577	0.612	35.082	26	0.454
67	0.006	0.149	0.014	0.359	0.414	0.425	24.355	35	0.611
68	0.003	0.086	0.008	0.197	0.436	0.450	25.762	30	0.524
69	0.004	0.100	0.006	0.141	0.707	0.758	43.450	18	0.314
70	0.005	0.132	0.010	0.264	0.498	0.522	29.900	27	0.471
71	0.005	0.132	0.010	0.266	0.496	0.519	29.708	32	0.559
72	0.006	0.142	0.010	0.261	0.544	0.574	32.896	26	0.454
73	0.004	0.107	0.007	0.168	0.637	0.688	39.427	22.5	0.393
74	0.004	0.107	0.007	0.168	0.636	0.687	39.359	23.5	0.410
75	0.004	0.092	0.005	0.134	0.692	0.755	43.240	22.5	0.393

No.	actual depth of cut (inches)	actual depth of cut (mm)	Cut chip thickness (inches)	Cut chip thickness (mm)	chip thickness ratio	phi calculated (radians)	phi calculated (degrees)	Psi calculated (degrees)	Psi-calculated (radians)
76	0.005	0.120	0.006	0.156	0.766	0.842	48.226	13.5	0.236
77	0.006	0.143	0.007	0.189	0.759	0.834	47.768	16.5	0.288
78	0.004	0.094	0.006	0.164	0.573	0.610	34.979	23.5	0.410
79	0.005	0.135	0.008	0.191	0.707	0.772	44.254	21.5	0.375
80	0.003	0.088	0.006	0.140	0.630	0.680	38.939	17.5	0.305
81	0.004	0.106	0.007	0.171	0.617	0.664	38.069	23.5	0.410
82	0.008	0.206	0.019	0.489	0.421	0.435	24.919	31.5	0.550
83	0.006	0.159	0.016	0.398	0.399	0.411	23.526	33.5	0.585
84	0.008	0.206	0.017	0.435	0.473	0.492	28.196	28.5	0.497
85	0.008	0.200	0.021	0.524	0.383	0.392	22.472	33.5	0.585
86	0.008	0.210	0.020	0.497	0.422	0.436	24.968	34.5	0.602
87	0.008	0.194	0.019	0.481	0.404	0.415	23.794	33.5	0.585
88	0.008	0.214	0.016	0.404	0.531	0.556	31.830	22.5	0.393
89	0.007	0.171	0.012	0.296	0.579	0.607	34.760	19.5	0.340
90	0.007	0.167	0.010	0.249	0.671	0.704	40.312	12.5	0.218
91	0.009	0.220	0.018	0.453	0.486	0.507	29.046	28	0.489
92	0.007	0.179	0.017	0.420	0.426	0.438	25.088	32	0.559
93	0.008	0.209	0.015	0.376	0.556	0.588	33.714	25	0.436
94	0.008	0.195	0.021	0.537	0.363	0.367	21.000	38	0.663
95	0.007	0.170	0.014	0.345	0.492	0.515	29.495	31	0.541
96	0.007	0.178	0.015	0.381	0.466	0.485	27.769	30	0.524
97	0.009	0.235	0.018	0.462	0.508	0.532	30.504	26	0.454
98	0.006	0.163	0.011	0.267	0.612	0.652	37.337	20	0.349
99	0.009	0.011	0.014	0.360	0.628	0.670	38.394	20	0.349
100	0.008	0.198	0.015	0.376	0.527	0.554	31.723	33.5	0.585
101	0.007	0.186	0.012	0.300	0.622	0.669	38.351	24.5	0.428
102	0.008	0.206	0.012	0.302	0.684	0.745	42.678	20.5	0.358
103	0.010	0.242	0.015	0.373	0.649	0.702	40.231	21.5	0.375
104	0.007	0.167	0.009	0.236	0.707	0.772	44.252	16.5	0.288
105	0.010	0.259	0.016	0.416	0.623	0.671	38.429	22.5	0.393
106	0.009	0.231	0.017	0.432	0.536	0.565	32.361	30.5	0.532
107	0.008	0.206	0.015	0.378	0.544	0.575	32.919	27.5	0.480
108	0.008	0.214	0.014	0.361	0.592	0.633	36.267	25.5	0.445
109	0.006	0.148	0.018	0.454	0.327	0.331	18.960	36.5	0.637
110	0.005	0.134	0.011	0.283	0.474	0.493	28.245	29.5	0.515
111	0.005	0.135	0.012	0.296	0.456	0.473	27.101	28.5	0.497
112	0.006	0.143	0.015	0.391	0.367	0.375	21.481	34.5	0.602
113	0.006	0.145	0.013	0.337	0.429	0.443	25.397	31.5	0.550
114	0.005	0.135	0.011	0.291	0.464	0.482	27.645	27.5	0.480

No.	actual depth of cut (inches)	actual depth of cut (mm)	Cut chip thickness (inches)	Cut chip thickness (mm)	chip thickness ratio	phi calculated (radians)	phi calculated (degrees)	Psi calculated (degrees)	Psi-calculated (radians)
115	0.005	0.124	0.009	0.233	0.529	0.553	31.699	21.5	0.375
116	0.006	0.146	0.012	0.306	0.476	0.496	28.396	26.5	0.463
117	0.005	0.121	0.010	0.249	0.487	0.507	29.070	27.5	0.480
118	0.005	0.133	0.009	0.241	0.551	0.577	33.032	24.5	0.428
119	0.005	0.122	0.012	0.317	0.386	0.396	22.676	32.5	0.567
120	0.005	0.135	0.013	0.334	0.405	0.417	23.885	32.5	0.567
121	0.006	0.159	0.014	0.364	0.436	0.450	25.786	34	0.593
122	0.005	0.135	0.021	0.530	0.255	0.248	14.219	44	0.768
123	0.005	0.135	0.010	0.248	0.546	0.576	33.010	25	0.436
124	0.007	0.175	0.015	0.390	0.449	0.465	26.658	33	0.576
125	0.005	0.130	0.012	0.294	0.443	0.458	26.241	34	0.593
126	0.005	0.130	0.010	0.248	0.525	0.552	31.621	27	0.471
127	0.005	0.130	0.013	0.335	0.390	0.397	22.733	34	0.593
128	0.006	0.153	0.014	0.359	0.426	0.439	25.141	34	0.593
129	0.005	0.130	0.012	0.302	0.432	0.446	25.534	33	0.576
130	0.005	0.130	0.010	0.241	0.539	0.568	32.569	29	0.506
131	0.004	0.107	0.007	0.187	0.576	0.611	35.008	22	0.384
132	0.006	0.158	0.013	0.342	0.462	0.479	27.457	31	0.541
133	0.006	0.160	0.017	0.424	0.379	0.388	22.213	31.5	0.550
134	0.009	0.229	0.021	0.524	0.438	0.453	25.978	30.5	0.532
135	0.009	0.239	0.025	0.644	0.372	0.381	21.808	36.5	0.637
136	0.010	0.247	0.019	0.478	0.518	0.541	30.998	25.5	0.445
137	0.009	0.228	0.030	0.774	0.295	0.296	16.984	39.5	0.689
138	0.007	0.186	0.012	0.314	0.591	0.620	35.538	21.5	0.375
139	0.006	0.163	0.013	0.324	0.503	0.525	30.058	27.5	0.480
140	0.010	0.249	0.023	0.584	0.427	0.441	25.262	34.5	0.602
141	0.010	0.242	0.021	0.528	0.459	0.476	27.275	29.5	0.515
142	0.006	0.165	0.015	0.377	0.437	0.452	25.910	29.5	0.515
143	0.006	0.143	0.016	0.406	0.353	0.360	20.621	37.5	0.654
144	0.008	0.207	0.023	0.578	0.358	0.365	20.938	35.5	0.620
145	0.006	0.159	0.017	0.434	0.366	0.370	21.179	37	0.646
146	0.008	0.214	0.016	0.402	0.531	0.560	32.068	29	0.506
147	0.009	0.229	0.030	0.756	0.304	0.301	17.218	42	0.733
148	0.006	0.153	0.013	0.322	0.474	0.493	28.249	31	0.541
149	0.008	0.192	0.016	0.401	0.480	0.500	28.652	31	0.541
150	0.007	0.175	0.015	0.373	0.470	0.489	28.030	32	0.559
151	0.009	0.221	0.025	0.637	0.346	0.348	19.932	38	0.663
152	0.007	0.175	0.015	0.388	0.452	0.468	26.835	32	0.559
153	0.008	0.205	0.015	0.375	0.547	0.578	33.125	25	0.436

No.	actual depth of cut (inches)	actual depth of cut (mm)	Cut chip thickness (inches)	Cut chip thickness (mm)	chip thickness ratio	phi calculated (radians)	phi calculated (degrees)	Psi calculated (degrees)	Psi-calculated (radians)
154	0.008	0.205	0.016	0.400	0.513	0.538	30.848	28	0.489
155	0.008	0.205	0.017	0.420	0.488	0.510	29.238	31	0.541
156	0.008	0.205	0.016	0.400	0.513	0.538	30.853	28	0.489
157	0.004	0.112	0.015	0.378	0.296	0.298	17.073	38.5	0.672
158	0.004	0.112	0.014	0.348	0.321	0.325	18.616	38.5	0.672
159	0.004	0.112	0.013	0.331	0.337	0.342	19.618	35.5	0.620
160	0.004	0.109	0.012	0.300	0.363	0.371	21.229	29.5	0.515
161	0.005	0.120	0.011	0.280	0.427	0.441	25.295	26.5	0.463
162	0.004	0.113	0.010	0.265	0.425	0.439	25.163	31.5	0.550
163	0.005	0.133	0.010	0.242	0.548	0.574	32.904	18.5	0.323
164	0.005	0.121	0.010	0.249	0.487	0.507	29.043	27.5	0.480
165	0.005	0.134	0.011	0.273	0.490	0.511	29.278	27.5	0.480
166	0.005	0.137	0.014	0.367	0.373	0.381	21.850	33.5	0.585
167	0.006	0.150	0.015	0.385	0.390	0.400	22.939	31.5	0.550
168	0.004	0.100	0.008	0.210	0.478	0.497	28.483	23.5	0.410
169	0.004	0.106	0.012	0.317	0.335	0.335	19.190	39	0.681
170	0.004	0.112	0.011	0.279	0.400	0.409	23.419	36	0.628
171	0.004	0.091	0.012	0.293	0.309	0.307	17.573	40	0.698
172	0.005	0.122	0.009	0.217	0.564	0.597	34.208	24	0.419
173	0.005	0.117	0.009	0.222	0.526	0.553	31.699	29	0.506
174	0.004	0.113	0.009	0.220	0.513	0.539	30.869	26	0.454
175	0.004	0.101	0.006	0.150	0.674	0.722	41.359	15	0.262
176	0.004	0.100	0.008	0.196	0.511	0.537	30.747	28	0.489
177	0.003	0.079	0.006	0.143	0.552	0.583	33.428	25	0.436
178	0.005	0.136	0.012	0.303	0.447	0.463	26.502	30	0.524
179	0.005	0.120	0.011	0.282	0.425	0.437	25.044	35	0.611
180	0.005	0.135	0.013	0.324	0.418	0.429	24.607	36	0.628
181	0.007	0.190	0.021	0.541	0.351	0.358	20.491	37.5	0.654
182	0.008	0.214	0.021	0.526	0.407	0.419	23.989	33.5	0.585
183	0.009	0.231	0.021	0.523	0.442	0.458	26.234	30.5	0.532
184	0.009	0.217	0.019	0.478	0.454	0.471	26.962	29.5	0.515
185	0.009	0.223	0.017	0.433	0.515	0.538	30.817	27.5	0.480
186	0.008	0.207	0.023	0.583	0.355	0.362	20.731	35.5	0.620
187	0.009	0.216	0.023	0.593	0.364	0.372	21.326	35.5	0.620
188	0.010	0.254	0.023	0.572	0.444	0.460	26.376	29.5	0.515
189	0.008	0.205	0.016	0.414	0.496	0.517	29.609	27.5	0.480
190	0.008	0.213	0.030	0.754	0.282	0.283	16.191	40.5	0.707
191	0.010	0.242	0.028	0.709	0.342	0.347	19.888	35.5	0.620
192	0.009	0.217	0.019	0.485	0.447	0.463	26.543	29.5	0.515

No.	actual depth of cut (inches)	actual depth of cut (mm)	Cut chip thickness (inches)	Cut chip thickness (mm)	chip thickness ratio	phi calculated (radians)	phi calculated (degrees)	Psi calculated (degrees)	Psi-calculated (radians)
193	0.009	0.230	0.020	0.498	0.463	0.481	27.554	33	0.576
194	0.008	0.200	0.023	0.591	0.338	0.339	19.414	39	0.681
195	0.010	0.244	0.017	0.424	0.575	0.610	34.928	28	0.489
196	0.009	0.228	0.017	0.436	0.523	0.550	31.512	28	0.489
197	0.008	0.207	0.014	0.360	0.576	0.611	34.985	25	0.436
198	0.008	0.207	0.018	0.468	0.442	0.457	26.171	32	0.559
199	0.008	0.196	0.012	0.311	0.632	0.674	38.641	23	0.401
200	0.008	0.205	0.018	0.447	0.459	0.476	27.286	31	0.541
201	0.009	0.226	0.021	0.528	0.429	0.441	25.280	34	0.593
202	0.006	0.165	0.012	0.298	0.552	0.583	33.426	28	0.489
203	0.005	0.135	0.012	0.295	0.460	0.477	27.340	29	0.506
204	0.007	0.184	0.013	0.338	0.544	0.574	32.912	26	0.454

No.	Friction Force (Newtons)	Normal Force (Newtons)	Friction Force (lb)	Normal Force (lb)	F/N Ratio	Fs Merchant (newtons)	Fn Merchant (newtons)	Fs Merchant (lb)	Fn Merchant (lb)	Fs Payton (newtons)
1	632.803	704.139	142.260	158.297	0.899	638.810	698.694	143.610	157.073	253.860
2	634.937	707.644	142.740	159.085	0.897	681.032	663.400	153.102	149.138	255.669
3	639.865	711.873	143.848	160.035	0.899	657.772	695.361	147.873	156.323	256.588
4	466.611	566.376	104.898	127.326	0.824	559.599	474.718	125.803	106.721	226.966
5	615.741	801.654	138.424	180.219	0.768	887.247	484.335	199.461	108.883	345.271
6	442.522	530.250	99.483	119.205	0.835	545.543	423.525	122.643	95.212	209.441
7	408.286	616.203	91.786	138.528	0.663	590.003	445.310	132.638	100.110	300.328
8	312.272	480.816	70.201	108.092	0.649	451.112	353.830	101.414	79.544	237.733
9	349.126	534.310	78.487	120.118	0.653	530.787	354.459	119.326	79.686	263.047
10	403.906	419.936	90.802	94.405	0.962	347.728	467.516	78.172	105.102	161.722
11	584.431	618.603	131.385	139.067	0.945	514.573	677.823	115.681	152.381	243.510
12	545.056	571.472	122.534	128.472	0.954	513.562	599.934	115.453	134.871	222.381
13	329.954	432.355	74.177	97.197	0.763	444.251	313.754	99.872	70.535	209.453
14	324.623	459.071	72.978	103.203	0.707	466.817	313.381	104.945	70.451	235.256
15	291.792	412.387	65.598	92.708	0.708	423.940	274.736	95.306	61.763	211.241
16	387.497	418.947	87.113	94.183	0.925	461.263	336.016	103.696	75.539	169.070
17	379.543	442.340	85.325	99.442	0.858	448.966	371.681	100.932	83.557	193.306
18	331.935	363.561	74.622	81.732	0.913	341.311	354.774	76.730	79.756	148.886

No.	Friction Force (Newtons)	Normal Force (Newtons)	Friction Force (lb)	Normal Force (lb)	F/N Ratio	F <sub>s</sub> Merchant (newtons)	F <sub>n</sub> Merchant (newtons)	F <sub>s</sub> Merchant (lb)	F <sub>n</sub> Merchant (lb)	F <sub>s</sub> Payton (newtons)
19	462.678	459.199	104.014	103.232	1.008	489.101	430.947	109.954	96.881	193.673
20	482.446	476.940	108.458	107.220	1.012	484.497	474.856	108.919	106.752	200.282
21	508.068	491.939	114.218	110.592	1.033	560.051	431.834	125.904	97.080	201.756
22	317.365	333.242	71.347	74.916	0.952	334.635	315.896	75.229	71.016	149.046
23	318.611	342.247	71.627	76.940	0.931	346.954	313.480	77.998	70.473	156.459
24	336.628	367.568	75.677	82.633	0.916	402.479	293.999	90.481	66.094	170.600
25	374.347	476.108	84.157	107.033	0.786	478.888	370.784	107.658	83.355	249.459
26	298.729	340.332	67.157	76.510	0.878	359.613	275.215	80.844	61.871	163.940
27	341.565	447.848	76.787	100.680	0.763	384.274	411.787	86.388	92.573	239.529
28	1112.448	1324.886	250.088	297.846	0.840	1417.389	991.903	318.642	222.989	519.679
29	1033.048	1206.075	232.239	271.136	0.857	1290.293	925.716	290.069	208.109	462.137
30	1096.447	1281.184	246.491	288.022	0.856	1330.952	1035.470	299.210	232.783	491.419
31	615.737	848.014	138.423	190.641	0.726	808.105	667.252	181.669	150.004	384.372
32	688.122	914.093	154.696	205.496	0.753	874.455	737.840	196.585	165.873	401.211
33	796.692	1115.368	179.103	250.745	0.714	1069.581	857.182	240.451	192.702	512.630
34	589.240	915.230	132.466	205.752	0.644	950.199	531.010	213.613	119.376	455.299
35	786.992	1326.638	176.923	298.240	0.593	1301.808	827.417	292.658	186.011	696.025
36	612.515	1053.809	137.699	236.906	0.581	1084.868	555.652	243.888	124.916	559.669
37	1180.380	1295.628	265.360	291.269	0.911	1299.849	1175.730	292.218	264.315	531.856
38	995.076	1045.851	223.702	235.117	0.951	960.237	1077.927	215.870	242.328	408.196
39	1067.798	1128.279	240.051	253.647	0.946	1161.435	1031.637	261.101	231.921	443.220
40	684.846	803.020	153.960	180.526	0.853	854.377	619.594	192.072	139.290	353.013
41	889.717	1083.580	200.016	243.599	0.821	1097.889	871.998	246.815	196.033	493.549
42	1072.125	1249.189	241.023	280.829	0.858	1294.376	1017.112	290.987	228.656	545.767
43	663.521	983.848	149.165	221.178	0.674	910.908	760.567	204.780	170.982	520.277
44	604.859	875.274	135.978	196.769	0.691	844.858	646.663	189.932	145.376	455.580
45	582.506	843.212	130.953	189.562	0.691	898.635	492.723	202.021	110.768	438.990
46	1009.222	1001.610	226.882	225.171	1.008	1159.111	823.538	260.579	185.139	422.432
47	886.583	801.393	199.312	180.160	1.106	919.858	762.969	206.792	171.522	301.466
48	969.974	892.136	218.059	200.560	1.087	1033.493	817.709	232.339	183.828	343.450
49	685.392	837.421	154.082	188.260	0.818	956.883	505.381	215.116	113.614	426.323
50	585.797	712.940	131.692	160.275	0.822	771.186	506.670	173.370	113.904	361.895

No.	Friction Force (Newtons)	Normal Force (Newtons)	Friction Force (lb)	Normal Force (lb)	F/N Ratio	F <sub>s</sub> Merchant (newtons)	F <sub>n</sub> Merchant (newtons)	F <sub>s</sub> Merchant (lb)	F <sub>n</sub> Merchant (lb)	F <sub>s</sub> Payton (newtons)
51	543.411	643.851	122.164	144.743	0.844	687.141	487.521	154.476	109.599	320.183
52	534.644	645.196	120.193	145.046	0.829	673.326	498.754	151.370	112.124	325.424
53	609.357	584.303	136.989	131.357	1.043	660.025	526.396	148.380	118.339	236.913
54	576.143	591.882	129.522	133.060	0.973	600.309	567.356	134.955	127.547	258.972
55	521.612	615.703	117.263	138.416	0.847	498.299	634.718	112.022	142.690	239.016
56	604.485	724.842	135.894	162.951	0.834	717.134	613.610	161.218	137.945	286.536
57	557.433	673.457	125.316	151.399	0.828	594.458	641.012	133.639	144.105	268.479
58	531.250	729.449	119.430	163.987	0.728	725.661	536.412	163.135	120.590	329.770
59	519.010	661.335	116.678	148.674	0.785	623.349	564.068	140.134	126.807	278.900
60	473.899	666.699	106.537	149.880	0.711	637.629	512.344	143.345	115.180	307.663
61	533.529	732.939	119.942	164.771	0.728	720.608	550.071	161.999	123.661	331.490
62	377.718	531.836	84.914	119.561	0.710	457.744	464.748	102.905	104.480	245.598
63	353.650	472.603	79.504	106.246	0.748	426.743	407.815	95.936	91.680	208.574
64	468.656	478.226	105.358	107.510	0.980	434.870	509.143	97.763	114.460	179.828
65	518.211	558.776	116.498	125.618	0.927	484.859	587.949	109.001	132.176	224.809
66	549.360	592.477	123.501	133.194	0.927	541.487	599.681	121.731	134.814	238.420
67	558.679	586.738	125.596	131.904	0.952	638.848	498.255	143.619	112.012	228.791
68	448.608	490.786	100.851	110.333	0.914	522.594	411.115	117.484	92.422	200.729
69	421.300	521.769	94.712	117.298	0.807	409.469	531.103	92.052	119.397	241.215
70	434.444	619.299	97.667	139.224	0.702	620.059	433.359	139.395	97.423	319.106
71	464.552	642.049	104.435	144.339	0.724	644.410	461.272	144.869	103.698	323.755
72	451.528	599.183	101.508	134.702	0.754	575.607	481.222	129.402	108.183	293.144
73	516.752	466.077	116.170	104.778	1.109	424.797	551.188	95.498	123.912	174.806
74	549.887	503.420	123.620	113.173	1.092	460.172	586.558	103.451	131.863	192.630
75	530.252	469.379	119.206	105.521	1.130	388.534	592.052	87.346	133.099	171.501
76	500.386	401.494	112.491	90.260	1.246	276.358	578.973	62.128	130.158	125.077
77	546.664	476.127	122.895	107.038	1.148	343.539	638.372	77.231	143.512	169.908
78	549.587	456.948	123.552	102.726	1.203	457.153	549.417	102.772	123.514	151.547
79	427.292	517.051	96.059	116.238	0.826	441.610	504.877	99.278	113.501	261.328
80	335.206	341.062	75.357	76.674	0.983	317.227	357.846	71.315	80.447	147.745
81	418.984	473.163	94.191	106.371	0.885	450.053	443.716	101.176	99.751	226.235
82	1222.467	1494.773	274.822	336.038	0.818	1496.507	1220.343	336.428	274.344	603.848

No.	Friction Force (Newtons)	Normal Force (Newtons)	Friction Force (lb)	Normal Force (lb)	F/N Ratio	F <sub>s</sub> Merchant (newtons)	F <sub>n</sub> Merchant (newtons)	F <sub>s</sub> Merchant (lb)	F <sub>n</sub> Merchant (lb)	F <sub>s</sub> Payton (newtons)
83	1078.046	1299.785	242.354	292.203	0.829	1327.094	1044.244	298.343	234.755	516.994
84	1098.903	1331.271	247.043	299.282	0.825	1267.930	1171.419	285.042	263.346	532.342
85	922.159	1205.666	207.310	271.045	0.765	1245.174	868.073	279.926	195.151	521.373
86	748.376	1052.363	168.242	236.581	0.711	1052.782	747.787	236.675	168.109	485.452
87	638.718	824.864	143.589	185.437	0.774	838.123	621.216	188.418	139.655	352.500
88	725.010	1040.871	162.989	233.997	0.697	947.265	843.647	212.954	189.659	488.314
89	694.957	1010.955	156.233	227.272	0.687	878.512	856.278	197.497	192.499	479.230
90	643.628	999.706	144.693	224.743	0.644	794.248	884.782	178.554	198.907	497.323
91	1079.348	1172.859	242.647	263.669	0.920	1190.669	1059.668	267.673	238.223	476.051
92	1057.460	1158.774	237.727	260.503	0.913	1245.070	954.349	279.903	214.546	474.798
93	997.933	1073.438	224.344	241.319	0.930	1006.541	1065.370	226.280	239.505	430.658
94	880.294	1078.830	197.898	242.531	0.816	1203.259	700.686	270.503	157.520	494.147
95	657.139	829.463	147.731	186.471	0.792	835.223	649.802	187.766	146.081	389.767
96	769.453	937.244	172.980	210.701	0.821	966.492	732.378	217.276	164.645	426.950
97	521.304	798.432	117.194	179.495	0.653	793.817	528.305	178.457	118.768	430.811
98	636.997	764.705	143.203	171.912	0.833	677.089	729.444	152.216	163.986	343.755
99	709.510	862.743	159.504	193.952	0.822	749.927	827.853	168.590	186.109	392.403
100	1113.446	1092.464	250.313	245.596	1.019	1154.321	1049.182	259.502	235.866	454.895
101	961.772	898.817	216.215	202.062	1.070	841.060	1012.668	189.078	227.657	353.163
102	962.049	909.300	216.277	204.419	1.058	772.618	1074.907	173.692	241.649	362.334
103	757.178	871.671	170.220	195.959	0.869	799.003	833.500	179.623	187.378	423.555
104	831.183	826.391	186.858	185.780	1.006	682.005	953.235	153.321	214.296	349.220
105	864.112	915.161	194.260	205.736	0.944	861.831	917.309	193.747	206.219	412.755
106	732.787	883.519	164.737	198.623	0.829	916.321	691.331	205.997	155.417	445.328
107	732.588	953.510	164.692	214.358	0.768	979.479	697.486	220.196	156.801	507.502
108	768.232	1048.088	172.706	235.620	0.733	1030.845	791.220	231.743	177.873	574.936
109	236.637	244.497	53.198	54.965	0.968	268.039	209.597	60.257	47.119	79.062
110	200.918	207.497	45.168	46.647	0.968	195.792	212.341	44.016	47.736	67.048
111	216.892	226.798	48.759	50.986	0.956	218.695	225.059	49.165	50.595	74.743
112	166.743	189.736	37.485	42.654	0.879	199.613	154.782	44.875	34.796	70.431
113	166.248	194.204	37.374	43.659	0.856	193.046	167.591	43.399	37.676	74.465
114	183.974	218.574	41.359	49.137	0.842	209.851	193.865	47.176	43.583	85.494
115	180.787	213.126	40.643	47.913	0.848	190.582	204.414	42.845	45.954	82.612

No.	Friction Force (Newtons)	Normal Force (Newtons)	Friction Force (lb)	Normal Force (lb)	F/N Ratio	Fs Merchant (newtons)	Fn Merchant (newtons)	Fs Merchant (lb)	Fn Merchant (lb)	Fs Payton (newtons)
116	173.491	204.977	39.002	46.081	0.846	194.341	185.327	43.690	41.663	79.659
117	169.083	217.808	38.011	48.965	0.776	205.259	184.115	46.144	41.391	92.849
118	154.255	162.416	34.678	36.513	0.950	139.268	175.436	31.309	39.440	54.099
119	140.102	158.511	31.496	35.635	0.884	164.061	133.560	36.882	30.026	58.410
120	158.202	184.090	35.565	41.385	0.859	187.134	154.589	42.069	34.753	70.258
121	179.339	174.700	40.317	39.274	1.027	187.407	166.016	42.131	37.322	61.625
122	182.012	180.409	40.918	40.558	1.009	223.110	126.086	50.157	28.345	65.233
123	191.881	187.195	43.137	42.083	1.025	176.860	201.446	39.760	45.287	66.175
124	162.677	167.925	36.571	37.751	0.969	177.121	152.613	39.818	34.309	64.088
125	159.185	183.863	35.786	41.334	0.866	193.905	146.788	43.592	32.999	79.638
126	155.055	163.719	34.858	36.805	0.947	159.266	159.626	35.804	35.885	64.257
127	150.285	144.083	33.785	32.391	1.043	161.935	130.852	36.405	29.417	49.637
128	194.678	200.254	43.765	45.019	0.972	216.023	177.017	48.564	39.795	76.086
129	190.756	193.876	42.884	43.585	0.984	208.142	175.080	46.792	39.360	72.524
130	149.388	188.229	33.584	42.316	0.794	181.344	157.675	40.768	35.447	88.318
131	117.336	165.441	26.378	37.193	0.709	154.567	131.330	34.748	29.524	84.608
132	128.907	164.472	28.979	36.975	0.784	170.029	121.483	38.224	27.310	77.983
133	394.637	427.029	88.718	96.000	0.924	445.710	373.410	100.200	83.946	148.115
134	356.129	371.855	80.061	83.596	0.958	365.726	362.421	82.218	81.476	122.272
135	390.712	416.399	87.836	93.610	0.938	437.508	366.921	98.356	82.487	141.258
136	321.000	350.939	72.164	78.894	0.915	315.475	355.914	70.922	80.013	123.506
137	299.405	343.294	67.309	77.176	0.872	381.690	248.610	85.807	55.890	128.661
138	303.376	368.948	68.202	82.943	0.822	307.241	365.736	69.071	82.221	148.164
139	279.760	359.997	62.892	80.930	0.777	333.929	310.410	75.070	69.783	153.303
140	232.182	352.656	52.197	79.280	0.658	351.589	233.794	79.040	52.559	172.676
141	230.252	350.475	51.763	78.790	0.657	341.058	243.984	76.673	54.850	171.873
142	198.687	340.318	44.667	76.507	0.584	337.121	204.064	75.788	45.875	180.267
143	219.113	352.883	49.259	79.331	0.621	368.583	191.531	82.861	43.058	179.889
144	224.613	363.369	50.495	81.689	0.618	378.368	198.307	85.061	44.581	185.778
145	315.449	323.190	70.916	72.656	0.976	367.741	262.157	82.672	58.935	122.166
146	434.063	370.733	97.581	83.344	1.171	354.830	447.157	79.769	100.525	104.033
147	461.766	362.650	103.809	81.527	1.273	455.827	370.088	102.474	83.199	83.181
148	228.561	267.983	51.383	60.245	0.853	274.843	220.264	61.787	49.517	117.799
149	253.237	294.891	56.930	66.294	0.859	300.766	246.230	67.615	55.355	128.764
150	230.299	273.134	51.773	61.403	0.843	280.891	220.771	63.147	49.631	121.391

No.	Friction Force (Newtons)	Normal Force (Newtons)	Friction Force (lb)	Normal Force (lb)	F/N Ratio	F <sub>s</sub> Merchant (newtons)	F <sub>n</sub> Merchant (newtons)	F <sub>s</sub> Merchant (lb)	F <sub>n</sub> Merchant (lb)	F <sub>s</sub> Payton (newtons)
151	225.919	275.552	50.789	61.947	0.820	310.804	174.268	69.872	39.177	125.676
152	203.447	261.638	45.737	58.819	0.778	272.473	188.690	61.254	42.419	124.862
153	227.155	284.612	51.067	63.983	0.798	271.807	242.332	61.105	54.478	132.904
154	188.415	279.479	42.357	62.829	0.674	276.661	192.529	62.196	43.282	147.829
155	192.232	294.727	43.215	66.257	0.652	297.258	188.294	66.826	42.330	159.125
156	187.116	271.182	42.065	60.964	0.690	268.368	191.131	60.332	42.968	141.293
157	188.843	242.670	42.454	54.554	0.778	266.395	153.570	59.888	34.524	103.200
158	201.397	260.337	45.276	58.526	0.774	281.116	171.201	63.197	38.487	111.356
159	203.009	261.656	45.638	58.823	0.776	279.543	177.573	62.844	39.920	111.602
160	145.129	213.056	32.626	47.897	0.681	222.139	130.803	49.939	29.406	101.712
161	132.011	200.409	29.677	45.054	0.659	199.727	133.041	44.900	29.909	98.094
162	132.198	202.261	29.719	45.470	0.654	201.883	132.774	45.385	29.849	99.555
163	140.159	197.520	31.509	44.404	0.710	176.370	165.989	39.650	37.316	91.279
164	137.749	223.290	30.967	50.198	0.617	213.022	153.150	47.889	34.430	114.308
165	121.805	213.124	27.383	47.912	0.572	203.444	137.363	45.736	30.880	114.301
166	99.446	181.770	22.356	40.864	0.547	186.961	89.307	42.030	20.077	99.871
167	120.920	217.876	27.184	48.980	0.555	222.084	113.006	49.926	25.405	118.784
168	105.393	197.544	23.693	44.410	0.534	190.776	117.199	42.888	26.347	109.979
169	174.716	209.872	39.278	47.181	0.832	238.918	132.251	53.711	29.731	94.397
170	173.528	208.568	39.011	46.888	0.832	227.082	148.480	51.050	33.380	93.861
171	171.765	207.224	38.614	46.586	0.829	239.333	123.146	53.804	27.684	93.579
172	113.611	162.486	25.541	36.528	0.699	153.711	125.228	34.556	28.152	83.912
173	113.470	155.726	25.509	35.009	0.729	152.293	118.037	34.237	26.536	78.128
174	116.073	171.791	26.094	38.620	0.676	170.012	118.664	38.220	26.677	90.739
175	136.897	196.018	30.776	44.067	0.698	165.214	172.824	37.142	38.852	101.308
176	133.017	183.300	29.903	41.208	0.726	181.552	135.394	40.814	30.438	92.234
177	137.171	194.742	30.837	43.780	0.704	186.191	148.570	41.857	33.400	100.066
178	116.035	168.126	26.086	37.796	0.690	174.891	105.562	39.317	23.731	87.584
179	133.591	187.321	30.032	42.111	0.713	198.162	116.908	44.549	26.282	95.429
180	138.926	191.316	31.232	43.010	0.726	203.527	120.329	45.755	27.051	96.222
181	317.488	435.390	71.374	97.880	0.729	459.002	282.276	103.188	63.458	196.618
182	319.782	443.149	71.890	99.624	0.722	448.724	311.911	100.877	70.120	201.930
183	336.889	474.187	75.736	106.601	0.710	466.824	347.020	104.946	78.013	218.915
184	220.568	364.374	49.586	81.914	0.605	356.609	232.913	80.169	52.361	188.799

No.	Friction Force (Newtons)	Normal Force (Newtons)	Friction Force (lb)	Normal Force (lb)	F/N Ratio	Fs Merchant (newtons)	Fn Merchant (newtons)	Fs Merchant (lb)	Fn Merchant (lb)	Fs Payton (newtons)
185	217.139	348.783	48.815	78.410	0.623	324.979	251.373	73.058	56.511	177.492
186	215.067	353.544	48.349	79.480	0.608	368.573	188.152	82.858	42.298	182.621
187	197.881	370.707	44.485	83.338	0.534	382.624	173.722	86.017	39.054	206.330
188	203.690	383.076	45.791	86.119	0.532	378.075	212.830	84.995	47.846	213.641
189	215.837	375.006	48.522	84.305	0.576	356.450	245.272	80.133	55.139	200.308
190	234.396	394.255	52.694	88.632	0.595	425.502	171.251	95.657	38.499	206.571
191	245.419	407.340	55.172	91.574	0.602	427.587	208.147	96.125	46.793	211.683
192	193.900	372.937	43.590	83.840	0.520	367.579	203.874	82.635	45.833	210.350
193	271.027	347.203	60.929	78.054	0.781	358.452	255.964	80.583	57.543	165.173
194	278.191	357.249	62.540	80.313	0.779	402.277	207.824	90.435	46.721	170.292
195	291.986	371.948	65.641	83.617	0.785	345.488	322.861	77.669	72.582	176.123
196	192.168	309.952	43.201	69.680	0.620	304.775	200.278	68.516	45.024	172.343
197	196.692	315.286	44.218	70.879	0.624	297.002	223.345	66.769	50.210	174.700
198	197.771	325.751	44.461	73.232	0.607	338.231	175.577	76.037	39.471	183.223
199	184.965	298.164	41.582	67.030	0.620	266.989	227.664	60.021	51.181	165.736
200	180.447	295.797	40.566	66.498	0.610	304.010	166.236	68.344	37.371	165.944
201	185.676	294.908	41.742	66.298	0.630	309.185	160.781	69.508	36.145	162.560
202	184.399	283.094	41.455	63.642	0.651	271.567	200.989	61.051	45.184	152.968
203	174.090	265.099	39.137	59.597	0.657	272.891	161.602	61.348	36.330	142.537
204	200.488	319.913	45.071	71.919	0.627	309.313	216.482	69.536	48.667	176.809

No.	Fs Payton (lbf)	Fn Payton (newtons)	Fn Payton (lbf)	Fs/Fn Payton (newtons)	Beta (degrees)	Shear Area, As Merchant (in^2)	Shear Area, As Payton (in^2)	Shear Area, As Chandrasekaran (in^2)	Shear Area, As Merchant (mm^2)
1	57.070	912.034	205.034	0.278	41.946	0.001	0.001	0.001	0.633
2	57.477	915.717	205.861	0.279	41.900	0.001	0.001	0.002	0.702
3	57.683	922.146	207.307	0.278	41.951	0.001	0.001	0.002	0.652
4	51.024	697.849	156.883	0.325	39.484	0.001	0.001	0.001	0.741
5	77.620	950.039	213.577	0.363	37.527	0.002	0.002	0.003	1.163
6	47.084	658.122	147.952	0.318	39.847	0.001	0.001	0.002	0.826
7	67.517	675.431	151.843	0.445	33.528	0.001	0.001	0.002	0.676
8	53.445	521.710	117.285	0.456	33.002	0.001	0.001	0.002	0.643
9	59.135	581.534	130.734	0.452	33.161	0.001	0.001	0.001	0.747

No.	Fs Payton (lbf)	Fn Payton (newtons)	Fn Payton (lbf)	Fs/Fn Payton (newtons)	Beta (degrees)	Shear Area, As Merchant (in^2)	Shear Area, As Payton (in^2)	Shear Area, As Chandrasekaran (in^2)	Shear Area, As Merchant (mm^2)
10	36.357	559.761	125.839	0.289	43.885	0.001	0.001	0.001	0.507
11	54.743	815.433	183.317	0.299	43.373	0.001	0.001	0.001	0.508
12	49.993	757.769	170.353	0.293	43.645	0.001	0.001	0.001	0.552
13	47.087	501.926	112.837	0.417	37.349	0.001	0.001	0.001	0.690
14	52.888	510.667	114.803	0.461	35.265	0.001	0.001	0.001	0.674
15	47.489	458.893	103.163	0.460	35.282	0.001	0.001	0.001	0.695
16	38.008	545.056	122.533	0.310	42.767	0.001	0.001	0.001	0.815
17	43.457	549.864	123.614	0.352	40.631	0.001	0.001	0.001	0.666
18	33.471	469.245	105.491	0.317	42.396	0.001	0.001	0.001	0.581
19	43.539	622.435	139.929	0.311	45.216	0.001	0.001	0.002	0.623
20	45.025	648.161	145.712	0.309	45.329	0.001	0.001	0.001	0.575
21	45.356	677.814	152.379	0.298	45.924	0.001	0.001	0.002	0.718
22	33.507	435.380	97.877	0.342	43.602	0.001	0.001	0.001	0.566
23	35.173	440.644	99.061	0.355	42.952	0.001	0.001	0.001	0.575
24	38.352	468.317	105.282	0.364	42.484	0.001	0.001	0.002	0.673
25	56.081	551.892	124.070	0.452	38.177	0.001	0.001	0.001	0.568
26	36.855	422.124	94.897	0.388	41.275	0.001	0.001	0.001	0.624
27	53.848	509.765	114.600	0.470	37.332	0.001	0.001	0.001	0.459
28	116.829	1650.089	370.955	0.315	40.019	0.003	0.003	0.003	1.889
29	103.892	1519.288	341.550	0.304	40.581	0.003	0.003	0.003	1.879
30	110.475	1613.114	362.643	0.305	40.557	0.003	0.003	0.004	1.698
31	86.410	974.944	219.176	0.394	35.983	0.002	0.002	0.003	1.349
32	90.196	1071.498	240.882	0.374	36.972	0.002	0.002	0.002	1.366
33	115.244	1271.210	285.779	0.403	35.538	0.002	0.002	0.003	1.367
34	102.355	988.712	222.271	0.460	32.774	0.003	0.003	0.004	1.766
35	156.473	1376.544	309.460	0.506	30.677	0.002	0.002	0.004	1.433
36	125.819	1082.801	243.424	0.517	30.167	0.003	0.003	0.004	1.726
37	119.566	1670.053	375.443	0.318	42.335	0.002	0.002	0.003	1.298
38	91.766	1384.687	311.290	0.295	43.575	0.002	0.002	0.002	1.132
39	99.640	1488.879	334.714	0.298	43.422	0.002	0.002	0.002	1.366
40	79.360	994.605	223.596	0.355	40.459	0.002	0.002	0.003	1.499
41	110.954	1312.307	295.019	0.376	39.389	0.002	0.002	0.003	1.328
42	122.693	1553.082	349.147	0.351	40.638	0.002	0.002	0.003	1.396
43	116.963	1066.550	239.770	0.488	33.996	0.002	0.002	0.002	1.101
44	102.418	961.460	216.145	0.474	34.646	0.002	0.002	0.003	1.191
45	98.689	926.071	208.189	0.474	34.637	0.002	0.002	0.003	1.580
46	94.967	1357.683	305.219	0.311	45.217	0.002	0.002	0.002	1.517
47	67.772	1156.451	259.981	0.261	47.889	0.002	0.002	0.003	1.432

No.	Fs Payton (lbf)	Fn Payton (newtons)	Fn Payton (lbf)	Fs/Fn Payton (newtons)	Beta (degrees)	Shear Area, As Merchant (in^2)	Shear Area, As Payton (in^2)	Shear Area, As Chandrasekaran (in^2)	Shear Area, As Merchant (mm^2)
48	77.211	1272.320	286.029	0.270	47.394	0.002	0.002	0.002	1.474
49	95.841	994.628	223.601	0.429	39.299	0.003	0.003	0.003	1.615
50	81.357	848.807	190.820	0.426	39.409	0.002	0.002	0.002	1.335
51	71.980	779.309	175.196	0.411	40.164	0.002	0.002	0.002	1.283
52	73.158	772.154	173.587	0.421	39.647	0.002	0.002	0.002	1.222
53	53.260	810.307	182.164	0.292	46.202	0.002	0.002	0.002	1.403
54	58.219	784.346	176.328	0.330	44.228	0.002	0.002	0.002	1.149
55	53.733	770.740	173.269	0.310	40.271	0.001	0.001	0.002	0.535
56	64.416	899.275	202.165	0.319	39.827	0.001	0.001	0.002	0.734
57	60.357	831.982	187.037	0.323	39.615	0.001	0.001	0.001	0.592
58	74.135	839.984	188.836	0.393	36.065	0.001	0.001	0.002	0.743
59	62.699	793.064	178.288	0.352	38.125	0.001	0.001	0.002	0.657
60	69.165	757.899	170.383	0.406	35.406	0.001	0.001	0.002	0.671
61	74.522	843.782	189.690	0.393	36.052	0.001	0.001	0.002	0.719
62	55.213	604.320	135.856	0.406	35.383	0.001	0.001	0.001	0.555
63	46.889	552.195	124.138	0.378	36.808	0.001	0.001	0.001	0.603
64	40.427	644.981	144.998	0.279	44.421	0.001	0.001	0.001	0.555
65	50.539	728.171	163.699	0.309	42.843	0.001	0.001	0.001	0.522
66	53.599	771.998	173.552	0.309	42.837	0.001	0.001	0.001	0.555
67	51.434	777.200	174.722	0.294	43.597	0.001	0.001	0.002	0.773
68	45.126	633.899	142.506	0.317	42.429	0.001	0.001	0.001	0.733
69	54.227	625.740	140.672	0.385	38.919	0.001	0.001	0.001	0.463
70	71.738	685.889	154.194	0.465	35.050	0.001	0.001	0.002	0.639
71	72.783	723.338	162.613	0.448	35.887	0.001	0.001	0.001	0.643
72	65.901	690.626	155.259	0.424	37.001	0.001	0.001	0.002	0.587
73	39.298	673.575	151.426	0.260	47.952	0.001	0.001	0.001	0.502
74	43.305	720.210	161.910	0.267	47.526	0.001	0.001	0.001	0.503
75	38.555	687.075	154.461	0.250	48.485	0.001	0.001	0.001	0.465
76	28.119	629.237	141.458	0.199	51.258	0.001	0.001	0.001	0.427
77	38.197	704.748	158.434	0.241	48.945	0.001	0.001	0.001	0.430
78	34.069	698.485	157.026	0.217	50.259	0.001	0.001	0.001	0.556
79	58.749	617.760	138.878	0.423	39.570	0.001	0.001	0.001	0.457
80	33.214	454.816	102.247	0.325	44.504	0.001	0.001	0.001	0.507
81	50.860	590.126	132.666	0.383	41.525	0.001	0.001	0.001	0.517
82	135.750	1834.159	412.336	0.329	39.277	0.002	0.002	0.003	1.513
83	116.225	1607.589	361.400	0.322	39.672	0.002	0.002	0.002	1.597
84	119.675	1642.096	369.158	0.324	39.538	0.002	0.002	0.003	1.349
85	117.209	1425.545	320.475	0.366	37.411	0.003	0.003	0.003	1.668

No.	Fs Payton (lbf)	Fn Payton (newtons)	Fn Payton (lbf)	Fs/Fn Payton (newtons)	Beta (degrees)	Shear Area, As Merchant (in^2)	Shear Area, As Payton (in^2)	Shear Area, As Chandrasekaran (in^2)	Shear Area, As Merchant (mm^2)
86	109.134	1196.608	269.008	0.406	35.418	0.002	0.002	0.003	1.510
87	79.245	981.888	220.737	0.359	37.752	0.002	0.002	0.003	1.580
88	109.777	1170.727	263.190	0.417	34.859	0.002	0.002	0.002	1.209
89	107.735	1129.307	253.878	0.424	34.506	0.002	0.002	0.002	1.118
90	111.803	1079.972	242.787	0.460	32.774	0.002	0.002	0.002	0.985
91	107.021	1521.172	341.973	0.313	42.622	0.002	0.002	0.003	1.313
92	106.739	1495.175	336.129	0.318	42.383	0.002	0.002	0.002	1.503
93	96.816	1400.954	314.947	0.307	42.912	0.002	0.002	0.002	1.148
94	111.089	1301.772	292.650	0.380	39.213	0.003	0.003	0.003	1.779
95	87.623	983.830	221.174	0.396	38.388	0.002	0.002	0.002	1.295
96	95.982	1134.987	255.155	0.376	39.385	0.002	0.002	0.002	1.368
97	96.850	850.679	191.240	0.506	33.141	0.002	0.002	0.003	1.256
98	77.279	934.008	209.973	0.368	39.794	0.002	0.002	0.002	1.051
99	88.216	1045.825	235.111	0.375	39.433	0.002	0.002	0.002	1.026
100	102.265	1492.083	335.434	0.305	45.545	0.002	0.002	0.002	1.212
101	79.394	1268.130	285.087	0.278	46.938	0.002	0.002	0.002	1.027
102	81.456	1273.216	286.230	0.285	46.615	0.001	0.001	0.002	0.940
103	95.219	1074.118	241.471	0.394	40.979	0.002	0.002	0.002	0.987
104	78.508	1118.853	251.528	0.312	45.166	0.001	0.001	0.001	0.913
105	92.791	1189.051	267.309	0.347	43.357	0.002	0.002	0.002	1.026
106	100.114	1057.954	237.838	0.421	39.672	0.002	0.002	0.002	1.191
107	114.091	1090.095	245.063	0.466	37.535	0.002	0.002	0.002	1.173
108	129.251	1165.384	261.989	0.493	36.241	0.002	0.002	0.002	1.078
109	17.774	330.945	74.400	0.239	44.064	0.002	0.002	0.003	0.987
110	15.073	280.940	63.158	0.239	44.077	0.001	0.001	0.002	0.678
111	16.803	304.783	68.518	0.245	43.721	0.001	0.001	0.002	0.704
112	15.833	242.574	54.533	0.290	41.309	0.001	0.001	0.002	0.876
113	16.740	244.558	54.979	0.304	40.565	0.002	0.002	0.002	1.495
114	19.220	272.602	61.283	0.314	40.087	0.002	0.002	0.002	1.382
115	18.572	266.987	60.021	0.309	40.307	0.002	0.002	0.001	1.220
116	17.908	256.454	57.653	0.311	40.244	0.002	0.002	0.002	1.348
117	20.873	259.632	58.368	0.358	37.822	0.002	0.002	0.001	1.320
118	12.162	217.363	48.865	0.249	43.524	0.002	0.002	0.001	1.176
119	13.131	203.329	45.710	0.287	41.472	0.003	0.003	0.002	1.663
120	15.795	232.338	52.232	0.302	40.675	0.002	0.002	0.002	1.584
121	13.854	242.662	54.553	0.254	45.751	0.001	0.001	0.002	0.737
122	14.665	247.832	55.715	0.263	45.253	0.002	0.002	0.003	1.305
123	14.877	259.771	58.399	0.255	45.708	0.001	0.001	0.001	0.589

No.	Fs Payton (lbf)	Fn Payton (newtons)	Fn Payton (lbf)	Fs/Fn Payton (newtons)	Beta (degrees)	Shear Area, As Merchant (in^2)	Shear Area, As Payton (in^2)	Shear Area, As Chandrasekaran (in^2)	Shear Area, As Merchant (mm^2)
124	14.408	224.845	50.547	0.285	44.091	0.001	0.001	0.002	0.715
125	17.903	229.790	51.659	0.347	40.885	0.001	0.001	0.002	0.725
126	14.446	216.141	48.590	0.297	43.443	0.001	0.001	0.001	0.612
127	11.159	202.192	45.455	0.245	46.207	0.001	0.001	0.002	0.830
128	17.105	268.723	60.411	0.283	44.191	0.001	0.001	0.002	0.755
129	16.304	262.138	58.931	0.277	44.535	0.001	0.001	0.002	0.744
130	19.855	223.488	50.242	0.395	38.437	0.001	0.001	0.001	0.596
131	19.021	184.337	41.441	0.459	35.345	0.001	0.001	0.001	0.559
132	17.531	193.873	43.584	0.402	38.088	0.001	0.001	0.002	0.695
133	33.298	562.276	126.405	0.263	42.742	0.003	0.003	0.003	1.696
134	27.488	500.154	112.439	0.244	43.762	0.002	0.002	0.003	1.464
135	31.756	553.255	124.377	0.255	43.177	0.003	0.003	0.004	1.726
136	27.765	459.288	103.252	0.269	42.449	0.002	0.002	0.003	1.245
137	28.924	436.967	98.234	0.294	41.093	0.003	0.003	0.005	2.195
138	33.309	454.101	102.086	0.326	39.430	0.002	0.002	0.002	1.103
139	34.464	429.373	96.527	0.357	37.851	0.002	0.002	0.002	1.280
140	38.819	385.302	86.619	0.448	33.360	0.002	0.002	0.003	1.503
141	38.639	382.502	85.990	0.449	33.304	0.002	0.002	0.003	1.399
142	40.526	350.424	78.778	0.514	30.278	0.002	0.002	0.002	1.468
143	40.441	374.402	84.169	0.480	31.837	0.003	0.003	0.002	1.821
144	41.765	384.675	86.478	0.483	31.722	0.003	0.003	0.003	1.795
145	27.464	434.782	97.743	0.281	44.306	0.003	0.003	0.003	1.775
146	23.387	561.276	126.180	0.185	49.499	0.002	0.002	0.002	1.208
147	18.700	581.227	130.665	0.143	51.856	0.003	0.003	0.004	2.166
148	26.482	331.931	74.621	0.355	40.461	0.002	0.002	0.002	1.355
149	28.947	366.755	82.450	0.351	40.654	0.002	0.002	0.002	1.337
150	27.290	336.011	75.538	0.361	40.137	0.002	0.002	0.002	1.365
151	28.253	333.428	74.958	0.377	39.348	0.003	0.003	0.004	1.881
152	28.070	307.009	69.018	0.407	37.868	0.002	0.002	0.002	1.421
153	29.878	339.028	76.217	0.392	38.594	0.002	0.002	0.002	1.174
154	33.233	302.912	68.097	0.488	33.986	0.002	0.002	0.002	1.251
155	35.773	313.841	70.554	0.507	33.114	0.002	0.002	0.002	1.313
156	31.764	297.639	66.912	0.475	34.606	0.002	0.002	0.002	1.250
157	23.200	289.655	65.117	0.356	37.890	0.002	0.002	0.002	1.125
158	25.034	309.735	69.631	0.360	37.725	0.002	0.002	0.002	1.035
159	25.089	311.804	70.096	0.358	37.807	0.002	0.002	0.002	0.984
160	22.866	236.875	53.252	0.429	34.262	0.001	0.001	0.002	0.912
161	22.052	219.017	49.237	0.448	33.373	0.001	0.001	0.002	0.773

No.	Fs Payton (lbf)	Fn Payton (newtons)	Fn Payton (lbf)	Fs/Fn Payton (newtons)	Beta (degrees)	Shear Area, As Merchant (in^2)	Shear Area, As Payton (in^2)	Shear Area, As Chandrasekaran (in^2)	Shear Area, As Merchant (mm^2)
162	22.381	220.169	49.496	0.452	33.169	0.001	0.001	0.002	0.777
163	20.520	224.336	50.433	0.407	35.359	0.001	0.001	0.002	0.608
164	25.698	236.150	53.089	0.484	31.671	0.001	0.001	0.001	0.680
165	25.696	217.240	48.838	0.526	29.749	0.001	0.001	0.002	0.675
166	22.452	181.537	40.811	0.550	28.683	0.001	0.001	0.002	0.888
167	26.704	219.047	49.244	0.542	29.030	0.001	0.001	0.002	0.848
168	24.724	195.027	43.844	0.564	28.081	0.001	0.001	0.001	0.693
169	21.221	256.245	57.606	0.368	39.777	0.002	0.002	0.002	1.005
170	21.101	254.563	57.228	0.369	39.760	0.001	0.001	0.002	0.831
171	21.037	252.365	56.734	0.371	39.655	0.002	0.002	0.002	1.094
172	18.864	179.633	40.383	0.467	34.961	0.001	0.001	0.001	0.588
173	17.564	176.131	39.596	0.444	36.079	0.001	0.001	0.001	0.629
174	20.399	186.418	41.908	0.487	34.046	0.001	0.001	0.001	0.644
175	22.775	216.566	48.686	0.468	34.930	0.001	0.001	0.001	0.500
176	20.735	206.846	46.501	0.446	35.968	0.001	0.001	0.001	0.646
177	22.496	216.164	48.596	0.463	35.160	0.001	0.001	0.001	0.600
178	19.690	184.552	41.489	0.475	34.612	0.001	0.001	0.002	0.740
179	21.453	209.354	47.065	0.456	35.495	0.001	0.001	0.002	0.780
180	21.632	215.971	48.552	0.446	35.986	0.001	0.001	0.002	0.793
181	44.201	501.702	112.787	0.392	36.100	0.003	0.003	0.003	1.887
182	45.396	507.805	114.159	0.398	35.815	0.003	0.003	0.003	1.625
183	49.214	538.910	121.152	0.406	35.392	0.002	0.002	0.003	1.495
184	42.444	381.803	85.833	0.494	31.188	0.002	0.002	0.003	1.457
185	39.902	370.535	83.300	0.479	31.905	0.002	0.002	0.003	1.290
186	41.055	371.344	83.482	0.492	31.313	0.003	0.003	0.003	1.866
187	46.385	366.071	82.296	0.564	28.093	0.003	0.003	0.003	1.817
188	48.028	377.617	84.892	0.566	28.001	0.002	0.002	0.003	1.487
189	45.031	383.526	86.220	0.522	29.923	0.002	0.002	0.002	1.337
190	46.439	409.521	92.064	0.504	30.733	0.004	0.004	0.004	2.369
191	47.588	425.847	95.734	0.497	31.069	0.003	0.003	0.004	1.942
192	47.288	363.912	81.811	0.578	27.471	0.002	0.002	0.003	1.478
193	37.132	408.317	91.793	0.405	37.976	0.002	0.002	0.003	1.428
194	38.283	419.545	94.317	0.406	37.908	0.003	0.003	0.003	1.988
195	39.594	438.842	98.656	0.401	38.133	0.002	0.002	0.002	1.154
196	38.744	321.398	72.253	0.536	31.799	0.002	0.002	0.002	1.264
197	39.274	327.983	73.734	0.533	31.958	0.002	0.002	0.002	1.152
198	41.190	334.151	75.120	0.548	31.263	0.002	0.002	0.003	1.498
199	37.259	309.266	69.526	0.536	31.813	0.002	0.002	0.002	1.058

No.	Fs Payton (lbf)	Fn Payton (newtons)	Fn Payton (lbf)	Fs/Fn Payton (newtons)	Beta (degrees)	Shear Area, As Merchant (in^2)	Shear Area, As Payton (in^2)	Shear Area, As Chandrasekaran (in^2)	Shear Area, As Merchant (mm^2)
200	37.306	304.170	68.380	0.546	31.385	0.002	0.002	0.003	1.441
201	36.545	308.254	69.298	0.527	32.195	0.002	0.002	0.003	1.547
202	34.388	301.241	67.722	0.508	33.079	0.001	0.001	0.002	0.600
203	32.044	283.316	63.692	0.503	33.293	0.002	0.002	0.002	1.438
204	39.748	333.584	74.993	0.530	32.075	0.004	0.004	0.002	2.432

No .	Shear Area, As Payton (mm^2 )	Shear Area, As Chandrasekaran (mm^2)	Shear Stress Ts Merchant (MPa)	Shear Stress, Ts Payton (MPa)	Shear Stress, Ts Chandrasekaran (MPa)	Shear Stress Ts Merchant (ksi)	Shear Stress, Ts Payton (ksi)	Shear Stress, Ts Chandrasekaran (ksi)	Friction Co-efficient
1	0.633	0.926	1008.593	400.809	274.195	146.246	58.117	39.758	0.732
2	0.702	1.106	969.887	364.110	231.078	140.634	52.796	33.506	0.731
3	0.652	1.043	1008.449	393.383	245.931	146.225	57.040	35.660	0.732
4	0.741	0.955	755.702	306.503	237.616	109.577	44.443	34.454	0.689
5	1.163	1.786	762.840	296.858	193.357	110.612	43.044	28.037	0.655
6	0.826	1.051	660.165	253.446	199.279	95.724	36.750	28.895	0.695
7	0.676	1.294	873.183	444.475	232.103	126.612	64.449	33.655	0.585
8	0.643	1.076	701.480	369.675	220.914	101.715	53.603	32.032	0.576
9	0.747	0.814	710.292	352.006	322.987	102.992	51.041	46.833	0.579
10	0.507	0.580	685.284	318.713	278.989	99.366	46.213	40.453	0.766
11	0.508	0.811	1013.001	479.380	300.098	146.885	69.510	43.514	0.757
12	0.552	0.794	931.070	403.169	280.072	135.005	58.460	40.610	0.762
13	0.690	0.756	644.053	303.655	276.891	93.388	44.030	40.149	0.652
14	0.674	0.897	692.926	349.205	262.184	100.474	50.635	38.017	0.615
15	0.695	0.772	610.158	304.030	273.650	88.473	44.084	39.679	0.616
16	0.815	0.935	565.723	207.359	180.788	82.030	30.067	26.214	0.746
17	0.666	0.854	674.529	290.424	226.408	97.807	42.112	32.829	0.709
18	0.581	0.809	587.241	256.165	184.083	85.150	37.144	26.692	0.740
19	0.623	1.158	784.694	310.722	167.191	113.781	45.055	24.243	0.789
20	0.575	0.714	841.948	348.046	280.469	122.083	50.467	40.668	0.791
21	0.718	0.995	780.373	281.126	202.802	113.154	40.763	29.406	0.802
22	0.566	0.653	591.267	263.350	228.239	85.734	38.186	33.095	0.761
23	0.575	0.960	603.727	272.250	163.026	87.540	39.476	23.639	0.750

No .	<b>Shear Area, As Payton (mm<sup>2</sup>)</b>	<b>Shear Area, As Chandrase karan (mm<sup>2</sup>)</b>	<b>Shear Stress Ts Merchant (MPa)</b>	<b>Shear Stress, Ts Payton (MPa)</b>	<b>Shear Stress, Ts Chandrase karan (MPa)</b>	<b>Shear Stress Ts Merchant (ksi)</b>	<b>Shear Stress, Ts Payton (ksi)</b>	<b>Shear Stress, Ts Chandras ekaran (ksi)</b>	<b>Friction Co-efficient</b>
24	0.673	1.014	598.459	253.670	168.296	86.777	36.782	24.403	0.741
25	0.568	0.954	842.408	438.820	261.572	122.149	63.629	37.928	0.666
26	0.624	0.762	576.697	262.905	215.100	83.621	38.121	31.189	0.720
27	0.459	0.662	837.142	521.815	361.752	121.386	75.663	52.454	0.652
28	1.889	2.220	750.179	275.050	234.102	108.776	39.882	33.945	0.698
29	1.879	2.223	686.522	245.887	207.921	99.546	35.654	30.149	0.708
30	1.698	2.365	783.659	289.345	207.785	113.630	41.955	30.129	0.708
31	1.349	1.765	598.889	284.860	217.816	86.839	41.305	31.583	0.628
32	1.366	1.593	640.177	293.722	251.901	92.826	42.590	36.526	0.645
33	1.367	1.935	782.697	375.132	264.864	113.491	54.394	38.405	0.620
34	1.766	2.470	537.973	257.776	184.324	78.006	37.377	26.727	0.572
35	1.433	2.383	908.598	485.791	292.128	131.747	70.440	42.359	0.535
36	1.726	2.677	628.667	324.321	209.097	91.157	47.027	30.319	0.527
37	1.298	1.964	1001.126	409.628	270.751	145.163	59.396	39.259	0.739
38	1.132	1.251	847.937	360.457	326.237	122.951	52.266	47.304	0.761
39	1.366	1.490	850.435	324.538	297.492	123.313	47.058	43.136	0.758
40	1.499	1.906	569.928	235.484	185.247	82.640	34.145	26.861	0.706
41	1.328	1.836	826.814	371.689	268.774	119.888	53.895	38.972	0.687
42	1.396	2.223	927.082	390.899	245.485	134.427	56.680	35.595	0.709
43	1.101	1.502	827.188	472.459	346.317	119.942	68.506	50.216	0.593
44	1.191	1.651	709.084	382.365	275.913	102.817	55.443	40.007	0.605
45	1.580	2.150	568.726	277.827	204.166	82.465	40.285	29.604	0.605
46	1.517	1.478	764.301	278.546	285.869	110.824	40.389	41.451	0.789
47	1.432	1.640	642.510	210.570	183.857	93.164	30.533	26.659	0.836
48	1.474	1.566	701.172	233.013	219.368	101.670	33.787	31.808	0.827
49	1.615	1.981	592.413	263.939	215.164	85.900	38.271	31.199	0.686
50	1.335	1.470	577.618	271.059	246.244	83.755	39.304	35.705	0.688
51	1.283	1.329	535.606	249.573	240.861	77.663	36.188	34.925	0.701
52	1.222	1.144	551.222	266.411	284.388	79.927	38.630	41.236	0.692
53	1.403	1.608	470.349	168.830	147.309	68.201	24.480	21.360	0.806
54	1.149	1.330	522.410	225.366	194.741	75.749	32.678	28.237	0.772

No .	<b>Shear Area, As Payton (mm<sup>2</sup>)</b>	<b>Shear Area, As Chandrase karan (mm<sup>2</sup>)</b>	<b>Shear Stress Ts Merchant (MPa)</b>	<b>Shear Stress, Ts Payton (MPa)</b>	<b>Shear Stress, Ts Chandrase karan (MPa)</b>	<b>Shear Stress Ts Merchant (ksi)</b>	<b>Shear Stress, Ts Payton (ksi)</b>	<b>Shear Stress, Ts Chandras ekaran (ksi)</b>	<b>Friction Co-efficient</b>
55	0.535	0.973	932.081	447.086	245.523	135.152	64.827	35.601	0.703
56	0.734	1.087	976.676	390.238	263.698	141.618	56.585	38.236	0.695
57	0.592	0.862	1003.347	453.149	311.369	145.485	65.707	45.149	0.691
58	0.743	1.381	976.865	443.927	238.794	141.645	64.369	34.625	0.629
59	0.657	1.009	948.736	424.486	276.466	137.567	61.550	40.088	0.665
60	0.671	1.026	950.846	458.793	299.995	137.873	66.525	43.499	0.618
61	0.719	1.527	1001.936	460.905	217.107	145.281	66.831	31.481	0.629
62	0.555	0.601	824.864	442.572	408.524	119.605	64.173	59.236	0.618
63	0.603	0.874	707.429	345.762	238.681	102.577	50.135	34.609	0.642
64	0.555	0.616	784.145	324.260	292.060	113.701	47.018	42.349	0.775
65	0.522	0.622	929.194	430.828	361.488	134.733	62.470	52.416	0.748
66	0.555	0.726	976.492	429.956	328.532	141.591	62.344	47.637	0.748
67	0.773	1.326	826.625	296.039	172.501	119.861	42.926	25.013	0.761
68	0.733	0.757	712.686	273.744	265.140	103.340	39.693	38.445	0.741
69	0.463	0.511	883.560	520.498	472.159	128.116	75.472	68.463	0.679
70	0.639	1.001	969.813	499.103	318.807	140.623	72.370	46.227	0.612
71	0.643	0.958	1002.028	503.425	337.865	145.294	72.997	48.990	0.626
72	0.587	0.968	980.892	499.546	302.700	142.229	72.434	43.891	0.646
73	0.502	0.606	846.501	348.339	288.323	122.743	50.509	41.807	0.837
74	0.503	0.600	915.661	383.299	320.995	132.771	55.578	46.544	0.829
75	0.465	0.465	835.148	368.638	368.727	121.096	53.453	53.465	0.846
76	0.427	0.563	646.680	292.681	222.201	93.769	42.439	32.219	0.895
77	0.430	0.665	798.114	394.732	255.683	115.727	57.236	37.074	0.854
78	0.556	0.611	822.294	272.591	247.891	119.233	39.526	35.944	0.877
79	0.457	0.666	966.939	572.199	392.287	140.206	82.969	56.882	0.691
80	0.507	0.534	625.576	291.355	276.926	90.709	42.247	40.154	0.777
81	0.517	0.619	870.722	437.700	365.520	126.255	63.467	53.000	0.725
82	1.513	1.862	989.186	399.141	324.331	143.432	57.875	47.028	0.686
83	1.597	1.505	831.040	323.747	343.506	120.501	46.943	49.808	0.692
84	1.349	1.652	939.866	394.604	322.173	136.281	57.218	46.715	0.690
85	1.668	2.006	746.663	312.639	259.911	108.266	45.333	37.687	0.653

No .	Shear Area, As Payton (mm^2 )	Shear Area, As Chandrase karan (mm^2)	Shear Stress Ts Merchant (MPa)	Shear Stress, Ts Payton (MPa)	Shear Stress, Ts Chandrase karan (MPa)	Shear Stress Ts Merchant (ksi)	Shear Stress, Ts Payton (ksi)	Shear Stress, Ts Chandras ekaran (ksi)	Friction Co-efficient
86	1.510	1.830	697.172	321.475	265.231	101.090	46.614	38.458	0.618
87	1.580	1.813	530.486	223.113	194.383	76.920	32.351	28.185	0.659
88	1.209	1.578	783.766	404.030	309.433	113.646	58.584	44.868	0.608
89	1.118	1.158	785.788	428.649	413.711	113.939	62.154	59.988	0.602
90	0.985	0.993	806.129	504.762	501.021	116.889	73.191	72.648	0.572
91	1.313	1.713	906.911	362.600	277.980	131.502	52.577	40.307	0.744
92	1.503	1.587	828.209	315.831	299.230	120.090	45.795	43.388	0.740
93	1.148	1.397	876.471	375.006	308.216	127.088	54.376	44.691	0.749
94	1.779	1.988	676.488	277.816	248.507	98.091	40.283	36.034	0.684
95	1.295	1.258	645.133	301.059	309.760	93.544	43.654	44.915	0.670
96	1.368	1.429	706.429	312.067	298.713	102.432	45.250	43.313	0.687
97	1.256	1.760	632.142	343.068	244.818	91.661	49.745	35.499	0.578
98	1.051	1.006	644.256	327.086	341.711	93.417	47.427	49.548	0.695
99	1.026	1.343	730.689	382.336	292.087	105.950	55.439	42.353	0.688
100	1.212	1.314	952.219	375.251	346.107	138.072	54.411	50.186	0.795
101	1.027	1.070	818.709	343.778	330.197	118.713	49.848	47.879	0.819
102	0.940	1.074	821.655	385.331	337.373	119.140	55.873	48.919	0.814
103	0.987	1.345	809.603	429.175	314.866	117.392	62.230	45.656	0.715
104	0.913	0.858	746.627	382.309	407.248	108.261	55.435	59.051	0.788
105	1.026	1.510	840.377	402.480	273.354	121.855	58.360	39.636	0.757
106	1.191	1.541	769.454	373.951	289.078	111.571	54.223	41.916	0.692
107	1.173	1.382	835.096	432.692	367.265	121.089	62.740	53.253	0.655
108	1.078	1.301	956.665	533.563	441.824	138.716	77.367	64.065	0.633
109	0.987	1.749	271.604	80.113	45.203	39.383	11.616	6.554	0.769
110	0.678	1.062	288.970	98.957	63.159	41.901	14.349	9.158	0.769
111	0.704	1.141	310.711	106.192	65.521	45.053	15.398	9.501	0.763
112	0.876	1.496	227.968	80.435	47.068	33.055	11.663	6.825	0.721
113	1.495	1.277	129.110	49.803	58.297	18.721	7.221	8.453	0.708
114	1.382	1.126	151.833	61.857	75.922	22.016	8.969	11.009	0.700
115	1.220	0.926	156.158	67.690	89.248	22.643	9.815	12.941	0.703
116	1.348	1.189	144.117	59.073	66.990	20.897	8.566	9.714	0.702

No .	Shear Area, As Payton (mm^2 )	Shear Area, As Chandrase karan (mm^2)	Shear Stress Ts Merchant (MPa)	Shear Stress, Ts Payton (MPa)	Shear Stress, Ts Chandrase karan (MPa)	Shear Stress Ts Merchant (ksi)	Shear Stress, Ts Payton (ksi)	Shear Stress, Ts Chandras ekaran (ksi)	Friction Co-efficient
11 7	1.320	0.947	155.515	70.348	98.092	22.550	10.200	14.223	0.660
11 8	1.176	0.907	118.381	45.986	59.633	17.165	6.668	8.647	0.760
11 9	1.663	1.224	98.629	35.114	47.708	14.301	5.092	6.918	0.724
12 0	1.584	1.274	118.153	44.360	55.162	17.132	6.432	7.999	0.710
12 1	0.737	1.338	254.249	83.605	46.075	36.866	12.123	6.681	0.798
12 2	1.305	1.979	170.909	49.970	32.957	24.782	7.246	4.779	0.790
12 3	0.589	0.928	300.493	112.43 5	71.297	43.571	16.303	10.338	0.798
12 4	0.715	1.435	247.842	89.677	44.649	35.937	13.003	6.474	0.770
12 5	0.725	1.074	267.379	109.81 4	74.176	38.770	15.923	10.756	0.714
12 6	0.612	0.922	260.425	105.07 1	69.705	37.762	15.235	10.107	0.758
12 7	0.830	1.271	195.163	59.822	39.042	28.299	8.674	5.661	0.806
12 8	0.755	1.329	286.230	100.81 4	57.245	41.503	14.618	8.300	0.771
12 9	0.744	1.123	279.806	97.494	64.556	40.572	14.137	9.361	0.777
13 0	0.596	0.872	304.451	148.27 3	101.294	44.145	21.500	14.688	0.671
13 1	0.559	0.706	276.547	151.37 9	119.779	40.099	21.950	17.368	0.617
13 2	0.695	1.274	244.501	112.14 0	61.223	35.453	16.260	8.877	0.665
13 3	1.696	1.668	262.759	87.318	88.782	38.100	12.661	12.873	0.746
13 4	1.464	1.995	249.801	83.515	61.291	36.221	12.110	8.887	0.764
13 5	1.726	2.402	253.449	81.831	58.819	36.750	11.865	8.529	0.754
13 6	1.245	1.818	253.353	99.186	67.929	36.736	14.382	9.850	0.741
13 7	2.195	2.946	173.862	58.606	43.672	25.210	8.498	6.332	0.717
13 8	1.103	1.189	278.474	134.29 1	124.648	40.379	19.472	18.074	0.688
13 9	1.280	1.221	260.815	119.73 8	125.576	37.818	17.362	18.209	0.661
14 0	1.503	2.148	233.975	114.91 2	80.407	33.926	16.662	11.659	0.582
14 1	1.399	2.005	243.720	122.82 0	85.704	35.339	17.809	12.427	0.581
14 2	1.468	1.452	229.702	122.82 7	124.139	33.307	17.810	18.000	0.528
14 3	1.821	1.517	202.421	98.793	118.621	29.351	14.325	17.200	0.556
14 4	1.795	2.201	210.842	103.52 3	84.388	30.572	15.011	12.236	0.554
14 5	1.775	1.623	207.174	68.824	75.279	30.040	9.980	10.915	0.773
14 6	1.208	1.460	293.763	86.128	71.248	42.596	12.489	10.331	0.864
14 7	2.166	2.793	210.399	38.394	29.786	30.508	5.567	4.319	0.905

No .	Shear Area, As Payton (mm^2 )	Shear Area, As Chandrase karan (mm^2)	Shear Stress Ts Merchant (MPa)	Shear Stress, Ts Payton (MPa)	Shear Stress, Ts Chandrase karan (MPa)	Shear Stress Ts Merchant (ksi)	Shear Stress, Ts Payton (ksi)	Shear Stress, Ts Chandras ekaran (ksi)	Friction Co-efficient
14 8	1.355	1.191	202.845	86.941	98.922	29.413	12.606	14.344	0.706
14 9	1.337	1.475	224.882	96.277	87.311	32.608	13.960	12.660	0.710
15 0	1.365	1.366	205.832	88.954	88.842	29.846	12.898	12.882	0.701
15 1	1.881	2.386	165.219	66.807	52.665	23.957	9.687	7.636	0.687
15 2	1.421	1.439	191.799	87.893	86.789	27.811	12.744	12.584	0.661
15 3	1.174	1.402	231.616	113.25 2	94.807	33.584	16.422	13.747	0.674
15 4	1.251	1.485	221.211	118.20 0	99.555	32.076	17.139	14.435	0.593
15 5	1.313	1.536	226.405	121.19 6	103.596	32.829	17.573	15.021	0.578
15 6	1.250	1.484	214.611	112.99 0	95.221	31.119	16.384	13.807	0.604
15 7	1.125	1.453	236.768	91.723	71.011	34.331	13.300	10.297	0.661
15 8	1.035	1.315	271.673	107.61 5	84.670	39.393	15.604	12.277	0.658
15 9	0.984	1.282	284.138	113.43 6	87.027	41.200	16.448	12.619	0.660
16 0	0.912	1.231	243.511	111.49 8	82.615	35.309	16.167	11.979	0.598
16 1	0.773	1.133	258.351	126.88 7	86.611	37.461	18.399	12.559	0.582
16 2	0.777	1.009	259.870	128.15 1	98.681	37.681	18.582	14.309	0.579
16 3	0.608	0.984	290.050	150.11 4	92.794	42.057	21.767	13.455	0.617
16 4	0.680	0.947	313.075	167.99 7	120.726	45.396	24.360	17.505	0.553
16 5	0.675	1.036	301.201	169.22 4	110.341	43.674	24.537	15.999	0.519
16 6	0.888	1.417	210.649	112.52 5	70.480	30.544	16.316	10.220	0.501
16 7	0.848	1.501	262.038	140.15 4	79.118	37.996	20.322	11.472	0.507
16 8	0.693	0.844	275.430	158.78 1	130.254	39.937	23.023	18.887	0.490
16 9	1.005	1.184	237.740	93.932	79.736	34.472	13.620	11.562	0.694
17 0	0.831	1.030	273.228	112.93 5	91.127	39.618	16.376	13.213	0.694
17 1	1.094	1.101	218.752	85.532	84.979	31.719	12.402	12.322	0.692
17 2	0.588	0.809	261.615	142.81 8	103.730	37.934	20.709	15.041	0.610
17 3	0.629	0.808	242.259	124.28 1	96.636	35.128	18.021	14.012	0.630
17 4	0.644	0.835	264.069	140.93 9	108.659	38.290	20.436	15.756	0.594
17 5	0.500	0.572	330.497	202.65 7	177.158	47.922	29.385	25.688	0.610
17 6	0.646	0.727	280.988	142.75 1	126.847	40.743	20.699	18.393	0.628
17 7	0.600	0.533	310.517	166.88 3	187.814	45.025	24.198	27.233	0.614
17 8	0.740	1.155	236.263	118.31 8	75.834	34.258	17.156	10.996	0.604

No .	Shear Area, As Payton (mm^2 )	Shear Area, As Chandrase karan (mm^2)	Shear Stress Ts Merchant (MPa)	Shear Stress, Ts Payton (MPa)	Shear Stress, Ts Chandrase karan (MPa)	Shear Stress Ts Merchant (ksi)	Shear Stress, Ts Payton (ksi)	Shear Stress, Ts Chandras ekaran (ksi)	Friction Co-efficient
17 9	0.780	1.032	253.947	122.29 4	92.501	36.822	17.733	13.413	0.620
18 0	0.793	1.180	256.557	121.29 3	81.575	37.201	17.587	11.828	0.628
18 1	1.887	2.027	243.214	104.18 3	96.982	35.266	15.107	14.062	0.630
18 2	1.625	1.980	276.142	124.26 6	101.988	40.041	18.019	14.788	0.625
18 3	1.495	1.988	312.349	146.47 4	110.145	45.291	21.239	15.971	0.618
18 4	1.457	1.821	244.740	129.57 2	103.706	35.487	18.788	15.037	0.544
18 5	1.290	1.615	252.008	137.63 8	109.899	36.541	19.958	15.935	0.557
18 6	1.866	2.227	197.485	97.850	82.017	28.635	14.188	11.893	0.547
18 7	1.817	2.250	210.632	113.58 3	91.694	30.542	16.470	13.296	0.490
18 8	1.487	2.194	254.242	143.66 6	97.366	36.865	20.832	14.118	0.489
18 9	1.337	1.565	266.579	149.80 4	128.003	38.654	21.722	18.560	0.522
19 0	2.369	2.866	179.588	87.186	72.085	26.040	12.642	10.452	0.536
19 1	1.942	2.737	220.175	109.00 1	77.348	31.925	15.805	11.215	0.542
19 2	1.478	1.855	248.639	142.28 5	113.384	36.053	20.631	16.441	0.479
19 3	1.428	1.814	250.992	115.65 6	91.034	36.394	16.770	13.200	0.663
19 4	1.988	2.203	202.396	85.678	77.311	29.347	12.423	11.210	0.662
19 5	1.154	1.512	299.420	152.63 9	116.475	43.416	22.133	16.889	0.666
19 6	1.264	1.608	241.125	136.35 0	107.167	34.963	19.771	15.539	0.555
19 7	1.152	1.319	257.763	151.61 9	132.477	37.376	21.985	19.209	0.558
19 8	1.498	1.750	225.807	122.32 2	104.708	32.742	17.737	15.183	0.546
19 9	1.058	1.122	252.359	156.65 4	147.735	36.592	22.715	21.422	0.555
20 0	1.441	1.669	210.955	115.15 0	99.442	30.589	16.697	14.419	0.548
20 1	1.547	1.949	199.861	105.08 0	83.386	28.980	15.237	12.091	0.562
20 2	0.600	1.078	452.883	255.09 9	141.848	65.668	36.989	20.568	0.577
20 3	1.438	1.124	189.713	99.091	126.849	27.508	14.368	18.393	0.581
20 4	2.432	1.255	127.199	72.709	140.890	18.444	10.543	20.429	0.560

No.	Shear Strain Y Merchant	Shear Strain Y Payton	Shear Strain Y Chandrasekaran	Resultant Force (newtons) payton	Resultant Force (lbf) Payton	Resultant Shear Stress Merchant (MPa)	Resultant Shear Stress Payton (MPa)	Resultant Shear Stress Chandrasekaran (MPa)
1	1.788	1.274	1.141	946.706	212.828	1494.718	1494.745	1022.544
2	1.974	1.274	0.933	950.739	213.735	1353.988	1354.013	859.295
3	1.839	1.274	1.149	957.179	215.182	1467.478	1467.505	917.423
4	2.081	1.274	0.885	733.831	164.972	990.991	991.009	768.263
5	3.308	1.274	0.436	1010.835	227.245	869.099	869.115	566.082
6	2.323	1.274	0.707	690.645	155.263	835.753	835.768	657.135
7	1.902	1.274	0.970	739.192	166.177	1093.977	1093.996	571.270
8	1.814	1.274	1.165	573.322	128.888	891.516	891.532	532.760
9	2.100	1.274	0.851	638.260	143.487	854.111	854.127	783.699
10	1.381	1.155	2.174	582.655	130.986	1148.264	1148.284	1005.144
11	1.382	1.155	1.449	851.016	191.316	1675.332	1675.362	1048.780
12	1.488	1.155	1.561	789.726	177.537	1431.746	1431.772	994.598
13	1.853	1.155	0.908	543.875	122.268	788.483	788.498	718.987
14	1.809	1.155	0.958	562.251	126.399	834.584	834.599	626.608
15	1.867	1.155	0.929	505.179	113.569	727.081	727.094	654.428
16	2.204	1.155	0.747	570.675	128.293	699.913	699.926	610.227
17	1.787	1.155	1.032	582.853	131.031	875.681	875.697	682.662
18	1.564	1.155	1.365	492.299	110.673	847.022	847.037	608.680
19	1.586	1.041	1.160	651.870	146.546	1045.835	1045.854	562.736
20	1.461	1.041	1.214	678.399	152.510	1178.907	1178.928	950.007
21	1.842	1.041	0.837	707.204	158.986	985.416	985.433	710.872
22	1.437	1.041	1.895	460.186	103.454	813.102	813.117	704.697
23	1.460	1.041	1.176	467.596	105.120	813.655	813.669	487.225
24	1.718	1.041	0.893	498.423	112.050	741.120	741.133	491.692
25	1.444	1.041	1.548	605.652	136.156	1065.397	1065.416	635.061
26	1.587	1.041	1.084	452.841	101.803	726.203	726.216	594.155
27	1.182	1.041	2.474	563.236	126.621	1227.011	1227.033	850.635
28	2.664	1.274	0.574	1729.989	388.917	915.629	915.645	779.315
29	2.650	1.274	0.577	1588.019	357.001	844.932	844.947	714.469
30	2.388	1.274	0.654	1686.307	379.097	992.890	992.908	713.017
31	1.899	1.274	1.035	1047.978	235.595	776.661	776.675	593.868
32	1.922	1.274	0.990	1144.150	257.215	837.618	837.633	718.356
33	1.923	1.274	0.959	1370.680	308.141	1003.036	1003.054	708.197
34	2.486	1.274	0.629	1088.508	244.706	616.279	616.290	440.673
35	2.014	1.274	0.862	1542.506	346.769	1076.593	1076.613	647.403
36	2.428	1.274	0.660	1218.888	274.017	706.330	706.342	455.385
37	1.743	1.155	0.965	1752.698	394.022	1349.903	1349.928	892.242

No.	Shear Strain Y Merchant	Shear Strain Y Payton	Shear Strain Y Chandrasekaran	Resultant Force (newtons) payton	Resultant Force (lbf) Payton	Resultant Shear Stress Merchant (MPa)	Resultant Shear Stress Payton (MPa)	Resultant Shear Stress Chandrasekaran (MPa)
38	1.525	1.155	1.458	1443.600	324.534	1274.772	1274.795	1153.751
39	1.834	1.155	0.917	1553.450	349.229	1137.479	1137.499	1042.686
40	2.019	1.155	0.790	1055.394	237.262	704.021	704.033	553.828
41	1.783	1.155	0.943	1402.049	315.193	1055.876	1055.895	763.519
42	1.876	1.155	0.897	1646.185	370.077	1179.061	1179.082	740.452
43	1.486	1.155	1.499	1186.683	266.777	1077.616	1077.635	789.904
44	1.601	1.155	1.281	1063.935	239.182	892.954	892.970	644.353
45	2.132	1.155	0.712	1024.851	230.396	648.606	648.618	476.639
46	1.954	1.041	0.733	1421.883	319.652	937.569	937.586	962.218
47	1.837	1.041	0.724	1195.098	268.669	834.762	834.777	728.864
48	1.895	1.041	0.674	1317.861	296.267	894.100	894.117	841.741
49	2.093	1.041	0.688	1082.144	243.276	669.962	669.974	546.154
50	1.705	1.041	0.925	922.736	207.439	691.129	691.142	627.857
51	1.635	1.041	0.991	842.520	189.406	656.719	656.731	633.795
52	1.553	1.041	1.073	837.927	188.374	685.975	685.987	732.263
53	1.798	1.041	0.833	844.231	189.791	601.618	601.629	524.929
54	1.459	1.041	1.216	825.993	185.691	718.807	718.820	621.126
55	1.552	1.274	1.983	806.951	181.410	1509.421	1509.448	828.920
56	2.088	1.274	0.831	943.821	212.180	1285.405	1285.428	868.594
57	1.700	1.274	1.250	874.229	196.534	1475.555	1475.581	1013.890
58	2.112	1.274	0.845	902.398	202.867	1214.783	1214.805	653.446
59	1.873	1.274	0.985	840.676	188.992	1279.508	1279.531	833.337
60	1.910	1.274	0.936	817.966	183.886	1219.767	1219.789	797.580
61	2.046	1.274	0.960	906.561	203.803	1260.486	1260.509	593.746
62	1.603	1.274	1.567	652.319	146.647	1175.492	1175.514	1085.060
63	1.728	1.274	1.381	590.273	132.699	978.521	978.539	675.477
64	1.513	1.155	1.534	669.581	150.528	1207.368	1207.390	1087.471
65	1.431	1.155	1.563	762.084	171.323	1460.473	1460.499	1225.417
66	1.513	1.155	1.311	807.976	181.640	1457.066	1457.093	1113.355
67	2.110	1.155	0.719	810.176	182.135	1048.311	1048.330	610.848
68	1.998	1.155	0.869	664.921	149.480	906.785	906.801	878.283
69	1.295	1.155	2.225	670.623	150.762	1447.083	1447.109	1312.693
70	1.737	1.155	1.098	756.487	170.065	1183.196	1183.217	755.778
71	1.748	1.155	0.935	792.487	178.158	1232.282	1232.304	827.024
72	1.597	1.155	1.239	750.265	168.666	1278.527	1278.550	774.723
73	1.294	1.041	1.660	695.888	156.442	1386.709	1386.734	1147.792
74	1.295	1.041	1.590	745.525	167.601	1483.463	1483.490	1242.332
75	1.208	1.041	1.790	708.156	159.200	1522.168	1522.195	1522.535

No.	Shear Strain Y Merchant	Shear Strain Y Payton	Shear Strain Y Chandrasekaran	Resultant Force (newtons) payton	Resultant Force (lbf) Payton	Resultant Shear Stress Merchant (MPa)	Resultant Shear Stress Payton (MPa)	Resultant Shear Stress Chandrasekaran (MPa)
76	1.128	1.041	3.195	641.548	144.226	1501.225	1501.252	1139.717
77	1.134	1.041	2.607	724.940	162.973	1684.190	1684.221	1090.915
78	1.429	1.041	1.438	714.736	160.679	1285.616	1285.639	1169.122
79	1.189	1.041	1.904	670.761	150.793	1468.683	1468.710	1006.898
80	1.306	1.041	2.090	478.212	107.506	943.040	943.057	896.335
81	1.330	1.041	1.546	632.006	142.081	1222.749	1222.771	1021.108
82	2.151	1.274	0.806	1931.003	434.107	1276.386	1276.409	1037.156
83	2.271	1.274	0.723	1688.675	379.629	1057.466	1057.485	1122.007
84	1.921	1.274	0.990	1726.230	388.072	1279.585	1279.608	1044.712
85	2.373	1.274	0.693	1517.896	341.237	910.199	910.216	756.691
86	2.147	1.274	0.745	1291.330	290.303	855.144	855.159	705.530
87	2.247	1.274	0.731	1043.245	234.531	660.316	660.328	575.287
88	1.731	1.274	1.378	1268.484	285.167	1049.542	1049.560	803.807
89	1.613	1.274	1.708	1226.782	275.792	1097.300	1097.320	1059.060
90	1.452	1.274	2.989	1188.978	267.293	1206.765	1206.786	1197.820
91	1.784	1.155	1.034	1593.923	358.328	1214.062	1214.083	930.736
92	2.050	1.155	0.800	1568.751	352.669	1043.519	1043.537	988.668
93	1.564	1.155	1.313	1465.653	329.492	1276.254	1276.277	1048.947
94	2.447	1.155	0.582	1392.405	313.025	782.828	782.842	700.241
95	1.759	1.155	0.956	1058.225	237.899	817.382	817.397	841.004
96	1.860	1.155	0.932	1212.635	272.611	886.340	886.356	848.411
97	1.706	1.155	1.158	953.547	214.366	759.340	759.354	541.876
98	1.440	1.155	1.773	995.258	223.743	946.997	947.014	989.340
99	1.410	1.155	1.816	1117.018	251.116	1088.364	1088.383	831.458
100	1.560	1.041	0.953	1559.885	350.676	1286.776	1286.799	1186.839
101	1.322	1.041	1.496	1316.388	295.936	1281.406	1281.429	1230.781
102	1.219	1.041	1.936	1323.769	297.595	1407.786	1407.811	1232.574
103	1.274	1.041	1.762	1154.611	259.567	1169.930	1169.951	858.325
104	1.189	1.041	2.457	1172.087	263.496	1283.145	1283.168	1366.846
105	1.320	1.041	1.624	1258.653	282.957	1227.321	1227.343	833.565
106	1.532	1.041	1.055	1147.860	258.049	963.882	963.899	745.117
107	1.508	1.041	1.177	1202.442	270.320	1025.192	1025.211	870.173
108	1.385	1.041	1.374	1299.489	292.137	1205.977	1205.998	998.626
109	2.805	1.274	0.546	340.258	76.493	344.785	344.791	194.540
110	1.918	1.274	0.961	288.830	64.932	426.287	426.295	272.077
111	1.991	1.274	0.955	313.814	70.548	445.851	445.859	275.093
112	2.480	1.274	0.647	252.592	56.785	288.473	288.478	168.805
113	2.113	1.274	0.821	255.644	57.471	170.975	170.978	200.137

No.	Shear Strain Y Merchant	Shear Strain Y Payton	Shear Strain Y Chandrasekaran	Resultant Force (newtons) payton	Resultant Force (lbf) Payton	Resultant Shear Stress Merchant (MPa)	Resultant Shear Stress Payton (MPa)	Resultant Shear Stress Chandrasekaran (MPa)
114	1.955	1.274	1.005	285.694	64.227	206.708	206.712	253.708
115	1.737	1.274	1.434	279.476	62.829	228.995	228.999	301.925
116	1.909	1.274	1.066	268.541	60.371	199.141	199.145	225.832
117	1.870	1.274	1.052	275.735	61.988	208.911	208.915	291.305
118	1.679	1.274	1.314	223.994	50.356	190.401	190.404	246.907
119	2.353	1.274	0.718	211.552	47.559	127.179	127.182	172.792
120	2.239	1.274	0.754	242.728	54.567	153.254	153.257	190.575
121	1.996	1.155	0.778	250.365	56.284	339.662	339.668	187.189
122	3.664	1.155	0.354	256.273	57.612	196.312	196.316	129.476
123	1.592	1.155	1.289	268.068	60.264	455.458	455.466	288.815
124	1.933	1.155	0.824	233.800	52.560	327.151	327.157	162.884
125	1.963	1.155	0.791	243.199	54.673	335.352	335.358	226.520
126	1.652	1.155	1.155	225.490	50.692	368.713	368.720	244.608
127	2.259	1.155	0.691	208.195	46.804	250.915	250.919	163.758
128	2.046	1.155	0.760	279.287	62.786	370.054	370.060	210.127
129	2.015	1.155	0.791	271.985	61.145	365.630	365.637	242.103
130	1.610	1.155	1.110	240.306	54.023	403.440	403.447	275.613
131	1.515	1.155	1.531	202.826	45.597	362.891	362.898	287.139
132	1.880	1.155	0.895	208.969	46.978	300.495	300.501	164.057
133	2.400	1.274	0.724	581.457	130.717	342.786	342.792	348.532
134	2.069	1.274	0.863	514.883	115.750	351.680	351.686	258.094
135	2.443	1.274	0.625	571.003	128.367	330.782	330.788	237.761
136	1.769	1.274	1.196	475.604	106.920	381.951	381.958	261.586
137	3.133	1.274	0.459	455.515	102.404	207.490	207.494	154.617
138	1.586	1.274	1.586	477.661	107.382	432.937	432.945	401.847
139	1.817	1.274	1.085	455.920	102.495	356.096	356.103	373.460
140	2.124	1.274	0.753	422.226	94.920	280.982	280.987	196.611
141	1.979	1.274	0.931	419.343	94.272	299.662	299.668	209.104
142	2.074	1.274	0.887	394.072	88.591	268.507	268.512	271.374
143	2.581	1.274	0.579	415.376	93.380	228.119	228.123	273.904
144	2.543	1.274	0.615	427.186	96.035	238.045	238.049	194.047
145	2.426	1.155	0.600	451.619	101.528	254.428	254.432	278.288
146	1.632	1.155	1.095	570.836	128.329	472.594	472.603	390.942
147	3.000	1.155	0.442	587.149	131.996	271.014	271.018	210.251
148	1.831	1.155	0.919	352.214	79.181	259.948	259.953	295.771
149	1.807	1.155	0.931	388.702	87.384	290.631	290.636	263.567
150	1.844	1.155	0.887	357.267	80.317	261.800	261.804	261.470
151	2.580	1.155	0.554	356.327	80.105	189.418	189.422	149.321

No.	Shear Strain Y Merchant	Shear Strain Y Payton	Shear Strain Y Chandrasekaran	Resultant Force (newtons) payton	Resultant Force (lbf) Payton	Resultant Shear Stress Merchant (MPa)	Resultant Shear Stress Payton (MPa)	Resultant Shear Stress Chandrasekaran (MPa)
152	1.921	1.155	0.852	331.429	74.508	233.300	233.304	230.369
153	1.587	1.155	1.293	364.148	81.864	310.303	310.309	259.766
154	1.689	1.155	1.092	337.059	75.774	269.503	269.508	226.991
155	1.773	1.155	0.948	351.876	79.105	268.004	268.009	229.085
156	1.689	1.155	1.092	329.473	74.069	263.476	263.480	222.040
157	3.117	1.274	0.472	307.490	69.127	273.292	273.297	211.581
158	2.857	1.274	0.513	329.145	73.995	318.088	318.093	250.265
159	2.711	1.274	0.578	331.175	74.451	336.619	336.625	258.249
160	2.508	1.274	0.735	257.789	57.953	282.591	282.596	209.388
161	2.121	1.274	0.958	239.981	53.950	310.420	310.426	211.888
162	2.131	1.274	0.814	241.631	54.321	311.036	311.041	239.509
163	1.684	1.274	1.712	242.195	54.448	398.304	398.311	246.214
164	1.872	1.274	1.051	262.361	58.981	385.588	385.595	277.091
165	1.858	1.274	1.059	245.475	55.185	363.429	363.435	236.972
166	2.439	1.274	0.674	207.196	46.579	233.448	233.452	146.219
167	2.327	1.274	0.746	249.181	56.018	294.011	294.016	165.972
168	1.904	1.274	1.196	223.900	50.335	323.252	323.258	265.177
169	2.682	1.155	0.522	273.079	61.391	271.733	271.738	230.666
170	2.193	1.155	0.676	271.316	60.994	326.451	326.457	263.413
171	2.937	1.155	0.470	269.157	60.509	246.011	246.016	244.420
172	1.545	1.155	1.382	198.265	44.572	337.446	337.452	245.091
173	1.649	1.155	1.084	192.681	43.316	306.506	306.511	238.328
174	1.688	1.155	1.170	207.328	46.609	322.032	322.037	248.275
175	1.337	1.155	2.553	239.090	53.750	478.278	478.286	418.098
176	1.694	1.155	1.089	226.479	50.914	350.522	350.528	311.471
177	1.575	1.155	1.304	238.202	53.550	397.258	397.265	447.083
178	1.944	1.155	0.892	204.280	45.924	275.965	275.970	176.875
179	2.054	1.155	0.738	230.078	51.724	294.848	294.853	223.018
180	2.089	1.155	0.708	236.437	53.153	298.042	298.047	200.446
181	2.597	1.274	0.575	538.854	121.139	285.525	285.530	265.789
182	2.230	1.274	0.737	546.481	122.854	336.302	336.308	276.008
183	2.051	1.274	0.871	581.676	130.766	389.196	389.203	292.666
184	2.000	1.274	0.921	425.932	95.753	292.317	292.322	233.962
185	1.778	1.274	1.109	410.852	92.363	318.599	318.605	254.390
186	2.567	1.274	0.610	413.820	93.030	221.729	221.733	185.852
187	2.497	1.274	0.626	420.214	94.468	231.326	231.330	186.746
188	2.041	1.274	0.902	433.863	97.536	291.757	291.763	197.731
189	1.840	1.274	1.070	432.684	97.271	323.591	323.597	276.499

No.	Shear Strain Y Merchant	Shear Strain Y Payton	Shear Strain Y Chandrasekaran	Resultant Force (newtons) payton	Resultant Force (lbf) Payton	Resultant Shear Stress Merchant (MPa)	Resultant Shear Stress Payton (MPa)	Resultant Shear Stress Chandrasekaran (MPa)
190	3.289	1.274	0.429	458.671	103.113	193.587	193.591	160.058
191	2.675	1.274	0.586	475.559	106.910	244.877	244.881	173.766
192	2.029	1.274	0.908	420.332	94.494	284.323	284.328	226.570
193	1.874	1.155	0.849	440.460	99.019	308.415	308.420	242.756
194	2.651	1.155	0.528	452.788	101.791	227.810	227.814	205.563
195	1.518	1.155	1.220	472.865	106.304	409.813	409.820	312.718
196	1.657	1.155	1.113	364.690	81.986	288.527	288.532	226.773
197	1.516	1.155	1.357	371.609	83.541	322.513	322.519	281.795
198	1.968	1.155	0.832	381.087	85.672	254.418	254.423	217.782
199	1.403	1.155	1.598	350.876	78.880	331.650	331.656	312.767
200	1.891	1.155	0.890	346.492	77.895	240.434	240.438	207.635
201	2.035	1.155	0.764	348.491	78.344	225.269	225.273	178.760
202	1.575	1.155	1.173	337.854	75.953	563.428	563.438	313.295
203	1.888	1.155	0.947	317.151	71.298	220.482	220.486	282.245
204	1.596	1.155	1.239	377.544	84.875	155.257	155.260	300.847

No.	Resultant Shear Stress Merchant (ksi)	Resultant Shear Stress Payton (ksi)	Resultant Shear Stress Chandrasekaran (ksi)	measured Ultimate Tensile Strength (Mpa)	measured Ultimate Tensile Strength (ksi)	Horsepower (hp)	Horsepower (W)	MRR(in^3/min)
1	216.734	216.738	148.269	728.173	105.613	0.046	34.503	0.005
2	196.328	196.332	124.598	728.173	105.613	0.046	34.659	0.005
3	212.784	212.788	133.026	728.173	105.613	0.047	34.884	0.005
4	143.694	143.696	111.398	728.173	105.613	0.036	27.070	0.004
5	126.019	126.022	82.082	728.173	105.613	0.050	37.596	0.005
6	121.184	121.186	95.285	728.173	105.613	0.034	25.435	0.004
7	158.627	158.629	82.834	728.173	105.613	0.037	27.852	0.006
8	129.270	129.272	77.250	728.173	105.613	0.029	21.631	0.005
9	123.846	123.848	113.636	728.173	105.613	0.032	24.071	0.003
10	166.498	166.501	145.746	728.173	105.613	0.029	21.550	0.004
11	242.923	242.927	152.073	728.173	105.613	0.042	31.545	0.006
12	207.603	207.607	144.217	728.173	105.613	0.039	29.239	0.005
13	114.330	114.332	104.253	728.173	105.613	0.028	20.551	0.004
14	121.015	121.017	90.858	728.173	105.613	0.029	21.331	0.004
15	105.427	105.429	94.892	728.173	105.613	0.026	19.166	0.004
16	101.487	101.489	88.483	728.173	105.613	0.028	21.205	0.004
17	126.974	126.976	98.986	728.173	105.613	0.029	21.826	0.004
18	122.818	122.820	88.259	728.173	105.613	0.025	18.319	0.004

No.	Resultant Shear Stress Merchant (ksi)	Resultant Shear Stress Payton (ksi)	Resultant Shear Stress Chandrasekaran (ksi)	measured Ultimate Tensile Strength (Mpa)	measured Ultimate Tensile Strength (ksi)	Horsepower (hp)	Horsepower (W)	MRR(in^3/min)
19	151.646	151.649	81.597	728.173	105.613	0.033	24.442	0.006
20	170.941	170.945	137.751	728.173	105.613	0.034	25.428	0.004
21	142.885	142.888	103.076	728.173	105.613	0.035	26.456	0.005
22	117.900	117.902	102.181	728.173	105.613	0.023	17.336	0.003
23	117.980	117.982	70.648	728.173	105.613	0.024	17.644	0.006
24	107.462	107.464	71.295	728.173	105.613	0.025	18.828	0.005
25	154.483	154.485	92.084	728.173	105.613	0.031	23.040	0.005
26	105.299	105.301	86.152	728.173	105.613	0.023	17.150	0.004
27	177.917	177.920	123.342	728.173	105.613	0.029	21.442	0.005
28	132.766	132.769	113.001	728.173	105.613	0.085	63.661	0.007
29	122.515	122.517	103.598	728.173	105.613	0.078	58.280	0.007
30	143.969	143.972	103.387	728.173	105.613	0.083	61.894	0.009
31	112.616	112.618	86.111	728.173	105.613	0.053	39.197	0.008
32	121.455	121.457	104.162	728.173	105.613	0.057	42.644	0.007
33	145.440	145.443	102.689	728.173	105.613	0.069	51.342	0.009
34	89.360	89.362	63.898	728.173	105.613	0.055	41.091	0.009
35	156.106	156.109	93.873	728.173	105.613	0.078	58.481	0.011
36	102.418	102.420	66.031	728.173	105.613	0.062	46.251	0.010
37	195.736	195.740	129.375	728.173	105.613	0.087	65.236	0.010
38	184.842	184.845	167.294	728.173	105.613	0.072	53.465	0.007
39	164.934	164.937	151.189	728.173	105.613	0.077	57.570	0.007
40	102.083	102.085	80.305	728.173	105.613	0.053	39.542	0.008
41	153.102	153.105	110.710	728.173	105.613	0.071	52.702	0.009
42	170.964	170.967	107.366	728.173	105.613	0.083	61.642	0.010
43	156.254	156.257	114.536	728.173	105.613	0.060	45.103	0.009
44	129.478	129.481	93.431	728.173	105.613	0.054	40.403	0.009
45	94.048	94.050	69.113	728.173	105.613	0.052	38.919	0.009
46	135.947	135.950	139.522	728.173	105.613	0.071	53.315	0.006
47	121.040	121.043	105.685	728.173	105.613	0.060	44.386	0.008
48	129.645	129.647	122.052	728.173	105.613	0.066	49.040	0.007
49	97.145	97.146	79.192	728.173	105.613	0.055	41.114	0.008
50	100.214	100.216	91.039	728.173	105.613	0.047	35.052	0.007
51	95.224	95.226	91.900	728.173	105.613	0.043	31.970	0.007
52	99.466	99.468	106.178	728.173	105.613	0.043	31.820	0.006
53	87.235	87.236	76.115	728.173	105.613	0.042	31.552	0.008
54	104.227	104.229	90.063	728.173	105.613	0.042	31.063	0.008
55	218.866	218.870	120.193	1068.636	154.993	0.040	29.659	0.006
56	186.384	186.387	125.946	1068.636	154.993	0.047	34.762	0.005

No.	Resultant Shear Stress Merchant (ksi)	Resultant Shear Stress Payton (ksi)	Resultant Shear Stress Chandrasekaran (ksi)	measured Ultimate Tensile Strength (Mpa)	measured Ultimate Tensile Strength (ksi)	Horsepower (hp)	Horsepower (W)	MRR(in^3/min)
57	213.955	213.959	147.014	1068.636	154.993	0.043	32.230	0.005
58	176.144	176.147	94.750	1068.636	154.993	0.045	33.742	0.006
59	185.529	185.532	120.834	1068.636	154.993	0.042	31.193	0.005
60	176.866	176.869	115.649	1068.636	154.993	0.041	30.652	0.005
61	182.770	182.774	86.093	1068.636	154.993	0.045	33.899	0.006
62	170.446	170.449	157.334	1068.636	154.993	0.033	24.446	0.003
63	141.886	141.888	97.944	1068.636	154.993	0.030	22.014	0.004
64	175.068	175.072	157.683	1068.636	154.993	0.033	24.707	0.003
65	211.769	211.772	177.686	1068.636	154.993	0.038	28.309	0.004
66	211.275	211.278	161.436	1068.636	154.993	0.040	30.014	0.004
67	152.005	152.008	88.573	1068.636	154.993	0.040	30.003	0.005
68	131.484	131.486	127.351	1068.636	154.993	0.033	24.740	0.003
69	209.827	209.831	190.340	1068.636	154.993	0.034	25.242	0.004
70	171.563	171.566	109.588	1068.636	154.993	0.039	28.710	0.005
71	178.681	178.684	119.918	1068.636	154.993	0.040	30.035	0.005
72	185.386	185.390	112.335	1068.636	154.993	0.038	28.372	0.005
73	201.073	201.076	166.430	1068.636	154.993	0.035	25.839	0.004
74	215.102	215.106	180.138	1068.636	154.993	0.037	27.728	0.004
75	220.714	220.718	220.768	1068.636	154.993	0.035	26.237	0.003
76	217.678	217.682	165.259	1068.636	154.993	0.031	23.466	0.004
77	244.208	244.212	158.183	1068.636	154.993	0.036	26.806	0.005
78	186.414	186.418	169.523	1068.636	154.993	0.035	26.271	0.003
79	212.959	212.963	146.000	1068.636	154.993	0.034	25.475	0.005
80	136.741	136.743	129.969	1068.636	154.993	0.024	17.970	0.003
81	177.299	177.302	148.061	1068.636	154.993	0.032	23.923	0.004
82	185.076	185.079	150.388	1068.636	154.993	0.096	71.299	0.008
83	153.333	153.335	162.691	1068.636	154.993	0.083	62.240	0.006
84	185.540	185.543	151.483	1068.636	154.993	0.085	63.663	0.008
85	131.979	131.981	109.720	1068.636	154.993	0.076	56.480	0.007
86	123.996	123.998	102.302	1068.636	154.993	0.065	48.389	0.008
87	95.746	95.748	83.417	1068.636	154.993	0.052	38.767	0.007
88	152.184	152.186	116.552	1068.636	154.993	0.064	47.616	0.008
89	159.108	159.111	153.564	1068.636	154.993	0.062	46.099	0.006
90	174.981	174.984	173.684	1068.636	154.993	0.060	44.884	0.006
91	176.039	176.042	134.957	1068.636	154.993	0.079	59.261	0.008
92	151.310	151.313	143.357	1068.636	154.993	0.078	58.379	0.007
93	185.057	185.060	152.097	1068.636	154.993	0.073	54.429	0.008
94	113.510	113.512	101.535	1068.636	154.993	0.070	52.366	0.007

No.	Resultant Shear Stress Merchant (ksi)	Resultant Shear Stress Payton (ksi)	Resultant Shear Stress Chandrasekaran (ksi)	measured Ultimate Tensile Strength (Mpa)	measured Ultimate Tensile Strength (ksi)	Horsepower (hp)	Horsepower (W)	MRR(in^3/min)
95	118.520	118.523	121.946	1068.636	154.993	0.053	39.887	0.006
96	128.519	128.522	123.020	1068.636	154.993	0.061	45.583	0.007
97	110.104	110.106	78.572	1068.636	154.993	0.049	36.276	0.009
98	137.315	137.317	143.454	1068.636	154.993	0.050	37.367	0.006
99	157.813	157.816	120.561	1068.636	154.993	0.056	41.983	0.008
100	186.582	186.586	172.092	1068.636	154.993	0.078	58.428	0.007
101	185.804	185.807	178.463	1068.636	154.993	0.066	49.070	0.007
102	204.129	204.133	178.723	1068.636	154.993	0.066	49.403	0.008
103	169.640	169.643	124.457	1068.636	154.993	0.059	43.751	0.009
104	186.056	186.059	198.193	1068.636	154.993	0.059	43.955	0.006
105	177.962	177.965	120.867	1068.636	154.993	0.064	47.446	0.010
106	139.763	139.765	108.042	1068.636	154.993	0.058	43.588	0.009
107	148.653	148.656	126.175	1068.636	154.993	0.061	45.768	0.008
108	174.867	174.870	144.801	1068.636	154.993	0.066	49.499	0.008
109	49.994	49.995	28.208	117.439	17.033	0.016	12.253	0.005
110	61.812	61.813	39.451	117.439	17.033	0.014	10.400	0.005
111	64.648	64.650	39.889	117.439	17.033	0.015	11.324	0.005
112	41.829	41.829	24.477	117.439	17.033	0.012	9.236	0.005
113	24.791	24.792	29.020	117.439	17.033	0.013	9.383	0.005
114	29.973	29.973	36.788	117.439	17.033	0.014	10.510	0.005
115	33.204	33.205	43.779	117.439	17.033	0.014	10.270	0.005
116	28.875	28.876	32.746	117.439	17.033	0.013	9.871	0.005
117	30.292	30.293	42.239	117.439	17.033	0.014	10.244	0.004
118	27.608	27.609	35.801	117.439	17.033	0.011	8.092	0.005
119	18.441	18.441	25.055	117.439	17.033	0.010	7.729	0.005
120	22.222	22.222	27.633	117.439	17.033	0.012	8.904	0.005
121	49.251	49.252	27.142	117.439	17.033	0.012	9.181	0.006
122	28.465	28.466	18.774	117.439	17.033	0.013	9.420	0.005
123	66.041	66.043	41.878	117.439	17.033	0.013	9.832	0.005
124	47.437	47.438	23.618	117.439	17.033	0.012	8.640	0.006
125	48.626	48.627	32.845	117.439	17.033	0.012	9.099	0.005
126	53.463	53.464	35.468	117.439	17.033	0.011	8.356	0.005
127	36.383	36.383	23.745	117.439	17.033	0.010	7.617	0.005
128	53.658	53.659	30.468	117.439	17.033	0.014	10.316	0.006
129	53.016	53.017	35.105	117.439	17.033	0.013	10.031	0.005
130	58.499	58.500	39.964	117.439	17.033	0.012	9.057	0.005
131	52.619	52.620	41.635	117.439	17.033	0.010	7.694	0.004
132	43.572	43.573	23.788	117.439	17.033	0.011	7.883	0.006

No.	Resultant Shear Stress Merchant (ksi)	Resultant Shear Stress Payton (ksi)	Resultant Shear Stress Chandrasekaran (ksi)	measured Ultimate Tensile Strength (Mpa)	measured Ultimate Tensile Strength (ksi)	Horsepower (hp)	Horsepower (W)	MRR(in^3/min)
133	49.704	49.705	50.537	117.439	17.033	0.028	21.100	0.006
134	50.994	50.994	37.424	117.439	17.033	0.025	18.575	0.008
135	47.963	47.964	34.475	117.439	17.033	0.028	20.670	0.009
136	55.383	55.384	37.930	117.439	17.033	0.023	17.287	0.009
137	30.086	30.087	22.419	117.439	17.033	0.022	16.675	0.008
138	62.776	62.777	58.268	117.439	17.033	0.024	17.625	0.007
139	51.634	51.635	54.152	117.439	17.033	0.023	16.935	0.006
140	40.742	40.743	28.509	117.439	17.033	0.021	15.916	0.009
141	43.451	43.452	30.320	117.439	17.033	0.021	15.809	0.009
142	38.933	38.934	39.349	117.439	17.033	0.020	14.950	0.006
143	33.077	33.078	39.716	117.439	17.033	0.021	15.713	0.005
144	34.517	34.517	28.137	117.439	17.033	0.022	16.164	0.008
145	36.892	36.893	40.352	117.439	17.033	0.022	16.673	0.006
146	68.526	68.527	56.687	117.439	17.033	0.027	20.501	0.008
147	39.297	39.298	30.486	117.439	17.033	0.028	20.763	0.008
148	37.692	37.693	42.887	117.439	17.033	0.018	13.196	0.006
149	42.141	42.142	38.217	117.439	17.033	0.020	14.554	0.007
150	37.961	37.962	37.913	117.439	17.033	0.018	13.399	0.006
151	27.466	27.466	21.652	117.439	17.033	0.018	13.396	0.008
152	33.828	33.829	33.403	117.439	17.033	0.017	12.509	0.006
153	44.994	44.995	37.666	117.439	17.033	0.018	13.718	0.008
154	39.078	39.079	32.914	117.439	17.033	0.017	12.811	0.008
155	38.861	38.861	33.217	117.439	17.033	0.018	13.387	0.008
156	38.204	38.205	32.196	117.439	17.033	0.017	12.512	0.008
157	39.627	39.628	30.679	300.443	43.576	0.015	11.420	0.004
158	46.123	46.124	36.288	300.443	43.576	0.016	12.232	0.004
159	48.810	48.811	37.446	300.443	43.576	0.016	12.304	0.004
160	40.976	40.976	30.361	300.443	43.576	0.013	9.694	0.004
161	45.011	45.012	30.724	300.443	43.576	0.012	9.046	0.004
162	45.100	45.101	34.729	300.443	43.576	0.012	9.113	0.004
163	57.754	57.755	35.701	300.443	43.576	0.012	9.077	0.005
164	55.910	55.911	40.178	300.443	43.576	0.013	9.928	0.004
165	52.697	52.698	34.361	300.443	43.576	0.012	9.320	0.005
166	33.850	33.851	21.202	300.443	43.576	0.011	7.878	0.005
167	42.632	42.632	24.066	300.443	43.576	0.013	9.470	0.006
168	46.872	46.872	38.451	300.443	43.576	0.011	8.518	0.004
169	39.401	39.402	33.447	300.443	43.576	0.014	10.253	0.004
170	47.335	47.336	38.195	300.443	43.576	0.014	10.188	0.004

No.	Resultant Shear Stress Merchant (ksi)	Resultant Shear Stress Payton (ksi)	Resultant Shear Stress Chandrasekaran (ksi)	measured Ultimate Tensile Strength (Mpa)	measured Ultimate Tensile Strength (ksi)	Horsepower (hp)	Horsepower (W)	MRR(in^3/min)
171	35.672	35.672	35.441	300.443	43.576	0.014	10.110	0.003
172	48.930	48.931	35.538	300.443	43.576	0.010	7.526	0.005
173	44.443	44.444	34.558	300.443	43.576	0.010	7.300	0.004
174	46.695	46.695	36.000	300.443	43.576	0.011	7.880	0.004
175	69.350	69.352	60.624	300.443	43.576	0.012	9.076	0.004
176	50.826	50.827	45.163	300.443	43.576	0.012	8.582	0.004
177	57.602	57.603	64.827	300.443	43.576	0.012	9.039	0.003
178	40.015	40.016	25.647	300.443	43.576	0.010	7.758	0.005
179	42.753	42.754	32.338	300.443	43.576	0.012	8.726	0.004
180	43.216	43.217	29.065	300.443	43.576	0.012	8.959	0.005
181	41.401	41.402	38.539	300.443	43.576	0.027	20.146	0.007
182	48.764	48.765	40.021	300.443	43.576	0.027	20.451	0.008
183	56.433	56.434	42.437	300.443	43.576	0.029	21.798	0.009
184	42.386	42.387	33.924	300.443	43.576	0.022	16.133	0.008
185	46.197	46.198	36.887	300.443	43.576	0.021	15.540	0.008
186	32.151	32.151	26.948	300.443	43.576	0.021	15.671	0.008
187	33.542	33.543	27.078	300.443	43.576	0.021	15.987	0.008
188	42.305	42.306	28.671	300.443	43.576	0.022	16.508	0.009
189	46.921	46.922	40.092	300.443	43.576	0.022	16.424	0.008
190	28.070	28.071	23.208	300.443	43.576	0.023	17.388	0.008
191	35.507	35.508	25.196	300.443	43.576	0.024	18.017	0.009
192	41.227	41.228	32.853	300.443	43.576	0.021	16.000	0.008
193	44.720	44.721	35.200	300.443	43.576	0.022	16.619	0.009
194	33.032	33.033	29.807	300.443	43.576	0.023	17.087	0.007
195	59.423	59.424	45.344	300.443	43.576	0.024	17.835	0.009
196	41.836	41.837	32.882	300.443	43.576	0.019	13.888	0.008
197	46.764	46.765	40.860	300.443	43.576	0.019	14.150	0.008
198	36.891	36.891	31.578	300.443	43.576	0.019	14.516	0.008
199	48.089	48.090	45.351	300.443	43.576	0.018	13.362	0.007
200	34.863	34.864	30.107	300.443	43.576	0.018	13.197	0.008
201	32.664	32.665	25.920	300.443	43.576	0.018	13.268	0.008
202	81.697	81.699	45.428	300.443	43.576	0.017	12.854	0.006
203	31.970	31.971	40.926	300.443	43.576	0.016	12.064	0.005
204	22.512	22.513	43.623	300.443	43.576	0.019	14.375	0.007

No.	MRR(m <sup>3</sup> /min)	Specific Horsepower, Hps (hp*min/in <sup>3</sup> )	Specific Horsepower, Hps (W*min/m <sup>3</sup> )	Ki (x) Merchant (radians)	Ki (x) Merchant (degrees)	Ki (x) Payton (radians)	Ki (x) Payton (degrees)
1	7.58E-08	10.003	455187927.8	0.741	42.436	0.271	15.554
2	8.11E-08	9.387	427169478.6	0.799	45.751	0.272	15.600
3	8.09E-08	9.473	431081486	0.758	43.409	0.271	15.549
4	6.52E-08	9.125	415220357.9	0.867	49.691	0.314	18.016
5	7.88E-08	10.485	477128569.7	1.071	61.371	0.349	19.973
6	6.52E-08	8.573	390136917.9	0.911	52.177	0.308	17.653
7	1.00E-07	6.120	278509301.4	0.924	52.956	0.418	23.972
8	8.52E-08	5.580	253903032.2	0.906	51.891	0.428	24.498
9	5.56E-08	9.519	433143659.7	0.982	56.265	0.425	24.339
10	5.93E-08	7.982	363222302.6	0.640	36.641	0.281	16.115
11	9.05E-08	7.660	348593924.9	0.649	37.204	0.290	16.627
12	7.52E-08	8.541	388660069.2	0.708	40.565	0.285	16.355
13	5.77E-08	7.823	355968420.7	0.956	54.768	0.395	22.651
14	6.99E-08	6.707	305220986.5	0.980	56.126	0.432	24.735
15	5.77E-08	7.295	331964585.7	0.996	57.055	0.431	24.718
16	5.83E-08	7.986	363420477.8	0.941	53.928	0.301	17.233
17	6.61E-08	7.255	330130887.3	0.879	50.380	0.338	19.369
18	7.24E-08	5.557	252878421.4	0.766	43.892	0.307	17.604
19	9.67E-08	5.554	252725212.6	0.849	48.617	0.302	17.284
20	6.71E-08	8.330	379040523	0.795	45.576	0.300	17.171
21	7.40E-08	7.862	357755030.6	0.914	52.366	0.289	16.576
22	5.61E-08	6.795	309223208.6	0.814	46.650	0.330	18.898
23	9.12E-08	4.253	193554067.2	0.836	47.902	0.341	19.548
24	8.16E-08	5.068	230630474.1	0.940	53.853	0.349	20.016
25	8.55E-08	5.919	269337069.9	0.912	52.251	0.425	24.323
26	6.50E-08	5.801	263993157.7	0.918	52.573	0.370	21.225
27	7.88E-08	5.983	272267538.9	0.751	43.021	0.439	25.168
28	1.21E-07	11.578	526854896.5	0.960	55.015	0.305	17.481
29	1.22E-07	10.519	478658137.6	0.948	54.343	0.295	16.919
30	1.45E-07	9.379	426798993.6	0.910	52.117	0.296	16.943
31	1.34E-07	6.447	293364035.7	0.881	50.454	0.376	21.517
32	1.20E-07	7.813	355539403	0.870	49.843	0.358	20.528
33	1.47E-07	7.659	348520641.9	0.895	51.291	0.383	21.962
34	1.44E-07	6.257	284747390.4	1.061	60.802	0.432	24.726
35	1.74E-07	7.390	336290948.4	1.005	57.560	0.468	26.823
36	1.59E-07	6.388	290696868.9	1.097	62.879	0.477	27.333
37	1.62E-07	8.833	401930316.3	0.835	47.870	0.308	17.665
38	1.15E-07	10.198	464053788	0.728	41.695	0.287	16.425

No.	MRR(m^3/min)	Specific Horsepower, Hps (hp*min/in^3)	Specific Horsepower, Hps (W*min/m^3)	Ki (x) Merchant (radians)	Ki (x) Merchant (degrees)	Ki (x) Payton (radians)	Ki (x) Payton (degrees)
39	1.15E-07	10.981	499684551.5	0.845	48.387	0.289	16.578
40	1.34E-07	6.504	295952206.5	0.943	54.050	0.341	19.541
41	1.47E-07	7.862	357754449.3	0.900	51.542	0.360	20.611
42	1.67E-07	8.108	368976549.2	0.905	51.840	0.338	19.362
43	1.44E-07	6.870	312627318.1	0.875	50.140	0.454	26.004
44	1.44E-07	6.154	280049739.3	0.918	52.569	0.443	25.354
45	1.44E-07	5.928	269765439.3	1.069	61.264	0.443	25.363
46	1.06E-07	11.057	503140395	0.953	54.607	0.302	17.283
47	1.29E-07	7.550	343567624.8	0.878	50.326	0.255	14.611
48	1.21E-07	8.893	404663690.1	0.901	51.649	0.264	15.106
49	1.32E-07	6.849	311665984.1	1.085	62.159	0.405	23.201
50	1.18E-07	6.511	296301932.3	0.990	56.695	0.403	23.091
51	1.11E-07	6.304	286880424.1	0.954	54.645	0.390	22.336
52	1.01E-07	6.908	314372393.6	0.933	53.471	0.399	22.853
53	1.24E-07	5.585	254162022.6	0.898	51.426	0.284	16.298
54	1.25E-07	5.453	248122205.7	0.814	46.617	0.319	18.272
55	9.14E-08	7.130	324444300.2	0.666	38.134	0.301	17.229
56	7.56E-08	10.111	460115214.4	0.863	49.448	0.308	17.673
57	7.56E-08	9.366	426200559.9	0.748	42.842	0.312	17.885
58	9.35E-08	7.933	360984232	0.934	53.528	0.374	21.435
59	7.97E-08	8.601	391410443.2	0.835	47.858	0.338	19.375
60	7.96E-08	8.460	384954425.8	0.894	51.218	0.386	22.094
61	1.04E-07	7.160	325820544.9	0.919	52.644	0.374	21.448
62	5.57E-08	9.639	438605024.7	0.778	44.565	0.386	22.117
63	7.20E-08	6.716	305620663.6	0.808	46.299	0.361	20.692
64	5.68E-08	9.558	434942388	0.707	40.501	0.272	15.579
65	6.36E-08	9.776	444863904.7	0.690	39.511	0.299	17.157
66	6.98E-08	9.446	429854871.3	0.734	42.081	0.300	17.163
67	9.01E-08	7.319	333066415.5	0.908	52.048	0.286	16.403
68	5.20E-08	10.462	476095090.1	0.904	51.808	0.307	17.571
69	6.04E-08	9.176	417573748.3	0.657	37.631	0.368	21.081
70	7.96E-08	7.924	360569183.7	0.961	55.050	0.435	24.950
71	7.97E-08	8.286	377036021.6	0.950	54.405	0.421	24.113
72	8.59E-08	7.258	330287626.5	0.874	50.104	0.401	22.999
73	6.49E-08	8.747	398036130.2	0.657	37.621	0.254	14.548
74	6.47E-08	9.418	428553495.9	0.665	38.115	0.261	14.974
75	5.59E-08	10.311	469215896.2	0.581	33.275	0.245	14.015
76	7.24E-08	7.127	324334337	0.445	25.516	0.196	11.242
77	8.66E-08	6.804	309618270.8	0.494	28.287	0.237	13.555

No.	MRR(m^3/min)	Specific Horsepower, Hps (hp*min/in^3)	Specific Horsepower, Hps (W*min/m^3)	Ki (x) Merchant (radians)	Ki (x) Merchant (degrees)	Ki (x) Payton (radians)	Ki (x) Payton (degrees)
78	5.69E-08	10.144	461611792.5	0.694	39.763	0.214	12.241
79	8.18E-08	6.843	311382571.3	0.719	41.176	0.400	22.930
80	5.34E-08	7.401	336793746.7	0.725	41.557	0.314	17.996
81	6.40E-08	8.211	373648886.6	0.792	45.406	0.366	20.975
82	1.24E-07	12.585	572699825.6	0.887	50.804	0.318	18.223
83	9.60E-08	14.242	648069043.4	0.904	51.802	0.311	17.828
84	1.24E-07	11.238	511369446.5	0.825	47.266	0.313	17.962
85	1.21E-07	10.243	466132181.9	0.962	55.118	0.351	20.089
86	1.27E-07	8.388	381701011.9	0.953	54.614	0.385	22.082
87	1.17E-07	7.263	330484760.1	0.933	53.454	0.345	19.748
88	1.30E-07	8.066	367050173.3	0.843	48.311	0.395	22.641
89	1.04E-07	9.777	444886796.3	0.798	45.734	0.401	22.994
90	1.01E-07	9.761	444189539.7	0.732	41.914	0.432	24.726
91	1.33E-07	9.797	445816626	0.844	48.332	0.303	17.378
92	1.08E-07	11.880	540589494.3	0.917	52.530	0.307	17.617
93	1.27E-07	9.454	430191078.4	0.757	43.374	0.298	17.088
94	1.18E-07	9.768	444496569.3	1.043	59.787	0.363	20.787
95	1.03E-07	8.534	388323779.2	0.910	52.117	0.377	21.612
96	1.07E-07	9.328	424463033.9	0.922	52.846	0.360	20.615
97	1.42E-07	5.618	255632175	0.984	56.355	0.469	26.859
98	9.87E-08	8.323	378746706	0.748	42.868	0.353	20.206
99	1.37E-07	6.742	306809623.4	0.736	42.172	0.359	20.567
100	1.20E-07	10.724	487998752.5	0.833	47.732	0.296	16.955
101	1.13E-07	9.569	435452068.3	0.693	39.711	0.272	15.562
102	1.25E-07	8.693	395579602.9	0.623	35.708	0.277	15.885
103	1.46E-07	6.568	298886141.8	0.764	43.789	0.376	21.521
104	1.01E-07	9.586	436193110.9	0.621	35.582	0.303	17.334
105	1.57E-07	6.660	303079455.4	0.754	43.214	0.334	19.143
106	1.40E-07	6.845	311491718	0.924	52.967	0.398	22.828
107	1.24E-07	8.079	367627671.3	0.952	54.545	0.436	24.965
108	1.29E-07	8.417	383038685	0.916	52.492	0.458	26.259
109	8.97E-08	3.003	136639314.4	0.907	51.976	0.235	13.436
110	8.11E-08	2.819	128293409.1	0.745	42.678	0.234	13.423
111	8.17E-08	3.044	138532643.2	0.771	44.178	0.240	13.779
112	8.67E-08	2.342	106554410.8	0.911	52.210	0.283	16.191
113	8.74E-08	2.358	107320589	0.856	49.037	0.296	16.935
114	8.18E-08	2.825	128536094.5	0.825	47.268	0.304	17.413
115	7.47E-08	3.021	137483832.5	0.750	42.994	0.300	17.193
116	8.83E-08	2.457	111810567.5	0.809	46.360	0.301	17.256

No.	MRR(m^3/min)	Specific Horsepower, Hps (hp*min/in^3)	Specific Horsepower, Hps (W*min/m^3)	Ki (x) Merchant (radians)	Ki (x) Merchant (degrees)	Ki (x) Payton (radians)	Ki (x) Payton (degrees)
117	7.33E-08	3.071	139744072.9	0.840	48.108	0.343	19.678
118	8.03E-08	2.215	100810815.8	0.671	38.444	0.244	13.976
119	7.39E-08	2.299	104627516.2	0.888	50.851	0.280	16.028
120	8.18E-08	2.391	108813106.8	0.880	50.440	0.294	16.825
121	9.60E-08	2.101	95593106.75	0.846	48.464	0.249	14.249
122	8.18E-08	2.530	115142820.9	1.056	60.528	0.257	14.747
123	8.18E-08	2.641	120177638.5	0.721	41.282	0.249	14.292
124	1.06E-07	1.790	81460922.35	0.860	49.251	0.278	15.909
125	7.87E-08	2.542	115657477.5	0.923	52.874	0.334	19.115
126	7.86E-08	2.335	106254878.9	0.784	44.935	0.289	16.557
127	7.89E-08	2.122	96553787.39	0.891	51.060	0.241	13.793
128	9.27E-08	2.446	111312151.8	0.884	50.668	0.276	15.809
129	7.89E-08	2.793	127097825.2	0.871	49.931	0.270	15.465
130	7.87E-08	2.529	115066243.1	0.855	48.994	0.376	21.563
131	6.50E-08	2.601	118376023.4	0.867	49.647	0.430	24.655
132	9.54E-08	1.815	82586711.54	0.950	54.455	0.382	21.912
133	9.70E-08	4.782	217603076.4	0.873	50.044	0.258	14.758
134	1.39E-07	2.941	133827270.4	0.790	45.260	0.240	13.738
135	1.45E-07	3.136	142703913.8	0.873	50.015	0.250	14.323
136	1.50E-07	2.540	115581509	0.725	41.553	0.263	15.051
137	1.38E-07	2.655	120805122.8	0.993	56.922	0.286	16.407
138	1.12E-07	3.448	156908069.3	0.699	40.032	0.315	18.070
139	9.87E-08	3.771	171601274.6	0.822	47.090	0.343	19.649
140	1.51E-07	2.319	105516755.6	0.984	56.378	0.421	24.140
141	1.47E-07	2.370	107863738.9	0.950	54.421	0.422	24.196
142	9.95E-08	3.301	150225290.3	1.026	58.813	0.475	27.222
143	8.67E-08	3.985	181339475.9	1.092	62.542	0.448	25.663
144	1.25E-07	2.837	129110028.6	1.088	62.340	0.450	25.778
145	9.60E-08	3.815	173606565.2	0.951	54.516	0.274	15.694
146	1.29E-07	3.483	158516025.7	0.671	38.433	0.183	10.501
147	1.39E-07	3.289	149667509.1	0.889	50.927	0.142	8.144
148	9.23E-08	3.141	142948222	0.895	51.291	0.341	19.539
149	1.16E-07	2.750	125161903.7	0.885	50.694	0.338	19.346
150	1.06E-07	2.777	126378315.1	0.905	51.834	0.347	19.863
151	1.33E-07	2.207	100434042.2	1.060	60.721	0.360	20.652
152	1.06E-07	2.593	117976304.9	0.965	55.297	0.386	22.132
153	1.24E-07	2.429	110532333.7	0.843	48.281	0.374	21.406
154	1.24E-07	2.268	103194839.6	0.963	55.166	0.454	26.014
155	1.24E-07	2.371	107888431.7	1.006	57.648	0.469	26.886

No.	MRR(m^3/min)	Specific Horsepower, Hps (hp*min/in^3)	Specific Horsepower, Hps (W*min/m^3)	Ki (x) Merchant (radians)	Ki (x) Merchant (degrees)	Ki (x) Payton (radians)	Ki (x) Payton (degrees)
156	1.24E-07	2.216	100842112	0.952	54.542	0.443	25.394
157	6.77E-08	3.708	168712086.4	1.048	60.038	0.342	19.610
158	6.76E-08	3.977	180996237.1	1.024	58.658	0.345	19.775
159	6.76E-08	4.001	182054368.8	1.005	57.575	0.344	19.693
160	6.59E-08	3.233	147121818.8	1.039	59.509	0.406	23.238
161	7.24E-08	2.744	124867748.6	0.983	56.332	0.421	24.127
162	6.83E-08	2.933	133475882.9	0.989	56.668	0.425	24.331
163	8.03E-08	2.483	113007776.6	0.816	46.737	0.386	22.141
164	7.32E-08	2.979	135561099.4	0.947	54.286	0.451	25.829
165	8.10E-08	2.530	115127564.6	0.977	55.973	0.484	27.751
166	8.28E-08	2.092	95175177.08	1.125	64.467	0.503	28.817
167	9.07E-08	2.294	104368028.8	1.100	63.031	0.497	28.470
168	6.05E-08	3.092	140694717.8	1.020	58.436	0.513	29.419
169	6.41E-08	3.513	159873414.5	1.065	61.034	0.353	20.223
170	6.76E-08	3.313	150739515	0.992	56.821	0.353	20.240
171	5.47E-08	4.058	184675155.1	1.096	62.772	0.355	20.345
172	7.38E-08	2.240	101919204.2	0.887	50.830	0.437	25.039
173	7.06E-08	2.272	103390796.1	0.911	52.222	0.417	23.921
174	6.84E-08	2.533	115268311.9	0.961	55.086	0.453	25.954
175	6.11E-08	3.263	148474279.8	0.763	43.710	0.438	25.070
176	6.05E-08	3.115	141748874.9	0.930	53.286	0.419	24.032
177	4.77E-08	4.162	189400916.8	0.897	51.412	0.434	24.840
178	8.20E-08	2.078	94578780.56	1.028	58.885	0.443	25.388
179	7.24E-08	2.650	120603648.8	1.038	59.461	0.428	24.505
180	8.19E-08	2.404	109413941.8	1.037	59.408	0.419	24.014
181	1.15E-07	3.850	175186837.5	1.019	58.409	0.374	21.400
182	1.29E-07	3.475	158126885	0.963	55.197	0.378	21.685
183	1.40E-07	3.422	155736641.2	0.932	53.374	0.386	22.108
184	1.31E-07	2.703	123022906.1	0.992	56.850	0.459	26.312
185	1.35E-07	2.533	115261835.4	0.912	52.278	0.447	25.595
186	1.25E-07	2.751	125204450	1.099	62.956	0.457	26.187
187	1.31E-07	2.687	122264331.3	1.145	65.581	0.513	29.407
188	1.54E-07	2.359	107351747.6	1.058	60.623	0.515	29.499
189	1.24E-07	2.909	132370843.2	0.968	55.468	0.481	27.577
190	1.29E-07	2.968	135074152.2	1.188	68.077	0.467	26.767
191	1.47E-07	2.702	122942945.2	1.118	64.043	0.461	26.431
192	1.31E-07	2.683	122092286.9	1.064	60.986	0.524	30.029
193	1.39E-07	2.621	119250025.7	0.951	54.470	0.384	22.024
194	1.21E-07	3.107	141370672.9	1.094	62.678	0.386	22.092

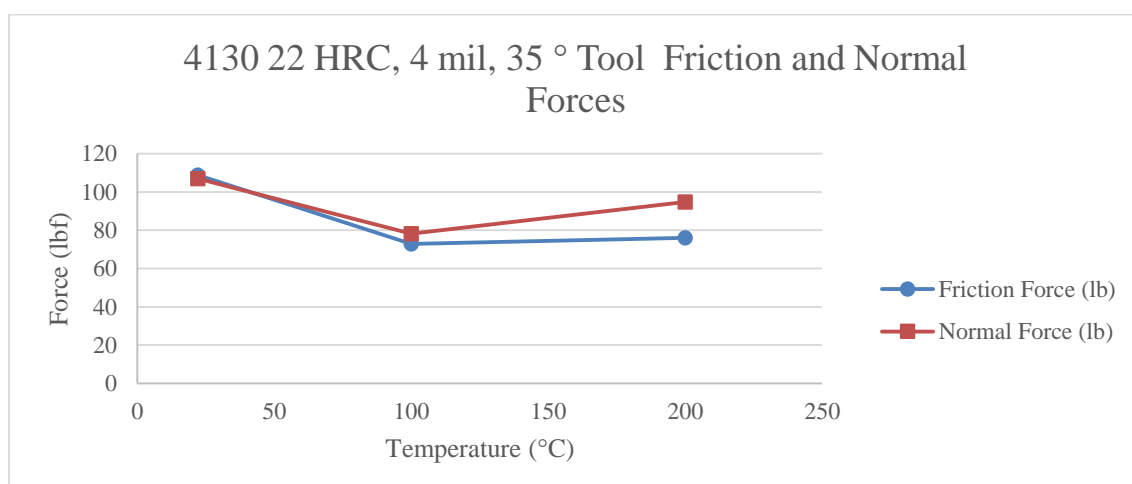
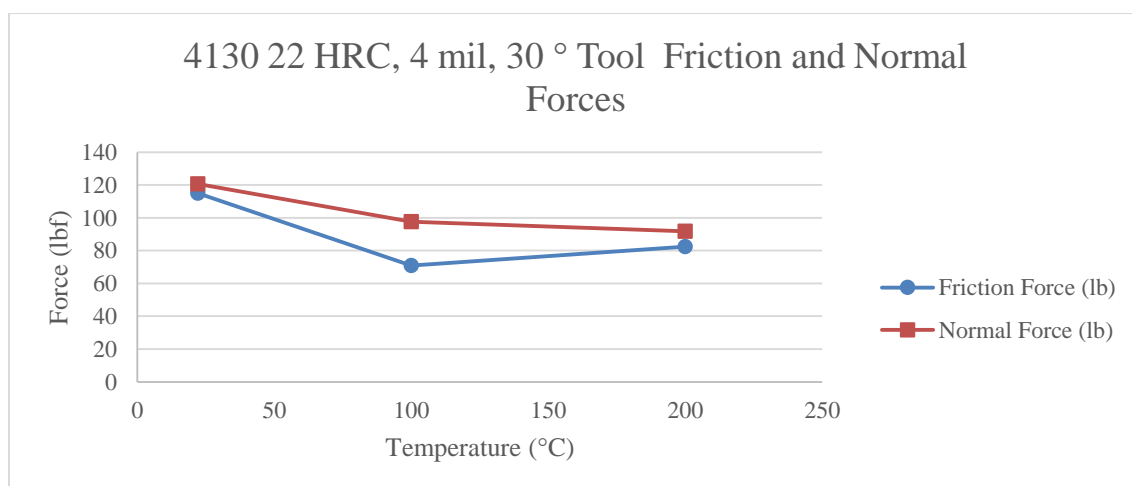
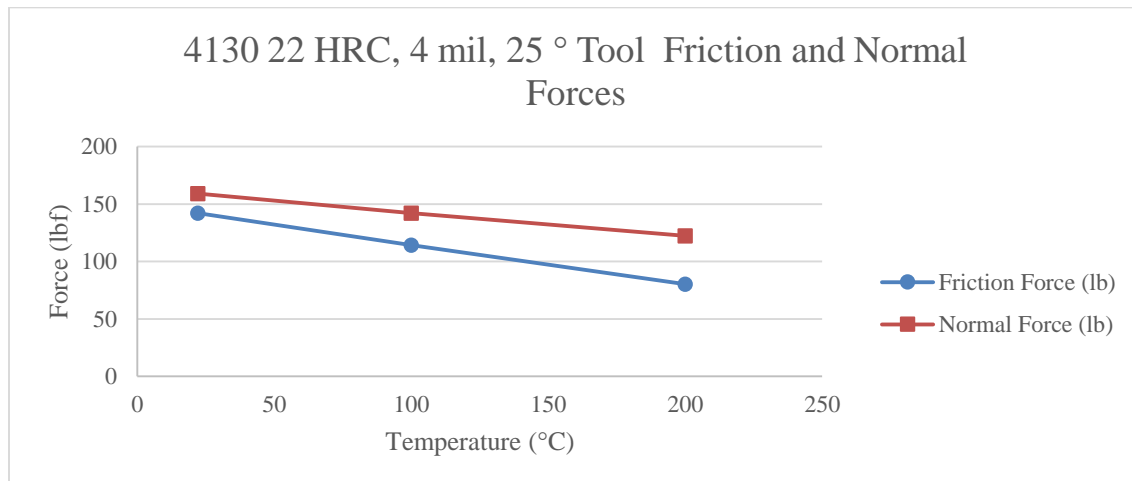
No.	MRR( $m^3/min$ )	Specific Horsepower, Hps ( $hp^*min/in^3$ )	Specific Horsepower, Hps ( $W^*min/m^3$ )	Ki (x) Merchant (radians)	Ki (x) Merchant (degrees)	Ki (x) Payton (radians)	Ki (x) Payton (degrees)
195	1.47E-07	2.659	120994449.9	0.819	46.939	0.382	21.867
196	1.38E-07	2.211	100613154.9	0.989	56.690	0.492	28.201
197	1.25E-07	2.484	113023928.3	0.926	53.057	0.489	28.042
198	1.25E-07	2.548	115946402.2	1.092	62.566	0.502	28.737
199	1.19E-07	2.472	112486826.8	0.865	49.545	0.492	28.187
200	1.24E-07	2.337	106336336.6	1.070	61.330	0.499	28.615
201	1.37E-07	2.131	96983105.81	1.091	62.525	0.485	27.805
202	9.96E-08	2.837	129102991.4	0.934	53.495	0.470	26.921
203	8.19E-08	3.236	147262457.9	1.036	59.367	0.466	26.707
204	1.11E-07	2.836	129057004.7	0.960	55.013	0.487	27.925

Pixel Conversion Table

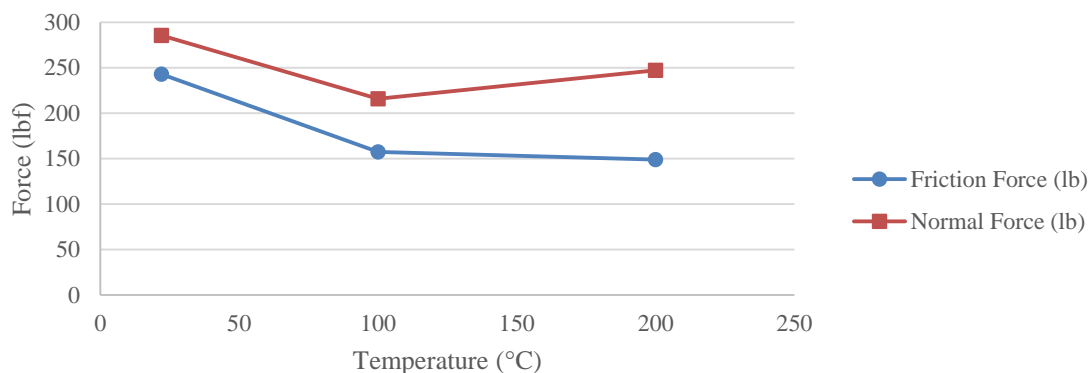
<b>Run</b>	<b>Valid Start Date</b>	<b>Valid End Date</b>	<b>Pixels (1 div x 10)</b>	<b>Scale</b>	<b>Conversion (pixels to in)</b>
pixel_calibration2 (Al)	7/23/2015	8/14/2015	195.11	1div = 0.1mm	0.000201784
4130_22_81415_3	8/14/2015	8/18/2015	176.9	1div = 0.1mm	0.000222556
4130_30_pixelcalib81815	8/18/2015	8/19/2015	199.05	1div = 0.1mm	0.00019779
t6_81915pixelcalib	8/19/2015	8/20/2015	194.56	1div = 0.1mm	0.000202354
4130_82015pixelcalib	8/20/2015	8/27/2015	16.35	1div = 0.1mm	0.002407956
t6_82715pixelcalib	8/27/2015	9/2/2015	174.71	1div = 0.1mm	0.000225345
9215pixelcalib	9/2/2015	10/16/2015	170.04	1div = 0.1mm	0.000231534
pixelcalib101615	10/16/2015	1/15/2016	176.34	1div = 0.1mm	0.000223262
pixelcalib11516	1/15/2016	4/7/2016	190.11	1div = 0.1mm	0.000207091

## Appendix.D: Friction and Normal Force Graphs

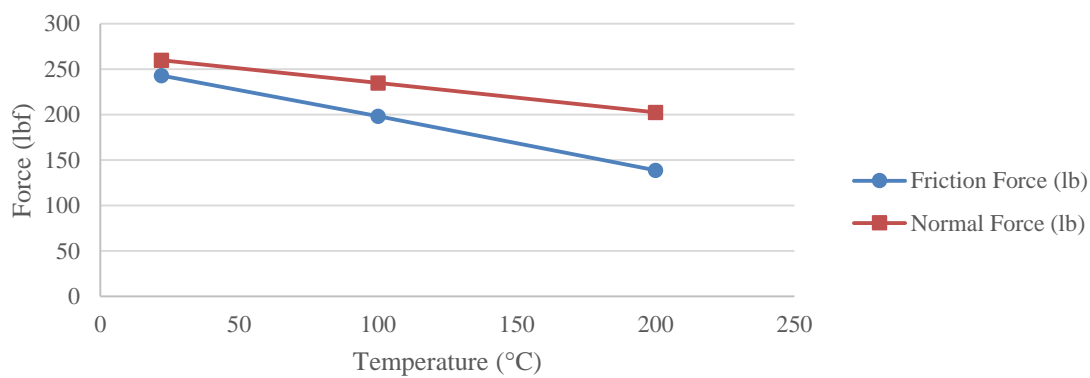
### 4130 22 HRC Steel Friction and Normal Force Graphs



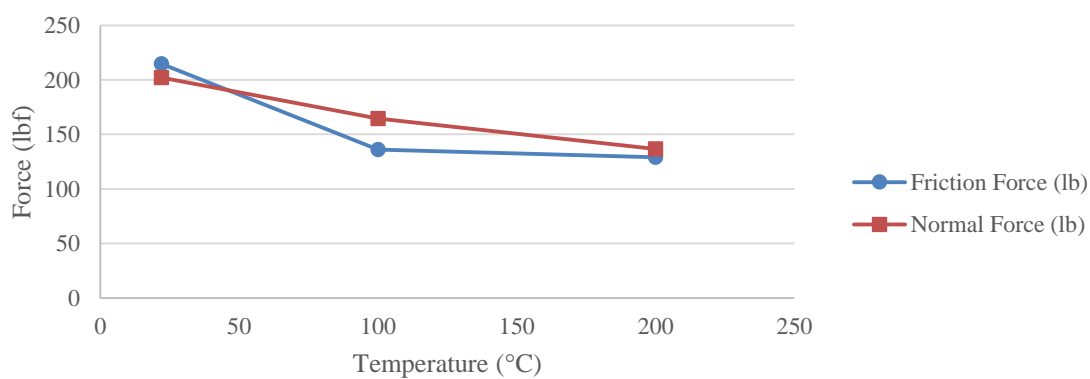
### 4130 22 HRC, 8 mil, 25 ° Tool Friction and Normal Forces



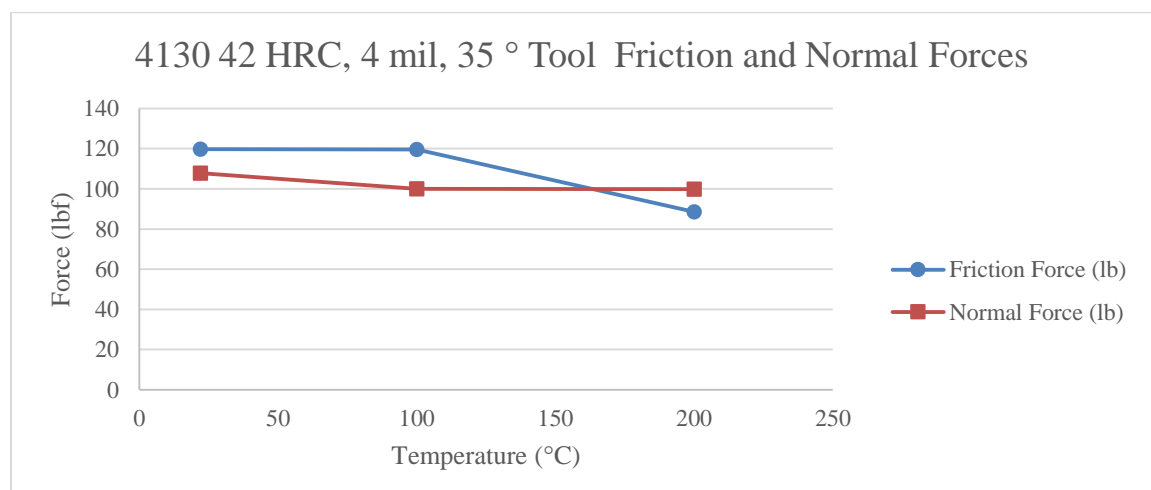
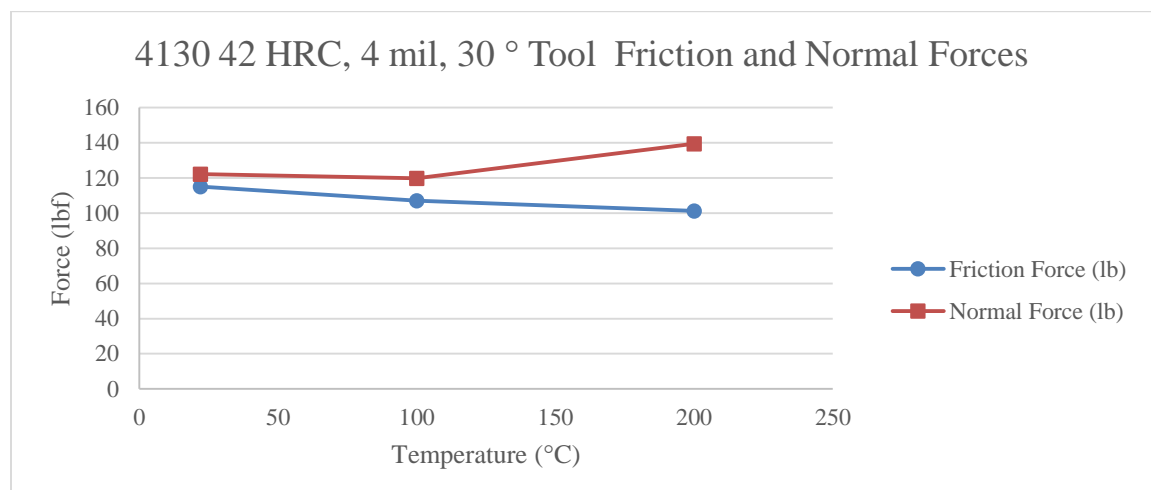
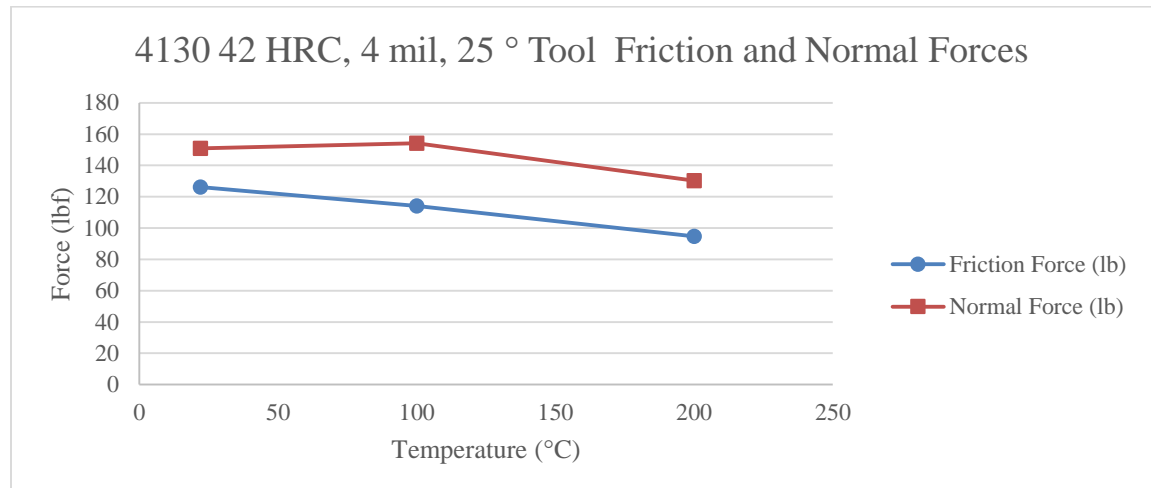
### 4130 22 HRC, 8 mil, 30 ° Tool Friction and Normal Forces



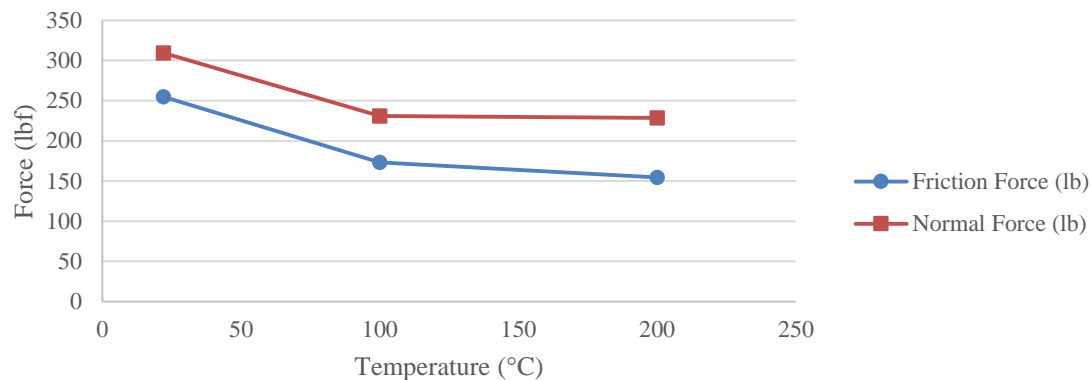
### 4130 22 HRC, 8 mil, 35 ° Tool Friction and Normal Forces



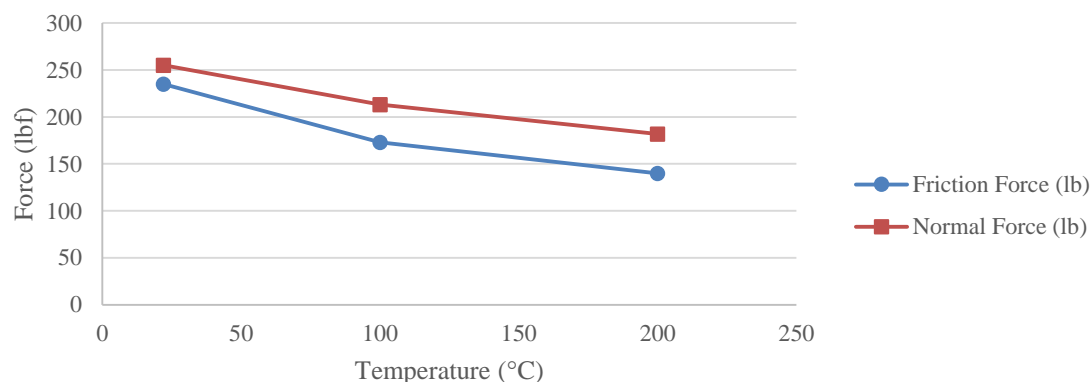
## 4130 42 HRC Steel Friction and Normal Force Graphs



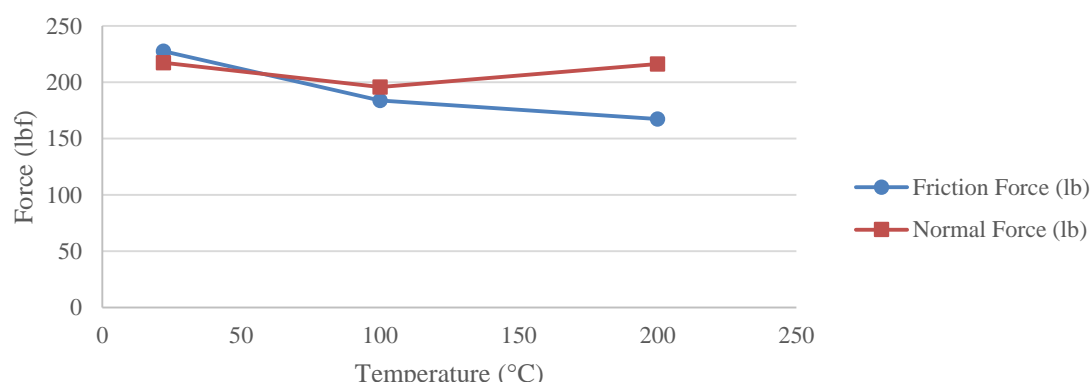
### 4130 42 HRC, 8 mil, 25 ° Tool Friction and Normal Forces



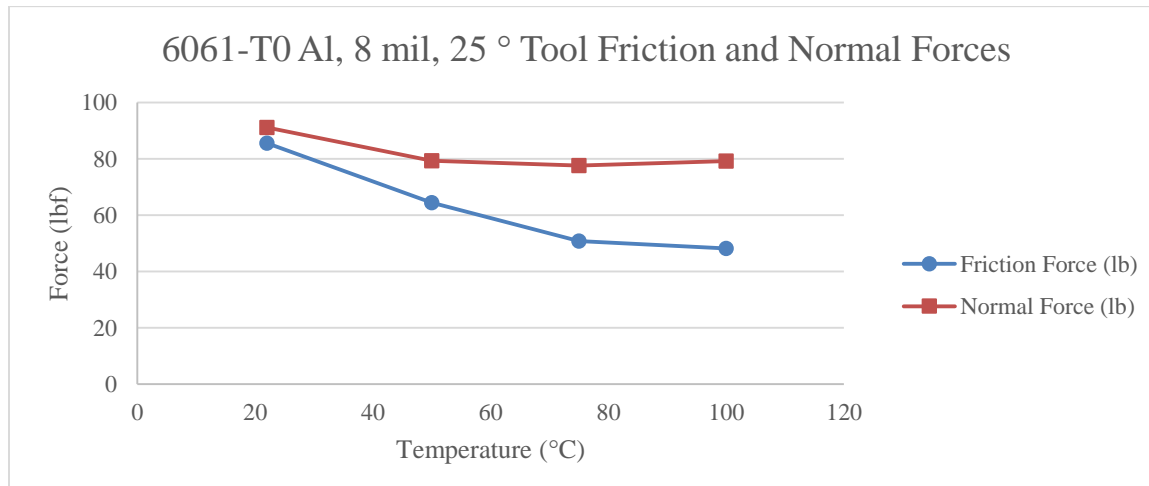
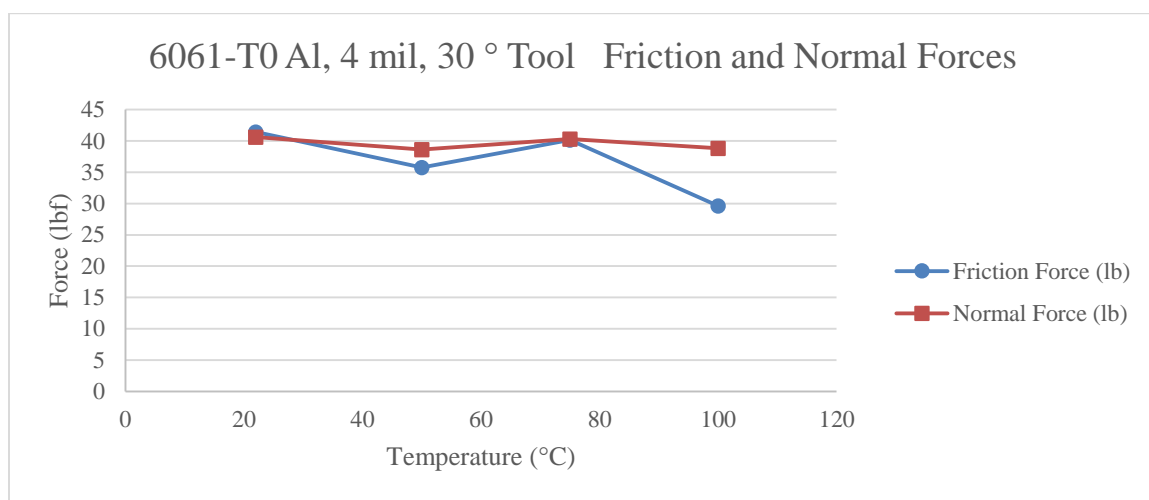
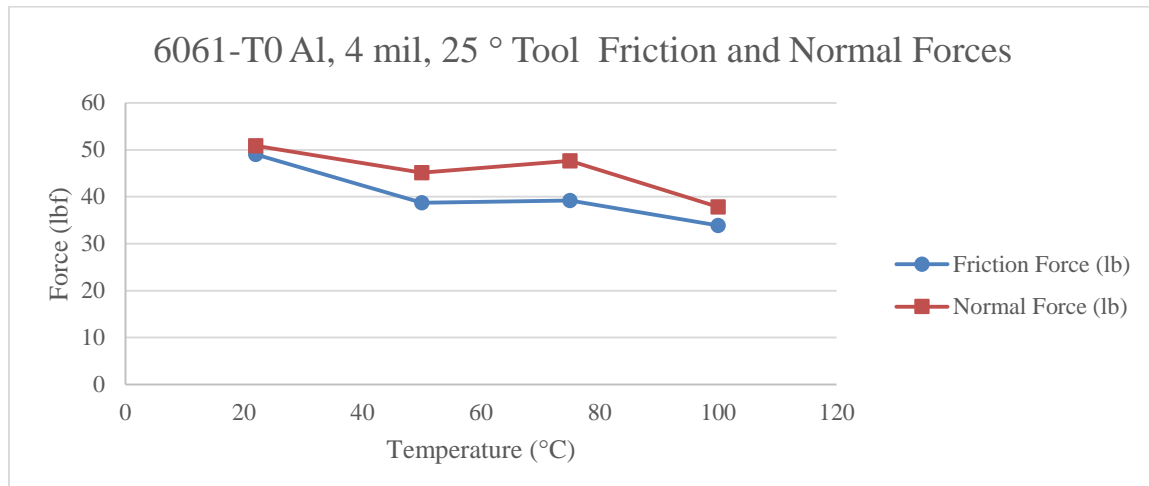
### 4130 42 HRC, 8 mil, 30 ° Tool Friction and Normal Forces



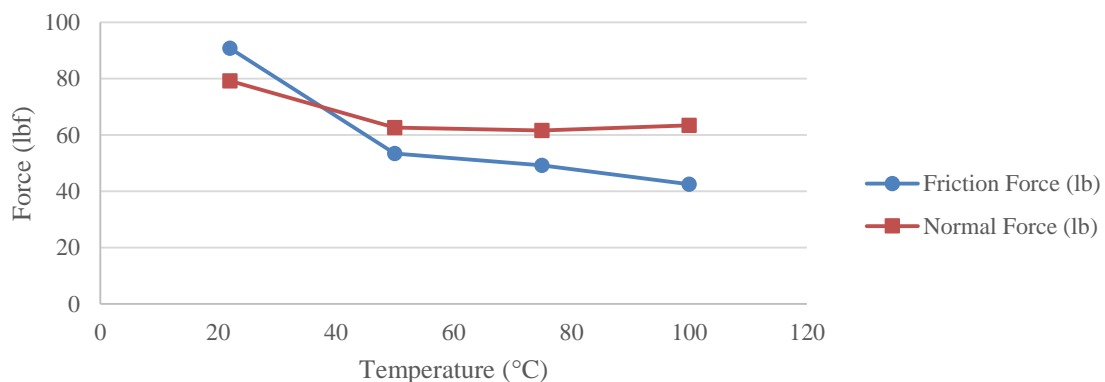
### 4130 42 HRC, 8 mil, 35 ° Tool Friction and Normal Forces



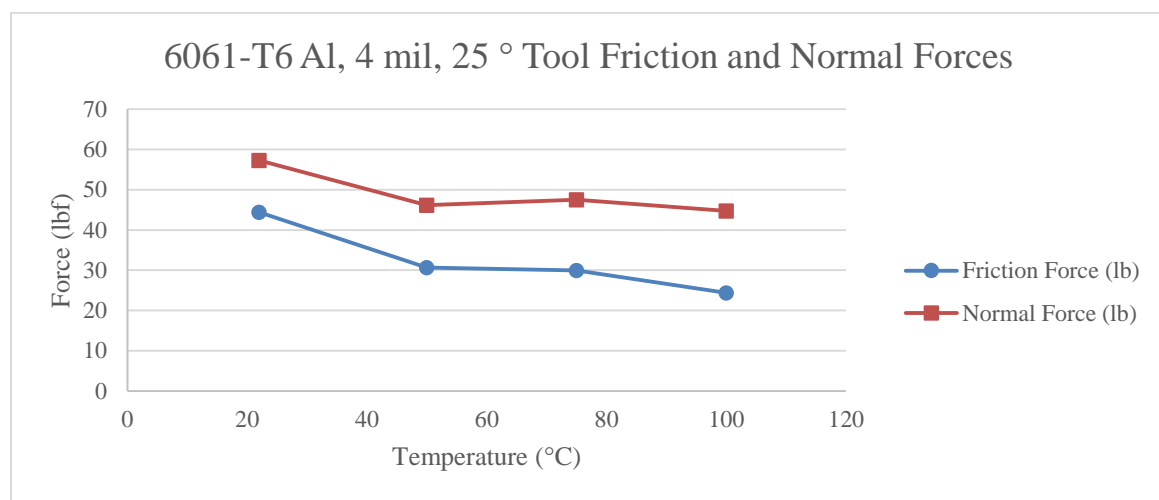
## 6061-T0 Al Friction and Normal Force Graphs



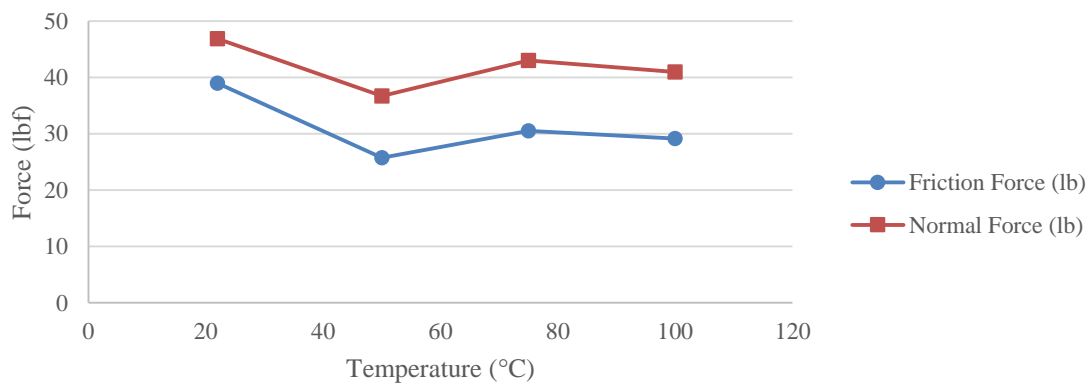
### 6061-T0 Al, 8 mil, 30 ° Tool Friction and Normal Forces



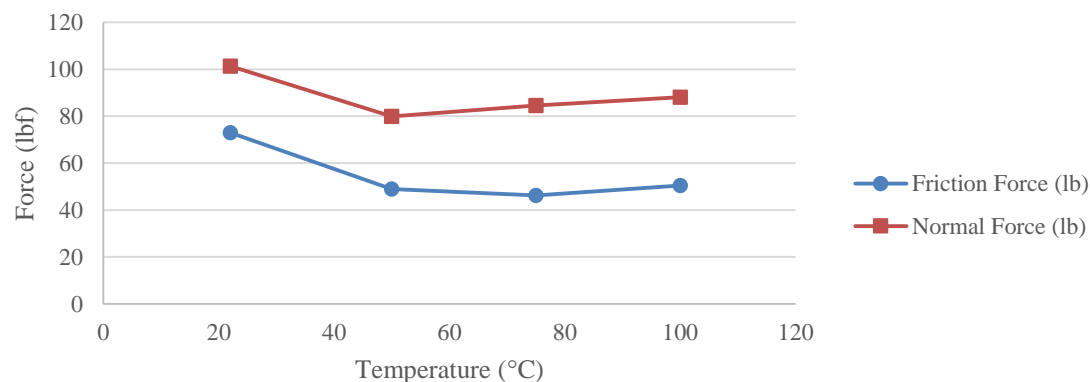
### 6061-T6 Al Friction and Normal Force Graphs



### 6061-T6 Al, 4 mil, 30 ° Tool Friction and Normal Forces

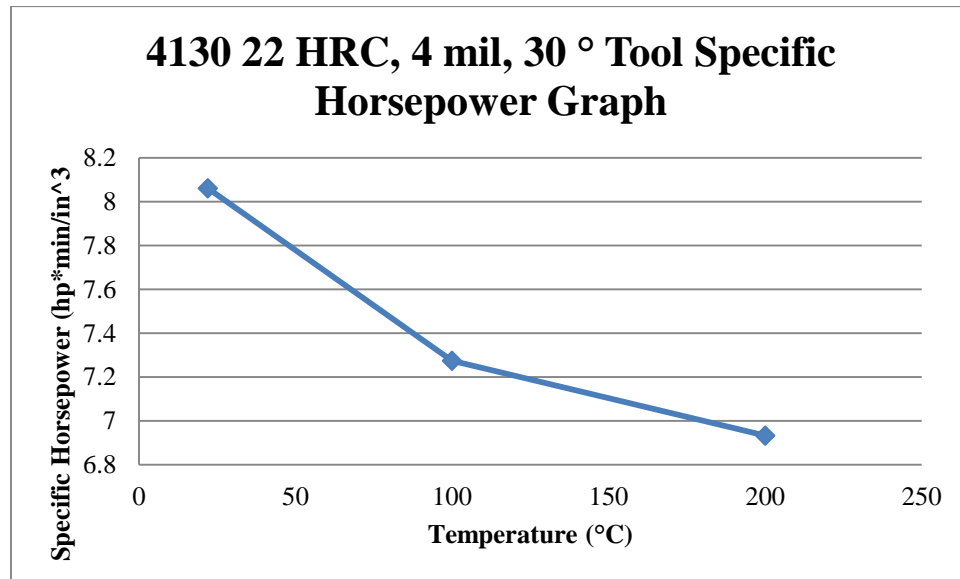
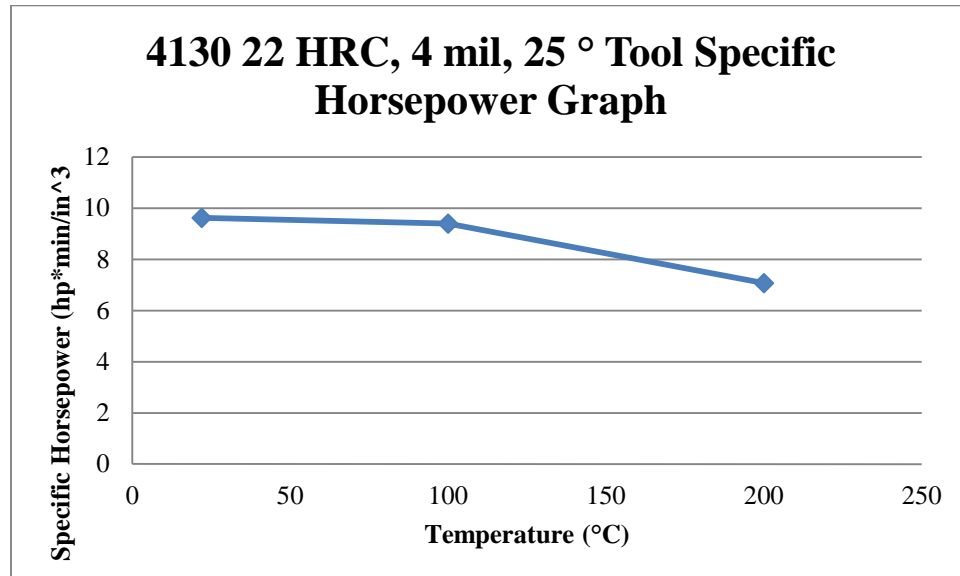


### 6061-T6 Al, 8 mil, 25 ° Tool Friction and Normal Forces

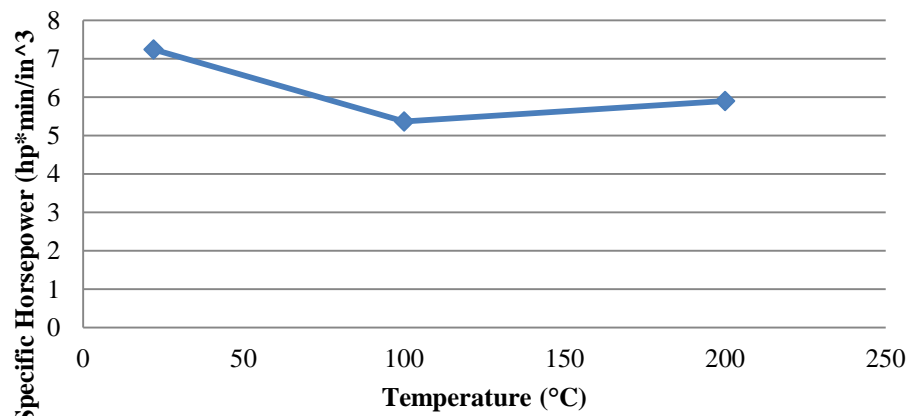


## Appendix.E: Specific Horsepower Graphs

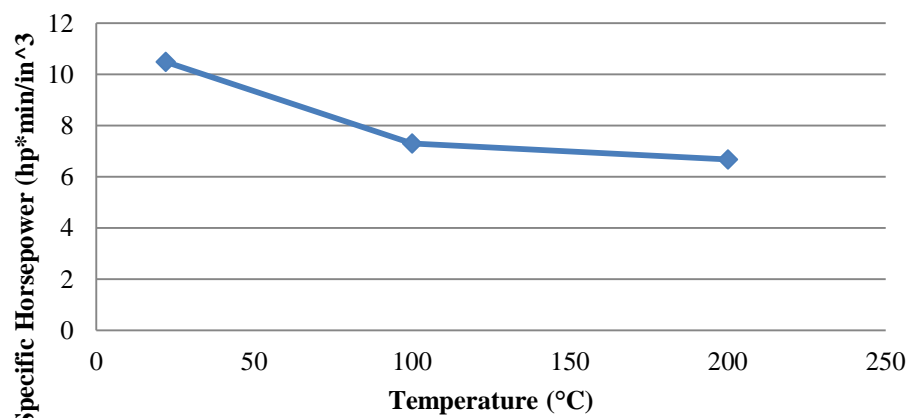
4130 22 HRC Steel Specific Horsepower Graphs



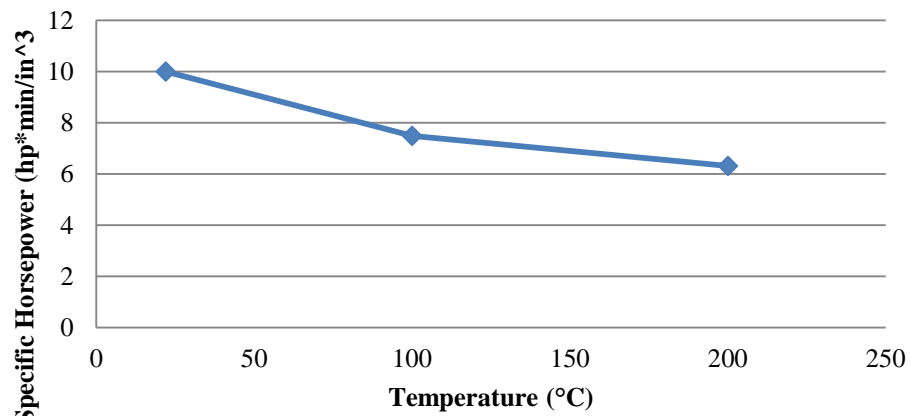
### **4130 22 HRC, 4 mil, 35 ° Tool Specific Horsepower Graph**



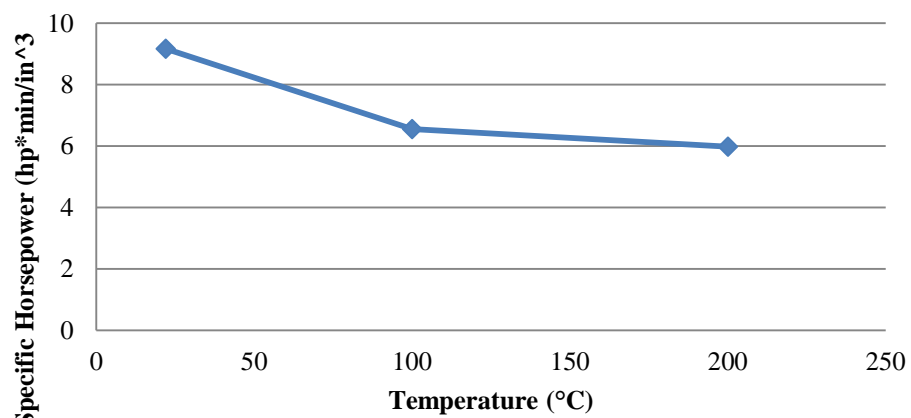
### **4130 22 HRC, 8 mil, 25 ° Tool Specific Horsepower Graph**



### **4130 22 HRC, 8 mil, 30 ° Tool Specific Horsepower Graph**

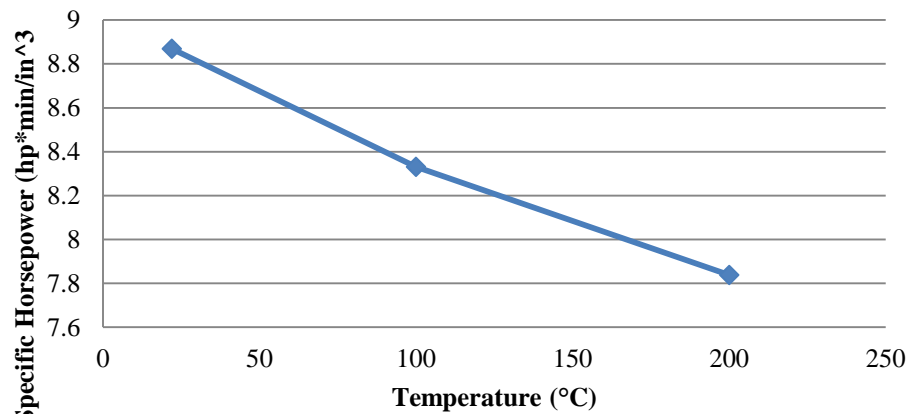


### **4130 22 HRC, 8 mil, 35 ° Tool Specific Horsepower Graph**

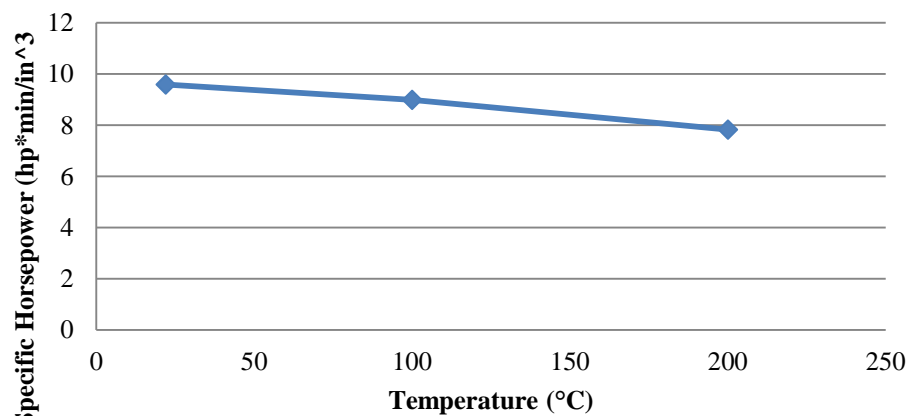


## 4130 42 HRC Steel Specific Horsepower Graphs

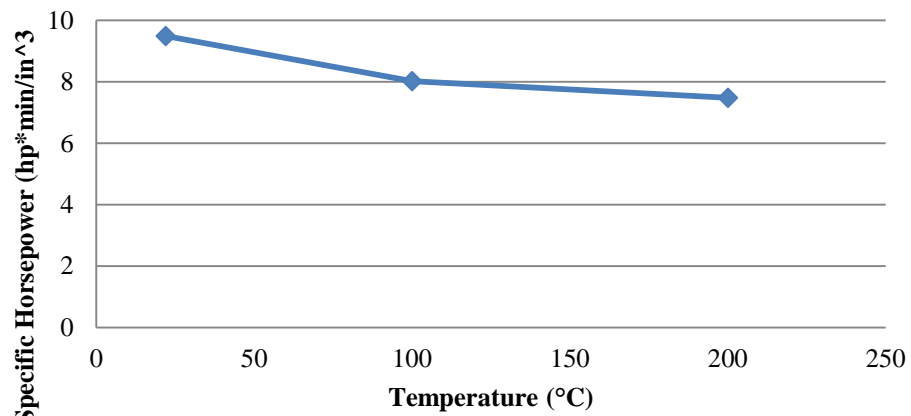
### 4130 42 HRC, 4 mil, 25 ° Tool Specific Horsepower Graph



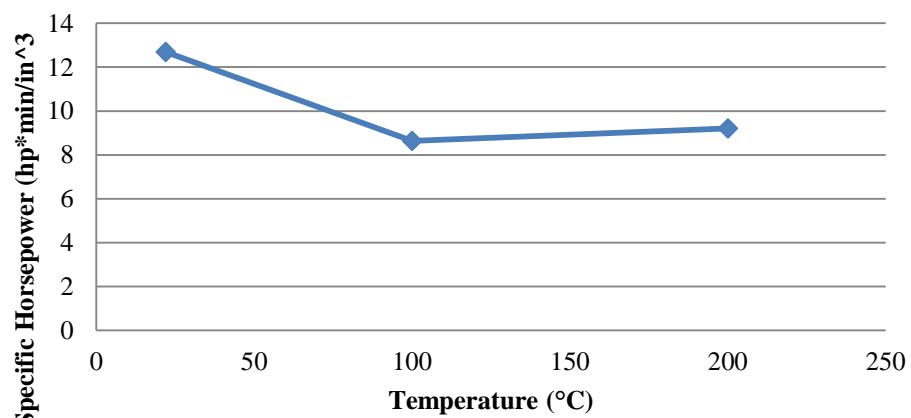
### 4130 42 HRC, 4 mil, 30 ° Tool Specific Horsepower Graph



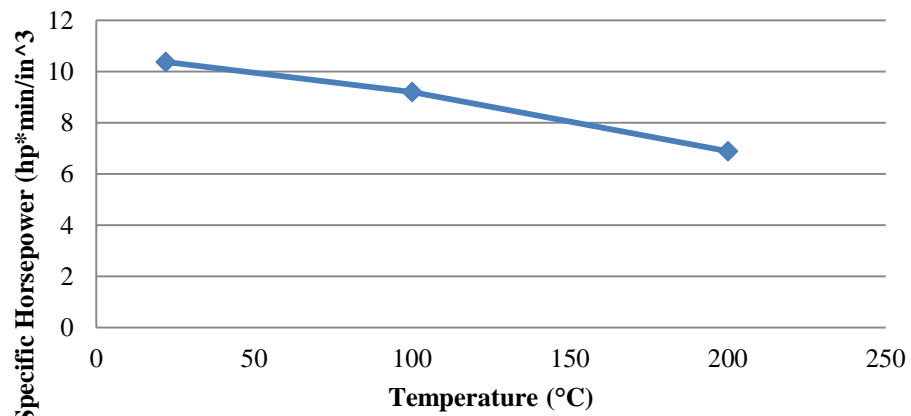
### **4130 42 HRC, 4 mil, 35 ° Tool Specific Horsepower Graph**



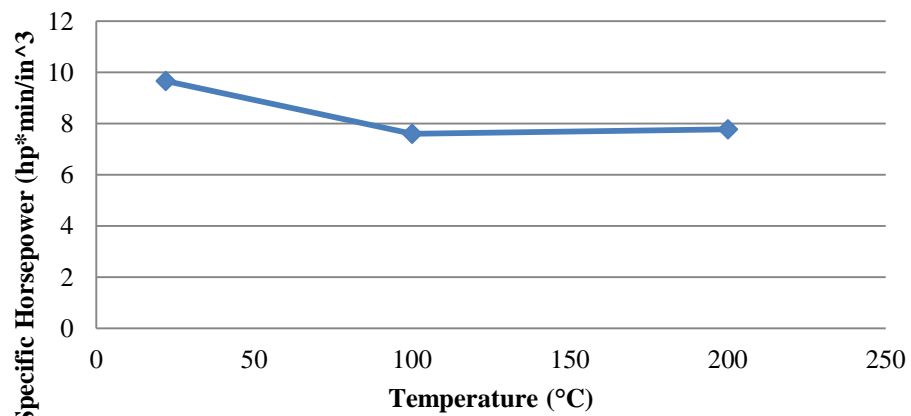
### **4130 42 HRC, 8 mil, 25 ° Tool Specific Horsepower Graph**



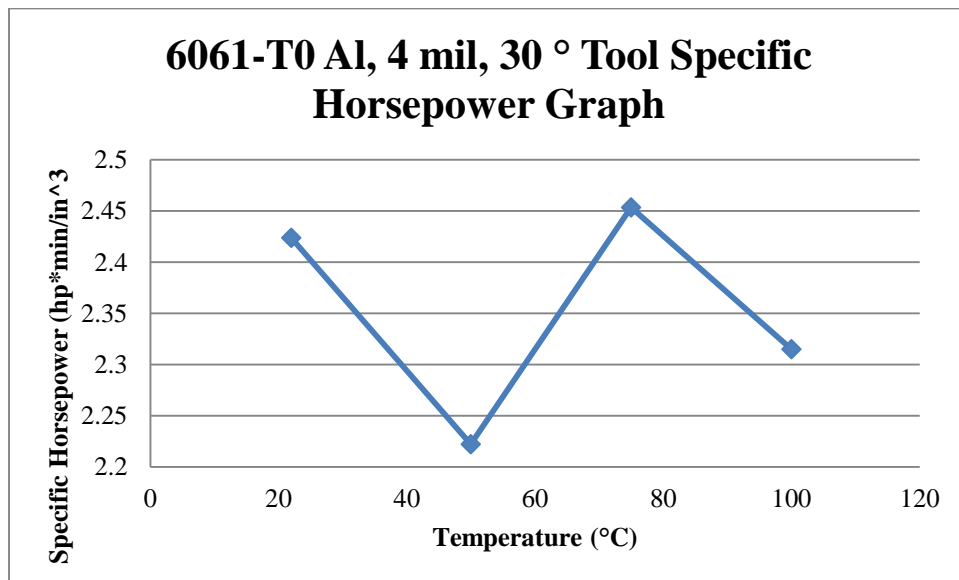
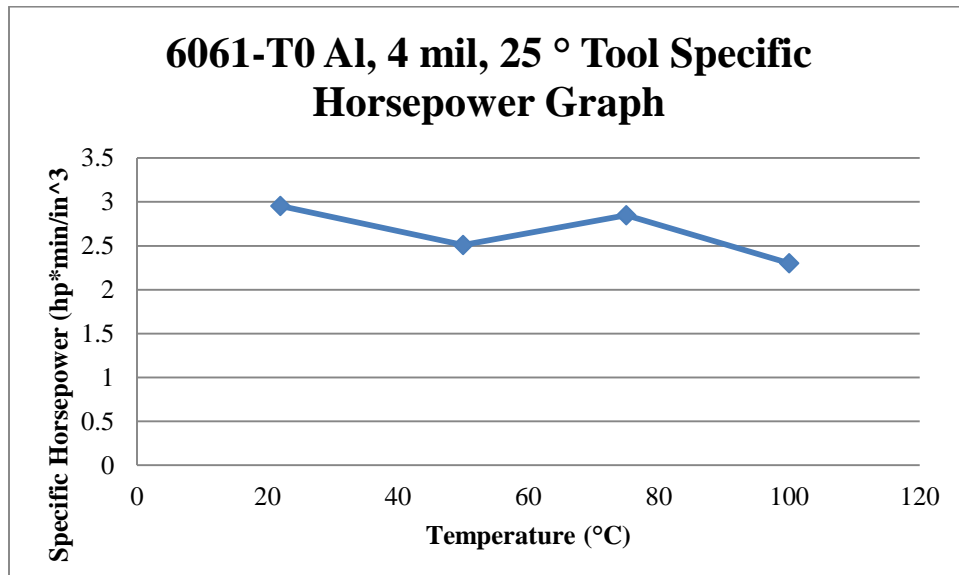
### **4130 42 HRC, 8 mil, 30 ° Tool Specific Horsepower Graph**



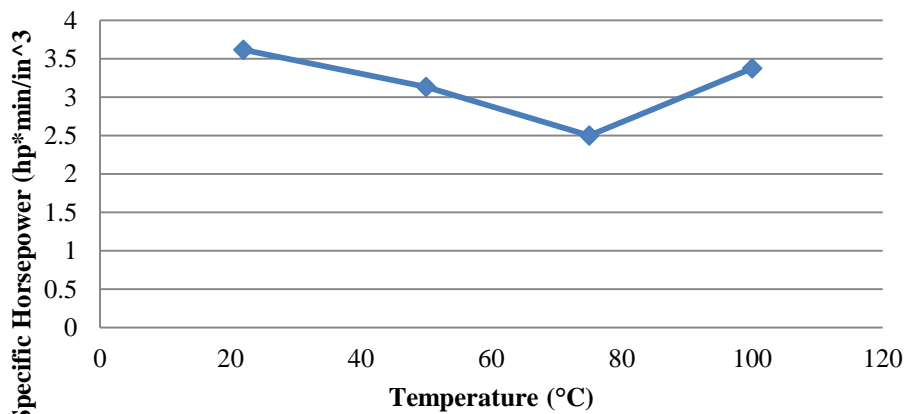
### **4130 42 HRC, 8 mil, 35 ° Tool Specific Horsepower Graph**



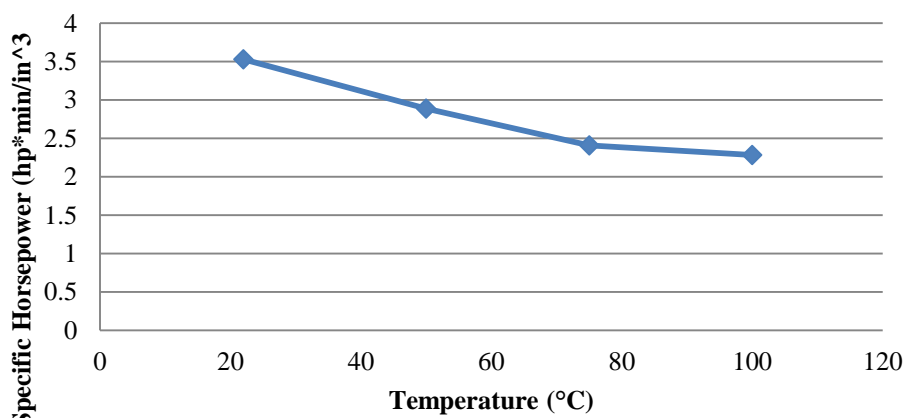
## 6061-T0 Al Specific Horsepower Graphs



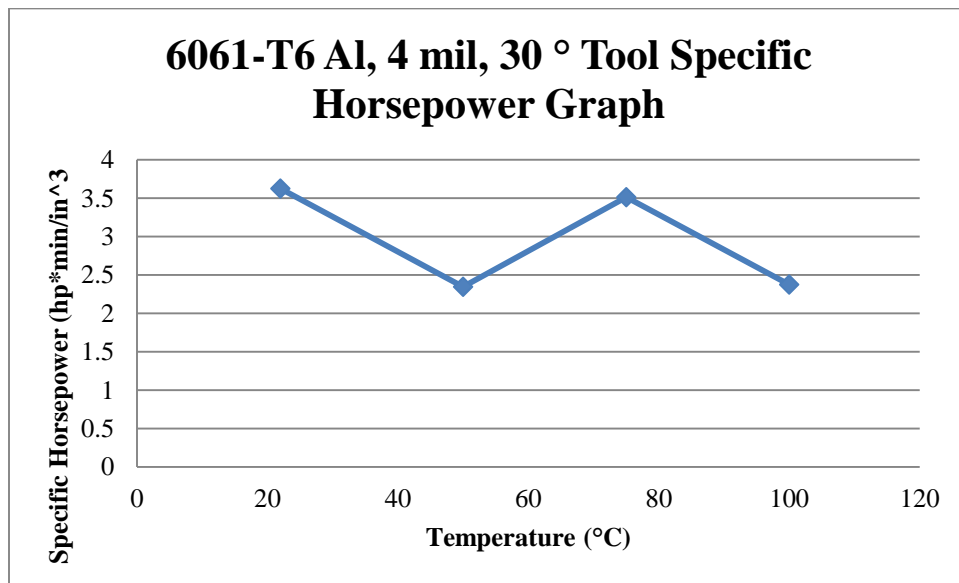
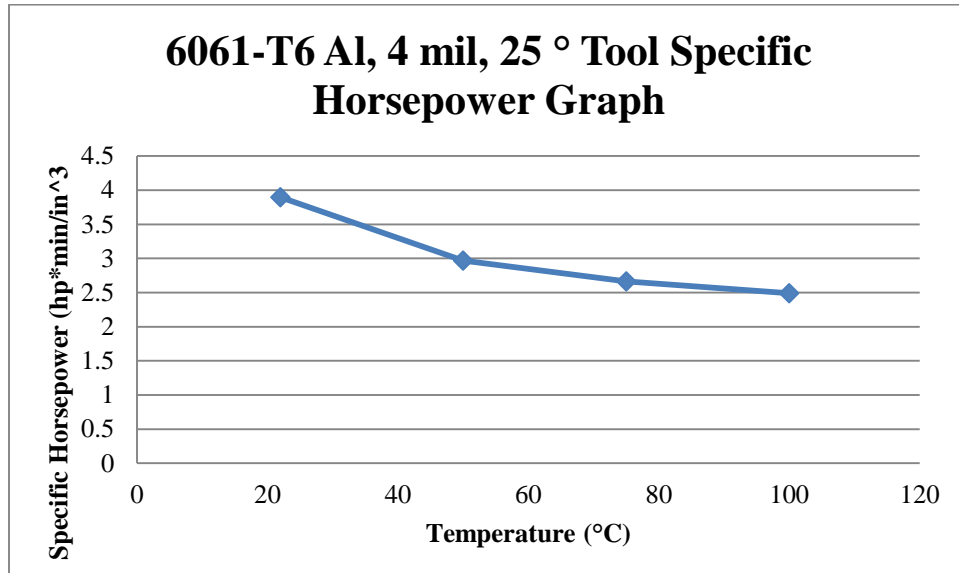
### **6061-T0 Al, 8 mil, 25 ° Tool Specific Horsepower Graph**



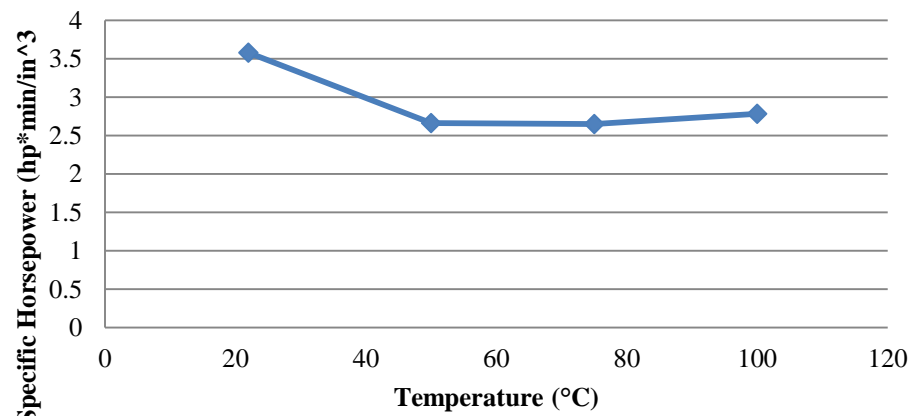
### **6061-T0 Al, 8 mil, 30 ° Tool Specific Horsepower Graph**



## 6061-T6 Al Specific Horsepower Graphs

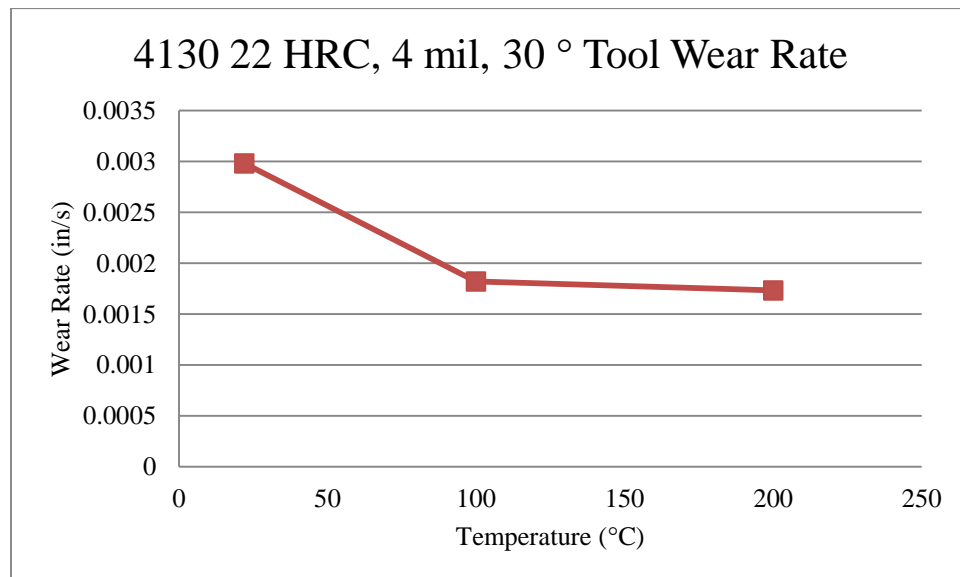
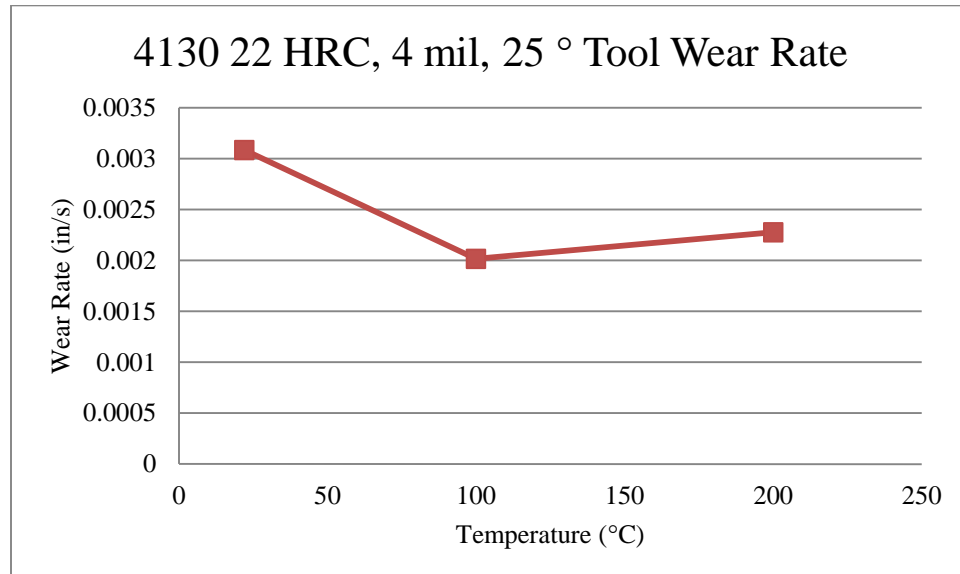


### **6061-T6 Al, 8 mil, 25 ° Tool Specific Horsepower Graph**

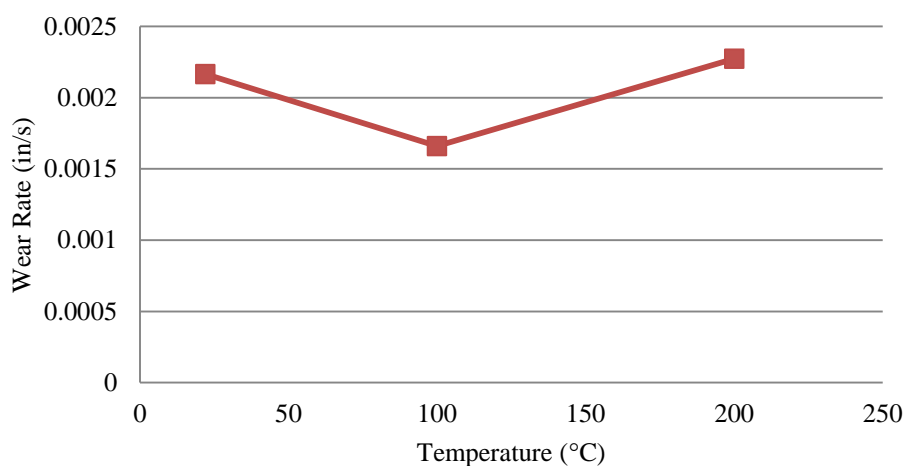


## Appendix.F: Wear Rate Graphs

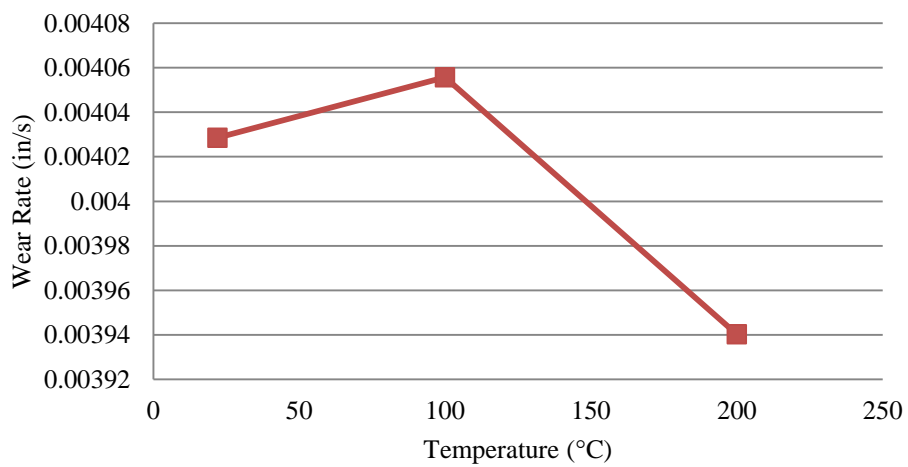
4130 22 HRC Steel Tool Wear Rate Graphs



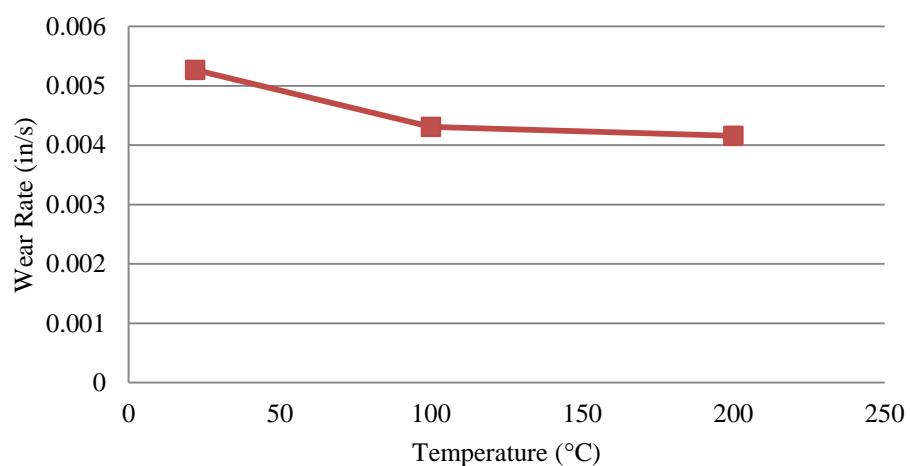
### 4130 22 HRC, 4 mil, 35 ° Tool Wear Rate



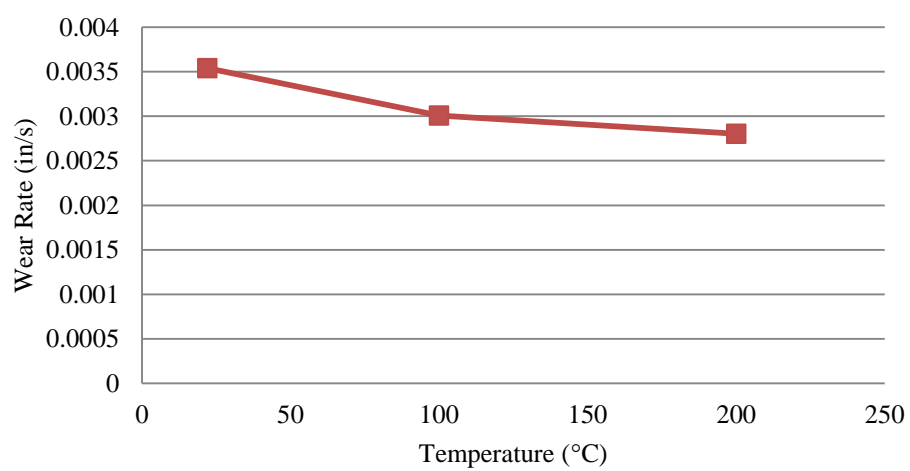
### 4130 22 HRC, 8 mil, 25 ° Tool Wear Rate



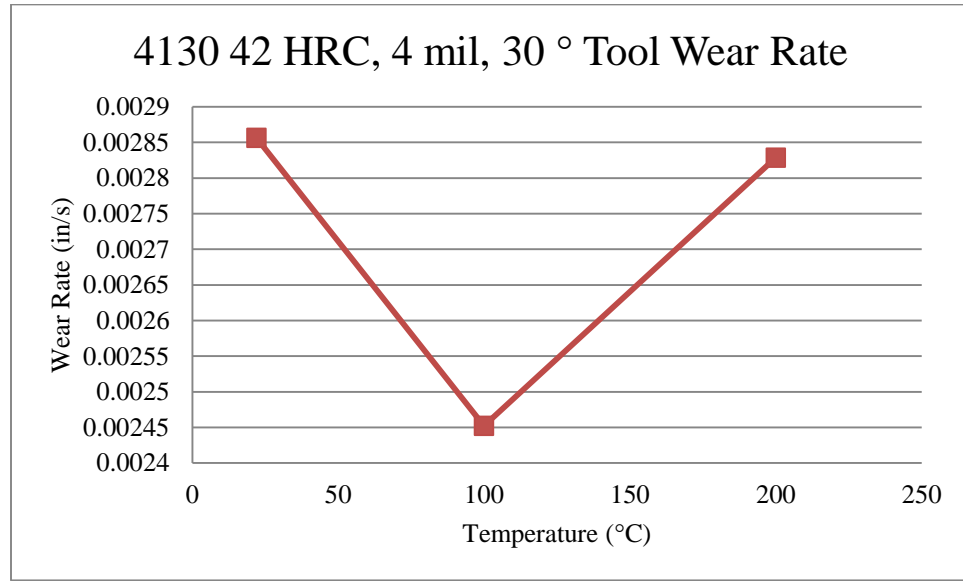
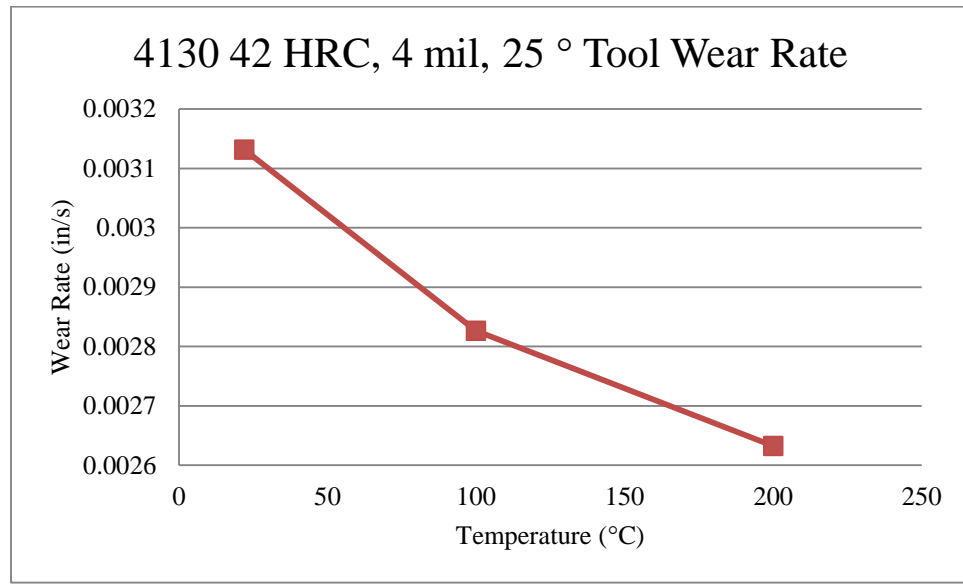
### 4130 22 HRC, 8 mil, 30 ° Tool Wear Rate



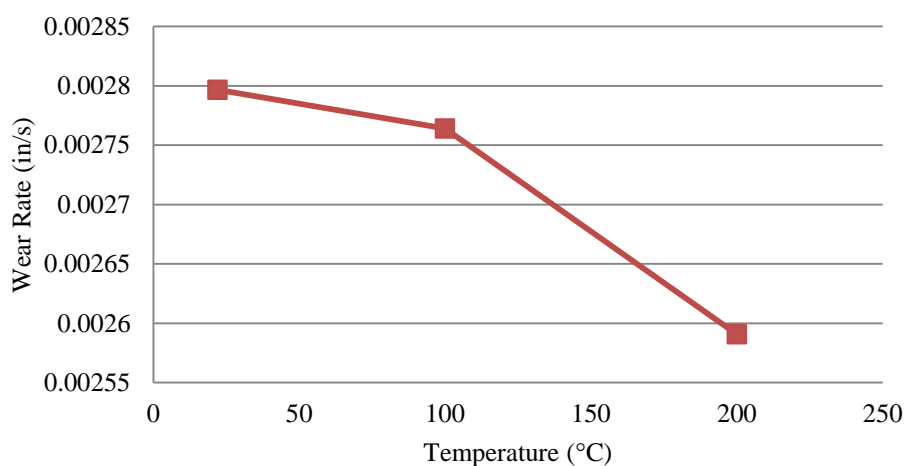
### 4130 22 HRC, 8 mil, 35 ° Tool Wear Rate



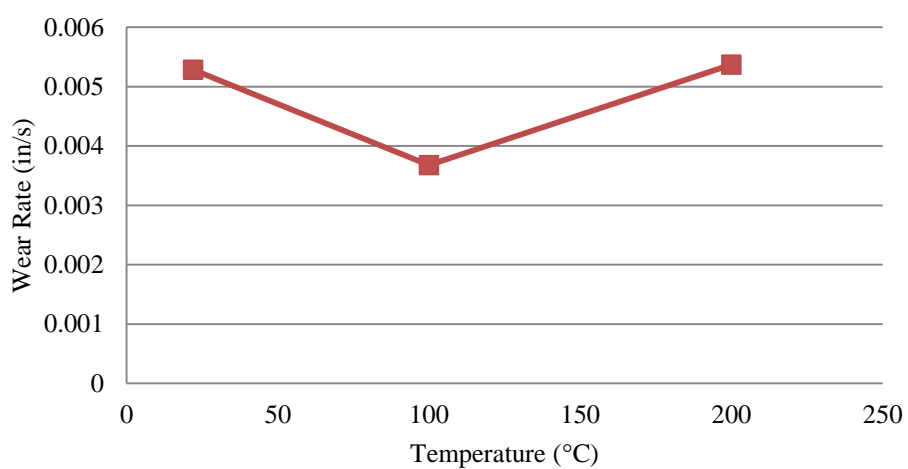
## 4130 42 HRC Steel Tool Wear Rate Graphs



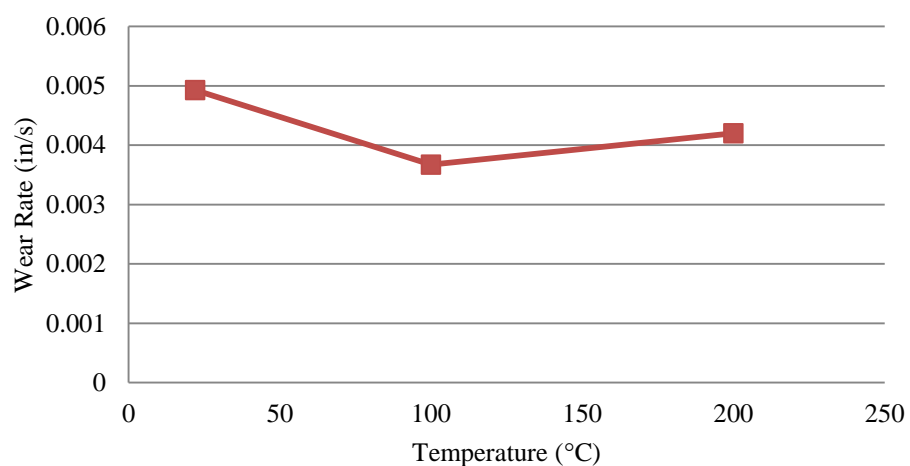
### 4130 42 HRC, 4 mil, 35 ° Tool Wear Rate



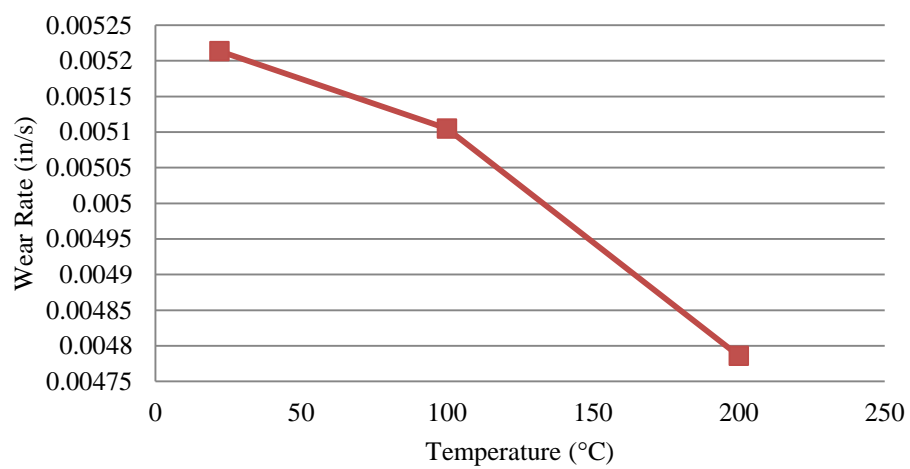
### 4130 42 HRC, 8 mil, 25 ° Tool Wear Rate



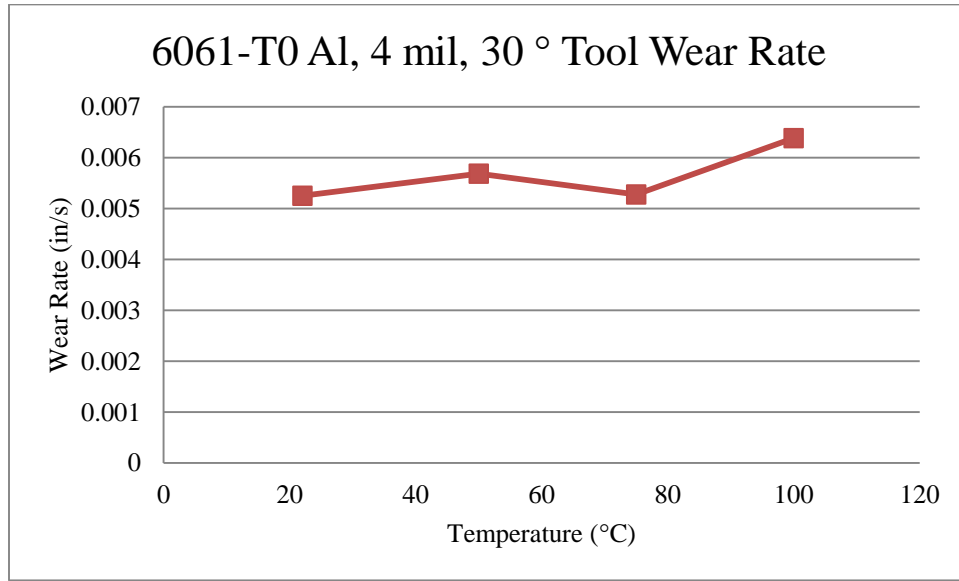
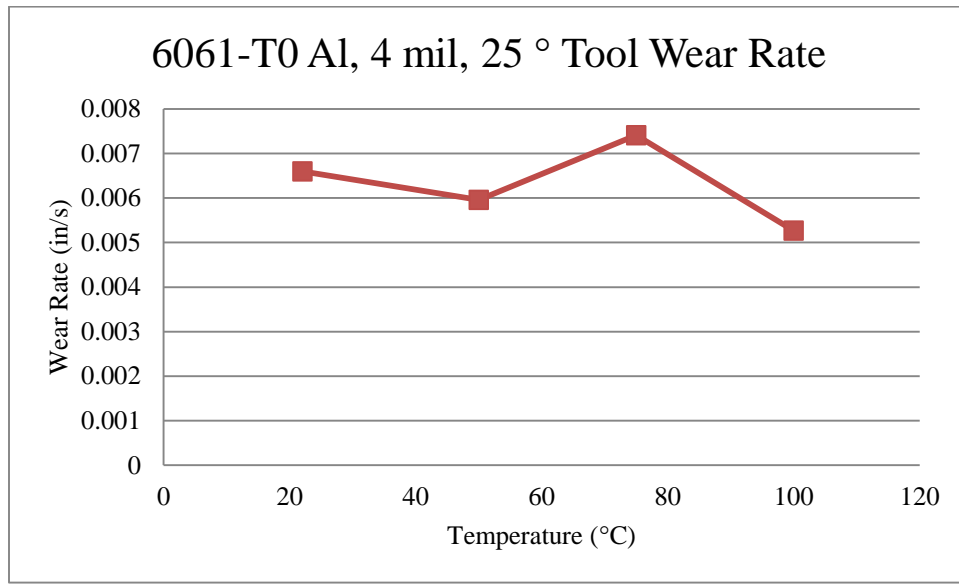
### 4130 42 HRC, 8 mil, 30 ° Tool Wear Rate



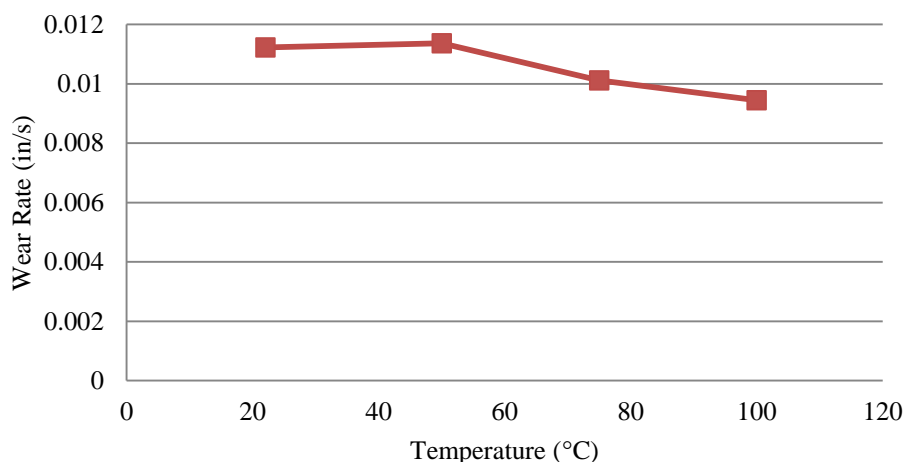
### 4130 42 HRC, 8 mil, 35 ° Tool Wear Rate



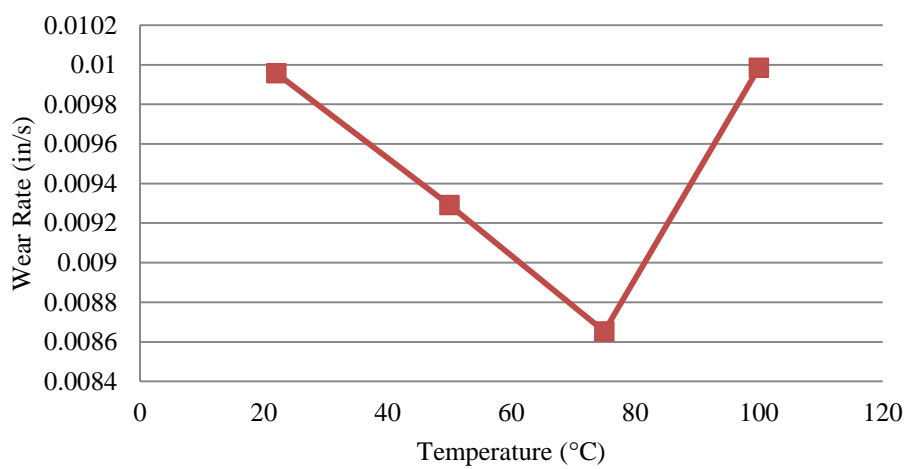
## 6061-T0 Al Tool Wear Rate Graphs



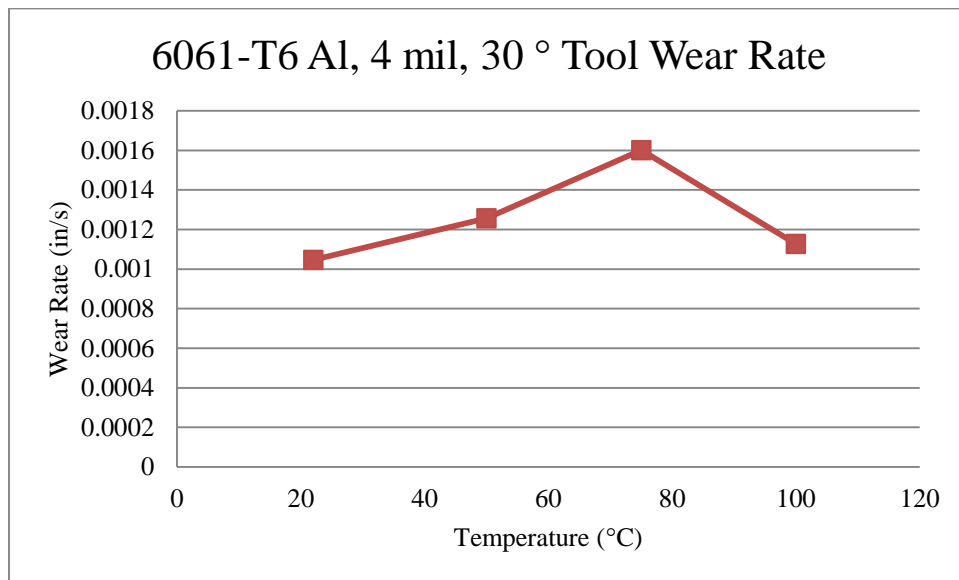
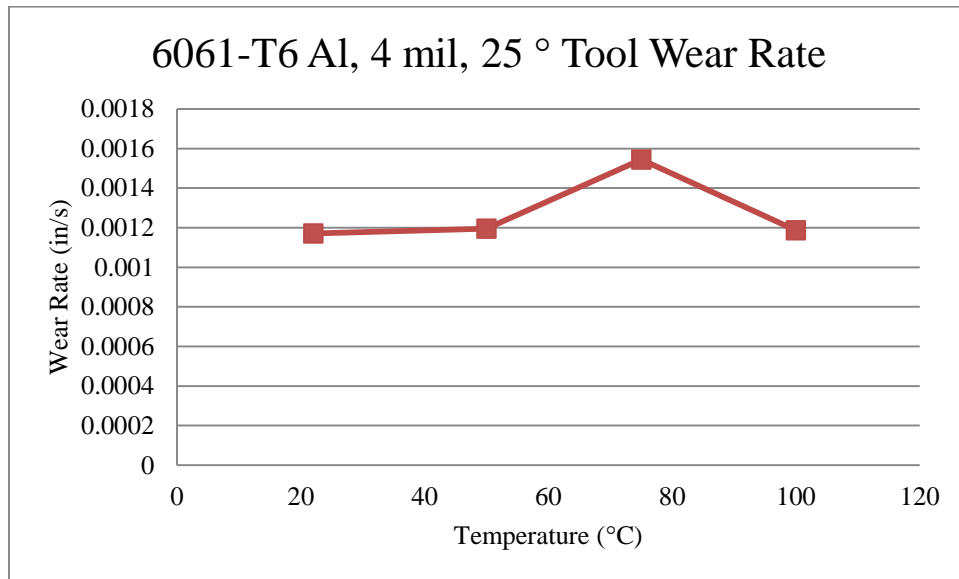
6061-T0 Al, 8 mil, 25 ° Tool Wear Rate



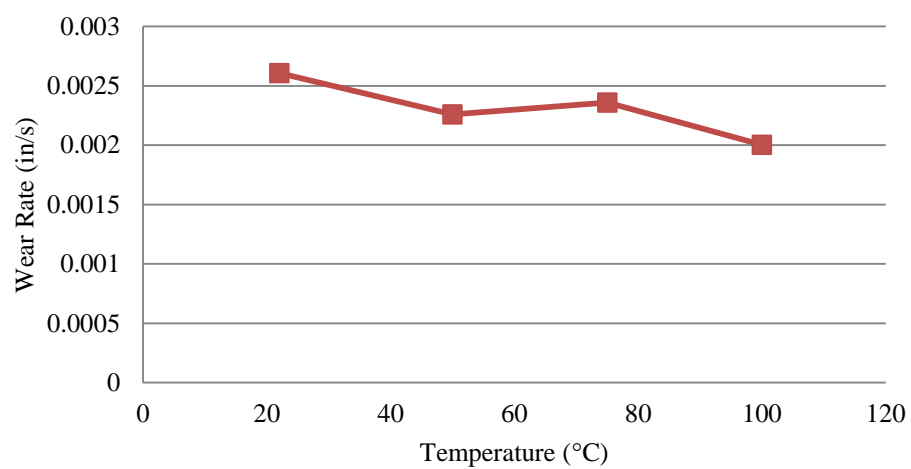
6061-T0 Al, 8 mil, 30 ° Tool Wear Rate



## 6061-T6 Al Tool Wear Rate Graphs



### 6061-T6 Al, 8 mil, 25 ° Tool Wear Rate



## Appendix.G: ANOVA Tables

### Steel Wear Rate Analysis

**Analysis of Variance for Wear Rate Payton (in/sec)**

Source	Sum of Squares	Df	Mean Square	F-Ratio	P-Value
A:Hardness/Temper	0.000016545	1	0.000016545	28.64	<b>0.0000</b>
B:Tool Angle (degrees)	4.69206E-9	1	4.69206E-9	0.01	0.9284
C:Depth of Cut (mils)	0.0000903731	1	0.0000903731	156.44	<b>0.0000</b>
D:Temperature (°C)	1.24132E-7	1	1.24132E-7	0.21	0.6439
AB	0.0000053196	1	0.0000053196	9.21	<b>0.0030</b>
AD	0.00000342487	1	0.00000342487	5.93	<b>0.0166</b>
Total error	0.0000595003	103	5.77673E-7		
Total (corr.)	0.00017293	109			

R-squared = **65.5929** percent

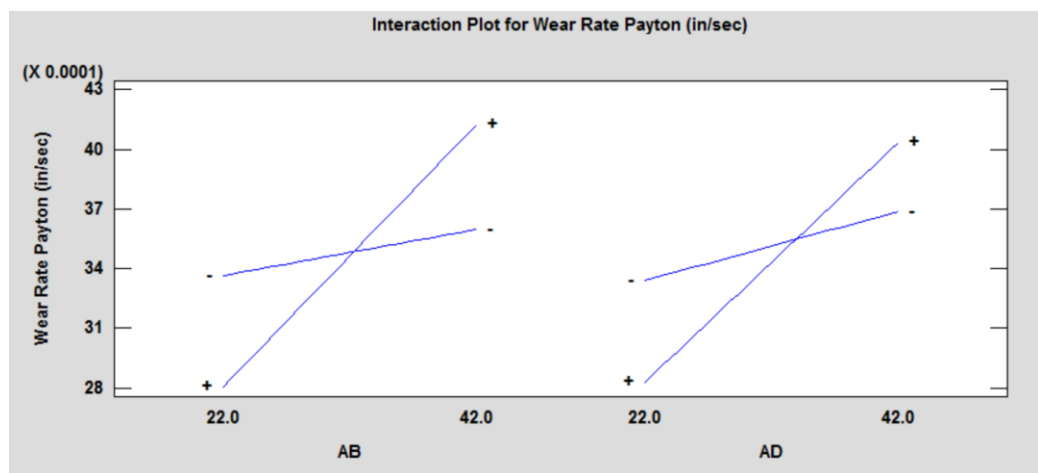
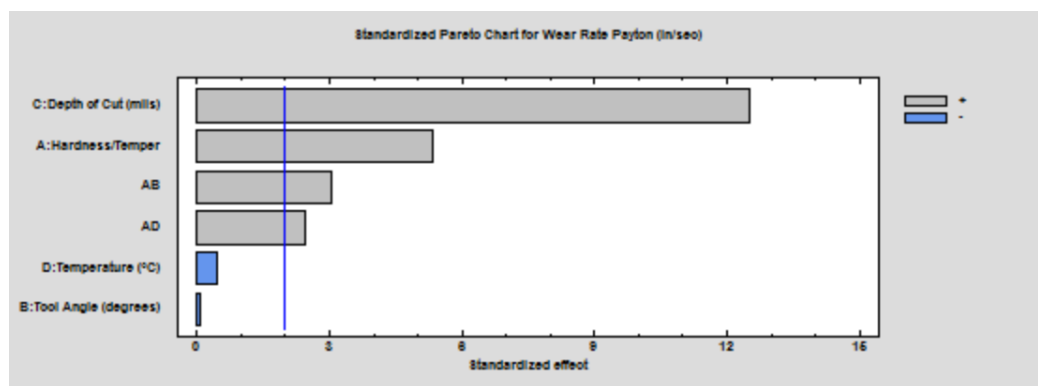
R-squared (adjusted for d.f.) = **63.5886** percent

Standard Error of Est. = **0.000760048**

Mean absolute error = **0.000582827**

Durbin-Watson statistic = 1.59519 (P=**0.0166**)

Lag 1 residual autocorrelation = 0.175949



Left: Interaction of Hardness and Tool Angle on Wear Rate

Right: Interaction of Hardness and Temperature on Wear Rate

## Steel Specific Horsepower Analysis

**Analysis of Variance for Specific Horsepower,  $HP_s$**

Source	Sum of Squares	Df	Mean Square	F-Ratio	P-Value
A:Hardness/Temper	33.9308	1	33.9308	22.35	0.0000
B:Tool Angle (degrees)	27.4187	1	27.4187	18.06	0.0000
C:Depth of Cut (mils)	9.75298	1	9.75298	6.42	0.0127
D:Temperature (°C)	112.742	1	112.742	74.27	0.0000
CD	6.60841	1	6.60841	4.35	0.0394
Total error	157.877	104	1.51805		
Total (corr.)	346.245	109			

R-squared = 54.4031 percent

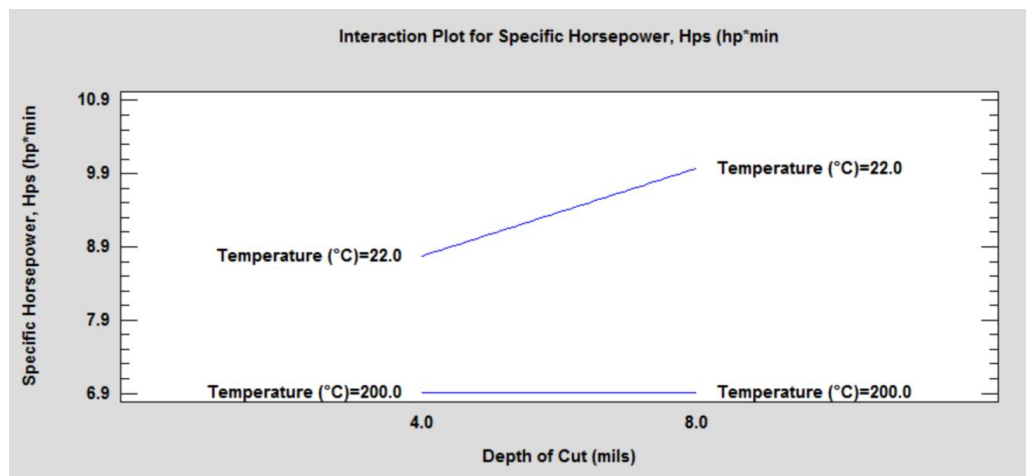
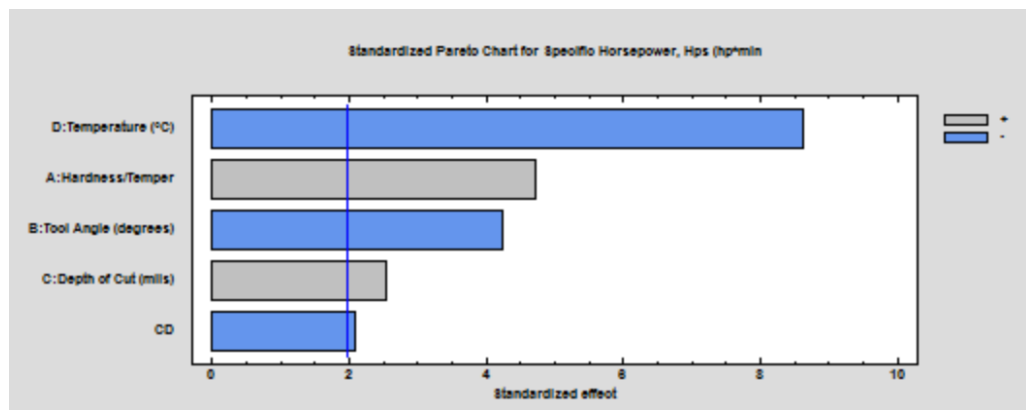
R-squared (adjusted for d.f.) = 52.211 percent

Standard Error of Est. = 1.23209

Mean absolute error = 0.96128

Durbin-Watson statistic = 1.8028 (P=0.1516)

Lag 1 residual autocorrelation = 0.0865409



Interaction of Depth of Cut with Temperature

## Steel Friction Co-Efficient

**Analysis of Variance for  $F_n$  Payton (lbf)**

Source	Sum of Squares	Df	Mean Square	F-Ratio	P-Value
A:Hardness/Temper	6635.04	1	6635.04	8.29	0.0049
B:Tool Angle (degrees)	30326.1	1	30326.1	37.89	0.0000
C:Depth of Cut (mils)	427156.	1	427156.	533.76	0.0000
D:Temperature (°C)	91424.2	1	91424.2	114.24	0.0000
AB	3934.45	1	3934.45	4.92	0.0289
AC	9.37753	1	9.37753	0.01	0.9140
AD	342.9	1	342.9	0.43	0.5143
BC	80.5166	1	80.5166	0.10	0.7518
BD	3226.77	1	3226.77	4.03	0.0474
CD	15723.5	1	15723.5	19.65	0.0000
DD	9477.03	1	9477.03	11.84	0.0009
Total error	78426.6	98	800.271		
Total (corr.)	671858.	109			

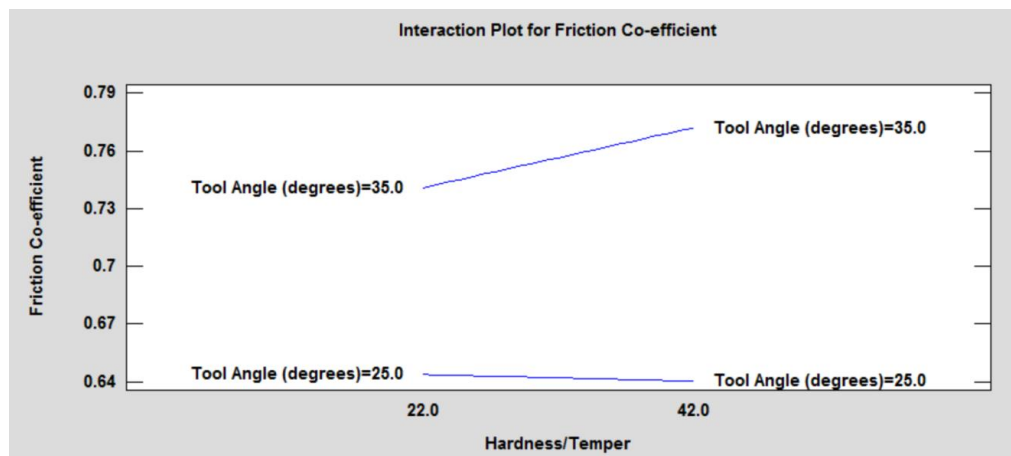
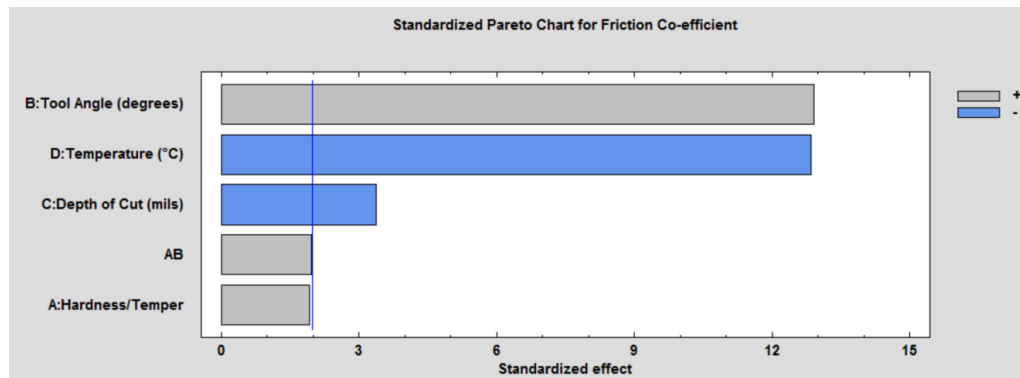
R-squared = 88.3269 percent

R-squared (adjusted for d.f.) = 87.0167 percent

Standard Error of Est. = 28.2891

Mean absolute error = 19.82

Durbin-Watson statistic = 1.71321 (P=0.0666)



Interaction of Tool angle and Hardness on Friction Coefficient

## Steel Normal Shear Force ( $F_n$ ) Analysis

**Analysis of Variance for  $F_n$  Payton (lbf)**

Source	Sum of Squares	Df	Mean Square	F-Ratio	P-Value
A:Hardness/Temper	6727.85	1	6727.85	7.56	0.0070
B:Tool Angle (degrees)	31408.1	1	31408.1	35.31	0.0000
C:Depth of Cut (mils)	425536.	1	425536.	478.39	0.0000
D:Temperature (°C)	86880.0	1	86880.0	97.67	0.0000
AB	3934.45	1	3934.45	4.42	0.0379
CD	16211.0	1	16211.0	18.22	0.0000
Total error	91620.6	103	889.52		
Total (corr.)	671858.	109			

R-squared = 86.3631 percent

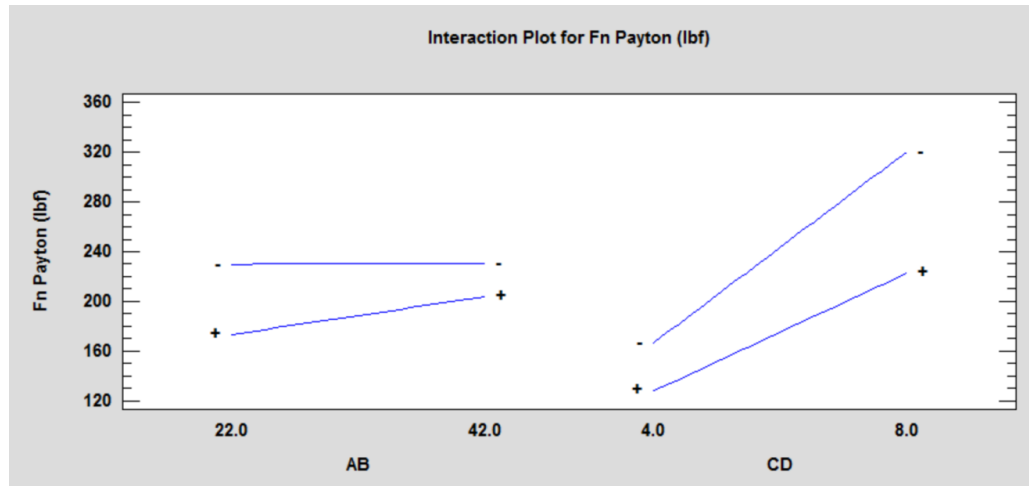
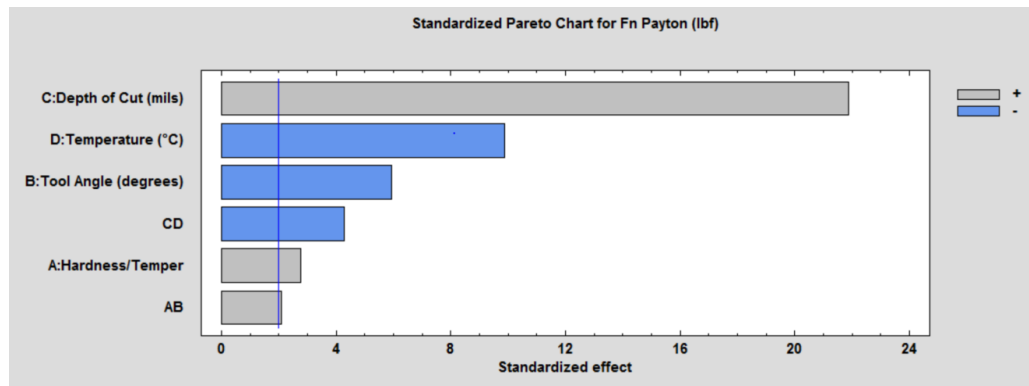
R-squared (adjusted for d.f.) = 85.5687 percent

Standard Error of Est. = 29.8248

Mean absolute error = 22.3574

Durbin-Watson statistic = 1.58805 (P=0.0150)

Lag 1 residual autocorrelation = 0.193199



Left: Interaction of Hardness and Tool Angle on Normal Shear Force ( $F_n$ )

Right: Interaction of Depth of Cut and Temperature on Normal Shear Force ( $F_n$ )

## Steel Analysis of internal shear force ( $F_s$ )

**Analysis of Variance for  $F_s$  Payton (lbf)**

Source	Sum of Squares	Df	Mean Square	F-Ratio	P-Value
A:Hardness/Temper	339.361	1	339.361	2.09	0.1517
B:Tool Angle (degrees)	7810.08	1	7810.08	47.99	0.0000
C:Depth of Cut (mils)	67963.2	1	67963.2	417.61	0.0000
D:Temperature (°C)	209.442	1	209.442	1.29	0.2592
Total error	17088.0	105	162.743		
Total (corr.)	93135.5	109			

R-squared = **81.6525** percent

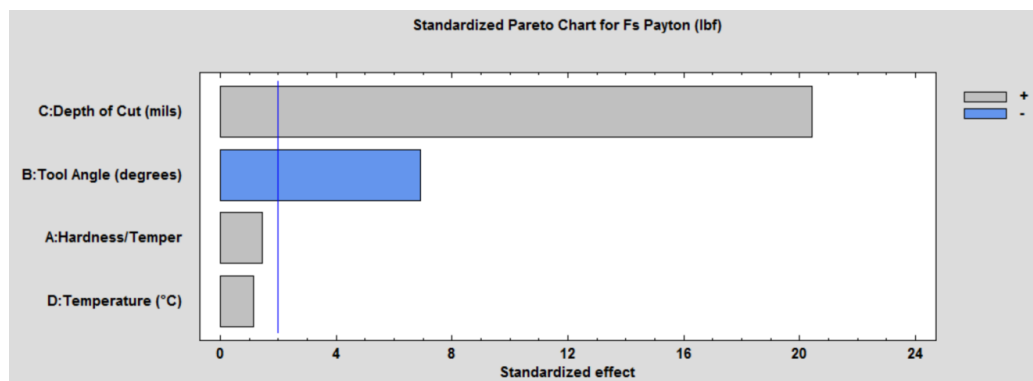
R-squared (adjusted for d.f.) = **80.9535** percent

Standard Error of Est. = **12.7571**

Mean absolute error = **9.6067**

Durbin-Watson statistic = 1.50668 (P=**0.0045**)

Lag 1 residual autocorrelation = 0.209369



No significant interactions on ( $F_s$ )

## Steel Normal Force (N)

**Analysis of Variance for Normal Force (lbf)**

Source	Sum of Squares	Df	Mean Square	F-Ratio	P-Value
A:Hardness/Temper	3040.81	1	3040.81	4.91	0.0289
B:Tool Angle (degrees)	46793.4	1	46793.4	75.56	0.0000
C:Depth of Cut (mils)	304186.	1	304186.	491.21	0.0000
D:Temperature (°C)	18600.9	1	18600.9	30.04	0.0000
BD	2325.35	1	2325.35	3.76	0.0554
CD	4411.12	1	4411.12	7.12	0.0088
Total error	63784.0	103	619.262		
Total (corr.)	448510.	109			

R-squared = 85.7787 percent

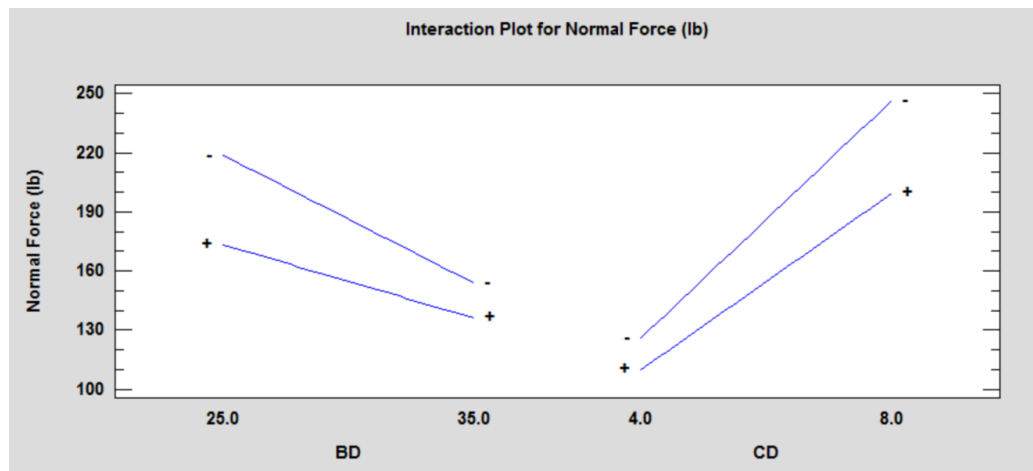
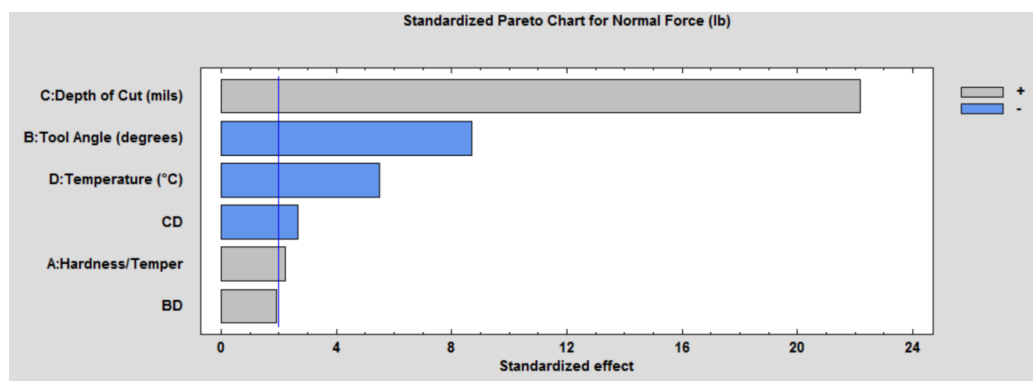
R-squared (adjusted for d.f.) = 84.9503 percent

Standard Error of Est. = 24.885

Mean absolute error = 18.6153

Durbin-Watson statistic = 1.58031 (P=0.0135)

Lag 1 residual autocorrelation = 0.19057



Left: Interaction of Tool Angle and Temperature on Normal Force (N)

Right: Interaction of Depth of Cut and Temperature on Normal Force (N)

## Steel Friction Force (**F**) Analysis

**Analysis of Variance for Friction Force (lbf)**

Source	Sum of Squares	Df	Mean Square	F-Ratio	P-Value
A:Hardness/Temper	4017.06	1	4017.06	9.16	0.0031
B:Tool Angle (degrees)	2079.7	1	2079.7	4.74	0.0317
C:Depth of Cut (mils)	188299.	1	188299.	429.20	0.0000
D:Temperature (°C)	68023.4	1	68023.4	155.05	0.0000
AB	2564.49	1	2564.49	5.85	0.0174
CD	11791.5	1	11791.5	26.88	0.0000
Total error	45188.2	103	438.72		
Total (corr.)	327143.	109			

R-squared = 86.187 percent

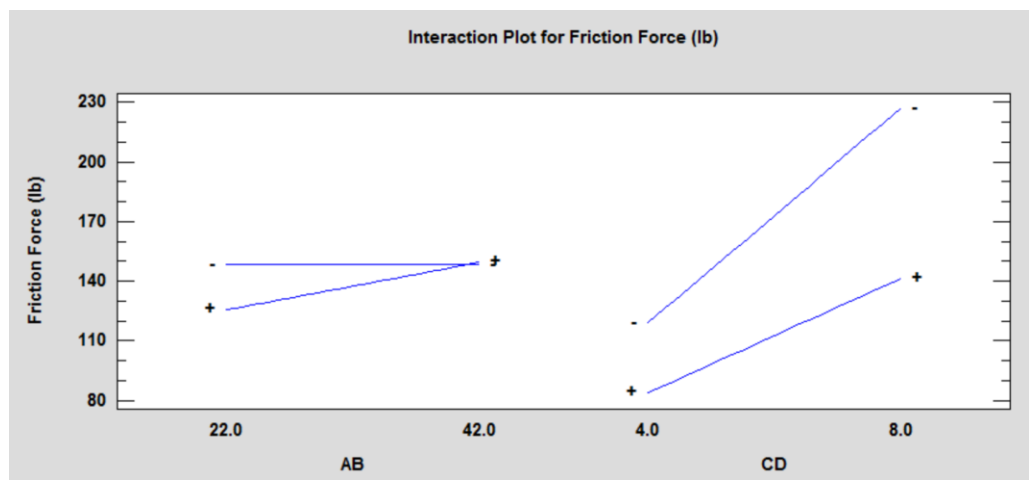
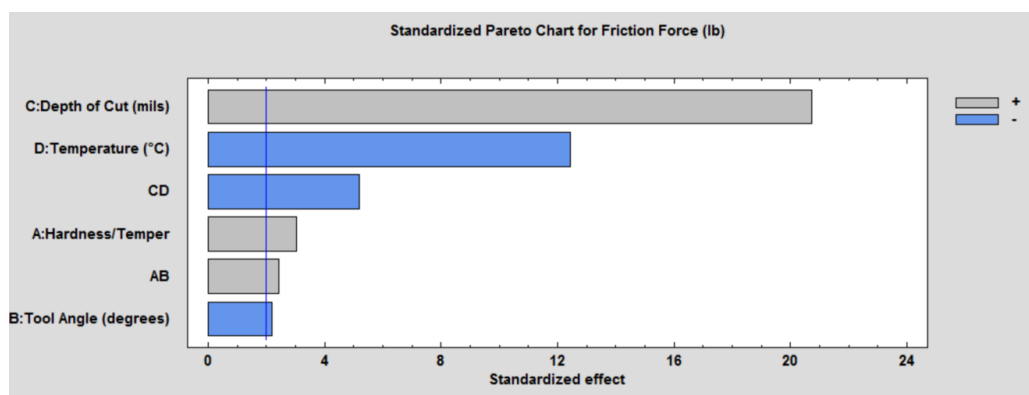
R-squared (adjusted for d.f.) = 85.3824 percent

Standard Error of Est. = 20.9456

Mean absolute error = 15.7194

Durbin-Watson statistic = 1.55948 (P=0.0101)

Lag 1 residual autocorrelation = 0.210048



Left: Interaction of Hardness and Tool Angle on Friction Force (**F**)

Right: Interaction of Depth of Cut and Temperature on Friction Force (**F**)

## Steel Analysis of Phi ( $\phi$ ) Plane Angle

**Analysis of Variance for phi calculated (degrees)**

Source	Sum of Squares	Df	Mean Square	F-Ratio	P-Value
A:Hardness/Temper	561.791	1	561.791	22.83	0.0000
B:Tool Angle (degrees)	1147.8	1	1147.8	46.64	0.0000
C:Depth of Cut (mils)	241.56	1	241.56	9.82	0.0023
D:Temperature (°C)	37.595	1	37.595	1.53	0.2193
AB	82.7412	1	82.7412	3.36	0.0696
CD	102.459	1	102.459	4.16	0.0439
Total error	2534.93	103	24.611		
Total (corr.)	4729.15	109			

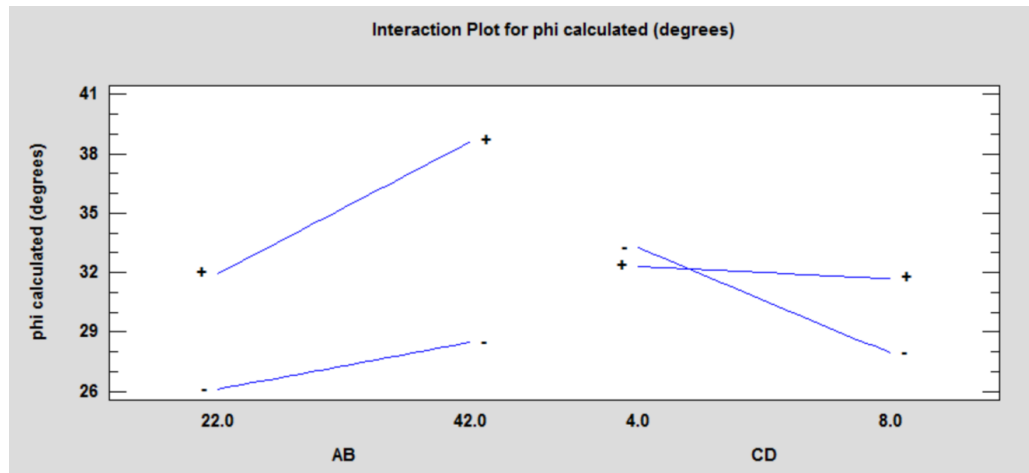
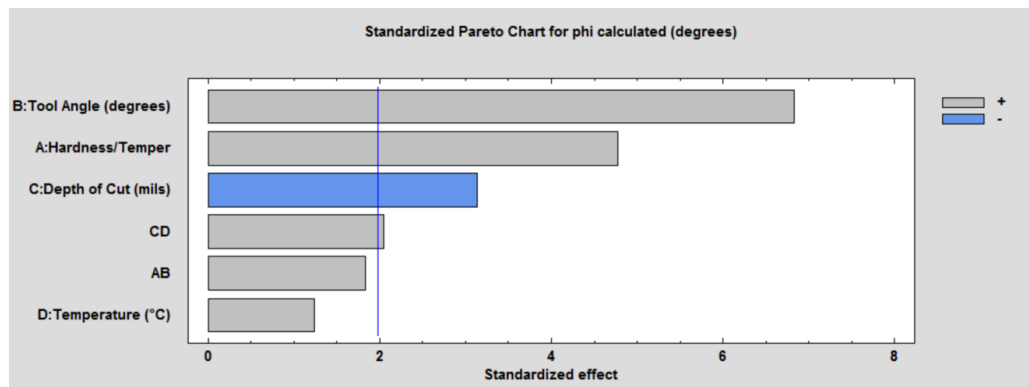
R-squared = 46.3976 percent

R-squared (adjusted for d.f.) = 43.2752 percent

Standard Error of Est. = 4.96095

Mean absolute error = 3.86325

Durbin-Watson statistic = 1.80006 (P=0.1483)



Left: Interaction of Hardness and Tool Angle on Phi ( $\phi$ ) Plane Angle

Right: Interaction of Depth of Cut and Temperature on Phi ( $\phi$ ) Plane Angle

## Steel Analysis of the Thrust Force ( $F_t$ )

**Analysis of Variance for thrust force (lbf)**

Source	Sum of Squares	Df	Mean Square	F-Ratio	P-Value
A:Hardness/Temper	522.806	1	522.806	5.73	0.0185
B:Tool Angle (degrees)	8598.95	1	8598.95	94.20	0.0000
C:Depth of Cut (mils)	10190.8	1	10190.8	111.64	0.0000
D:Temperature (°C)	26176.9	1	26176.9	286.76	0.0000
BC	431.631	1	431.631	4.73	0.0320
BD	665.544	1	665.544	7.29	0.0081
CD	3822.52	1	3822.52	41.87	0.0000
Total error	9310.98	102	91.2841		
Total (corr.)	60399.9	109			

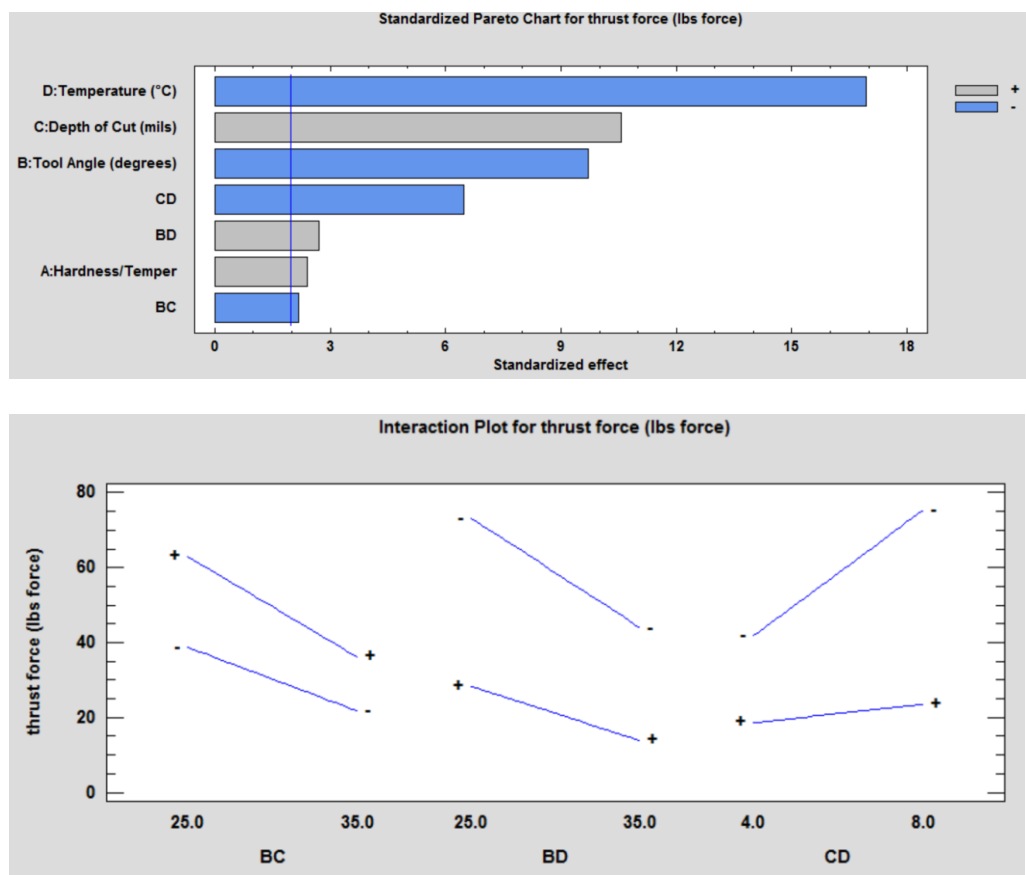
R-squared = 84.5844 percent

R-squared (adjusted for d.f.) = 83.5265 percent

Standard Error of Est. = 9.55427

Mean absolute error = 7.1874

Durbin-Watson statistic = 1.34796 (P=0.0002)



Left: Interaction of Tool Angle and Depth of Cut on Thrust Force ( $F_t$ )

Middle: Interaction of Tool Angle and Temperature on Thrust Force ( $F_t$ )

Right: Interaction of Depth of Cut and Temperature on Thrust Force ( $F_t$ )

## Steel Analysis of Cutting Force ( $F_c$ )

**Analysis of Variance for cutting force (lbf)**

Source	Sum of Squares	Df	Mean Square	F-Ratio	P-Value
A:Hardness/Temper	6540.63	1	6540.63	6.83	0.0103
B:Tool Angle (degrees)	33299.6	1	33299.6	34.79	0.0000
C:Depth of Cut (mils)	482867.	1	482867.	504.53	0.0000
D:Temperature (°C)	61146.2	1	61146.2	63.89	0.0000
AB	3840.38	1	3840.38	4.01	0.0478
CD	12391.1	1	12391.1	12.95	0.0005
Total error	98577.7	103	957.065		
Total (corr.)	707584.	109			

R-squared = 86.0684 percent

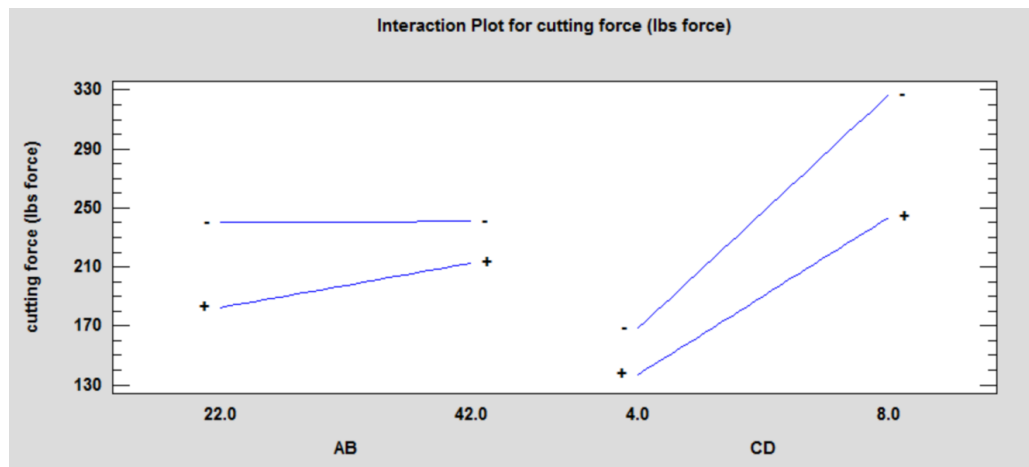
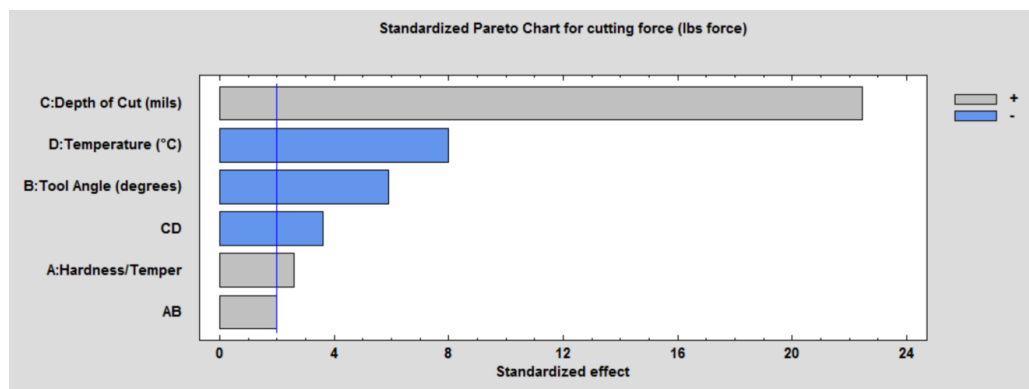
R-squared (adjusted for d.f.) = 85.2569 percent

Standard Error of Est. = 30.9365

Mean absolute error = 23.2812

Durbin-Watson statistic = 1.60911 (P=0.0199)

Lag 1 residual autocorrelation = 0.179219



Left: Interaction of Hardness and Tool Angle on Cutting Force ( $F_c$ )

Right: Interaction of Depth of Cut and Temperature on Cutting Force ( $F_c$ )

## Aluminum Wear Rate Analysis

**Analysis of Variance for Wear Rate Payton (in/sec)**

Source	Sum of Squares	Df	Mean Square	F-Ratio	P-Value
A:Hardness/Temper	0.000800166	1	0.000800166	222.81	0.0000
B:Tool Angle (degrees)	1.12921E-8	1	1.12921E-8	0.00	0.9554
C:Depth of Cut (mils)	0.0000708057	1	0.0000708057	19.72	0.0000
D:Temperature (°C)	3.90298E-7	1	3.90298E-7	0.11	0.7424
AC	0.0000179135	1	0.0000179135	4.99	0.0281
Total error	0.000316035	88	0.00000359131		
Total (corr.)	0.00121519	93			

R-squared = 73.9929 percent

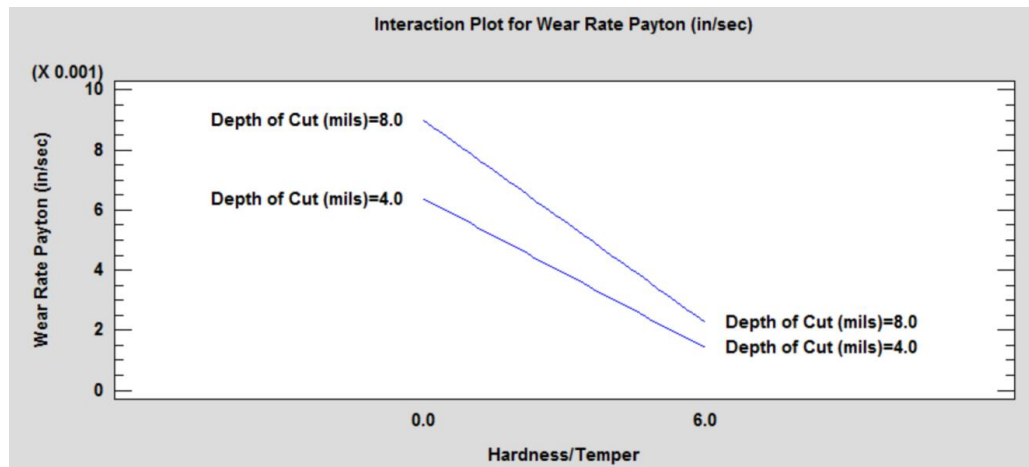
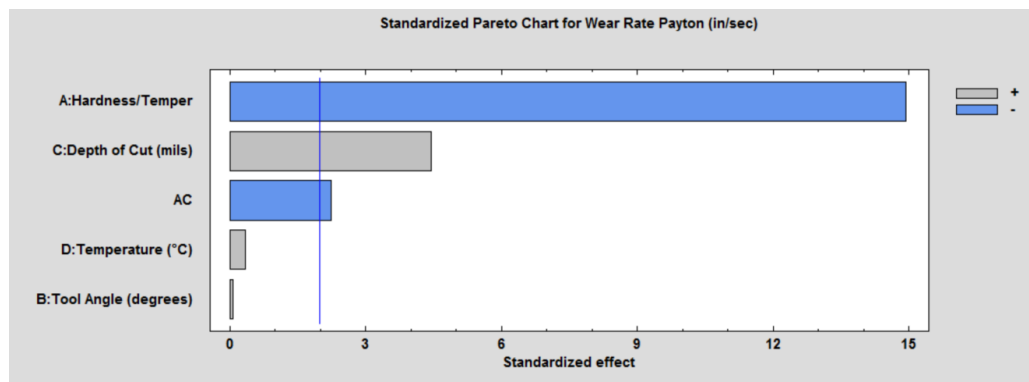
R-squared (adjusted for d.f.) = 72.5152 percent

Standard Error of Est. = 0.00189507

Mean absolute error = 0.00102425

Durbin-Watson statistic = 1.53616 (P=0.0027)

Lag 1 residual autocorrelation = 0.230316



Interaction of Hardness and Depth of Cut on Aluminum Wear Rate

## Aluminum Analysis Specific Horsepower ( $HP_s$ )

### Analysis of Variance for Specific Horsepower, $HP_s$

Source	Sum of Squares	Df	Mean Square	F-Ratio	P-Value
A:Hardness/Temper	0.281664	1	0.281664	1.40	0.2395
B:Tool Angle (degrees)	0.949883	1	0.949883	4.73	0.0323
C:Depth of Cut (mils)	0.443318	1	0.443318	2.21	0.1409
D:Temperature (°C)	5.48731	1	5.48731	27.32	0.0000
AC	2.90077	1	2.90077	14.44	0.0003
Total error	17.6724	88	0.200823		
Total (corr.)	27.6168	93			

R-squared = 36.0083 percent

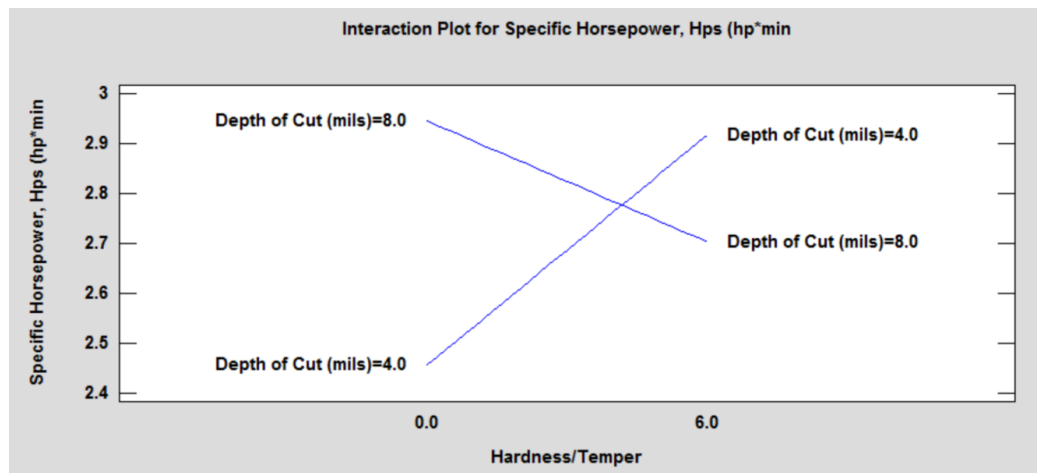
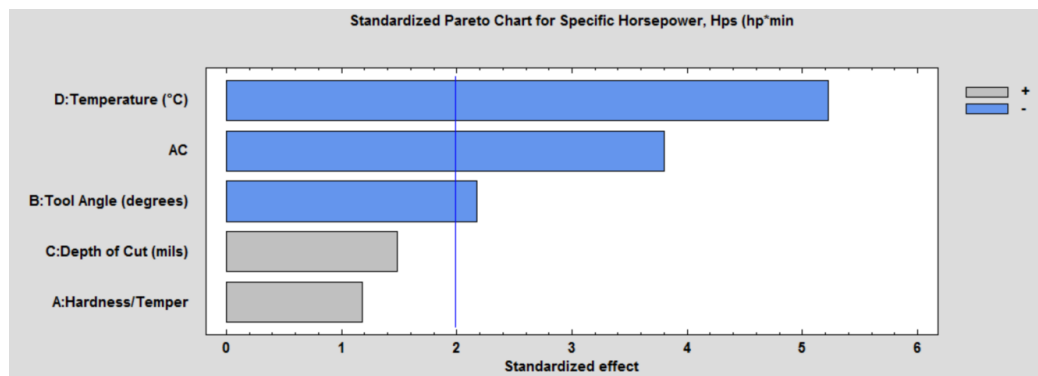
R-squared (adjusted for d.f.) = 32.3724 percent

Standard Error of Est. = 0.448133

Mean absolute error = 0.3485

Durbin-Watson statistic = 1.54209 (P=0.0030)

Lag 1 residual autocorrelation = 0.21959



## Interaction of Hardness and Depth of Cut on Specific Horsepower ( $HP_s$ )

## Aluminum Friction Coefficient Analysis

### Analysis of Variance for Friction Co-efficient

Source	Sum of Squares	Df	Mean Square	F-Ratio	P-Value
A:Hardness/Temper	0.38422	1	0.38422	239.24	0.0000
B:Tool Angle (degrees)	0.0528997	1	0.0528997	32.94	0.0000
C:Depth of Cut (mils)	0.0459857	1	0.0459857	28.63	0.0000
D:Temperature (°C)	0.202249	1	0.202249	125.94	0.0000
CD	0.0124072	1	0.0124072	7.73	0.0067
Total error	0.141325	88	0.00160597		
Total (corr.)	0.821486	93			

R-squared = 82.7964 percent

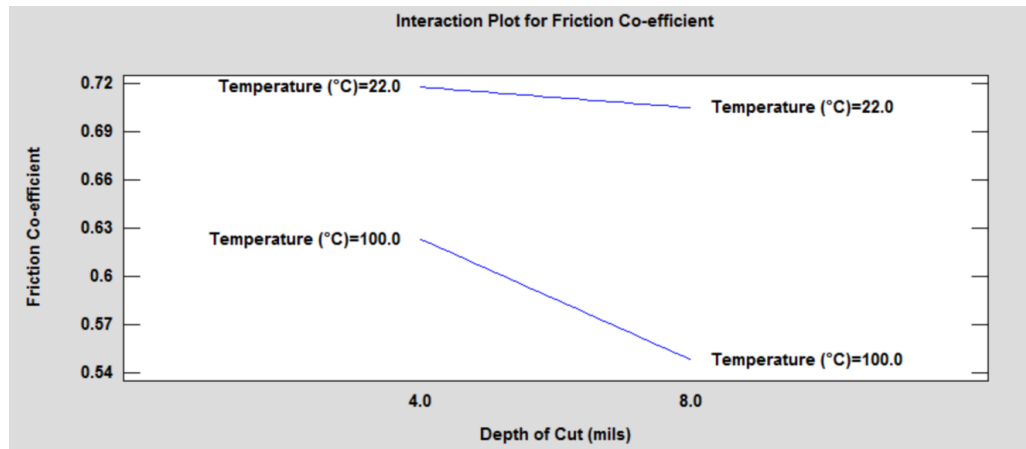
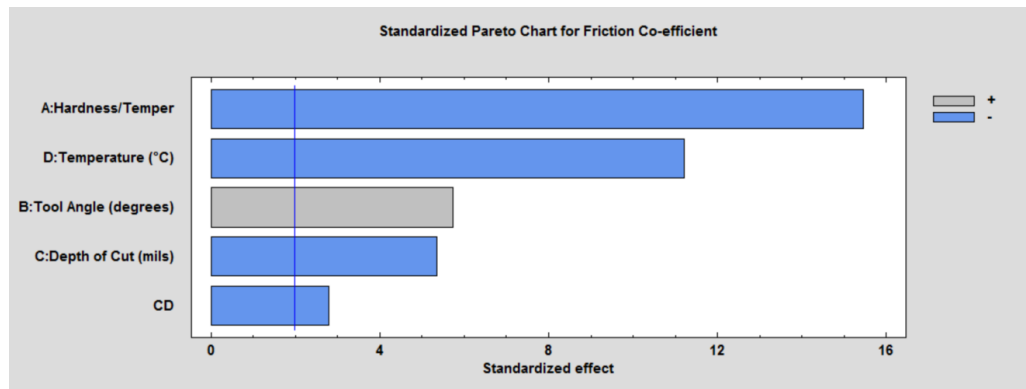
R-squared (adjusted for d.f.) = 81.8189 percent

Standard Error of Est. = 0.0400746

Mean absolute error = 0.030088

Durbin-Watson statistic = 1.08324 (P=0.0000)

Lag 1 residual autocorrelation = 0.440626



Interaction of Depth of Cut and Temperature on Aluminum Friction Coefficient

## Aluminum Analysis on Normal Shear Force ( $F_n$ )

### Analysis of Variance for $F_n$ Payton (lbf)

Source	Sum of Squares	Df	Mean Square	F-Ratio	P-Value
A:Hardness/Temper	856.35	1	856.35	8.97	0.0036
B:Tool Angle (degrees)	1897.11	1	1897.11	19.88	0.0000
C:Depth of Cut (mils)	31165.6	1	31165.6	326.53	0.0000
D:Temperature (°C)	5937.54	1	5937.54	62.21	0.0000
CD	642.744	1	642.744	6.73	0.0111
Total error	8399.12	88	95.4446		
Total (corr.)	49724.6	93			

R-squared = 83.1087 percent

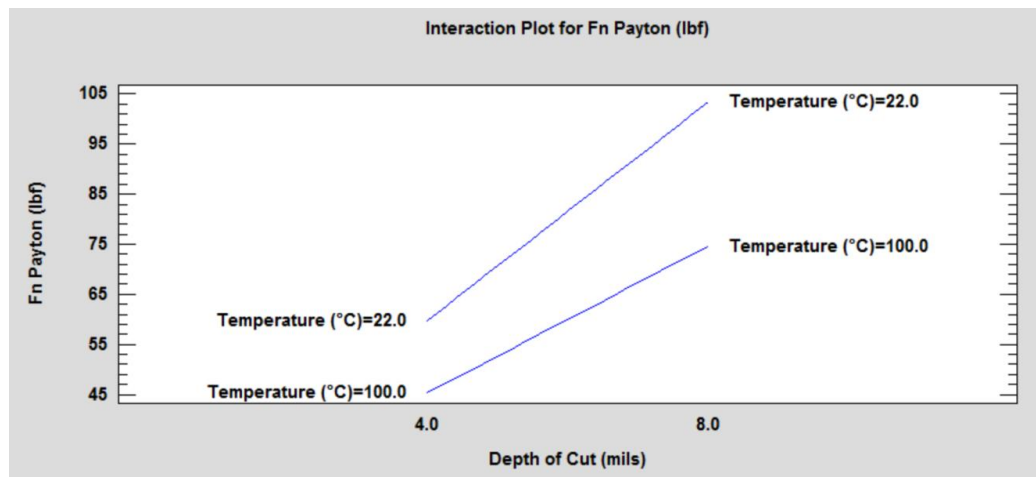
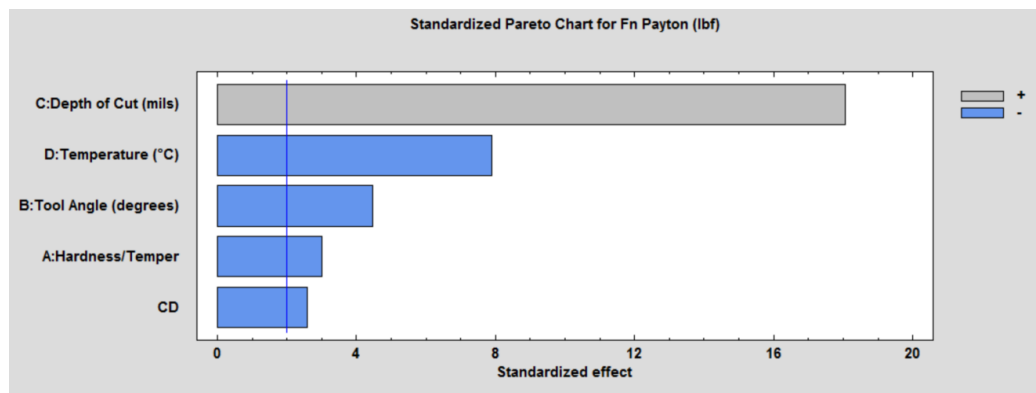
R-squared (adjusted for d.f.) = 82.149 percent

Standard Error of Est. = 9.76957

Mean absolute error = 7.26818

Durbin-Watson statistic = 1.22676 (P=0.0000)

Lag 1 residual autocorrelation = 0.383605



### Interaction of Depth of Cut and Temperature on Normal Shear Force ( $F_n$ )

## Aluminum Analysis of the Internal Shear Force ( $F_s$ )

### Analysis of Variance for $F_s$ Payton (lbf)

Source	Sum of Squares	Df	Mean Square	F-Ratio	P-Value
A:Hardness/Temper	1586.26	1	1586.26	160.18	0.0000
B:Tool Angle (degrees)	454.702	1	454.702	45.92	0.0000
C:Depth of Cut (mils)	7019.83	1	7019.83	708.88	0.0000
D:Temperature (°C)	145.191	1	145.191	14.66	0.0002
AB	43.2785	1	43.2785	4.37	0.0396
AC	92.9465	1	92.9465	9.39	0.0029
AD	88.5613	1	88.5613	8.94	0.0037
BC	102.548	1	102.548	10.36	0.0018
CD	99.161	1	99.161	10.01	0.0022
Total error	831.831	84	9.90275		
Total (corr.)	10480.8	93			

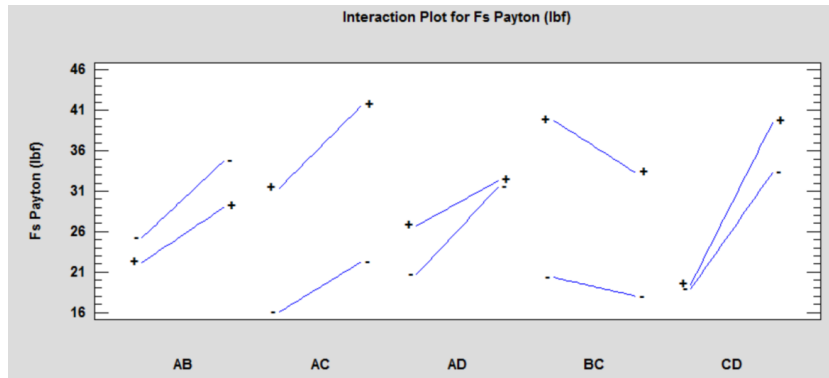
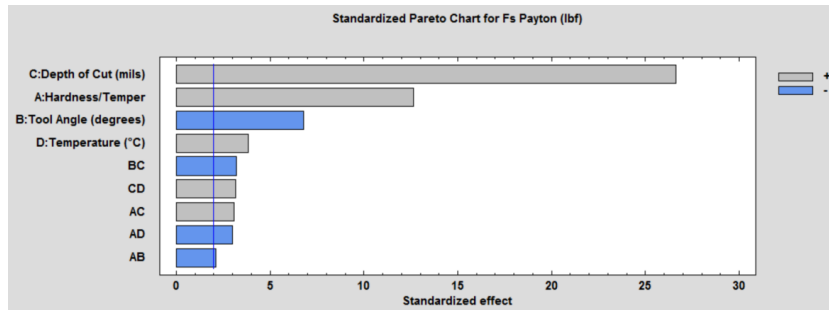
R-squared = 92.0633 percent

R-squared (adjusted for d.f.) = 91.2129 percent

Standard Error of Est. = 3.14686

Mean absolute error = 2.29125

Durbin-Watson statistic = 1.50379 (P=0.0004)



AB: Interaction of Hardness and Tool Angle on Normal Shear Force ( $F_n$ )

AC: Interaction of Hardness and Depth of Cut on Normal Shear Force ( $F_n$ )

AD: Interaction of Hardness and Temperature on Normal Shear Force ( $F_n$ )

BC: Interaction of Tool Angle and Depth of Cut on Normal Shear Force ( $F_n$ )

## CD: Interaction of Depth of Cut and Temperature on Normal Shear Force ( $F_n$ )

### Aluminum Analysis of Normal Force ( $N$ )

#### Analysis of Variance for Normal Force (lbf)

Source	Sum of Squares	Df	Mean Square	F-Ratio	P-Value
A:Hardness/Temper	349.356	1	349.356	8.39	0.0048
B:Tool Angle (degrees)	2573.98	1	2573.98	61.79	0.0000
C:Depth of Cut (mils)	26560.2	1	26560.2	637.61	0.0000
D:Temperature (°C)	908.038	1	908.038	21.80	0.0000
AB	166.824	1	166.824	4.00	0.0485
BC	310.379	1	310.379	7.45	0.0077
Total error	3624.07	87	41.656		
Total (corr.)	35197.2	93			

R-squared = 89.7035 percent

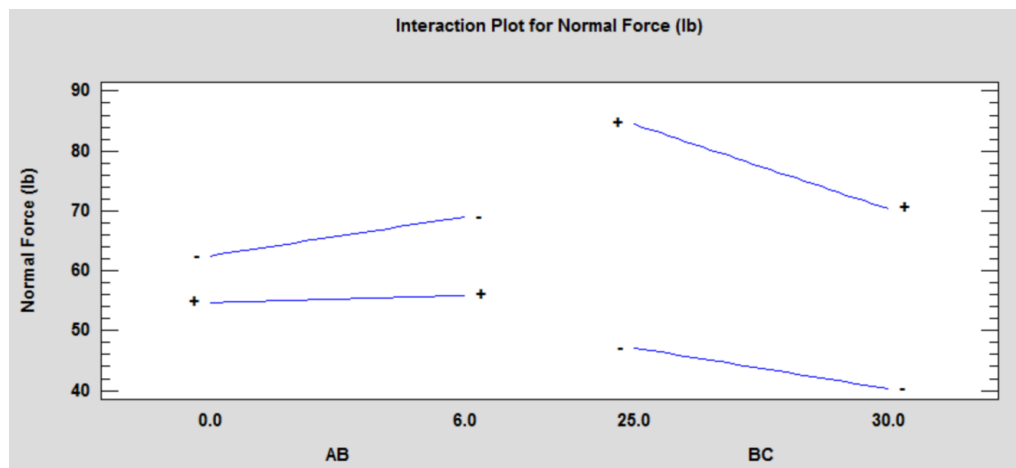
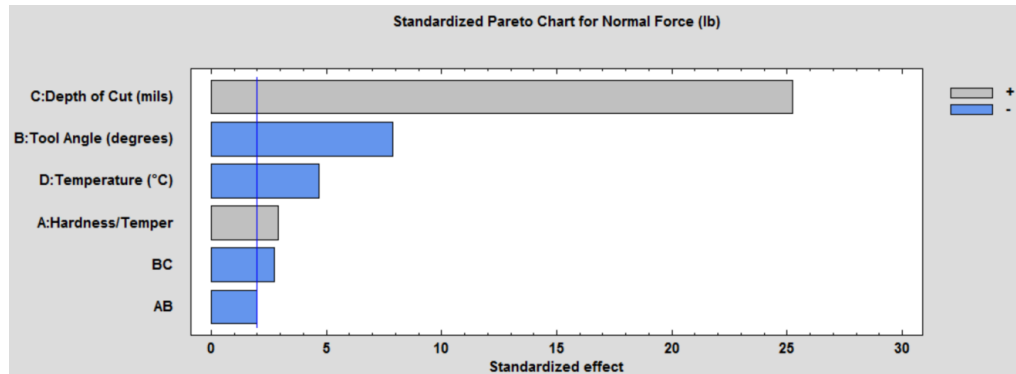
R-squared (adjusted for d.f.) = 88.9934 percent

Standard Error of Est. = 6.45415

Mean absolute error = 4.90758

Durbin-Watson statistic = 1.4298 (P=0.0003)

Lag 1 residual autocorrelation = 0.277286



Left: Interaction of Hardness and Tool Angle on Normal Force ( $N$ )

Right: Interaction of Tool Angle and Depth of Cut on Normal Force ( $N$ )

## Aluminum Analysis of the Friction Force ( $F$ )

### Analysis of Variance for Friction Force (lbf)

Source	Sum of Squares	Df	Mean Square	F-Ratio	P-Value
A:Hardness/Temper	2162.89	1	2162.89	35.35	0.0000
B:Tool Angle (degrees)	197.328	1	197.328	3.22	0.0760
C:Depth of Cut (mils)	11315.7	1	11315.7	184.94	0.0000
D:Temperature (°C)	5304.43	1	5304.43	86.69	0.0000
AC	176.424	1	176.424	2.88	0.0931
CD	776.502	1	776.502	12.69	0.0006
Total error	5323.28	87	61.1871		
Total (corr.)	25476.7	93			

R-squared = 79.1053 percent

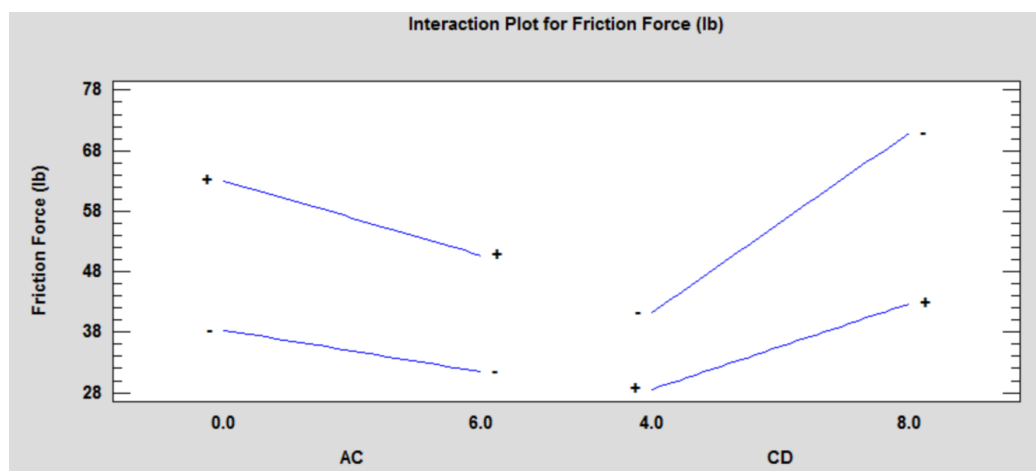
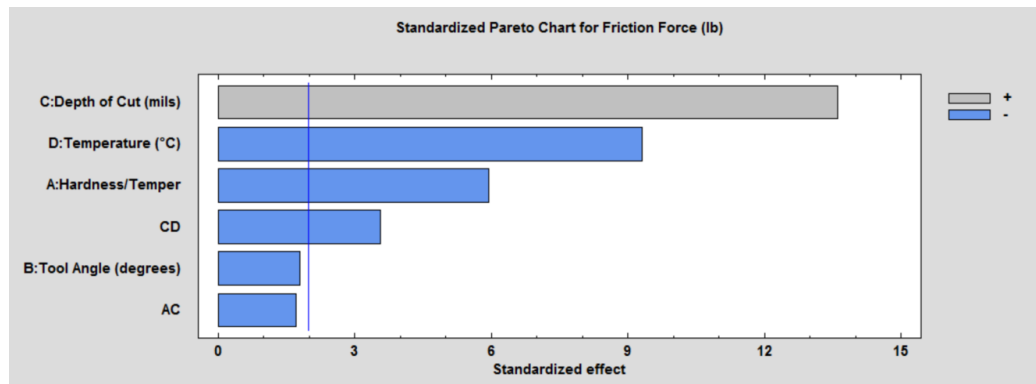
R-squared (adjusted for d.f.) = 77.6643 percent

Standard Error of Est. = 7.82222

Mean absolute error = 5.59861

Durbin-Watson statistic = 1.20508 (P=0.0000)

Lag 1 residual autocorrelation = 0.388931



Left: Interaction of Hardness and Depth of Cut on Friction Force ( $F$ )

Right: Interaction of Depth of Cut and Temperature on Friction Force ( $F$ )

## Aluminum Analysis of Phi ( $\phi$ ) Plane Angle

**Analysis of Variance for Phi Measured (degrees)**

Source	Sum of Squares	Df	Mean Square	F-Ratio	P-Value
A:Hardness/Temper	48.3856	1	48.3856	1.80	0.1831
B:Tool Angle (degrees)	370.922	1	370.922	13.80	0.0004
C:Depth of Cut (mils)	120.886	1	120.886	4.50	0.0367
D:Temperature (°C)	262.389	1	262.389	9.76	0.0024
BC	107.844	1	107.844	4.01	0.0482
Total error	2364.78	88	26.8725		
Total (corr.)	3253.49	93			

R-squared = 27.3156 percent

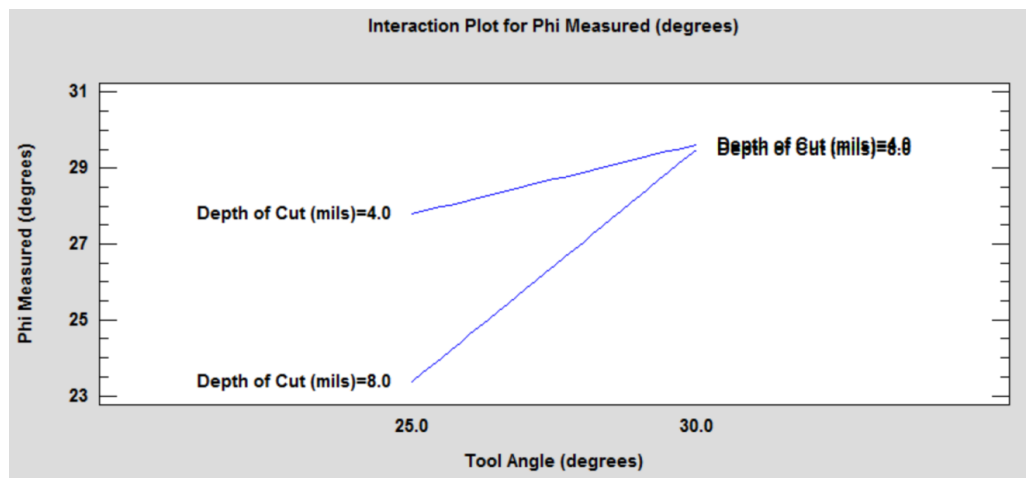
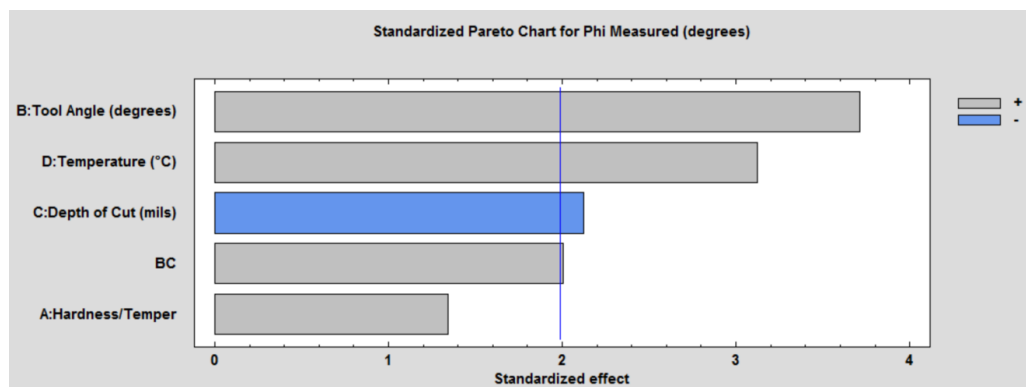
R-squared (adjusted for d.f.) = 23.1859 percent

Standard Error of Est. = 5.18387

Mean absolute error = 4.14294

Durbin-Watson statistic = 1.58438 (P=0.0057)

Lag 1 residual autocorrelation = 0.204709



Interaction of Tool Angle and Depth of Cut on Phi ( $\phi$ ) Plane Angle

## Aluminum Analysis of Thrust Force ( $F_t$ )

**Analysis of Variance for thrust force (lbf)**

Source	Sum of Squares	Df	Mean Square	F-Ratio	P-Value
A:Hardness/Temper	2427.09	1	2427.09	111.71	0.0000
B:Tool Angle (degrees)	417.565	1	417.565	19.22	0.0000
C:Depth of Cut (mils)	394.07	1	394.07	18.14	0.0001
D:Temperature (°C)	2586.35	1	2586.35	119.04	0.0000
AC	167.729	1	167.729	7.72	0.0067
AD	111.789	1	111.789	5.15	0.0258
CD	479.484	1	479.484	22.07	0.0000
Total error	1868.56	86	21.7274		
Total (corr.)	8170.22	93			

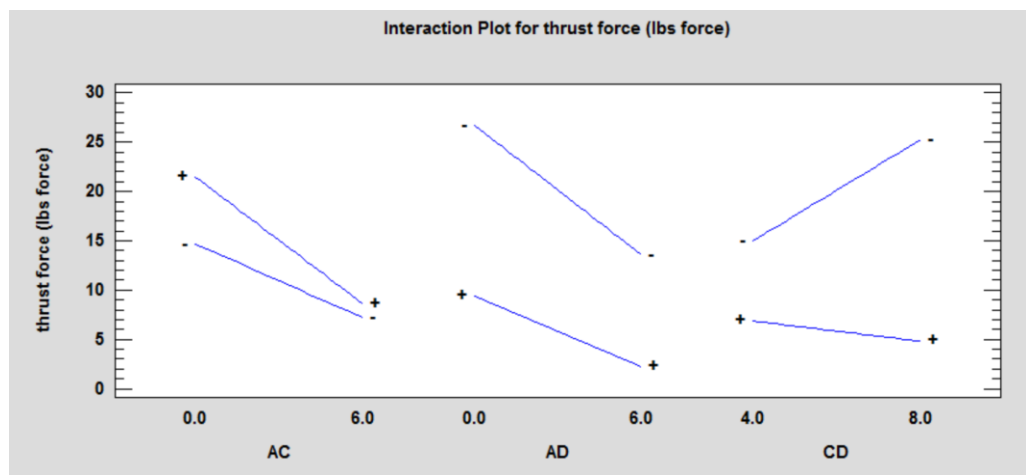
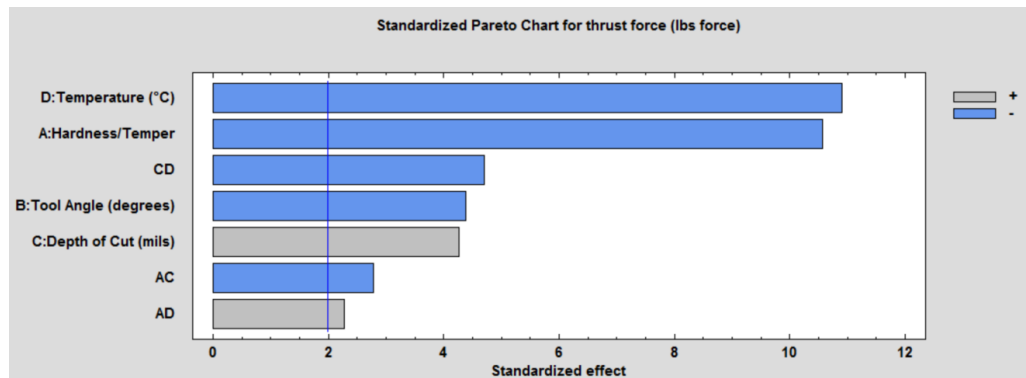
R-squared = 77.1296 percent

R-squared (adjusted for d.f.) = 75.2681 percent

Standard Error of Est. = 4.66127

Mean absolute error = 3.43847

Durbin-Watson statistic = 1.16326 (P=0.0000)



Left: Interaction of Hardness and Depth of Cut on Thrust Force ( $F_t$ )

Middle: Interaction of Hardness and Temperature on Thrust Force ( $F_t$ )

Right: Interaction of Depth of Cut and Temperature on Thrust Force ( $F_t$ )

## Aluminum Analysis of the Cutting Force ( $F_c$ )

**Analysis of Variance for cutting force (lbf)**

Source	Sum of Squares	Df	Mean Square	F-Ratio	P-Value
A:Hardness/Temper	21.5351	1	21.5351	0.26	0.6091
B:Tool Angle (degrees)	2090.35	1	2090.35	25.57	0.0000
C:Depth of Cut (mils)	37744.2	1	37744.2	461.74	0.0000
D:Temperature (°C)	3550.37	1	3550.37	43.43	0.0000
AB	320.647	1	320.647	3.92	0.0508
CD	276.689	1	276.689	3.38	0.0692
Total error	7111.61	87	81.7426		
Total (corr.)	52076.9	93			

R-squared = 86.344 percent

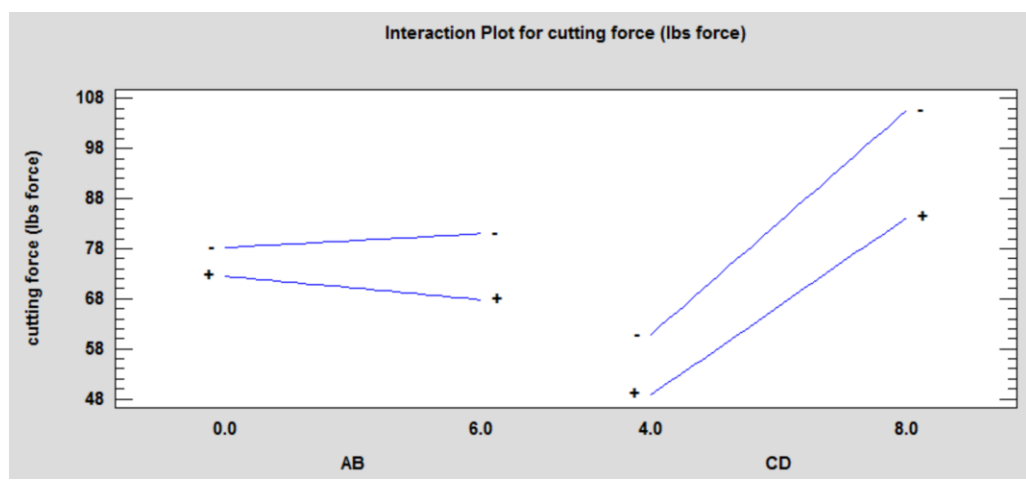
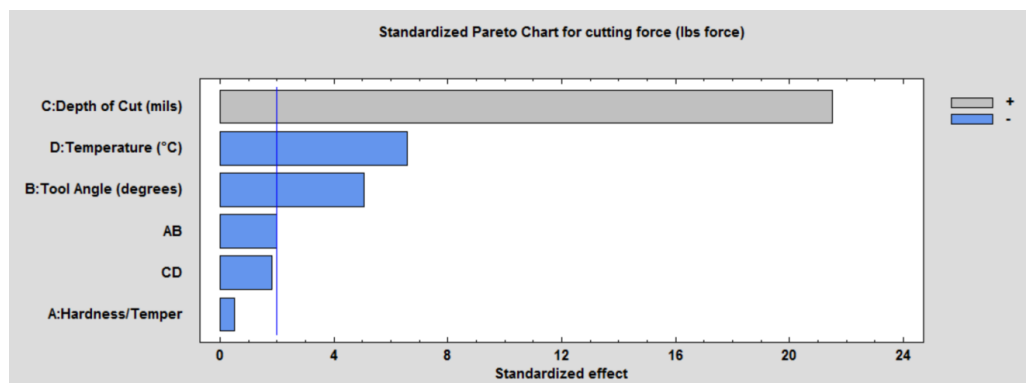
R-squared (adjusted for d.f.) = 85.4022 percent

Standard Error of Est. = 9.04116

Mean absolute error = 6.81619

Durbin-Watson statistic = 1.34639 (P=0.0001)

Lag 1 residual autocorrelation = 0.322076



Left: Interaction of Hardness and Tool Angle on Cutting Force ( $F_c$ )

Right: Interaction of Depth of Cut and Temperature on Cutting Force ( $F_c$ )

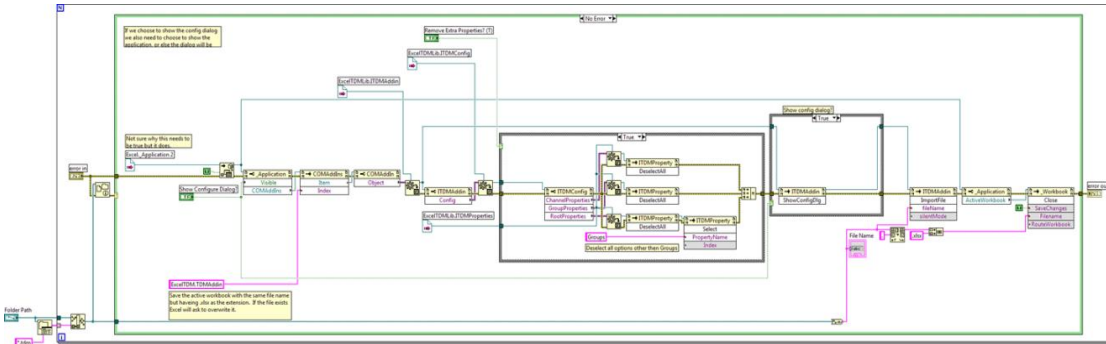
## Appendix.H: Tool Edge Summary Table

Material	Temperature(degrees C)	Tool Angle (degrees)	Min Profile Height (in)	Avg Profile Height (in)	Max Profile Height (in)	Uncut Edge Length (in)	Cutting Edge Length (in)	Edge Length Difference (in)	Edge Length Used (%)
A0	22	25	2.598E-06	0.0003878	0.000591	0.0599606	0.0575591	0.0024016	4.0052528
A0	22	30	0.0005452	0.0009587	0.0018207	0.0591732	0.0546457	0.0045276	7.6513639
A0	50	25	3.937E-05	4.698E-05	5.968E-05	0.0569685	0.0561811	0.0007874	1.38217
A0	50	30	0.0001424	0.0001994	0.0002535	0.0595669	0.056811	0.0027559	4.6265697
A0	75	25	3.937E-05	4.953E-05	6.601E-05	0.0585039	0.053189	0.005315	9.0847914
A0	75	30	0.0001899	0.0004366	0.0007498	0.0580315	0.0472835	0.010748	18.521031
A0	100	25	3.937E-05	0.0005807	0.0037938	0.0677559	0.071063	-0.0033071	4.8808832
A0	100	30	0.0005127	0.0008481	0.0013952	0.0596063	0.053937	0.0056693	9.5112285
A6	22	25	0.0002828	0.0004244	0.0006729	0.0578346	0.057874	-3.937E-05	0.0680735
A6	22	30	0.0004577	0.0006067	0.0007122	0.0587795	0.0572441	0.0015354	2.6121902
A6	50	25	0.0001964	0.0004182	0.0005551	0.0584252	0.0547244	0.0037008	6.3342318
A6	50	30	0.0001191	0.0002505	0.0003985	0.0535827	0.0503543	0.0032283	6.0249816
A6	75	25	0.0002487	0.000462	0.0005899	0.0546457	0.0512598	0.0033858	6.1959654
A6	75	30	8.843E-05	0.0003951	0.0004741	0.0588583	0.0444882	0.0143701	24.414716
A6	100	25	0.0001006	0.000216	0.0004438	0.0604724	0.0537402	0.0067323	11.132813
A6	100	30	0.0003273	0.0004736	0.0006308	0.0568898	0.0435039	0.0133858	23.529412
S22	22	25	8.362E-05	0.0002088	0.000322	0.053622	0.051063	0.0025591	4.7723935
S22	22	30	0.0007489	0.000934	0.0010992	0.059252	0.0537402	0.0055118	9.3023256
S22	22	35	0.0005977	0.0007261	0.000836	0.0620079	0.0551575	0.0068504	11.047619
S22	100	25	0.0010326	0.0012056	0.0014079	0.060315	0.0525591	0.0077559	12.859008
S22	100	30	0.0007421	0.0009577	0.0012802	0.0596063	0.0513386	0.0082677	13.870542
S22	100	35	0.00051	0.0006821	0.0007873	0.0579921	0.0479921	0.01	17.24372
S22	200	25	0.0004446	0.0005815	0.0008373	0.0580709	0.0512992	0.0067717	11.661017
S22	200	30	0.0005684	0.0007312	0.0008454	0.051378	0.0359449	0.0154331	30.038314
S22	200	35	0.0015801	0.0022842	0.003333	0.0594488	0.0463386	0.0131102	22.05298
S42	22	25	0.0004761	0.000586	0.0007027	0.0564961	0.0512598	0.0052362	9.2682927
S42	22	30	0.0001495	0.0002205	0.0003597	0.058189	0.0518504	0.0063386	10.893099
S42	22	35	0.0002299	0.0003332	0.0006468	0.0580315	0.051378	0.0066535	11.4654
S42	100	25	0.0005373	0.000666	0.0007854	0.0608268	0.0562598	0.0045669	7.5080906

Material	Temperature(degrees C)	Tool Angle (degrees)	Min Profile Height (in)	Avg Profile Height (in)	Max Profile Height (in)	Uncut Edge Length (in)	Cutting Edge Length (in)	Edge Length Difference (in)	Edge Length Used (%)
S42	100	30	0.0007426	0.0011616	0.0016563	0.058708	0.050518	0.008189	13.950369
S42	100	35	0.0003539	0.0006828	0.0010094	0.0616142	0.0533071	0.0083071	13.482428
S42	200	25	0.0006706	0.0010381	0.0014372	0.0596457	0.056811	0.0028346	4.7524752
S42	200	35	0.0006126	0.0008804	0.0013532	0.0594094	0.0559055	0.0035039	5.8979457
UC	N/A	25	0.0011975	0.0020121	0.0025206	0.0545669	N/A	N/A	N/A
UC	N/A	25	0.0002488	0.0011159	0.0019178	0.0563386	N/A	N/A	N/A
UC	N/A	25	0.0002605	0.0012097	0.0022098	0.0569291	N/A	N/A	N/A
UC	N/A	25	0.0004926	0.0017788	0.0032677	0.0577165	N/A	N/A	N/A
UC	N/A	30	0.0011651	0.0016135	0.0021376	0.0564567	N/A	N/A	N/A
UC	N/A	30	0.0002639	0.0008289	0.0015498	0.0570866	N/A	N/A	N/A
UC	N/A	30	0.0003568	0.0011321	0.0017593	0.0565354	N/A	N/A	N/A
UC	N/A	30	0.0002619	0.0008357	0.0012341	0.0562992	N/A	N/A	N/A
UC	N/A	35	0.0005963	0.0009229	0.0016687	0.0543701	N/A	N/A	N/A
UC	N/A	35	0.0001346	0.0009477	0.0013487	0.0572047	N/A	N/A	N/A
UC	N/A	35	0.0004212	0.0007638	0.0016975	0.0557874	N/A	N/A	N/A

## Appendix.I: Program Files

The figure below shows the LabVIEW file used to convert the force data from collection into an Excel file for further analysis.



The Matlab file shown below was used to compare the heated runs with the conventional (validation) runs and display the graphical and statistical results

```
% Data Comparison/ Outputting

clear all; clc;

% Input
%-----
-----
% Note: The first excel file imported needs to be the standard data set
% not
% the experimental data set.

fid = input('Enter the name of the first excel file with the extension: ','s');
sht = input('Which sheet should be imported: ');
% out = input('Input graph number and output file number w/ file type: ');
[num_m,txt_m] = xlsread(fid,sht);

fid2 = input('Enter the name of the second excel file with the
extension: ','s');
sht2 = input('Which sheet should be imported: ');
% out = input('Input graph number and output file number w/ file type: ');
[num_m2,txt_m2] = xlsread(fid2,sht2);

% Calculations
%-----
-----
% Force Vectors
```

```

Time = linspace(1,15,length(num_m)); T_l = length(Time);
Fx_v = num_m(:,1); Fy_v = num_m(:,2); Fz_v = num_m(:,3);
Time2 = linspace(1,15,length(num_m2)); T_l2 = length(Time2);
Fx_v2 = num_m2(:,1); Fy_v2 = num_m2(:,2); Fz_v2 = num_m2(:,3);

% Data Comparison
xc = 1; yc = 1; zc = 1; xc2 = 1; yc2 = 1; zc2 = 1; c = 5;

% Equalising Lengths
if T_l >= T_l2
    N = T_l2;
    Fx_v = Fx_v(1:N);
    Fy_v = Fy_v(1:N);
    Fz_v = Fz_v(1:N);
    X = Time2;
elseif T_l < T_l2
    N = T_l;
    Fx_v2 = Fx_v2(1:N);
    Fy_v2 = Fy_v2(1:N);
    Fz_v2 = Fz_v2(1:N);
    X = Time;
end

% Quantifying Differences
for j = 2:N
    if Fx_v(j-1)-Fx_v(j) <= c
        Fx_ssv(xc) = Fx_v(j);
        xc = xc+1;
    end
    if Fy_v(j-1)-Fy_v(j) <= c
        Fy_ssv(yc) = Fy_v(j);
        yc = yc+1;
    end
    if Fz_v(j-1)-Fz_v(j) <= c
        Fz_ssv(zc) = Fz_v(j);
        zc = zc+1;
    end
    if Fx_v2(j-1)-Fx_v2(j) <= c
        Fx_ssv2(xc2) = Fx_v2(j);
        xc2 = xc2+1;
    end
    if Fy_v2(j-1)-Fy_v2(j) <= c
        Fy_ssv2(yc2) = Fy_v2(j);
        yc2 = yc2+1;
    end
    if Fz_v2(j-1)-Fz_v2(j) <= c
        Fz_ssv2(zc2) = Fz_v2(j);
        zc2 = zc2+1;
    end
end
end

% Below the average of the steady state vectors is calculated. A
vector
% of the difference between the first excel sheet data and the
second

```

```

% excel sheet data is created. The max, min, and avg is determined
for % those difference vectors. Then the average steady state values
are % subtracted from one another and divided by the first excel data
to % get the percent difference.

Fx_ss = mean(Fx_ssv); Fy_ss = mean(Fy_ssv); Fz_ss = mean(Fz_ssv);
Fx_ss2 = mean(Fx_ssv2); Fy_ss2 = mean(Fy_ssv2); Fz_ss2 =
mean(Fz_ssv2);

for n = 1:N
    Fx_diff(n) = abs(Fx_v(n) - Fx_v2(n));
    Fy_diff(n) = abs(Fy_v(n) - Fy_v2(n));
    Fz_diff(n) = abs(Fz_v(n) - Fz_v2(n));
end

Fx_diff_max = max(Fx_diff); Fx_diff_min = min(Fx_diff);
Fx_diff_avg = mean(Fx_diff); Fx_ss_diff = abs(Fx_ss-Fx_ss2);

Fy_diff_max = max(Fy_diff); Fy_diff_min = min(Fy_diff);
Fy_diff_avg = mean(Fy_diff); Fy_ss_diff = abs(Fy_ss-Fy_ss2);

Fz_diff_max = max(Fz_diff); Fz_diff_min = min(Fz_diff);
Fz_diff_avg = mean(Fz_diff); Fz_ss_diff = abs(Fz_ss-Fz_ss2);

if Fx_ss > Fx_ss2
    Px_diff = -(Fx_ss_diff/Fx_ss)*100;
else
    Px_diff = -(Fx_ss_diff/Fx_ss)*100;
end
if Fy_ss > Fy_ss2
    Py_diff = -(Fy_ss_diff/Fy_ss)*100;
else
    Py_diff = -(Fy_ss_diff/Fy_ss)*100;
end
if Fz_ss > Fz_ss2
    Pz_diff = -(Fz_ss_diff/Fz_ss)*100;
else
    Pz_diff = -(Fz_ss_diff/Fz_ss)*100;
end

% Statistical Data
[hx,px,ci_x,stats_x] = ttest2(Fx_v,Fx_v2);
if hx == 0
    nullx = 'not rejected';
else
    nullx = 'rejected';
end
[hy,py,ci_y,stats_y] = ttest2(Fy_v,Fy_v2);
if hy == 0
    nully = 'not rejected';
else

```

```

        nully = 'rejected';
    end
    [hz,pz,ci_z,stats_z] = ttest2(Fz_v,Fz_v2);
    if hz == 0
        nullz = 'not rejected';
    else
        nullz = 'rejected';
    end

% Data Output
%-----  

% Graphical
% X Forces
subplot(4,1,2)
plot(X,[Fx_v,Fx_v2])
title('Fx')
xlabel('N')
ylabel('Forces, lbf')
legend(fid,fid2,'Location','northoutside')

% Y Forces
subplot(4,1,3)
plot(X,[Fy_v,Fy_v2])
title('Fy')
xlabel('N')
ylabel('Forces, lbf')

% Z Forces
subplot(4,1,4)
plot(X,[Fz_v,Fz_v2])
title('Fz')
xlabel('N')
ylabel('Forces, lbf')

% Text File
fprintf('\nX Forces\nMax diff = %g lbf\nMin diff = %g lbf\nAvg diff
= %g lbf\n',Fx_diff_max, Fx_diff_min, Fx_diff_avg)
    fprintf('SS diff = %g\nPercent diff = %g %%\n\n',Fx_ss_diff,
Px_diff)
    fprintf('Y Forces\nMax diff = %g lbf\nMin diff = %g lbf\nAvg diff =
%g lbf\n',Fy_diff_max, Fy_diff_min, Fy_diff_avg)
    fprintf('SS diff = %g\nPercent diff = %g %%\n\n',Fy_ss_diff,
Py_diff)
    fprintf('Z Forces\nMax diff = %g lbf\nMin diff = %g lbf\nAvg diff =
%g lbf\n',Fz_diff_max, Fz_diff_min, Fz_diff_avg)
    fprintf('SS diff = %g\nPercent diff = %g %%\n\n',Fz_ss_diff,
Pz_diff)

    fprintf('ttest p value for X Forces = %g\nNull hypothesis = %s\n',
px, nullx)
    fprintf('ttest p value for Y Forces = %g\nNull hypothesis = %s\n',
py, nully)

```

```

fprintf('ttest p value for Z Forces = %g\nNull hypothesis = %s\n',
pz, nullz)

fprintf('\nX Confidence Interval\n')
fprintf('Upper Int: %g\nLower Int: %g\n',ci_x(2),ci_x(1))
fprintf('Y Confidence Interval\n')
fprintf('Upper Int: %g\nLower Int: %g\n',ci_y(2),ci_y(1))
fprintf('Z Confidence Interval\n')
fprintf('Upper Int: %g\nLower Int: %g\n\n',ci_z(2),ci_z(1))

fprintf('X Stats\n')
disp(stats_x)
fprintf('Y Stats\n')
disp(stats_y)
fprintf('Z Stats\n')
disp(stats_z)

```

Below is the Matlab program which was used to create the ANOVA tables seen in the main report

```

% ANOVA Calculator

clear all; clc;

% Input
%-----
% Note: Columns 3,4,5,6,8,11,12 go as follows: material, hardness,
temperature,
% depth of cut, tool angle, cutting force, thrust force.

% [anova_data,anova_txt] = xlsread('Shear Stress Summary.xlsx');

[anova_data,anova_txt] = xlsread('Shear Stress Summary
(revised).xlsx');

% Vector Formation
%-----
sum_length = size(anova_data); sum_length2 = length(anova_txt);

stemp = anova_data(1:108,5);
sTangle = anova_data(1:108,8);
sdepth = anova_data(1:108,6);
sFcum = anova_data(1:108,11);
sFthrust = anova_data(1:108,12);
sHardness = anova_data(1:108,4);

atemp = anova_data(109:204,5);
aTangle = anova_data(109:204,8);
adepth = anova_data(109:204,6);
afcum = anova_data(109:204,11);

```

```

aFthrust = anova_data(109:204,12);
aHardness = anova_data(109:204,4);

% Anova Tables
%-----
-----
% Steel
% Prime Factor Tables
sAnova_Fcut =
anovan(sFcutf,{stemp,sTangle,sdepth,sHardness}, 'varnames', {'Temp','Tool_angle','Depth','Hardness'});
sAnova_Fthrust =
anovan(sFthrust,{stemp,sTangle,sdepth,sHardness}, 'varnames', {'Temp','Tool_angle','Depth','Hardness'});

% Secondary Interaction Tables
sIntanova_Fcut =
anovan(sFcutf,{stemp,sTangle,sdepth,sHardness}, 'model', 'interaction', 'varnames', {'Temp','Tool_angle','Depth','Hardness'});
sIntanova_Fthrust =
anovan(sFthrust,{stemp,sTangle,sdepth,sHardness}, 'model', 'interaction', 'varnames', {'Temp','Tool_angle','Depth','Hardness'});

% Full Interaction Tables
sFullanova_Fcut =
anovan(sFcutf,{stemp,sTangle,sdepth,sHardness}, 'model', 'full', 'varnames', {'Temp','Tool_angle','Depth','Hardness'});
sFullanova_Fthrust =
anovan(sFthrust,{stemp,sTangle,sdepth,sHardness}, 'model', 'full', 'varnames', {'Temp','Tool_angle','Depth','Hardness'});

% Aluminum
% Prime Factor Tables
aAnova_Fcut =
anovan(aFcutf,{atemp,aTangle,adepth,aHardness}, 'varnames', {'Temp','Tool_angle','Depth','Hardness'});
aAnova_Fthrust =
anovan(aFthrust,{atemp,aTangle,adepth,aHardness}, 'varnames', {'Temp','Tool_angle','Depth','Hardness'});

% Secondary Interaction Tables
aIntanova_Fcut =
anovan(aFcutf,{atemp,aTangle,adepth,aHardness}, 'model', 'interaction', 'varnames', {'Temp','Tool_angle','Depth','Hardness'});
aIntanova_Fthrust =
anovan(aFthrust,{atemp,aTangle,adepth,aHardness}, 'model', 'interaction', 'varnames', {'Temp','Tool_angle','Depth','Hardness'});

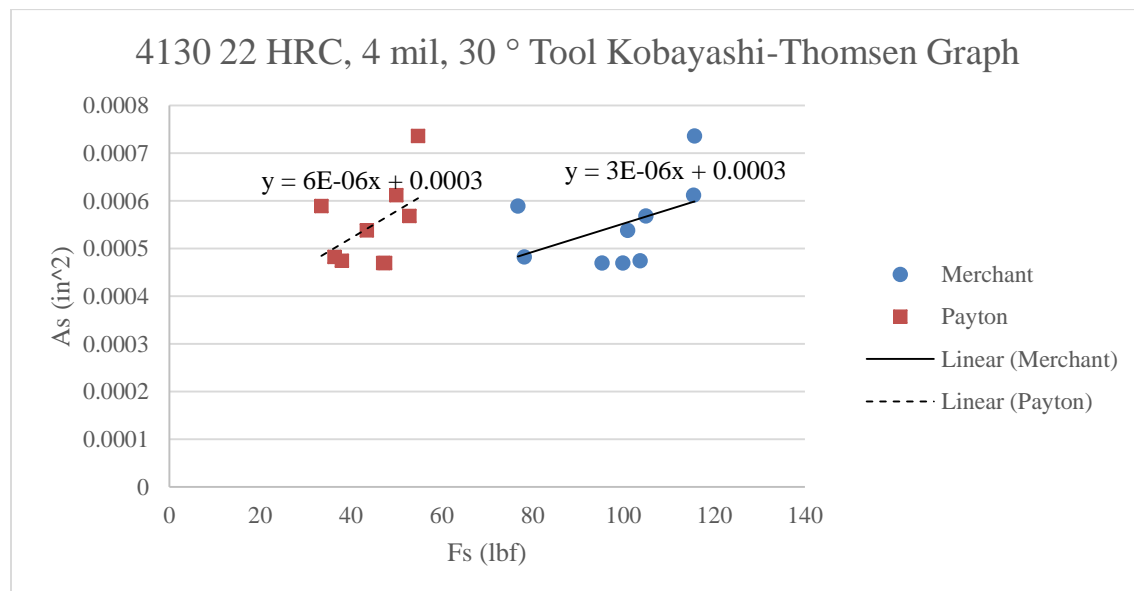
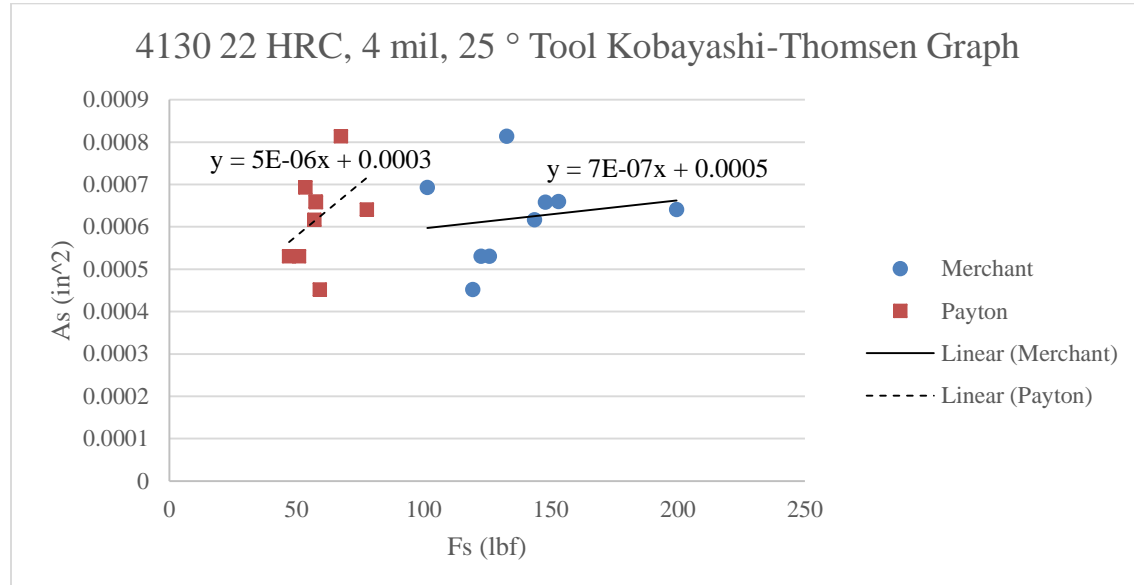
% Full Interaction Tables
aFullanova_Fcut =
anovan(aFcutf,{atemp,aTangle,adepth,aHardness}, 'model', 'full', 'varnames', {'Temp','Tool_angle','Depth','Hardness'});

```

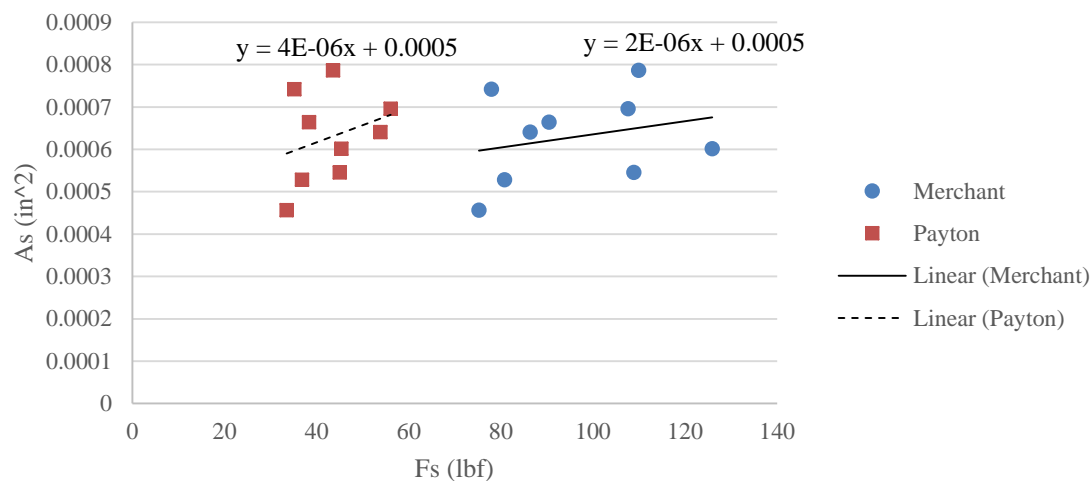
```
aFullanova_Fthrust =  
    anovan(aFthrust,{atemp,aTangle,aDepth,aHardness},'model','full','varnames',{'Temp','Tool_angle','Depth','Hardness'});
```

## Appendix.J: Kobayashi-Thomsen Graphs

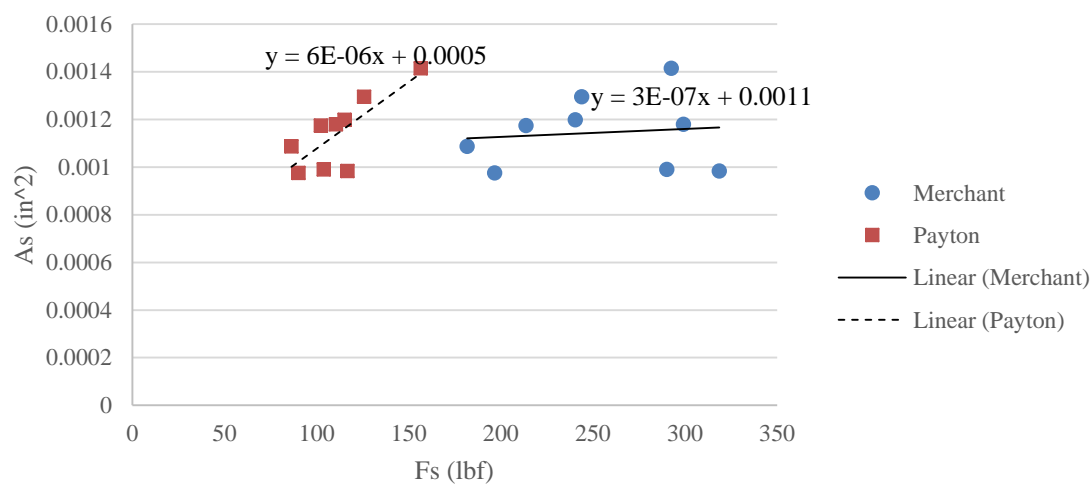
### 4130 22 HRC Steel Graphs



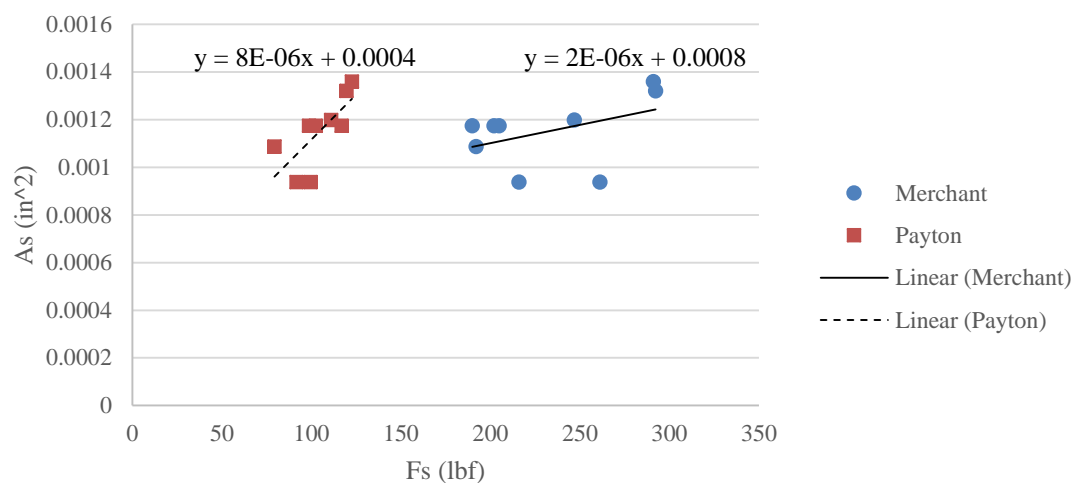
### 4130 22 HRC, 4 mil, 35 ° Tool Kobayashi-Thomsen Graph



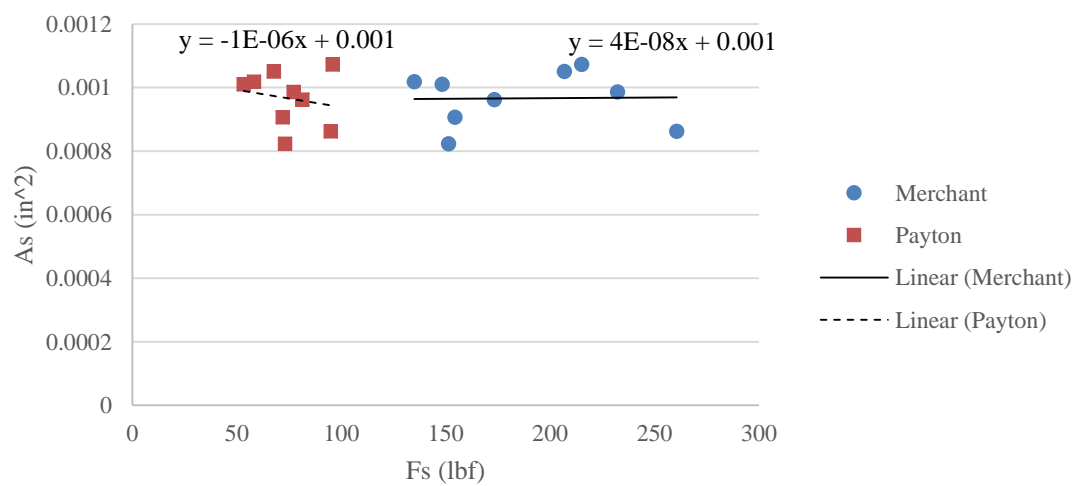
### 4130 22 HRC, 8 mil, 25 ° Tool Kobayashi-Thomsen Graph



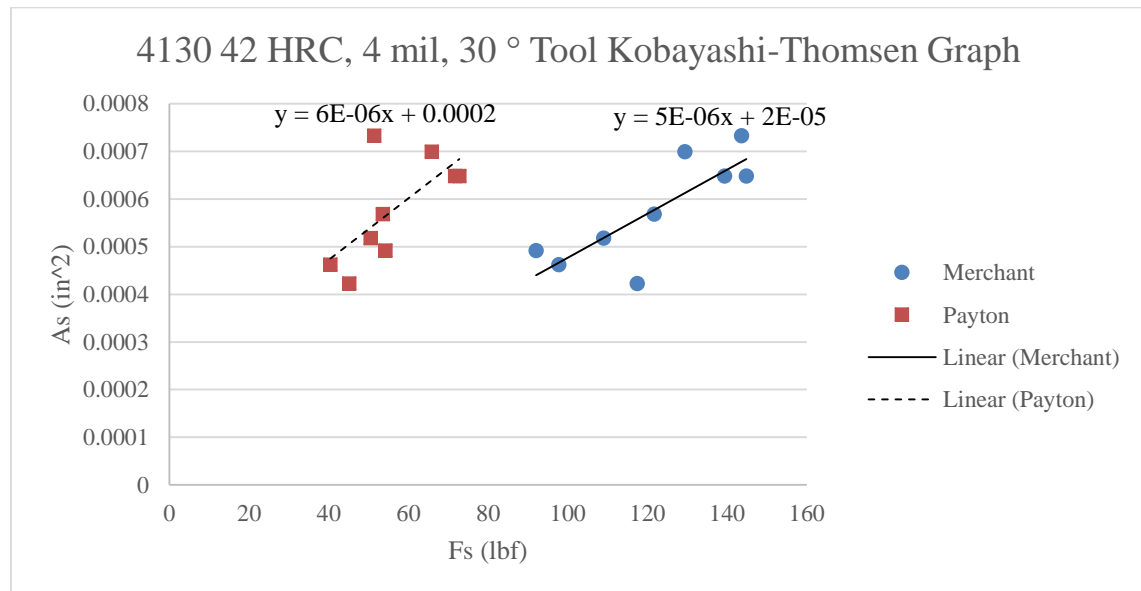
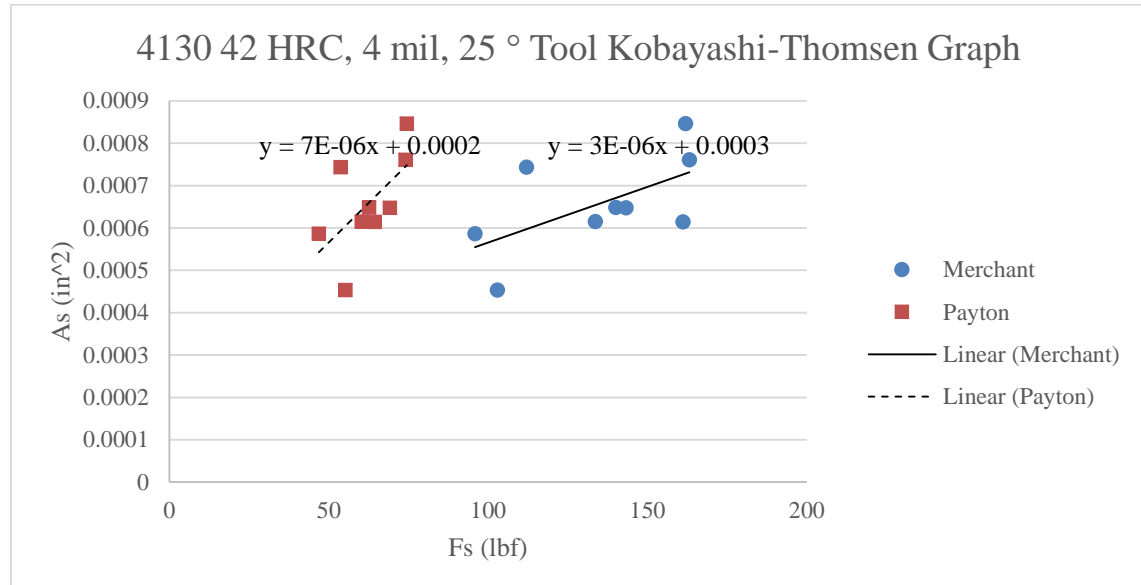
4130 22 HRC, 8 mil, 30 ° Tool Kobayashi-Thomsen Graph



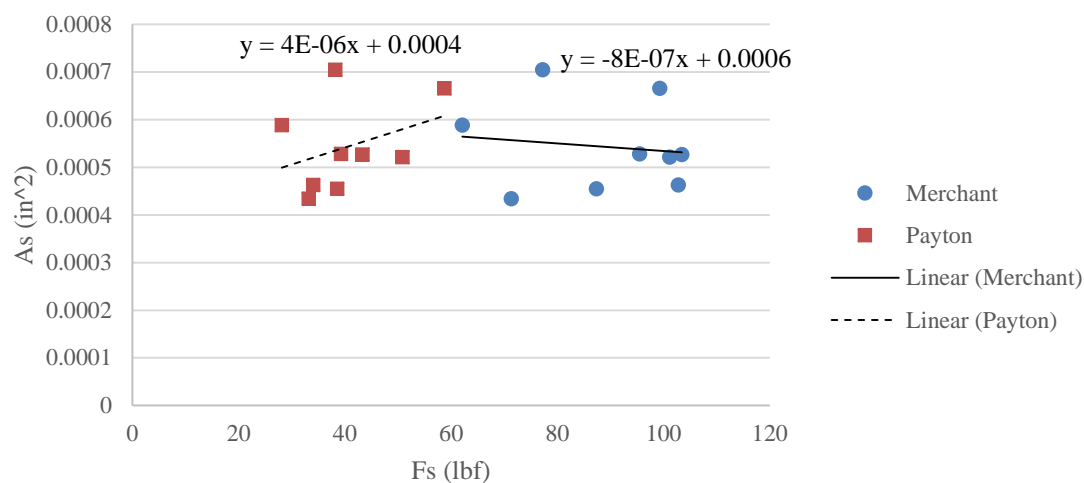
4130 22 HRC, 8 mil, 35 ° Tool Kobayashi-Thomsen Graph



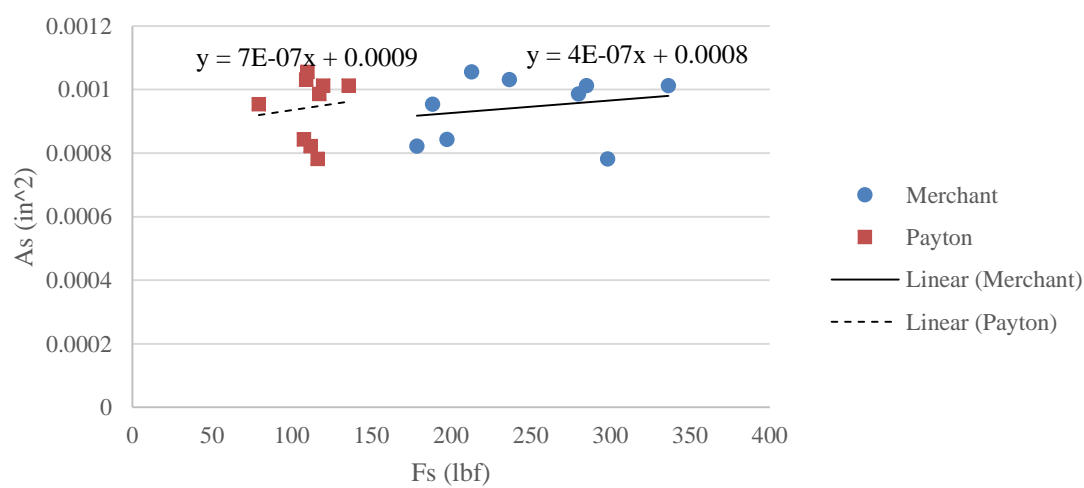
## 4130 42 HRC Steel Graphs



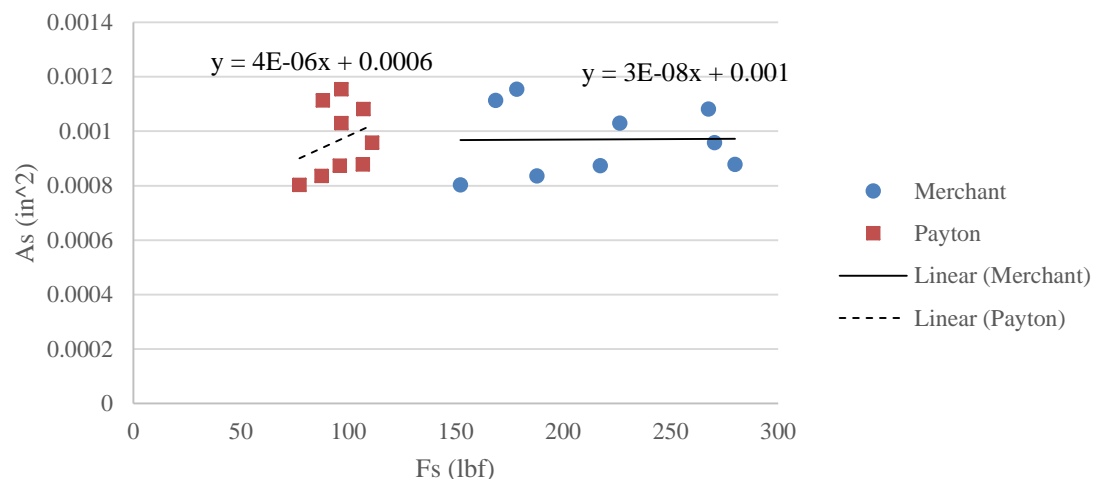
4130 42 HRC, 4 mil, 35 ° Tool Kobayashi-Thomsen Graph



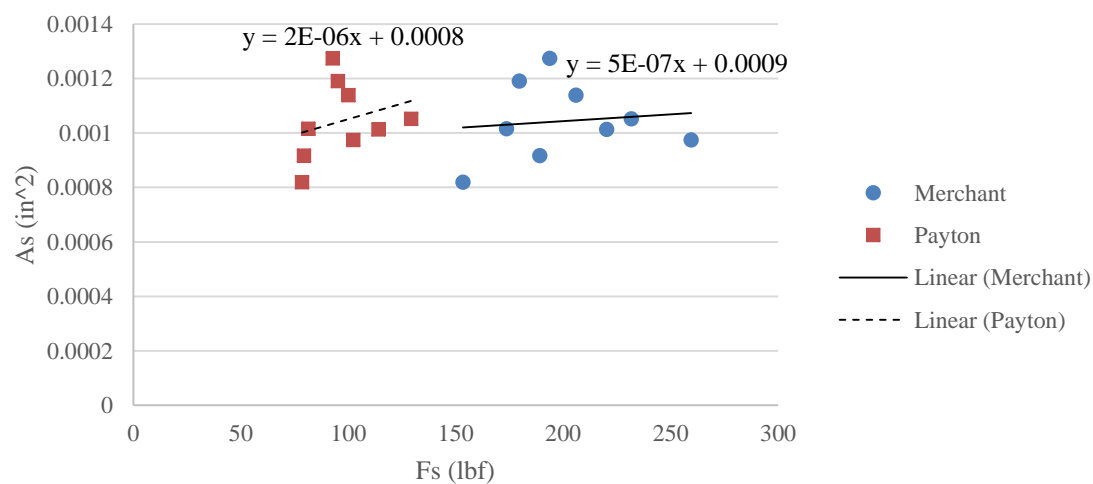
4130 42 HRC, 8 mil, 25 ° Tool Kobayashi-Thomsen Graph



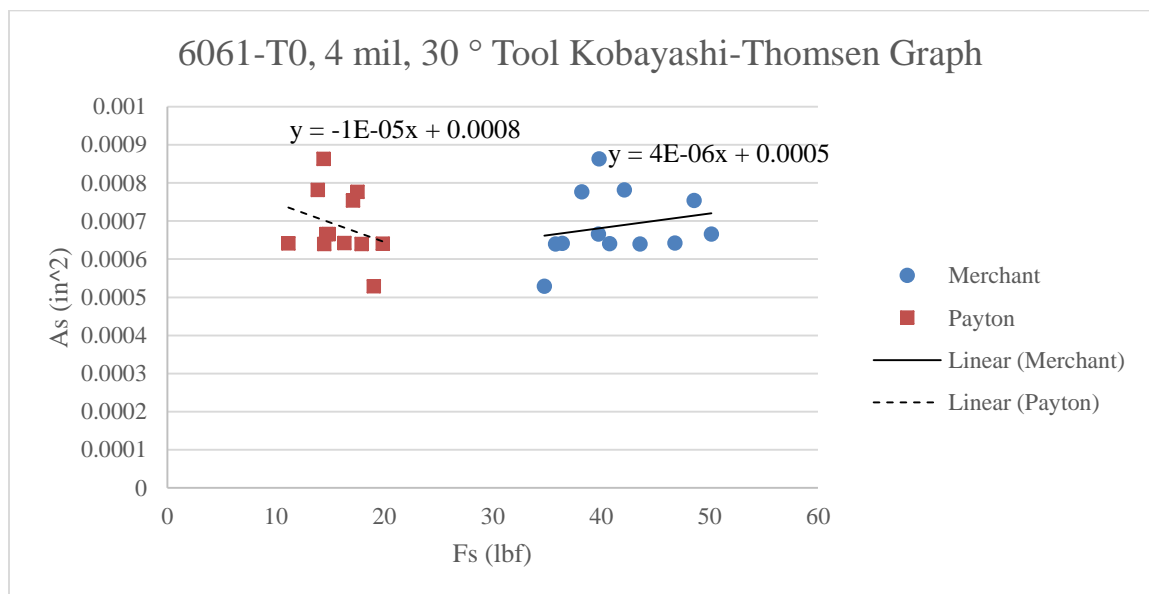
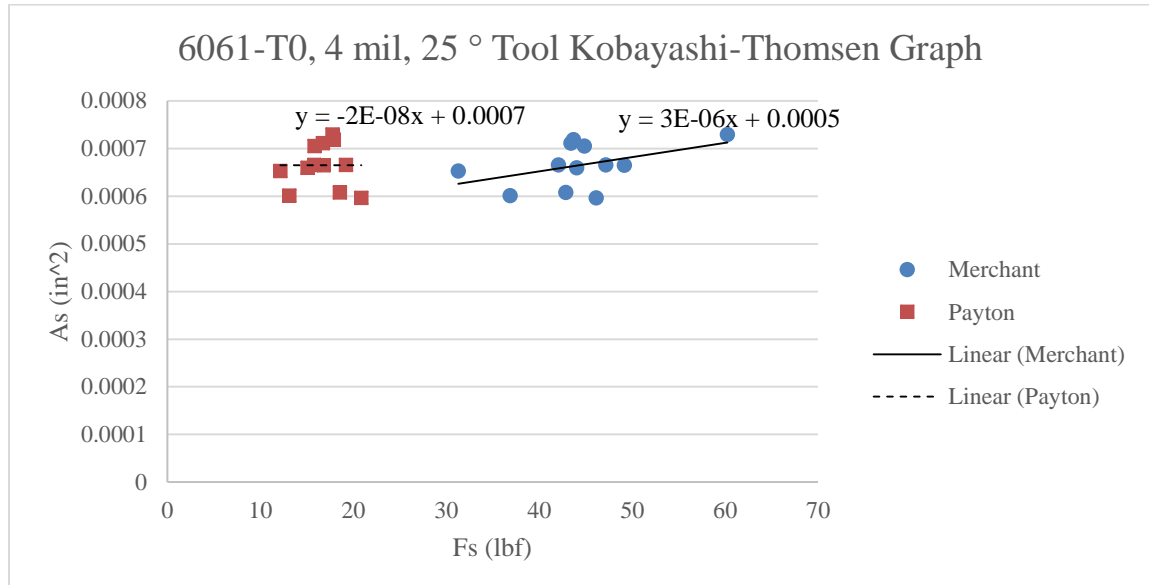
### 4130 42 HRC, 8 mil, 30 ° Tool Kobayashi-Thomsen Graph



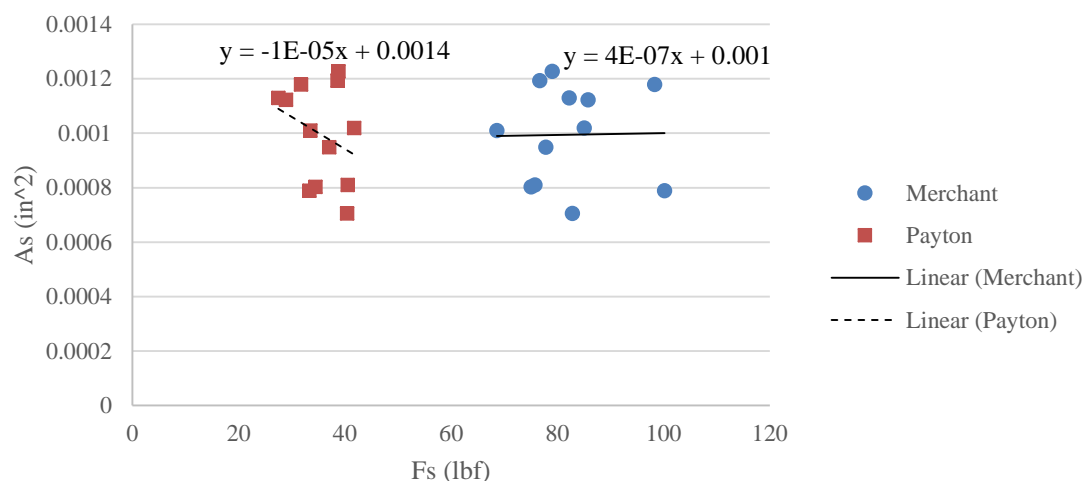
### 4130 42 HRC, 8 mil, 35 ° Tool Kobayashi-Thomsen Graph



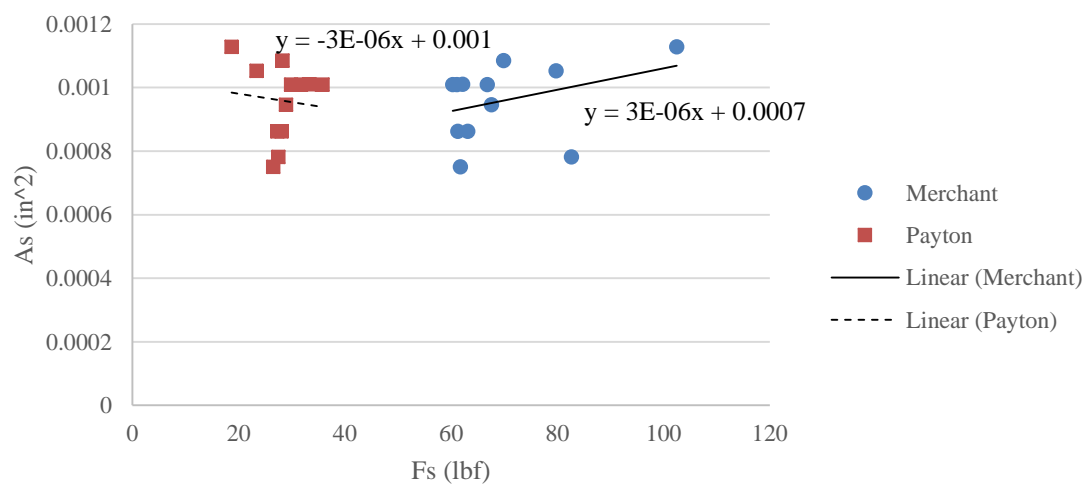
## 6061-T0 Aluminum Graphs



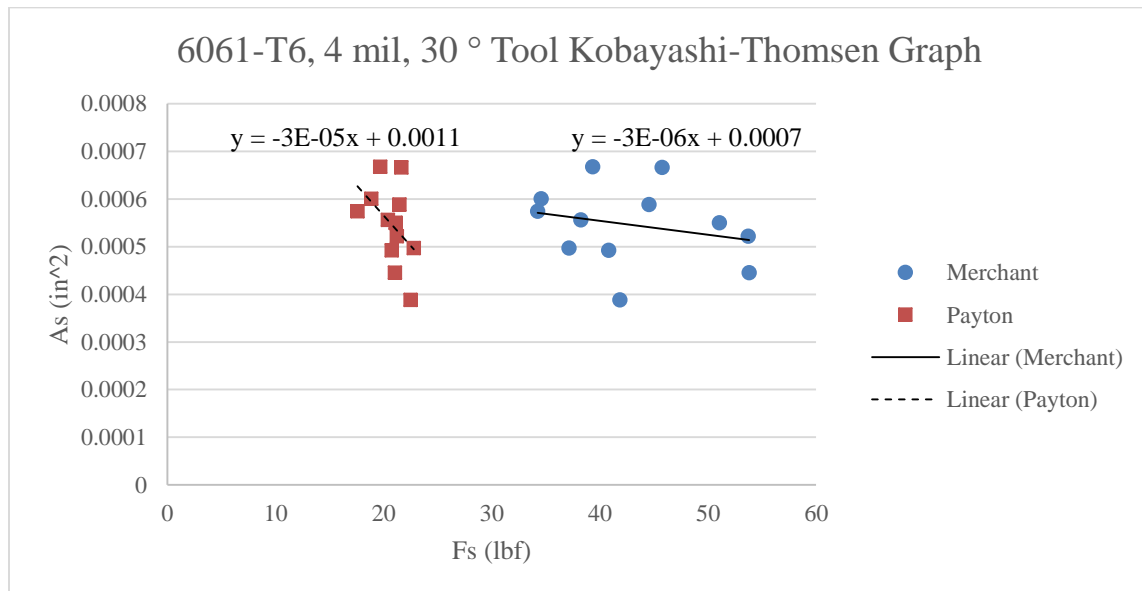
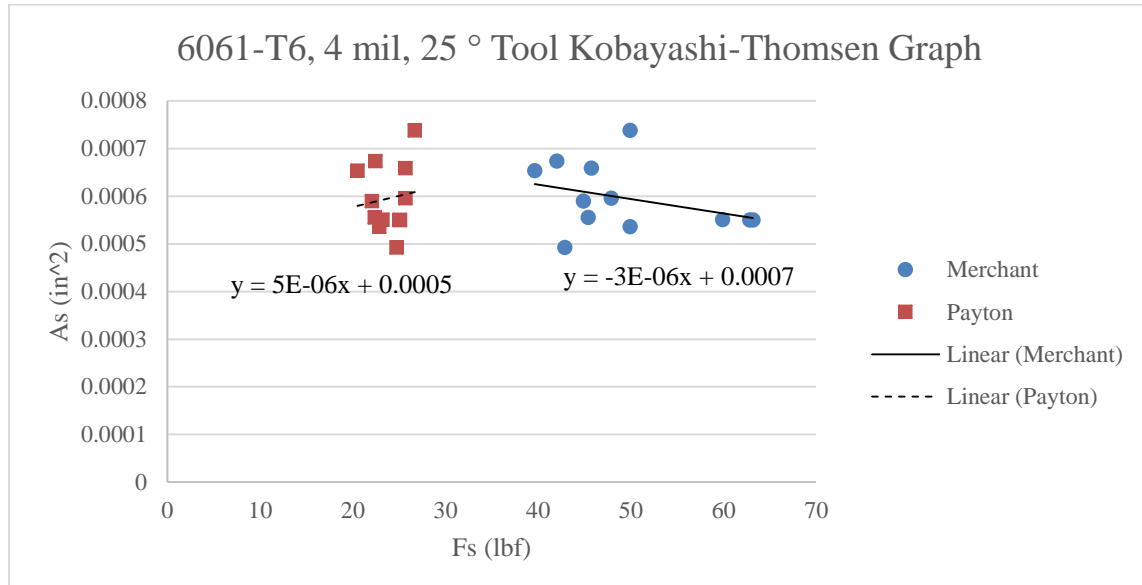
6061-T0, 8 mil, 25 ° Tool Kobayashi-Thomsen Graph



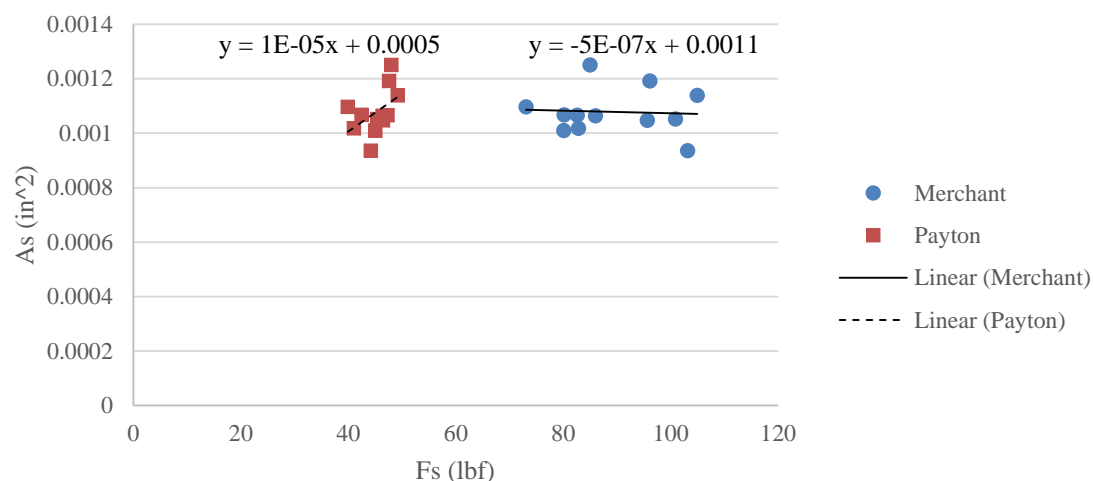
6061-T0, 8 mil, 30 ° Tool Kobayashi-Thomsen Graph



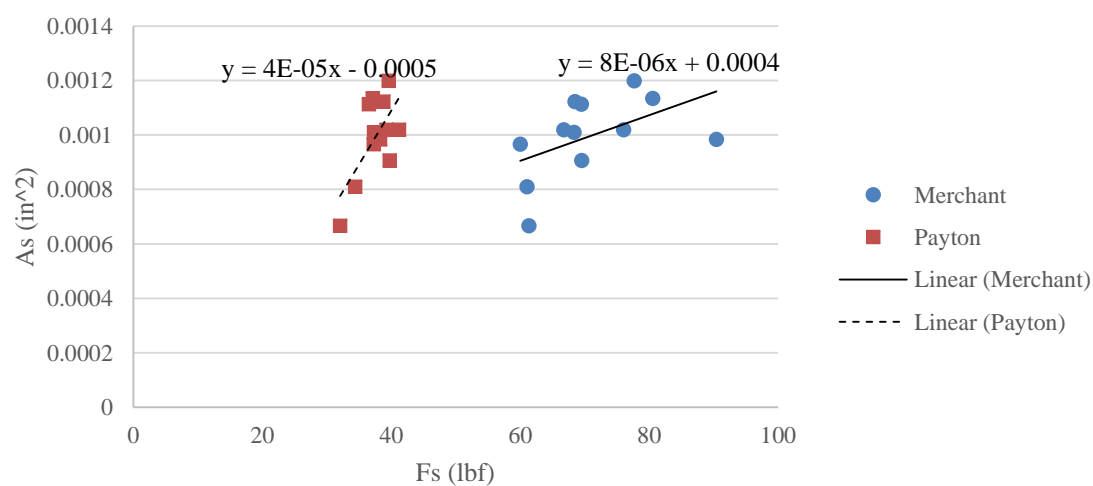
## 6061-T6 Aluminum Graphs



### 6061-T6, 8 mil, 25 ° Tool Kobayashi-Thomsen Graph



### 6061-T6, 8 mil, 30 ° Tool Kobayashi-Thomsen Graph



## Appendix.K: Load Cell Calibration Certificate

### Relevant Calibration and Specification Certificates

The calibration certificate for the Kistler 9257A dynamometer is given below.

